THÈSE

Présentée par Fatma Abid

pour l'obtention du

GRADE DE DOCTEUR

École Doctorale : École Centrale Paris (ED287)

Spécialité : Mécanique

Laboratoire d'accueil : LISMMA (EA2336), SUPMECA Paris

Reduction of coupled field models for the simulation of electrical machines and power electronic modules

---

Soutenue le : 11 juin 2015

Devant un jury composé de :

LARDIES Joseph	Rapporteur	FEMTO-ST, France
GARIBALDI Luigi	Rapporteur	Politecnico di Torino, Italie
DAUCHEZ Nicolas	Directeur de thèse	UTC Compiègne, France
CHEVALLIER Gaël	Co-directeur de thèse	FEMTO-ST, France
RENAUD Franck	Co-encadrant	SUPMECA Paris, France
ARGOUL Pierre	Examinateur	ENPC, France
DION Jean-Luc	Examinateur	SUPMECA Paris, France
BLANCHARD Jean-Louis	Examinateur	VALEO, France
BISSON Jean-François	Invité	VALEO, France

2015 - 2015ECAP0032

Résumé

Dans le domaine automobile, les modules électroniques de puissance des produits mécatroniques voient leur puissance sans cesse s'accroître, tout en étant confinés dans des volumes de plus en plus réduits. Au cours de leur fonctionnement, les composants semi-conducteurs et leur assemblage subissent ainsi des contraintes électro-thermo-mécaniques sévères, susceptibles d'entraîner leur destruction et de provoquer la défaillance du produit. L'étude de la fiabilité et le calcul de la durée de vie de tels produits dépendent des températures de jonction calculées au niveau des puces des composants de puissances. De surcroît, le contexte d'applications embarquées requiert de maîtriser, outre les paramètres électriques et mécaniques, les paramètres thermiques tels que les températures de jonctions et les puissances dissipées au niveau des composants, qu'il est nécessaire de réguler et contrôler en temps réel afin d'assurer le bon fonctionnement du produit.

L'objectif de cette thèse est ainsi de proposer une méthode d'identification de modèles réduits dans le but d'estimer le comportement thermique des modules électroniques de puissance, en se fondant uniquement sur les données d'entrées et les résultats issus d'une simulation numérique d'un modèle détaillé du système étudié.

Une première partie est consacrée (i) à une vue d'ensemble sur les technologies et pratiques industrielles adaptées à la modélisation, à la prévision de fiabilité et au contrôle des modules électroniques de puissance ; (ii) à la description de la méthode d'identification actuellement utilisée à Valeo pour générer un modèle thermique compact et à la mise en évidence de ses limitations lors de traitement de problèmes non-linéaires typiquement liés à la convection naturelle ; (iii) à une étude théorique de la physique des problèmes couplés solide/fluide permettant de déduire un modèle détaillé de référence considéré comme une boîte noire dans le problème d'identification.

Un état de l'art est ensuite consacré aux méthodes de réduction de modèles, classées en catégories intrusives et non-intrusives. Les méthodes intrusives s'appuient sur la projection du modèle détaillé de référence sur une base réduite d'un sous-espace ou bien sur l'approximation *a priori* des équations locales du problème étudié. Les méthodes non-intrusives, également dénommées méthodes d'identification, produisent un modèle réduit reliant les entrées aux sorties du modèle détaillé, tout en considérant ce dernier comme une boite noire.

Dans une seconde partie, nous présentons la nouvelle méthode d'identification développée dans cette thèse, nommée "Kernel Identification Method". Cette méthode

identifie des modèles réduits relatifs à des problèmes thermiques couplés solide/fluide dont le comportement est linéaire ou approximativement linéaire. Le modèle est representé en termes d'états, sous forme modale. Dans cette méthode, le noyau du problème thermique est identifié indépendemment de l'excitation thermique grâce à la projection orthogonale calculée par la décomposition LQ. Le noyau thermique est, en effet, constitué par les valeurs propres dominantes qui correspondent à l'opposé de l'inverse des constantes de temps thermiques dominantes, placées sur la diagonale de la matrice d'état. Les vecteurs propres associés se trouvent dans les vecteurs colonnes de la matrice d'observation. Les matrices de commande et de gain statique sont à leur tour identifiées par la résolution d'un problème aux moindres carrés. La méthode est évaluée sur un premier cas-test numérique avant d'être validée sur une application industrielle traitant d'un problème thermique couplé solide/fluide dont le comportement est essentiellement régi par de la convection forcée.

Dans une dernière partie, nous proposons une étude exploratoire portant sur l'identification de problèmes non linéaires où la convection naturelle joue le rôle dominant. En premier lieu, nous proposons à cet effet une extension de la méthode Kernel Identification Method. Cette extension est non paramétrique puisque les opérateurs non-linéaires du modèle réduit sont identifiés sans présumer de la nature des non linéarités,

Ces opérateurs sont estimés à partir de différents modèles réduits linéaires identifiés par la méthode Kernel Identification Method qui est alors appliquée par morceaux pour différents niveaux d'excitation thermique. Ces excitations sont générées par la variation des puissances dissipées par les composants et éventuellement par celle des conditions aux limites. Cette méthode est évaluée sur un cas-test numérique constituée par un problème comportant une seule entrée et une seule sortie. En second lieu, nous proposons une deuxième méthode d'identification non-linéaire, de nature non paramétrique, basée sur la variante dite *Unscented* du filtre de Kalman. Cette méthode identifie des modèles réduits en représentation d'état en se fondant également sur les données d'entrées et de sorties issues d'un modèle détaillé de référence. Le défi sous-jacent à cette proposition est d'identifier simutanément, en temps réel, les variables d'état et les paramètres présents dans les différents opérateurs du modèle réduit. Cette méthode est d'abord appliquée au cas test précédemment utilisé pour l'évaluation de l'approche étendue de Kernel Identification Method, mais cette fois dans un cadre linéaire. Elle est ensuite testée sur un cas linéaire représentatif d'une application industrielle. Les résultats obtenus soulignent les difficultés rencontrées par cette méthode quant au choix des paramètres du filtre de Kalman. L'étape d'initialisation des paramètres à identifier s'avère également délicate lorsque leur nombre devient important. De ce fait, la méthode n'est pas étendue au cas non-linéaire. En tant que perspective, nous proposons enfin de combiner l'extension de notre méthode Kernel Identification Method avec l'approche fondée sur la variante *Unscented* du filtre de Kalman dans le but d'identifier, en représentation d'état, des modèles réduits non-linéaires comportant plusieurs entrées et sorties.

Contents

List of Figures

List of Tables

Acronyms

ARMA	Auto-Regressive with Moving Average
ARMAX	Auto-Regressive with Moving Average with eXogenous input
CFD	Computational Fluid Dynamics
DCB	Direct Copper Bonding
DOF	Degree Of Freedom
FE	Finite Element (model)
FEM	Finite Element Method
FVM	Finite Volume Method
IGBT	Integrated Gate Bipolar Transistor
IML	Insert Molded Leadframe
IR camera	Infrared camera
KIM	Kernel Identification Method
LSQ	Least-SQuares (method/problem)
LTI	Linear-Time-Invariant (model)
MIM	Modal Identification Method
MIMO	multiple-input multiple-output (model)
MOESP	Multi Output-Error State Space Subspace approach
MOR	Model Order Reduction
MOS	Metal Oxide Semiconductor
MOSFET	Metal Oxide Semiconductor
MTBF	Time Between Failures
NTC thermistor	Negative Temperature Coefficient thermistor
PCB	Printed Circuit Board
ROM	Reduced Order Model
PEM	Prediction Error Method
SISO	single-input single-output (model)
SMI	Insulated Metal Substrate
SubCVA	Canonical Variate Analysis Subspace identification approach
Zth method	Thermal Impedance method

Nomenclature

S	Surface $[m^2]$
$\vec{f}$	Volume force applied on the fluid $[Nm^{-3}]$
$\vec{g}$	Gravitational acceleration $[ms^{-2}]$
$\vec{x}$	Space variable in $\mathbb{R}^d$
t	Time variable
$\frac{\partial .}{\partial t} = \partial_t$	Partial derivative with time
T_j	Junction Temperature [K or °C]
$R(t)$	Reliability function
λ_p	Failure rate [number of failures per unit time]
Subscripts	
$_f$	Fluid
$_s$	Solid
$_{i,j}$	Nodal quantities
Superscripts	
^{w}	Quantities on the interface Γ^w
*	For test function
^{h}	Approximation in a subspace
^{T}	Vector/Matrix transpose
Domain and spaces	
d	Order of the real space $\mathbb{R}^d, d = 2$ or 3
Ω	Bounded domain of $\mathbb{R}^d$
$\Gamma = \partial\Omega$	Boundary of the domain Ω
$\vec{n}$	Normal unit vector exterior to the solid domain Ω_s
Γ^w	Fluid-Solid interface of unit normal vector $\vec{n}$
Γ_s^i	Solid interface on which the imposed heat flux q_{imp} is imposed
$H^0(\Omega)$	Sobolev space of order 0 on Ω
$H^1(\Omega)$	Sobolev space of order 1 on Ω
$\mathcal{L}$	Subspace of H^0 for the pressure in the fluid domain
$\mathcal{H}$	Subspace of H^1 for the velocity in the fluid domain
$\mathcal{R}$	Subspace of H^1 for the temperature in both fluid and solid domains
$\mathcal{L}_h$	Subspace of $\mathcal{L}$ for the pressure approximation
$\mathcal{H}_h$	Subspace of $\mathcal{H}$ for the velocity approximation
$\mathcal{R}_h$	Subspace of $\mathcal{R}$ for the temperature approximation

Material properties	
k	Thermal conductivity $[W\ m^{-1}\ K^{-1}]$
ρ	Density $[kg\ m^{-3}]$
c_p	Specific heat $[Jkg^{-1}K^{-1}]$
μ	Fluid dynamic viscosity $[P_a\ s]$
ζ	Fluid bulk viscosity $[P_a\ s]$
β	Thermal expansion coefficient of the fluid $[K^{-1}]$
h	Convective heat transfer coefficient $[W\ m^{-2}\ K^{-1}]$
ϵ	Emissivity coefficient
σ	Stephan-Boltzman constant
Discretization	
l	Number of Degrees of Freedom of pressure
N	Number of Degrees of Freedom of temperature
m	Number of Degrees of Freedom of each velocity component
$M = d \times m$	Total number of Degrees of Freedom of velocity variable)
flux	
Q	Rate of heat flux / Power $[W$ (Watt)]
q	Heat flux (Power per unit area) $[W\ m^{-2}]$
Fluid / Solid Temperature	
T	Temperature variable in the subspace $\mathcal{R}$ [K or °C]
χ_j	Shape function of the temperature fluid / solid in the subspace $\mathcal{R}_h$, $j = 1, \cdots, l$
$\mathbf{T}$	Nodal vector of temperatures of dimension $l \times 1$
Fluid Velocity	
$\vec{u}$	Velocity variable in the subspace $\mathcal{H}$ $[ms^{-1}]$
ϕ_j	Shape function of the fluid velocity in the subspace $\mathcal{H}_h$, $j = 1, \cdots, N$
$\mathbf{U}$	Nodal vector of the fluid velocity components of dimension $N \times 1$
Fluid Pressure	
p	Pressure variable in the subspace $\mathcal{L}$ $[P_a]$
ψ_j	Shape function of pressure the fluid / solid in the subspace $\mathcal{L}_h$, $j = 1, \cdots, m$
$\mathbf{P}$	Nodal vector of the fluid pressure of dimension $m \times 1$
Differential operators	
∇	Gradient operator
$\nabla.(\ )$	Divergence operator
$\Delta = \nabla.(\ \nabla)$	Laplacian operator
Mathematical Symbols	
δ_{ij}	Kronecker delta

Other notations

N_{snap}	Number of time steps of the FE model simulation (or experimental measurements)
N_{ex}	Number of excitations (heat flux densities and BCs) in thermal input vector
N_{obs}	Number of observations selected from FE model nodes
n	ROM order
U	Thermal inputs vector
Y	Observed temperatures
$\dot{.}$	Derivation with respect to time
$diag\,(a_1, \ldots, a_n)$	Diagonal matrix of a_i
$\mathbf{I_n}$	Identity matrix of dimension n
$\mathbf{R^n}$	Space of dimension n
$\|.\| = \|.\|_2$	The 2-norm (or Euclidean norm)
F_s	Sampling frequency
$X\,(t)$	Continuous variable X at time t
$X\,[k]$	Discrete variable at time $t_k = k\Delta t$, Δt being the sampling time

Introduction

Industrial context and objectives

Mechatronics products are complex hardware widely used today in many areas of applications. As microprocessors gain speed and reliability, more electronic controls and electrical content are being applied to traditional mechanical processes in the new mechatronics products. An example of a mechatronics products is depicted in Fig. 0.1. This example shows a Start/Stop system designed for micro hybrid vehicles. Its function is to automatically shut and restart the internal combustion engine. This innovative solution has the relevant potential to save fuel, and reduce the CO2 emissions especially in traffic jam. The power electronics modules/systems guaranty the conversion and control of electrical power for mechatronics systems. Power electronics modules are mainly composed of power switches and a controller as it can be seen in Fig. 1(b). They are being made smaller and smaller while keeping the same power capability which leads to a rise in power density. The increasing power density results in higher junction temperature, generally located in the chip in silicon of power-handling components, which in turn causes further increase of the device power consumption. The safe operation of electronic devices requires then the prevention of an excessive chip temperature. As reliability is tightly related to electronic devices operating temperature, particularly the junction temperatures of power components, knowledge and control of these temperatures is required in order to ensure system reliability and control of the lifetime. The reliability of a product is strongly influenced by decisions made during the design process. An efficient thermal management should be therefore addressed at the start of design phase to avoid subsequent cost and schedule delays. The "cost of change" curve, that was first introduced by Barry Boehm [1], illustrates that the cost of an engineering change increases drastically with time (Fig. 0.2).

The thermal analysis of power electronics modules is usually performed by means of multiphysics simulation tools including electrical, mechanical, thermal, and fluidic effects. These tools are based on the discretization of the governing equations of the different field quantities taking into account the full coupling between these fields. Discretization-based methods such as Finite Difference, Finite Element and Finite Volume methods can easily lead to several hundred thousand degrees of freedom resulting in detailed models of high complexity. In addition, the reduction of

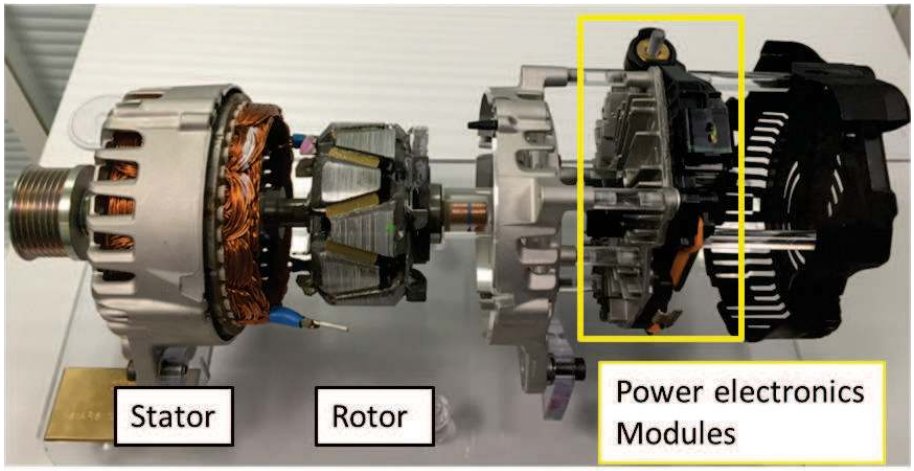

(a) Exploded view of Start/Stop Valeo system.

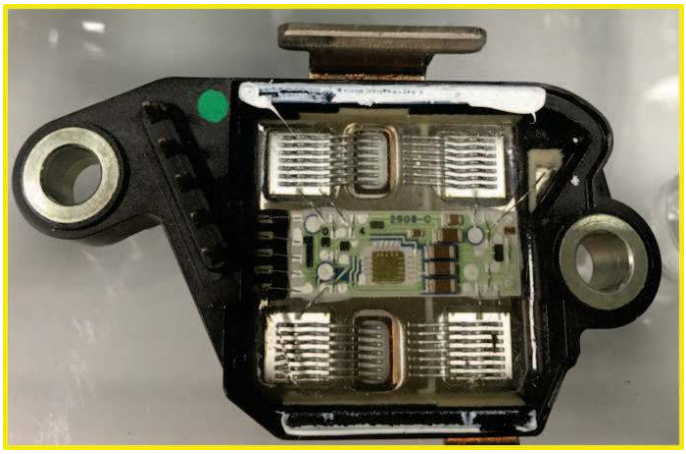

(b) Zoom on a power module.

Figure 0.1. Mechatronic hardware example: a control and power module for an automatic Start/Stop system in micro hybrid vehicles.

real prototyping requires producing reliable and accurate virtual models. This leads in practice to retain many details of the design to simulate. By contrast, almost paradoxically, these simulations aim at computing junction temperatures of electronic components, whose number is often limited compared to the detailed model size. Furthermore, the processing of transient regimes generally involve complex variations of the power dissipated by power components with time. This requires the use of very short integration time steps hampering large model simulations over long periods of time, in particular when several power profiles have to be processed. These facts show the need for a simplified thermal model to speed up the transient thermal simulation of mechatronics models.

The aim of this work is to develop an identification method of a thermal Reduced Order Model (ROM) in order to estimate the transient junction temperatures of the

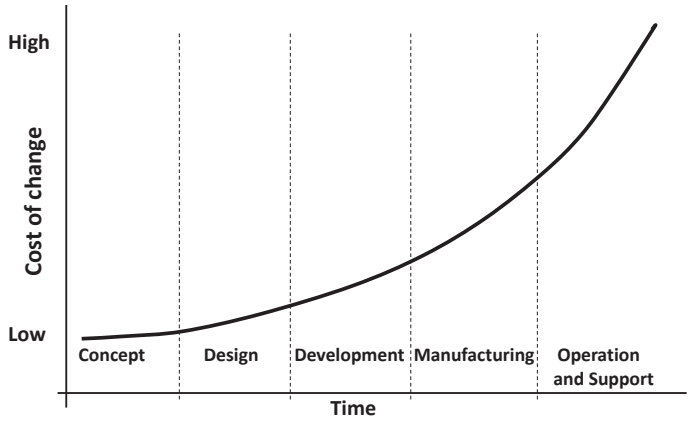

Figure 0.2. Cost of design change [1].

power-handling components on which mission profiles are applied. The identification method, as its name implies, must take into account the locked access to the source code of commercial simulation tool, in order to derive reduced models independently of the target tool. The method has to be implemented as an offline tool that post-processes the inputs and outputs of a discrete detailed reference model considered as a black box.
With regard to the thermal management of power electronics, the ROM use has a twofold purpose (Fig. 0.3):

- **Reliability analysis**: The key factor in this analysis is the individual component temperatures. The ROM intent is to produce an accurate estimate of the junction temperatures under a given mission profile. Initially identified into state-space form, the ROM can be then converted into an RC-network so that it can be implemented into SPICE (Simulation Program with Integrated Circuit Emphasis) simulator [2] or similar platforms to conclude on the system reliability assessment.

- **Control application** : The demand for reduced models also arises from control application that become increasingly necessary for system performance optimization. Generally, the order of a controller is approximately the same as that of the system to be controlled. Hence, if the latter has high complexity, so will the controller. Therefore, the implementation of the controller will become much more complex, if not infeasible, to design because of storage, accuracy, robustness and computational aspects problems [3]. A thermal reduced thermal model is intended to be implemented in a command law in order to provide an accurate temperature estimation, which constitutes a major information to ensure a safe system operation. The targeted ROM, besides being accurate enough, must be in a state-space representation, a form particularly appropriate for a Simulink implementation in view of its further inclusion in a command law.

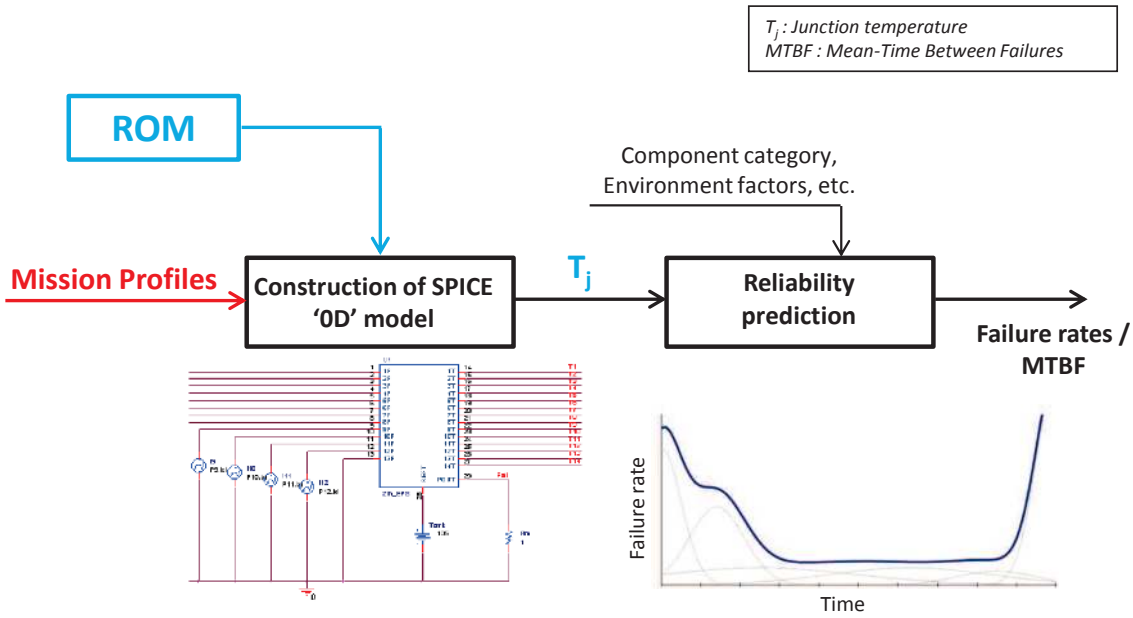

(a) Reliability analysis.

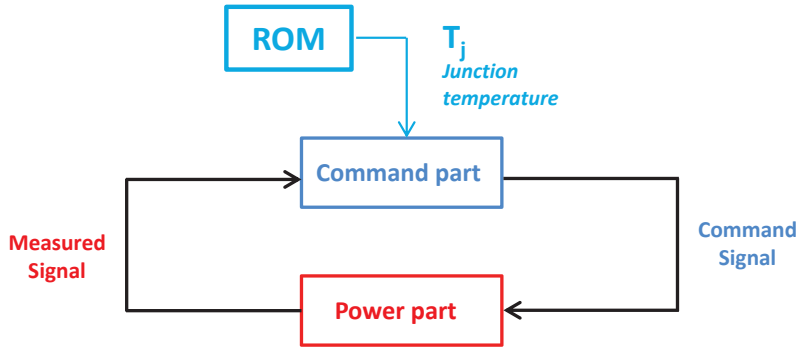

(b) Control process.

Figure 0.3. Schematic positioning of the reduced model in the targeted applications: Reliability analysis (a) and control in a command law (b).

Thesis contributions and overview

In this thesis, the development framework has been deliberately restricted to "non-intrusive" reduction methods, also known as the "identification" methods in experimental works. The identification method is aimed at producing reduced order models (ROMs) of transient thermal simulation of large scale mechatronics products. The ROM is identified into a multiple-input multiple-output (MIMO) state-space form. Our main contributions to this class of methods are the followings:

- We develop a new identification method named the "Kernel Identification Method" (KIM), in a non-intrusive framework. It is implemented as an offline tool that post-processes the inputs and outputs of a detailed reference model

considered as a black box. The state matrix, assumed to be diagonal, is formed of the dominant eigenvalues of the thermal problem. The name of the method reflects that the identification process is based on the kernel of the thermal problem through eigenvectors and eigenvalues independent of the input. A main feature of KIM comes from its use of robust linear algebra tools enabling the identification of generic reduced models valid for any signal input given the same initial and boundary conditions. We successfully validate KIM method on two applications: (1) a small-scale linear conduction problem; and (2) an industrial large-scale water-cooled CFD problem mainly governed by forced convection.

- we develop an extended KIM for the identification of non-linear reduced thermal models of convective heat transfer problems. This is handled with a non-parametric model. In order to describe the dynamic behavior of the non-linear system, we identify a linear multimodel consisting of KIM linear models suited for different operating points covering the entire range of operation. We validate the identification methodology on a single-input-single-output (SISO) academic problem.

- We explore and develop an on-line identification method based on Kalman Filter techniques aimed at processing non-linear thermal problems. The Kalman Filter-based method particularly accommodates adaptive control in the real-time processing problems due to its recursive working principle. Two variants are selected, The Extended Kalman Filter and the Unscented Kalman Filter. First, we focus on the identification of linear problems. An original Kalman model is proposed in order to identify a linear thermal reduced model in a discrete-time state-space form. In their present state, the Kalman variants methods give satisfactory results on an academic linear 10 degrees of freedom model but show difficulties when applied to a 3D larger-scale model.

Thesis outline

This thesis is organized in the following order:

- Chapter 1 gives a basic background in the thermal management of power electronics system, a key point to understand the targeted applications of this study. It also review the currently used identification method in Valeo named Thermal Impedance Method,

- Chapter 2 describes the derivation of the discrete model of a thermally coupled fluid solid problem using Finite Element method. Three different discrete models are then deduced; (1) a linear model for a heat conduction problem, (2) a linear forced convection governed problem and (3) a non-linear model for

a natural convection governed problem. These models play a key role in the choice of the ROM structure in the identification process.

- Chapter 3 reviews existing intrusive and non-intrusive model order reduction methods but provides more insight into the second category, i.e. identification methods including the Prediction Error Methods (PEM), the Modal Identification Method (MIM) and the Subspace method. This latter, in particular, has fruitfully contributed to the development of our method.

- Chapter 4 presents one of the original contributions of this thesis. It describes the Kernel Identification Method (KIM) method principle and compares it to three Subspace approaches on a 3D linear thermal model. KIM method is validated on two linear thermal problems (1) a small-scale conduction problem and (2) a large-scale water-cooled CFD problem of an industrial product.

- Chapter 5 proposes the non-linear identification approaches for the processing of non-linear thermal problems coupled with natural convection. An extended KIM method is developed as a non-parametric identification method and is validated on an academic problem. A parametric based-KIM methodology is also suggested but not tested in this work. The last section in this chapter presents the two variants of Kalman Filter technique, Extended Kalman Filter and Unscented Kalman Filter for the on-line identification of thermal problems, validates the approach on a linear academic test case and illustrates the current difficulties encountered when dealing with larger scale models.

- Finally the conclusion summarizes the main results of the work and discusses the related future work.

References

[1] B. Boehm. *Software Engineering Economics*. Prentice Hall, 1981.

[2] M.H. Rashid. *SPICE for Power Electronics and Electric Power, Third Edition*. CRC Press, Taylor & Francis Group, 2012.

[3] M.D. Gunzburger and J.S. Petersen. The reduced basis method in control problems. In *The Proceeding of Computation and Control, Birkhäuser, Berlin*, pages 211–218, 1993.

Chapter 1

Background

This chapter gives a basic background in thermal management of power electronics systems. After introducing the power electronics systems, we will present the reliability analysis as well as the derating process applied to power electronics in order to control temperatures of the most important components, i.e. those with the greatest power dissipation or those that are the most sensitive to high temperatures. We will also provide a brief overview of the physical mechanisms involved in electronic cooling. Finally, we shall review the thermal impedance method constituting the currently used in Valeo to estimate the junction temperature of power electronic components.

Contents

1.1 Power electronics systems

Power electronics systems are gaining more and more importance in the automotive applications due to the steady progress of partially or fully electric powered vehicles. Considering the various power electronic systems necessary in these modern vehicles, the most common solution today is to integrate power modules composed of multiple power semiconductors into a compact structure for cost and space reduction purposes. The result is an increasing heat flux density at both components and circuit board levels in addition to the increased coupling effect of neighbouring components. Fig. 1.1 depicts two examples of Valeo power modules with different substrate tech-

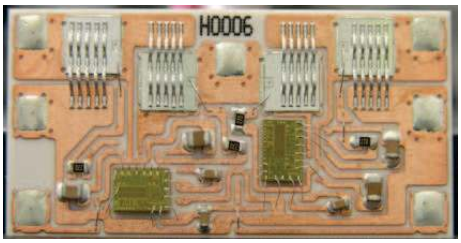

(a) DCB Power Module.

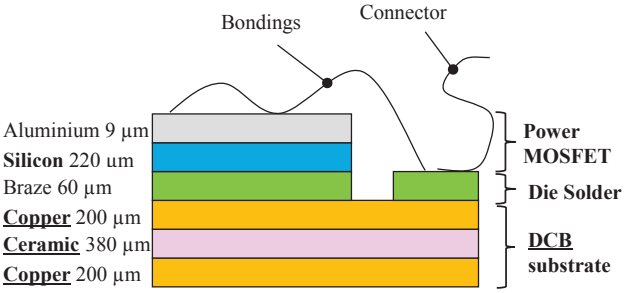

(b) Schematic Cross section of DCB Power Module.

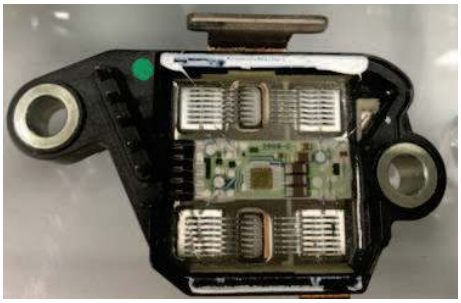

(c) IML Power Module.

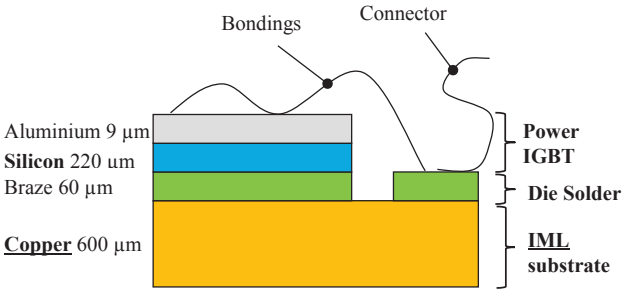

(d) Schematic Cross section of IML Power Module.

Figure 1.1. Two examples of Valeo power modules : DCB and IML technologies and their corresponding schematic cross sections.

nologies: the DCB module (Direct Copper Bonding) and the IML IGBT (Insert Molded Leadframe) module. This latter constitutes an innovative technology developed at Valeo [1], allowing for high power densities with high efficiency in comparison with other technologies (DCB, SMI (Insulated Metal Substrate), FR4, etc.). The cross sections with DCB and IML technologies are given in Figs. 1.1(b) and 1.1(d), respectively. The junction temperature of a component, T_j, is defined as the average temperature of the silicon die. This is also a key parameter for components, especially critical semiconductors such as IGBTs (Integrated Gate Bipolar Transistors), diodes and MOSFETs (Metal Oxide Semiconductor Field Effect Transistor).

Indeed, these components are particularly sensitive to temperature. Consequently, they must operate below a maximum allowed junction temperature specified by the semiconductor manufacturers under every operating conditions. Examples of temperature limits are $150 - 175°C$ for MOSFETs [2] and IGBTs, 150°C for diodes, 120°C for capacitors, and so forth).

1.1.1 Reliability analysis

The reliability of a power module depends on the technology of the components, their semiconductor material properties and on interactions with internal and external stresses. Improvements in semiconductors technology have resulted in higher power densities and lower power-temperature tolerances. This can lead to difficult thermal management problems in order to prevent junction temperatures attaining values beyond which reliability would be seriously affected.

Failure mechanisms

Electronic components can fail because of several mechanisms (fatigue, corrosion, wear, etc.). Fatigue is a common cause of failure of power components subjected to repetitive stress, for example from repeated electrical, thermal, mechanical stresses. There are strong interactions between these stresses. On the one hand, electrical and thermal stresses take place since current flow generates heat, and therefore increase temperature. On the other hand, if the system is subjected to vibration, thermal and vibration cycling can strongly interact. The most contributing stress factor to failure rates of the power semiconductor devices are related to temperature. Increased junction temperature may accelerate many fatigue failure mechanisms. The most typical ones are bond wires (Fig. 1.2(a)) and solder joints failure (Fig. 1.2(b)). The latter failure type generally appears due to the difference in thermal expansion coefficients of different materials at interfaces resulting in fatigue and eventually failure. Moreover, the lifetime of a power module is reduced if it is used consistently in extreme operating conditions. For instance, Fig. 1.3 illustrates that even a small variation of the junction temperature of 10 K may result in a factor 2.5 times reduction in device lifetime.

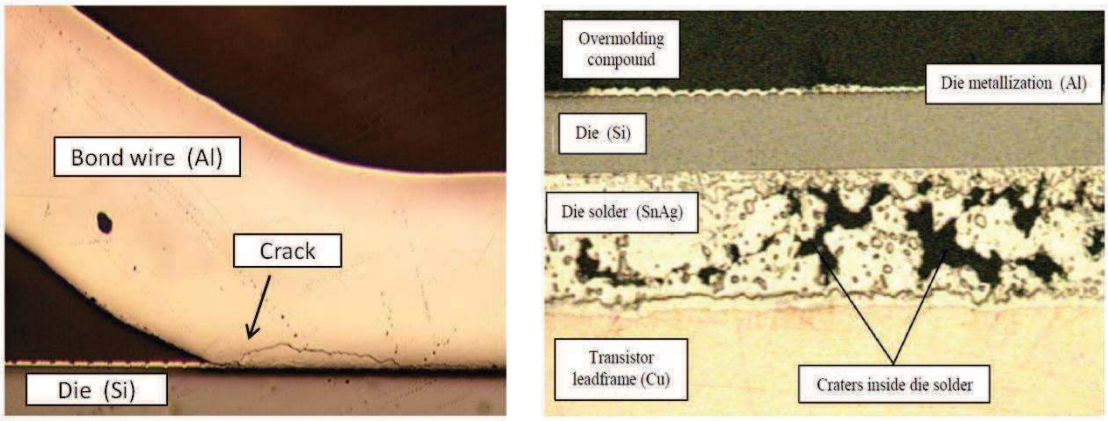

(a) Wire bond cracking of an IGBT as result of thermo-mechanical fatigue during power cycling.

(b) Solder voids between Mosfet and substrate.

Figure 1.2. Defects due to wire bond (a) [3] and die solder (b) [2] degradation.

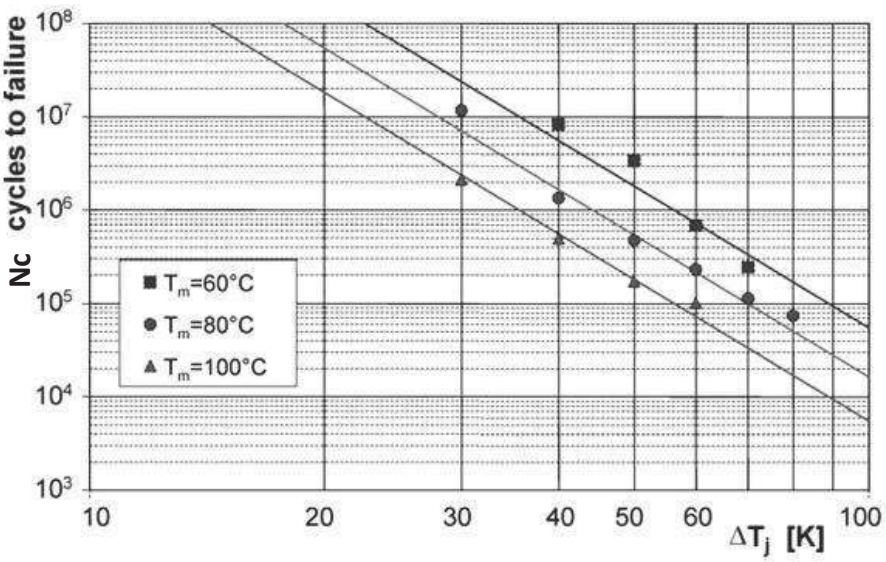

Figure 1.3. Number of cycles to failure depending on ΔT_j and different medium temperatures T_m; power cycle tests performed on IGBT modules [4].

Reliability prediction

Reliability can be defined as the ability of an item to perform a required function under given conditions for a given time interval. Another definition is that reliability is the probability of an item to perform a required function without incidents under given conditions for a given time interval too [5]. The second definition shows that the reliability can be a quantitative performance that must be achieved. Many

models and methods have been used for reliability prediction, an exhaustive list can be found in [5]. Among them, we will focus on describing failure-rate based prediction methods. The failure rate, denoted as λ_p, is the fundamental variable that quantifies reliability, expressed in terms of failures per unit of time. It is driven by the applied stress levels during operation (thermal, electrical, mechanical and radiation stresses). Thermal stresses, and in particular the system operating temperature, receive special focus due to its major influence on the overall reliability. For instance, the failure rate of MOS (Metal Oxide Semiconductor) transistor depends exponentially on the amplitude of its junction temperature based on NASA failure rate model [6].
The failure rate of electronics parts and equipment has often been represented by an idealized graph named the "bathtub curve" [5] directed by three regions as shown in Fig. 1.4:

- an early "infant mortality" failure period : the higher initial failure rate is due to manufacturing or material defects. Generally, a component or a system is operated in the factory for a period of time so that any infant mortality failures are eliminated before to be shipped to the customer. A common example of this testing process is the *burn-in* technique [7].

- a useful life period: the failure rate within this period is assumed constant. A constant rate represents failures that are generated by the application of overstress levels at a constant average rate. During this period, as the failure rate is assumed constant, reliability can also be quantified by the Mean Time Between Failures, denoted by $MTBF$ and defined by $MTBF = 1$ / failure rate.

- a final wear-out failure period : the increasing failure rate signifies the end of the useful life or lifetime of the device due to incremental physical damage or fatigue during normal load operation.

There exist several reliability prediction standards for electronic components and systems. The commonly used ones include the best known source US MIL-HDBK-217 [9] for US defense systems, RDF 2000 (UTEC 80810) [10] for Telecom and Automotive in France, FIDES (UTEC 80811) [11] for aeronautics and defense systems in France, and so on. These methods are based on empirical failure rate models based on a set of collected failure data over years and assume constant failures rates during the useful life period. These standards use two methods of reliability prediction : "parts count" and "parts stress" methods [5]. The parts count method considers stress levels as a means of providing a very early design estimate of the failure rates. The estimation of the failure rate equation contains several π-factors corresponding typically to product environment, application environment, temperature factor and quality, as well as information related to components categories (Eq. 1.1). The parts stress method, however, requires greater detailed informations, i.e. the failure rate equation contains more π factors. In addition, it is applied in the later phase of design (see [5] for more details). Herein, we focus on the parts

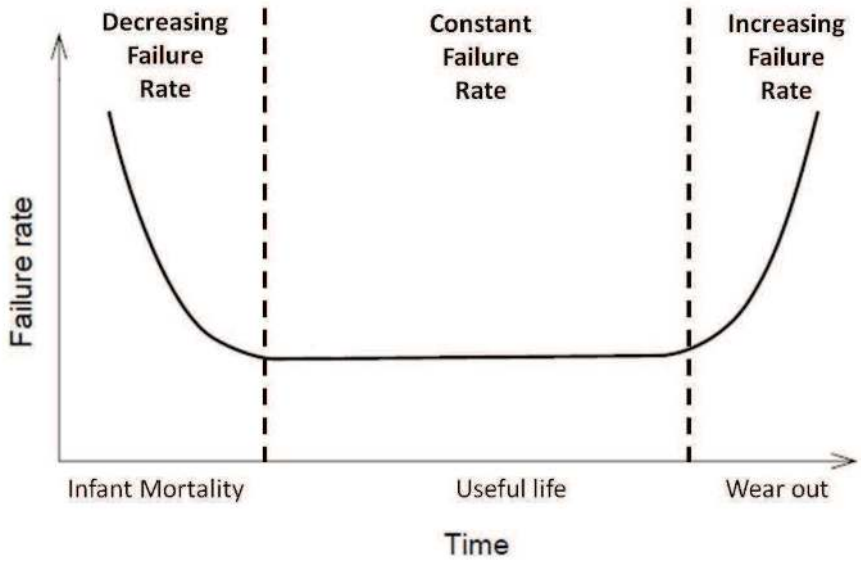

Figure 1.4. Reliability "Bathtub" curve - failure rate as a function of time during lifetime [8].

count method. The total equipment failure rate during the useful life period, can be calculated as the sum of the failure rates of the different equipment components as follows:

$$\lambda_p^{EQUIP} \;=\; \sum_{i=1}^{n} N_i \; \pi_{Q_i} \; \lambda_{pi} \tag{1.1}$$

where n is the number of parts categories (transistor, capacitor, etc.), N_i the quantity of ith part, π_{Q_i} the quality factor for ith part and λ_{pi} the base failure rate of ith part.
For instance, the predicted failure rate model, λ_p, for a transistor in low frequency, takes a form of (MIL-HDBK-2017)

$$\lambda_p \;=\; \lambda_b \; \pi_T \; \pi_A \; \pi_Q \; \pi_E \;\; \text{Failures}/10^6 \text{ Hours} \tag{1.2}$$

where λ_b is the base failure rate usually expressed by a model relating the influence of electrical and temperature stresses on the part, π_T, π_A, π_Q, π_E are temperature, application, quality and environment factors respectively. The π factors vary for components types and categories. π_T is in turn a function of the junction temperature. This fully justifies the need for an accurate determination of the components junction temperatures.
The reliability function of the equipment component, $R(t)$, is related to λ_p^{EQUP} in Eq. (1.1) by the following relationship:

$$R_i(t) = \exp\left(-\lambda_p^{EQUIP} \; t\right) \tag{1.3}$$

System reliability can be improved by controlling its operating stresses, in particular the junction temperature and environment conditions. These can be controlled by reducing the electrical stresses, such as current and voltage to prevent temperature extremes, or/and by managing the airflow and the ambient temperature. The former is referred to as "derating technique", the latter is generally performed by means of external cooling such as conduction and convection heat transfer modes. This will be the subject of the following paragraph.

1.1.2 Control strategies

The advancements in power electronics systems largely rely on the control effectiveness, therefore it is essential to apply the appropriate control strategies to the electronic devices and system to obtain the targeted performance. For electronic components, ambient temperature and power dissipation represent the main source of junction temperatures extremes that can damage components. Designers should therefore apply control strategies over each of the component power dissipation, referred to as derating technique, and over the ambient temperature through external cooling. Fig. 1.5 shows an application of control process to an electric drive system. In this example, the power electronics module (controller, power inverter, etc.) controls the stator current (and other parameters) by proper regulation to produce the reference torque. Given the appropriate command signals, the inverter (three-leg inverter for three-phase motor) turns on and off its power switches to provide a controlled alternating current (AC) supply from the DC source. The controller receives a temperature signal of power components. This information would be estimated by the ROM given the applied power dissipation computed by means of a power losses model. Then, in accordance with a derating curve scheme (Fig. 1.6), the controller calculates a derated value for the current amplitude just before the current regulation step in the feedback loop. The majority of heat is produced by power devices of the controller and inverter. This power inverter is sensitive to the temperature, especially the three IGBTs, temperature changes will affect the device turn-on and turn-off process, affecting further the controller performance. Therefore, a proper thermal design should also contain a cooling system design in order to absorb heat from the power electronics and then dissipate it to the environment.

Derating process

Derating power electronics systems has been common practice for decades to improve device reliability and extend lifetime [12], [5]. Heat-generating components such as power transistors (MOS transistors, IGBTs, etc.), are key components in power modules as they are very sensitive to their operating temperature. These components need to be monitored through a thermal derating process. "Derating" is the controlled limitation of the power dissipated of the components in applications that have high operating temperature. This is achieved by limiting the current flow-

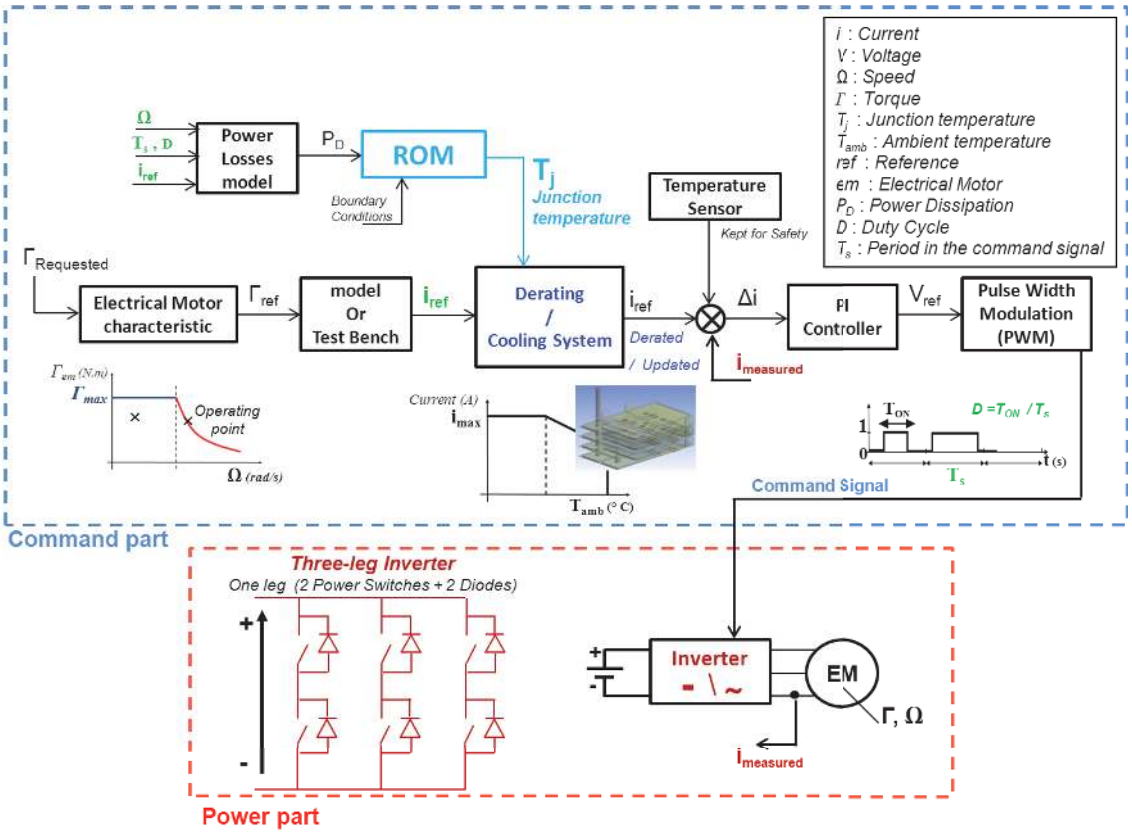

Figure 1.5. The positioning of the ROM in the the control process : Application to an Electric Drive System.

ing through these components, which in turn lower the components output electric power. Device manufacturers usually provide a "derating curve" associated to each type of component. Fig. 1.6 shows an example of a LED (Light-Emitting Diode) derating curve, where current is the derated parameter adjusted according to the ambient temperature. However, the accuracy of the derating curve is limited by that of the ambient temperature measurement.

Thermistors are the most common devices used for temperature measurement in an operating system. In the current state, NTC (Negative Temperature Coefficient) thermistors whose resistance goes up as the temperature goes down, are used. Thanks to their compact size, NTC thermistors can be integrated directly in close proximity to hot spots (the power components producing the most heat) on the PCB. It has been proven that NTC thermistors are highly reliable sensors of temperature measurement. This measurement, however, concerns the ambient temperature (surrounding) of the power components. In order to calculate how close to a maximum safe temperature the internal components may get, designers are conducted to consider an additional temperature margin. This margin is usually approximated based on thermal simulations or IR (Infrared) camera measurements. Hence, a high accu-

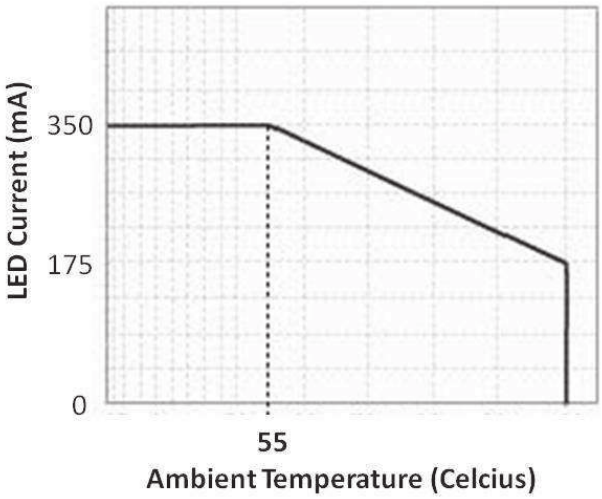

Figure 1.6. Temperature-current derating curve for LEDs [13].

racy can be achieved by measuring directly the junction temperature, which is not possible with thermistors. The purpose of this study is to replace the thermistors by a mathematical thermal model producing an estimation of the junction temperature of power components. However, thermistors will be still kept for safety reasons. For instance, thermistors can eliminate short circuits in the case of excessive continuous currents inside equipment [14].

Cooling strategies

The cooling system design of power electronics devices directly affect the system stability and reliability. Cooling technologies rely on three basic heat transfer mechanisms that often take place together : heat conduction, convection and radiation. The first two mechanisms are generally the most significant in power electronics devices in the automotive applications. In fact,the amount of power transferred is a function of the difference between the object and its surrounding's temperatures to the 4^{th} power (see Table 1.1). In automotive electronics systems, the "surroundings" is usually the ambient air in proximity to the component or PCB. In that respect, the role of radiation is further decreased when forced convection is used, since this will reduce the difference between the ambient and the object surface temperature. This situation contrasts for instance with lighting systems (Light-emitting diodes (LED) systems) where the radiation contribution may reach 27/% of the total heat transfer and may even be greater than that of the natural convection [15]. Other applications where radiation plays a dominant role include tablets and smart phones (over half of the heat transfer is due to radiation) [16], and the space applications, where radiation is the only relevant heat transfer mechanism. As far as the power electronics systems are concerned, we are going to briefly describe the conduction as well as convection, air cooled and water cooled systems [17].

Table 1.1
Comparison of the mathematical models for each transfer mode.

Conduction	Convection	Radiation
$Q = k\ S\ \vec{grad}(T) \cdot \vec{n}$	$Q = h\ S\ \ (T_S - T_f)$	$Q = S\ \epsilon\ \sigma\ (T_S - T_{Sur})^4$
S : Surface area of object $[m^2]$	S : Surface area of object being cooled $[m^2]$	S : Effective surface area of object $[m^2]$
k : Material thermal conductivity $[Wm^{-1}K^{-1}]$	h : Convective heat transfer coefficient $[Wm^{-2}K^{-1}]$	σ : Stefan-Boltzmann constant
$\vec{grad}(T)$: Temperature gradient $[Km^{-1}]$	$(T_S - T_f)$: Temperature difference between the object and the cooling fluid $[K]$	$(T_S - T_{Sur})$: Temperature difference between the object and surroundings $[K]$

Conduction cooling The rate of conductive heat flow depends on the temperature gradient and the thermal conductivity of the material as can be seen by the Fourier's law in Table 1.1. Conduction cooling is of major importance in electronics systems design. Even if a system is designed for convection cooling, conduction is still the dominant heat transfer mechanism within the components and circuit board. This is especially true for power electronics where power losses are concentrated on the power semiconductors such as silicon die. Heat sinks are the most common means to achieve the thermal dissipation necessary to reduce the components internal temperature. In fact, the primary function of a heat sink is to allow for the spreading of heat from components with high power dissipation generally mounted to its surface, as can be shown in Fig. 1.7, so that that heat can be dissipated by the convective cooling mechanisms to the surrounding environment.

Convection cooling Convection is defined as the heat transfer from the surface of an object to a moving fluid. If the fluid flow is created by external source such as fans, it is referred to as forced convection. If the fluid flow is created by gravitational forces on the fluid as its density varies, then it is referred to as natural convection. As can be seen in Table 1.1), the heat flow equation, the Newton's law, is the same for both natural and forced convection heat transfer. The difference lays in the convective heat transfer coefficient, h, values range. For instance, the value of the convection coefficient for air will typically be in the range of 5 to 25 for natural convection and in the range of 10 to 500 for forced convection. A commonly used method of cooling power semiconductors is air-cooling, which includes natural air

cooling and forced air cooling, as shown in Fig. 1.7 with an application to a power electronics device intended to control a ventilation motor. The forced air convection is able to remove a greater amount of heat than by natural convection but requires more control systems, such as for fan operation. Noise can also be a concern. A more effective heat removal method is water-cooling at the expense of higher cost and more difficult integration. Coolant loops can be combined with the thermal control of the power modules. This type of cooling can be used for very high power components (Kilowatts range). An illustration of water-cooling of a high power inverter electronics for electric drive system is given in Fig. 1.8.

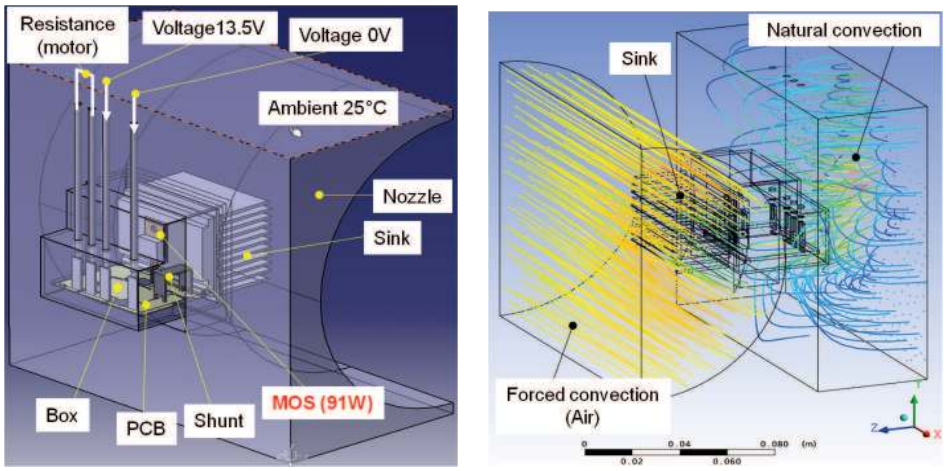

(a) MOS module attached to a forced air cooled heat sink.

(b) Air streamlines.

Figure 1.7. An illustration of air cooled MOS power module system for the control of a ventilation motor [18].

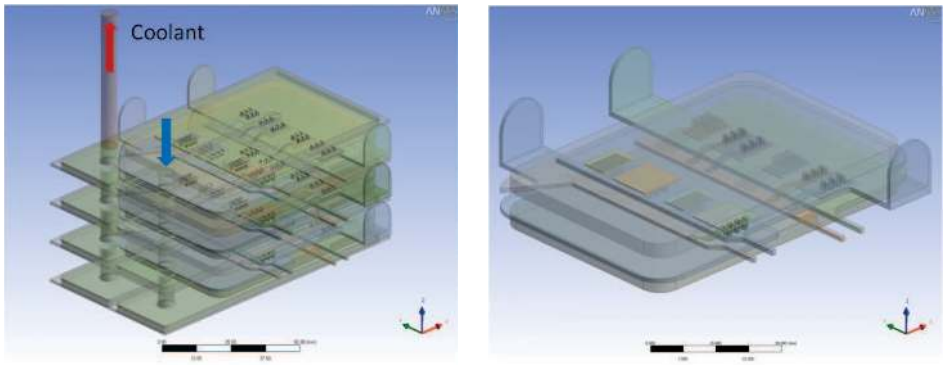

(a) Inverter model.

(b) Zoom on a power module.

Figure 1.8. Water cooled Inverter (composed of three power modules) [19].

1.2 Thermal Impedance Method

Traditionally, in order to estimate the junction temperature, designers use the thermal impedance specified in the datasheet for electronic components under standardized environment conditions [20], such as that specified by the JEDEC JESD51 standard [21], in order to estimate junction temperatures of their devices used in their systems. Unfortunately, standardized thermal impedance cannot accurately predict the thermal performance of a component in a user application, since it is not a characteristic of the component package by itself but also of many other characteristics such as the design and layout of the PCB (Printed Circuit Board) on which the components are mounted as well as other environmental factors. Consequently, it is appropriate to measure the thermal impedance from experimental measurement or a detailed 3D model simulation. The Thermal impedance method, also named the Zth method [22], [23], [24], is the current used method in Valeo [25] in order to predict the junction temperature based on the measured thermal impedance curves. In fact, the dynamic behaviour of a thermal system can be described either in the frequency domain by its transfer function or else by its impulse response, which is the derivative of the thermal impedance. The former process is referred to as the "compact model synthesis" [26] and enables the extraction of equivalent thermal RC-network models. The latter process is called the "direct approach" based on the convolution product [27], [28]. This technique is a practical tool for estimating directly the transient temperature response to any arbitrary power dissipation profiles by means of a convolution integral between input power and the time derivative of the thermal impedance in time domain.
The practical use of the thermal impedance (Zth) method in Valeo is explained in the publication [25]. More details are available in the internal Valeo report in [29]. The process consists of 3 steps:

- A measurement step to extract the thermal impedance Zth,
- An identification step to derive an equivalent RC network (compact thermal model) intended to be included into 0D electronic simulators such as Pspice,
- A validation step when the power profile (introduced below) is applied. This step can be performed by either (1) the convolution method acting directly on the extracted Zth (2) or a 0D electronic simulation including the identified RC network. The results, i.e. the temperatures evolution at observation points, are then compared to the reference solution issued from either a numerical simulation or IR camera measurements when the same power profile is applied.

Thereafter, after introducing the power profiles used in the 3D thermal simulations, we review the Zth measurement method as well as the principle of the two Zth method techniques, the compact model synthesis and the convolution-based direct

approaches. Then, we illustrate the Zth limitations on a fictitious test case representative of an industrial application.

1.2.1 The power profiles

The thermal management of power electronics systems is generally performed for few operating conditions. These latter are determined through the mission profile of the vehicle specified in the very start of the system design. A mission profile consists of a description of vehicle driving cycles. Fig. 1.9 depicts four typical ARTEMIS driving cycles (jam, urban, road and highway) developed by the European ARTEMIS project for an electrical vehicle. A *combined cycle* representative of the vehicle life is then computed (4 Jam + 3 Urban + 2 Road + 1 Highway). In Fig. 1.9, the combined cycle of 2 hours 30 minutes made of about 95,000 points. Starting from a mission profile, electronic designers can compute the power losses applied to the module components by means of *power losses model* as it was showed in Fig. 1.5. Like the vehicle mission, the computed power losses are long and complex transient signals. Although these latter can be handled in SPICE-like electronic simulators, it is impossible to process them in 3D thermal simulations which in turn involve several hundred of degrees of freedom. Thus, thermal designers are provided instead with averaged power losses generally taking the form of square signals. These signals, named the power profiles, are those used in the validation step in the Zth method. The idea is then to process in separate phases: (1) identify an equivalent RC networks of the 3D thermal model valid for the power profiles (2) then integrate that RC model into a 0D thermal-electrical model and (3) run the 0D model for the complex power losses signals to convert those latter into temperature profiles intended for reliability analysis.

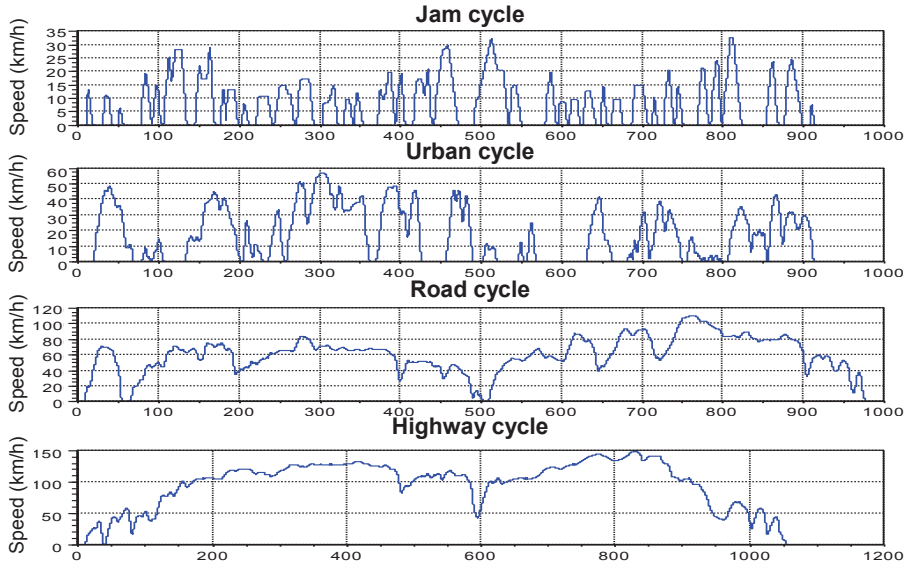

Figure 1.9. ARTEMIS electrical vehicle driving cycles.

1.2.2 Zth measurement

Since a well-established analogy exists between electrical and thermal, equivalent circuit models of thermal systems are a convenient method for thermal analysis [30], [31]. In thermal analysis, temperature and heat flux are analogous to voltage and current, respectively. Hence, equivalently to electrical resistance, defined by $R = \Delta V/I$, the thermal resistance, in steady-state, can be expressed with Eq. (1.4):

$$R^{th} = \frac{\Delta T_{j-ref}}{P} \tag{1.4}$$

where ΔT_{j-ref} is a temperature difference between the junction and a reference point and P the dissipated power. Heat is generated in the central junction position of the power device (the semiconductor die surface) and released to the surrounding environment through several thermal resistance paths. Steady-state junction temperature can be fully described through the thermal resistance parameter. However, in transient state, as far as linear thermal systems are concerned, the dynamic thermal behaviour is described based on the thermal impedance denoted by $Z^{th}(t)$. This latter represents the thermal step response, i.e. temperature response when a step signal is applied at different locations.

The thermal impedance response can be obtained, either from experimental measurements, or from physical simulation using 3D solvers based on finite element, finite differences or finite volumes. The thermal impedance based methods assumes that the systems are sufficiently linear under the operation conditions, allowing for the application of the superposition principle and the scaling of power dissipation. In practice, the thermal impedance measurement consists in applying *in turn* step power profiles to each dissipation source of the detailed model and in collecting the temperature responses performed up to the steady regime at all observation points. Those latter typically refer to junction temperatures and sensors at critical locations. For instance, the entry Z_{ij}^{th} in Eq. (1.5) correponds to the observed step response at point i when a step signal is applied at point j.

$$Z_{ij}^{th}(t) = \frac{T_i(t) - T_{ref}}{P_j} \tag{1.5}$$

In this relationship, $T_i(t)$ is the junction temperature at point i, T_{ref} the reference temperature (usually the ambient) and P_j the amplitude of the power dissipation step at point j. A schematic illustration of the Zth technique is given in Fig. 1.10. In this illustration, the time-functions $Z_{11}(t)$, $Z_{22}(t)$ and $Z_{33}(t)$ are called the driving point thermal impedances, or also the self impedances, for heating and measurement take place at the same location and constitutes the diagonal elements of the impedance matrix. The off-diagonal elements, however, are called the transfer thermal impedances and concern the case of different heating and measurement locations.

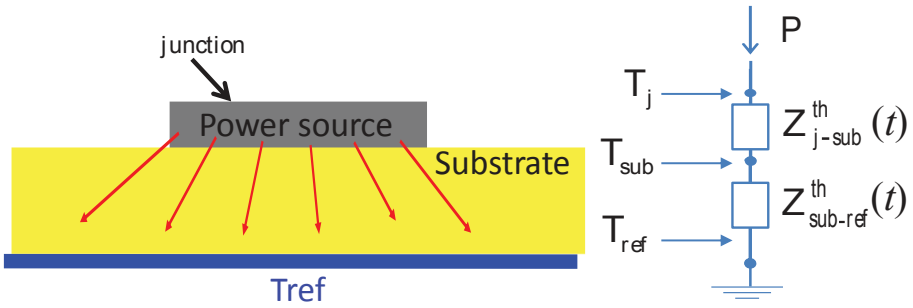

(a) Thermal impedance model for the exploration of the junction-to-ambient heat flow path.

$$Z^{th}_{j-sub}(t) = \begin{bmatrix} Z_{11}(t) & Z_{12}(t) & Z_{13}(t) \\ Z_{21}(t) & Z_{22}(t) & Z_{23}(t) \\ Z_{31}(t) & Z_{32}(t) & Z_{33}(t) \end{bmatrix}$$

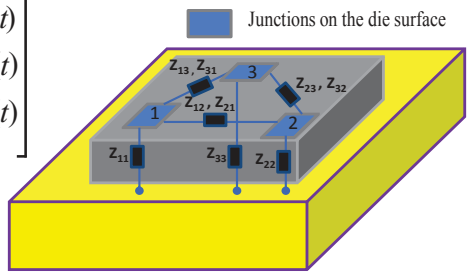

(b) Thermal impedance matrix; Z_{ii} are the self impedances and Z_{ij} the transfer impedances.

Figure 1.10. Schematic illustration of the Thermal impedance method on a Power component.

1.2.3 Compact model synthesis approach: equivalent RC networks

The thermal impedance in Laplace domain $Z^{th}(p)$ is represented by the so-called *time-constant representation* [23] given in Eq. (1.6):

$$Z^{th}(s) = \sum_{i=1}^{p} \frac{R_i}{1 + s\tau_i} \tag{1.6}$$

where s is the Laplace variable, τ_i the response time-constants and R_i the corresponding magnitudes. In the time domain, the corresponding temperature rise step response is given by a finite number of exponential terms (Eq. (1.7)):

$$Z^{th}(t) = \sum_{i=1}^{p} R_i \left(1 - \exp\left(-\frac{t}{\tau_i}\right)\right) \tag{1.7}$$

The unit step response (thermal impedance) represents the Foster-network model in Eq. (1.7). In this model, each time-constant τ_i equals the product of the thermal resistance R_i and thermal capacitance C_i. Hence, Doing so for each entry Z^{th}_{ij} (Eq. (1.5)), a reliable equivalent circuit structured as a low-pass network with n_{RC}

RC cells is obtained as shown in Fig. 1.11(a). It is necessary to retain a low number of RC cells to avoid unnecessary model complexity in electronic simulators. In-house experience proves that up to nine RC elements per Z_{ij}^{th} entry are sufficient for an acceptable approximation of a real measured thermal transient curve. The equivalent Foster-network is used for the thermal system characterization. However, it has not a physical interpretation, a Foster-to-Cauer network transformation is then used to calculate the physical heat capacitances of the heat flow structure [22]. The Cauer equivalent of the Foster network is depicted in Fig. 1.11(b).

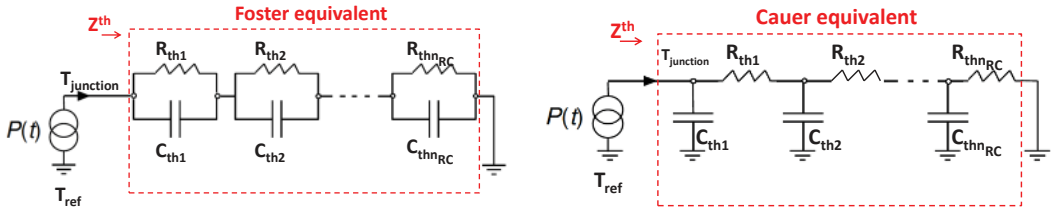

(a) Foster Rc-network. (b) Cauer Rc-network.

Figure 1.11. (a) Foster and (b) Cauer RC-networks representations of thermal impedance with applied power source $P(t)$.

To extract equivalent RC-networks model, various approaches have been developed. Szekely [22] first proposed the Network Identification by Deconvolution (NID) method. This technique differentiates the thermal impedance response in the logarithm of the time, applies a deconvolution method in order to obtain the signal containing the time-constant spectrum information density and then computes a Foster-to-Cauer transformation [32]. Since then, extended approaches of NID method has been proposed, such as the Thermal Resistance Analysis by Induced Transient (TRAIT) method in [33] and the Multi-Exponential Transient Spectroscopy (METS) method in [24] and so on.
Another well-known method enabling the extraction of compact thermal model is the "Thermal Impedance method". This method enables the extraction of compact thermal models as well, by directly fitting the step response, i.e. the thermal impedance, with RC-elements in series according to the equation (1.7) [26], [28] (Foster-network model). This technique has been introduced since 2010 by Dubus *et al.* [25] and is named the "Zth method". It is mainly used in order to cast a compact thermal model as an equivalent RC-networks that electronic designers can employ on their own in circuit simulators [25].

1.2.4 Direct approach : convolution product

As far as linear thermal systems are concerned (or sufficiently linear under operating conditions), the thermal impedance response $Z^{th}(t)$ matrix serves to compute the temperature $T(t)$ (Eq. (1.8)) at observation points for any input profile $P(t)$ by the

convolution product of $P(t)$ with the time derivative of $Z^{th}(t)$ denoted $\frac{dZ_th}{dt}$, which corresponds to the thermal impulse response of the system.

$$T\left(t\right) \; - \; T_{ref} \;\; = \;\; \frac{dZ_th}{dt} \otimes P\left(t\right) \tag{1.8}$$

or equivalently,

$$T\left(t\right) \; - \; T_{ref} \;\; = \;\; \int_0^t \frac{dZ_th}{dt}\left(t-s\right) P(s) \; \mathrm{ds} \tag{1.9}$$

The direct approach has been also implemented and is illustrated in a Valeo internal report [34]. Using the convolution theorem, the convolution operation is carried out by transforming the arbitrary input signal to the frequency domain and multiplying it with the system transfer function (Fourier transform of the impulse response). The inverse Fourier transform of this product is the output temperature response of the arbitrary input signal. A cubic spline interpolation [35] as proposed in [36] enables an accurate fitting of the Zth curves at the sample points of the arbitrary input time vector (often much larger than those of the thermal impedance data),as well as the derivative of the interpolated $Z^{th}(t)$ [34].

1.2.5 Thermal impedance method limitations

The Zth method in Valeo proved to be quite useful in the presence of non-linear conduction and radiation when carefully used, at least in automotive applications (approximately 10% of the global heat transfer modes). For instance, any non-zero level of power dissipation could be theoretically be used during the reference model simulations. Actually, these levels must be close to the ones involved by the real product, allowing for the problem linearization around the targeted operating condition. However, despite these precautions, Valeo experience revealed that this method may lead to significant errors, in particular for systems cooled by natural convection.

Given the Zth principle, this method necessitates as much simulations as the number of the dissipating power sources. This leads to a large number of simulations that may be prohibitively computationally expensive especially when dealing with a high-number of power sources. For instance, the simulation of a non-linear multiphysics hardware, involving non-linear conduction and natural convection, composed of 62 power sources with a Finite Volume model of size 10 million cells (about 50 millions of unknowns) lasts 15 hours, which lead to 62 simulations (about 5.5 weeks).

Moreover, the Zth method is theoretically strictly limited to linear systems, even if it can be extended to non-linear applications, typically when temperature dependence of material properties and the radiation effects are involved, when carefully used with regard to the operating conditions [24]. However, when natural convection is involved, the method may produce significant error levels. This fact has been revealed through the same aforementioned industrial example of 62 dissipating power

sources involving internal and external natural convection. The simulations have shown significant error in steady-state leading to an overestimation of junction temperature by 30% [37]. This status has led to set up a fictitious test case (Fig. 1.12) to investigate the reasons of the discrepancy in steady state regime. The model consists of 25 power components mounted onto a Printed Circuit Board (PCB) all encapsulated into an enclosure. Internal and external convection take place with the ambient air at 25 °C.

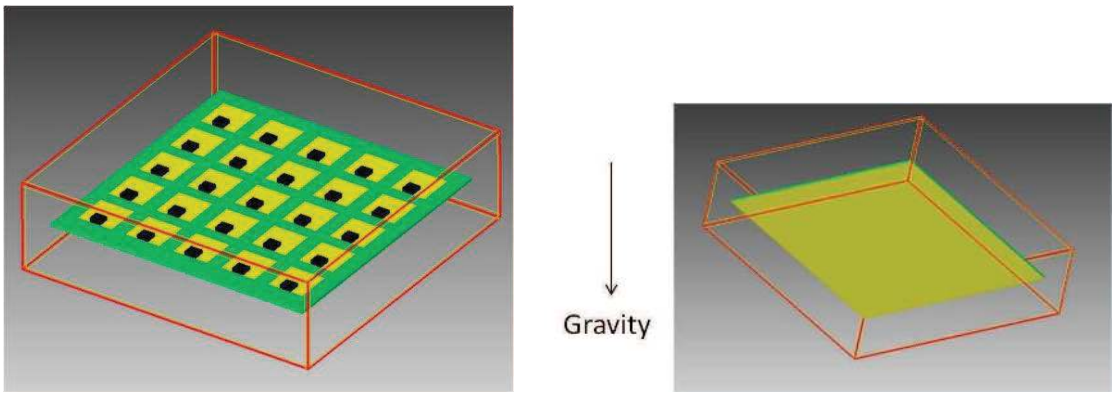

(a) Top view. (b) Bottom view.

Figure 1.12. Test case for illustration of the Thermal impedance method limitations.

In order to extract the R_{th} matrix, 25 simulations are performed where components are powered. After that the temperatures values are collected at 25 observation points placed in the upper center of the components. Then, for comparison purposes, the components are powered simultaneously. The applied power is put into a vector P whose multiplication by the R^{th} matrix produces the junction temperatures. Three scenario are tested:

- Test 1 : internal and external natural convection separated by the enclosure encapsulating the PCB and components as illustrated in Fig. 1.12. The power per component is 1 W,

- Test 2 : The enclosure is removed, but the board is still cooled by natural convection and the power per component is 1 W,

- Test 3 : The enclosure is removed and the board is cooled by forced convection. The power per component is 1 W.

In Fig. 1.13, we compare the temperature responses at observation points identified by the Rth model and those of the Finite Volume reference model. One can see that,

for tests 1 and 2 that involve natural convection, the relative error is very significant, with an overestimation in the range [34 %, 36 %] and [22 %, 24 %], respectively. However, in forced convection in test 3, the error is comprised between 0 % and 0.4 %. Thus, as opposed to the natural convection case, the role of non-linearities is less significant in both conduction and forced convection. The particularly discrepancy in the natural convection case can be also be explained by the differences between the flow patterns as illustrated by Figs. 1.14 and 1.15. Based on the same scale, we can notice the strong differences between the flow patterns of the reference and the Rth identified models.

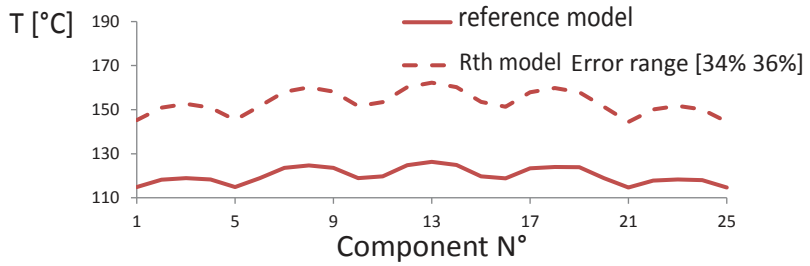

(a) Test 1: Natural convection with enclosure.

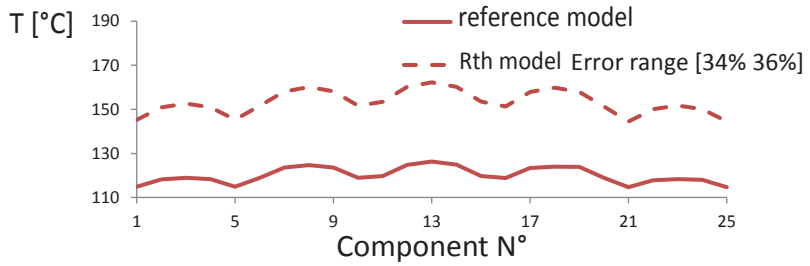

(b) Test 2 : Natural convection without enclosure.

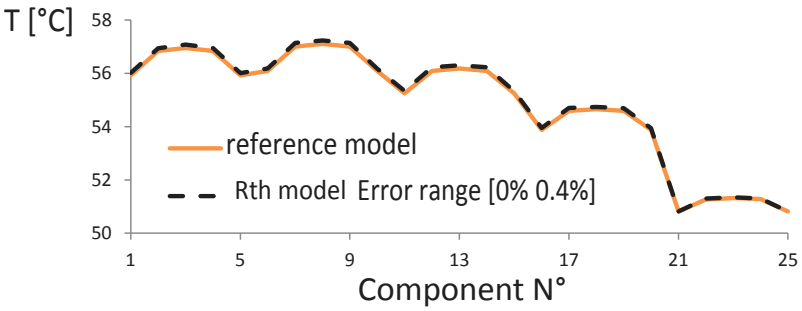

(c) Test 3 : Forced convection without enclosure.

Figure 1.13. Steady-state temperature responses of the model components. Comparison between the reference and Rth models results involving natural convection.

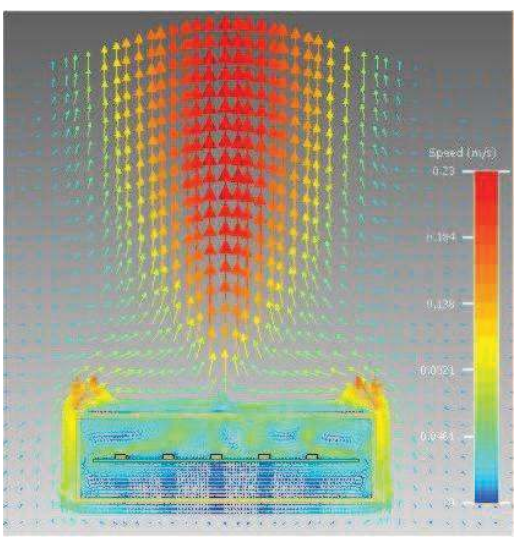

(a) Reference model when all components are powered with 1 W.

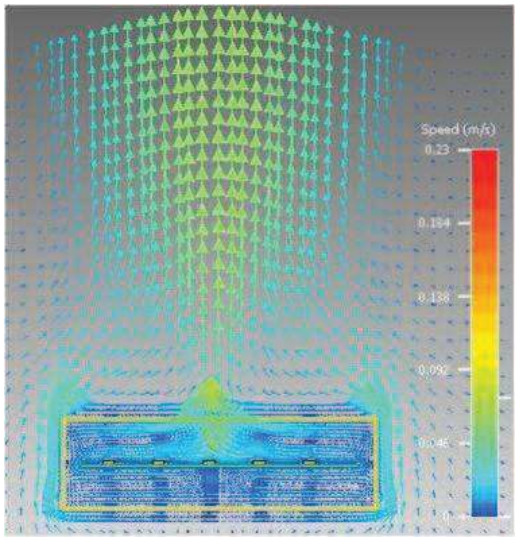

(b) Rth model when one component is powered with 1 W.

Figure 1.14. Flow patterns of Test 1 (Natural convection with enclosure). Comparison between the reference (a) and Rth (b) models results.

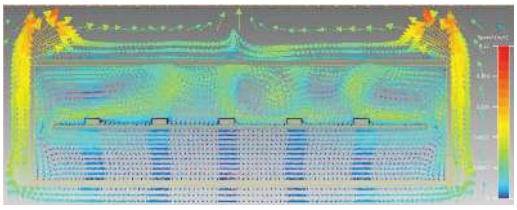

(a) Reference model when all components are powered with 1 W.

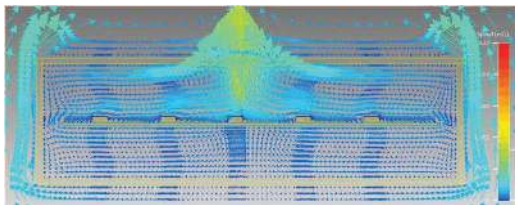

(b) Rth model when one component is powered with 1 W.

Figure 1.15. Zoom on flow patterns of Test 1 (Natural convection with enclosure) inside the enclosure. Comparison between the reference (a) and the Rth (b) models results.

1.3 Conclusion

In this section, we showed that the thermal design is one of the major keys to successful power electronics systems. The primary factor in the thermal management is the junction temperature of power components. These latter can be controlled by adopting derating process in command laws and by reducing their heat rise by means of cooling mechanisms. We also presented the Thermal Impedance method, denoted the Zth method, constituting the current used method in Valeo to estimate

the junction temperature based on either 3D model numerical simulations or Infrared Camera measurements. The investigation of an industrial use case revealed its practical difficulties and limitations typically in natural convection. Being based on the superposition principle, it is also difficult to extend the Zth method for the processing of non-linear models. All these limitations call for an alternative reduction method of non-linear problems with a broader scope regarding the processing of non-linear phenomena related above all to the natural convection. Prior to that, we will review the theoretical derivation of the discrete reference model of a thermally coupled fluid solid problem.

References

[1] J.M. Morelle. IML Mechatronic packaging technology, an innovative solution for automotive power electronics, Valeo presentation of the EC project HOPE. In ECPE Workshop, editor, *ECPE - HOPE Symposuim. Automotive power electronics - High density power electronics for hybrid traction, Germany*, 2008.

[2] P. Sardat. Power MOSFETs users guide. Technical report, VALEO: Group Electronic Expertise and Development Services, 2009.

[3] D. Newcombe D. Chamund. *IGBT module reliability*, 2010. DynexApplication Note.

[4] M. Held, P. Jacob, G. Nicoletti, P. Scacco, M.-H. Poech. Fast power cycling test for IGBT modules in traction application. In *The Proceeding of Power Electronics and Drive Systems*, 1997.

[5] P. D. T. O'Connor and A. Kleyner. *Practical reliability engineering - fifth edition.* John Wiley & Sons, Ltd, 2012.

[6] M. White, M. Cooper, Y. Chen and J. Bernstein. Impact of junction temperature on microelectronic device reliability and considerations for space applications. In *IEEE International Integrated reliability Workshop, CA, USA*, pages 133–136, 2003.

[7] A. Vassighi, M. Sachdev. Thermal runaway in integrated circuits. In *The Proceeding of Device and Materials Reliability (IEEE Transactions)*, volume 6, pages 300–305, 2006.

[8] Power module reliability - Mitsubishi electric. `http://www.mitsubishielectric.com/semiconductors/products/pdf/reliability/0512_e.pdf`.

[9] *Military Handbook, reliability prediction of electronic equipment.* the United States Department of Defense, 1990.

[10] *Recueil de Données de Fiabilité - Modèle universel pour le calcul de la fiabilite prévisionnelle des composants, cartes et équipements électroniques - RDF 2000 (UTEC 80810).* Association Française de Normalisation (AFNOR), 2005.

[11] *Reliability methodology for Electronic Defense Systems - FIDES Guide (UTEC 80811).* Association Française de Normalisation AFNOR), 2009.

[12] *Military standard. NASA standard Electrical, Electronic and Electromechanical (EEE) parts list.* National aeronautics and space administration. Washington, D.C. 20546, 1994.

[13] S. Roberts. Thermal derating of LEDs. http://docs-europe.origin.electrocomponents.com/webdocs/0e28/0900766b80e289cf.pdf, 2009. Recom Technical Support.

[14] NTC and PTC thermistors - reliable limiting of current surges. TDK EPCOS http://www.epcos.com/epcos-en/374108/tech-library/articles/products---technologies/products---technologies/reliable-limiting-of-current-surges/172842, 2012.

[15] S-H. Yu, D. Jang and K-S. Lee. Effect of radiation in a radial heat sink under natural convection. *International Journal of Heat and Mass Transfer*, 55:505–509, 2012.

[16] G.R. Wagner. A study of the maximum theoretical power dissipation of tablets under natural convection conditions. In *The Proceeding of the 20th international workshop on Thermal Investigations of ICs and Systems (THERMINIC)*, pages 1–5, 2014.

[17] S. S. Kang. Advanced cooling for power electronics. In *The proceeding of the 7th international conference on Integrated Power Electronics Systems (CIPS 2012), Nuremberg, Germany*, pages 1–8, 2012.

[18] J-L. Blanchard. Simulation électrique et thermohydraulique de systèmes mécatroniques en éléments finis. Seminaire NAFEMS France: Les defis de la Simulation Multiphysique: http://www.nafems.org/events/nafems/2008/multiphysics_paris/, 2008.

[19] J-L. Blanchard. CEE project reporting & visual management: FE-multiphysics Simulation use cases. 2009.

[20] A. Poppe. Thermal measurements and modelling - the transient and multichip issues. http://cmp.imag.fr/conferences/therminic/therminic05/APoppe_Tutorial.pdf, 2005. 11th THERMINIC workshop, Belgirate, Italy.

[21] *JEDEC Standard. Guidelines for Reporting and Using Electronic Package Thermal Information. JESD51-12.* JEDEC Solid State Technology Association 2005. Arlington, VA 22201-3834, 1999.

[22] V. Szekely and T. Van Bien. Fine structure of heat flow path in semiconductor devices: a measurement and identification method. *Solid-Slate Electronics*, 31:1363–1368, 1988.

[23] V. Szekely. On the representation of infinite length distributed RC one-ports. *IEEE Transactions on Circuits and Systems*, 38:711–719, 1991.

[24] M. Carmona, S. Marco, J. Palacn, and J. Samitier. A time-domain method for the analysis of thermal impedance response preserving the convolution form. *IEEE Transactions on components and packaging technology*, 22(2):238–244, 1999.

[25] P. Dubus, R. Leon, D. Le Guyader and L. Caves. Thermal pre-dimensioning methodology based on thermal impedance. In *The Proceedings of the 6th International Conference on Integrated Power Electronics Systems (CIPS 2010), Nuremberg, Germany*, pages 1–6, 2010.

[26] J.W. Sofia. Analysis of thermal transient data with synthesized dynamic models for semiconductor devices. *IEEE Components, Packaging, and Manufacturing Technology Society*, 18:39–47, 1995.

[27] F. Christiaens and E. Beyne. Transient thermal modeling and characterization of a hybrid component. In *The Proceeding of the 46th Electronic Components and Technology Conference, Orlando, FL*, pages 154–164, 1996.

[28] Y.C. Gerstenmaier and G. Wachutka. Calculation of the temperature development in electronic systems by convolution integrals. In *The Proceeding of the 16th Semiconductor Thermal Measurement and Management Symposium (SEMITHERM 2000) , San Jose, CA*, pages 50–59, 2000.

[29] P. Dubus and L. Caves. OD electro thermal models methodology. Technical report, VALEO: Group Electronic Expertise and Development Services, 2010.

[30] M. März, P. Nance. Thermal modeling of power-electronic systems. `http://peufeu.free.fr/audio/articles/Thermal%20modeling%20of%20power%20systems.pdf`. Accessed: 2014-08-29.

[31] F. N. Masana. A new approach to the dynamic thermal modelling of semiconductor packages. *Microelectronics Reliability*, 41(6):901–912, 2001.

[32] L. Weinberg. *Network analysis and synthesis.* McGraw-Hill, New-York, 1962.

[33] P.E. Bagnoli, C. Casarosa, M. Ciampi and E. Dallago. Thermal Resistance Analysis by Induced Transient (TRAIT) method for power electronic devices thermal characterizationpart I: Fundamentals and Theory. *IEEE Transactions on Power Electronics*, 13:1208–1219, 1998.

[34] J.-L. Blanchard. Technological development plan: model order reduction - bibliographic study. Technical report, VALEO: Group Electronic Expertise and Development Services, 2011.

[35] W.H. Press, S.A. Teukolsky, W.T. Vetterling, and B.P. Flannery. *Numerical recipes in C: The art of scientific computing, 2nd ed., Cambridge.* Cambridge University Press, 1992.

[36] D. Schweitzer. Thermal transient multisource simulation using cubic spline interpolation of Zth functions. In *The Proceedings of the 13th International Workshop on Thermal Investigations of ICs and Systems (THERMINIC 2006), Nice, Cte dAzur, France*, pages 123–127, 2006.

[37] R. Leon. Debrifing vd46. Technical report, VALEO: Group Electronic Expertise and Development Services, 2012.

Chapter 2

Theory : thermally coupled fluid-solid problem

Choice of the reduced model form plays a prominent role in the success of the identification process. For this purpose, it is essential to first understand the physics of the investigated problem. In this chapter, we present the mathematical background of a thermally coupled fluid-solid problem that will be used to derive a discrete reference model. The derivation of the discrete model in the fluid and solid domains is performed separately, starting each time from their corresponding governing equations. Then, coupling mechanisms are considered based either on a "weak" or "strong" coupling. Both types of coupling will be described.

Contents

2.1 Reference problem and notations

Let us consider Ω_f and Ω_s the spatial bounded domains in $\mathbb{R}^d$ $(d = 2 \text{ or } 3)$ for fluid and solid domains, respectively. The subscripts $._f$ and $._s$ stand for the fluid and the solid quantities. Let Γ_s^i denotes the solid interface on which the heat flux q_{imp} is imposed and Γ^w the fluid-solid interface and $\vec{n}$ its normal unit vector. The vector $\vec{n}$, chosen exterior to the solid domain Ω_s. Let $\vec{f}$ be the body forces per unit mass acting on the fluid (Fig. 2.1). The unknown variables in that problem are the solid temperature $T_s(\vec{x}, t)$. The unknown variables in the fluid problem are $(p, \vec{u}, T_f)$ for the pressure, velocity field and temperature, respectively.

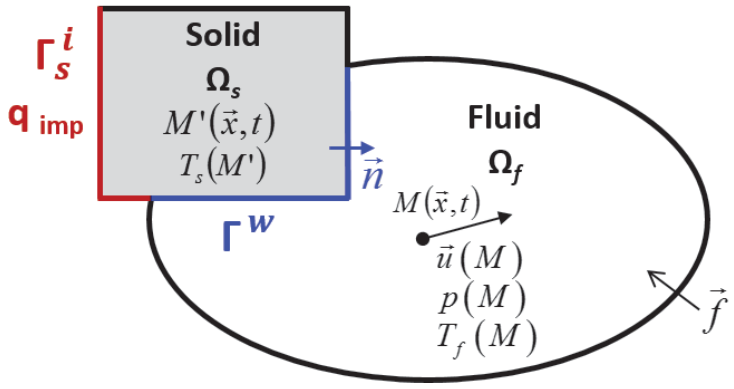

Figure 2.1. Schematic representation of the reference problem: a thermally coupled fluid-solid problem along the interface Γ^w.

Function spaces Let $H^0(\Omega) = L^2(\Omega)$ the space of square integrable functions defined on a bounded domain Ω of $\mathbb{R}^d$ (Sobolev space of order 0). The scalar product of H^0 on Ω is denoted by $(.,.)$ or also $(.,.)_\Omega$ and the norm by $|\ |_0$ or also $|\ |_{\Omega,0}$:

$$(a,b) = \int_\Omega a(x).b(x)\ \mathrm{d}\Omega; \qquad |a|_{\Omega,0} = |a|_0 = (a,a)^{\frac{1}{2}}$$

Similarly, the scalar product of H^0 on a boundary of Ω, $\partial\Omega = \Gamma$, is denoted by $(.,.)_\Gamma$.

$$(a,b) = \int_\Gamma a(x).b(x)\ \mathrm{d}\Gamma$$

Let $H^1(\Omega)$ the Sobolev space of order 1 on Ω. The scalar product is defined in the same way as for H^0 on Ω and Γ. The associated norm is denoted $\|.\|_1$.

$$H^1(\Omega) \quad = \quad = \left\{ v \in L^2(\Omega),\ \partial_{x_i} v \in L^2(\Omega),\ 1 \leq i \leq d \right\}$$

Let $\mathcal{H} \subset H^1(\Omega_f)$ the function space for the fluid flow velocity such as (no-slip condition for viscous fluid in contact with immobile solid):

$$\mathcal{H} \quad = \quad \left\{ \vec{u} \in H^1(\Omega_f),\ \vec{u} = 0 \ \text{ on } \partial\Omega_f \right\} \tag{2.1}$$

Let $\mathcal{L} \subset H^0(\Omega_f)$ the function space for the fluid pressure, and $\mathcal{R} \subset H^1(\Omega)$ the function space for the temperature for both the solid and the fluid domains.

2.2 Finite element method

Although Finite volume methods are well established for fluid flow problems [1], [2], we choose herein the Finite Element Method (FEM) to discretize both the fluid and solid domains based on the Galerkin approach. The spatial discretization using the finite element method (FEM) is realized by dividing the spatial domain into non-overlapping elements. The distribution of these elements in domain is called a mesh. We consider a tetrahedral mesh (triangular in 2D domain) of both the spatial fluid and solid domains. Thereafter, an approximation field can be constructed by means of interpolation between the discrete solutions at the mesh nodes using shape functions. These latter should have a prescribed behaviour per element, i.e. constant, linear or quadratic. In addition, the shape function associated with a node of an element should have the value of 1 on that node and 0 on the other nodes. The resolution of the governing equations of the fluid problem using FEM, in particular, restricts the number of applicable elements, especially for the pressure-velocity variables [3]. A general accepted rule is that the order of approximation of the pressure must be lower than that of the velocity. For example, if the velocity is approximated by a quadratic element, then the pressure is approximated by a linear or a constant element. The list of admissible elements for incompressible and weakly compressible fluid flows is given in [4].

Shape functions of the fluid domain

Consider for example the mesh $\mathbb{T}_h$ of a 2D fluid domain depicted in Fig. 2.2, based upon triangular elements with l points at the centroid of each element for the pressure, N vertices for the temperature, and N vertices together with m_t midpoints of the edges for the velocity. Each triangular element contains seven nodal points, one center node, three vertices and three edge midpoints. The pressure variable is determined by its values on the l center nodes of the mesh. Let $\mathcal{L}_h$ denote a subspace of dimension l of $\mathcal{L}$ and $\{\psi_1(\vec{x}), \cdots, \psi_l(\vec{x})\}$ its basis functions, where

$\psi_j(\vec{x}), j = 1, \ldots, l$ is the shape function in $\mathcal{L}_h$ (2.3). For temperature and velocity, we consider higher order shape functions. We choose linear shape functions $\{\chi_1(\vec{x}), \cdots, \chi_N(\vec{x})\}$ for the temperature in the subspace $\mathcal{R}_h \subset \mathcal{R}$ (2.5). The velocity variable is approximated by quadratic shape functions in the subspace $\mathcal{H}_h \subset \mathcal{H}$. Let $m = N + m_t$ denotes the number of vertices and edges in the mesh. We define then the shape functions $\{\varphi_{11}(\vec{x}), \cdots, \varphi_{m1}(\vec{x})\}$, $\{\varphi_{12}(\vec{x}), \cdots, \varphi_{m2}(\vec{x})\}$, and $\{\varphi_{13}(\vec{x}), \cdots, \varphi_{m3}(\vec{x})\}$ for the velocity components u_1, u_2 and u_3, respectively (2.4). We may combine the velocity shape functions into a vector form by:

$$\vec{\varphi}_{j1}(\vec{x}) = \begin{pmatrix} \varphi_j(\vec{x}) \\ 0 \\ 0 \end{pmatrix}, \vec{\varphi}_{j2}(\vec{x}) = \begin{pmatrix} 0 \\ \varphi_j(\vec{x}) \\ 0 \end{pmatrix}, \vec{\varphi}_{j3}(\vec{x}) = \begin{pmatrix} 0 \\ 0 \\ \varphi_j(\vec{x}) \end{pmatrix} \tag{2.2}$$

The approximations of the pressure, velocity and temperature variables, $\left(p^h, \vec{u}^h, T_f^h\right) \in (\mathcal{L}_h, \mathcal{H}_h, \mathcal{R}_h)$, are defined as follows:

$$p(\vec{x}, t) \approx p^h(\vec{x}, t) = \sum_{j=1}^{l} \psi_j(\vec{x}) p_j(t) \tag{2.3}$$

$$\begin{aligned} \vec{u}(\vec{x}, t) \approx \vec{u}^h(\vec{x}, t) &= \sum_{j=1}^{m} \vec{\varphi}_{j1}(\vec{x}) u_{1j}(t) + \vec{\varphi}_{j2}(\vec{x}) u_{2j}(t) + \vec{\varphi}_{j3}(\vec{x}) u_{3j}(t) \\ &= \sum_{j=1}^{M} \varphi_j(\vec{x}) u_j(t) \end{aligned} \tag{2.4}$$

$$T_f(\vec{x}, t) \approx T_f^h(\vec{x}, t) = \sum_{j=1}^{N} \chi_j(\vec{x}) T_{f_j}(t) \tag{2.5}$$

In the equation (2.4), u_j is defined by $u_j(t) = u_{1j}(t)$, $u_{j+m}(t) = u_{2j}(t)$, $u_{j+2m}(t) = u_{3j}(t)$, $(j = 1 \ldots m)$ and $\varphi_j(\vec{x})$ in the same way. In what follows, we assume $M = 3m$ the number of degrees of freedom of the velocity field. The number M is equal to $2m$ in the case of 2D problem for example. The subscript $_j$ stands for the jth node in the fluid domain mesh. The variables $u_j(t)$, $p_j(t)$ and $T_{f_j}(t)$ are the velocity, pressure and fluid temperature unknowns at the jth node.

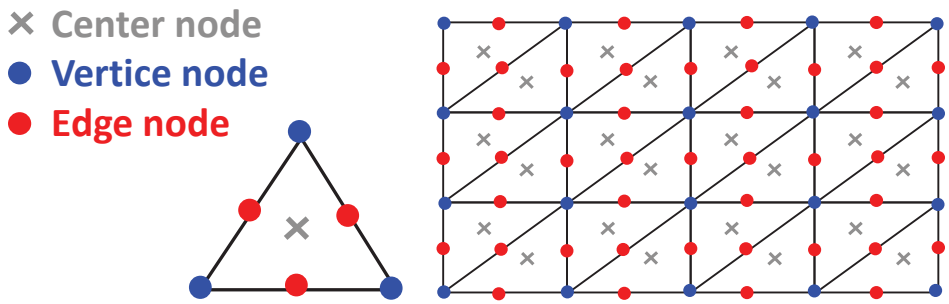

(a) Triangular element. (b) All elements in domain Ω_f, $l = 24$, $N = 20$, $m_t = 43$.

Figure 2.2. Example of triangular mesh of a 2D fluid domain.

Shape functions in the solid domain

For simplicity, the shape functions for the solid temperature are taken the same as in the fluid in the subspace $\mathcal{R}_h$ as follows:

$$T_s(\vec{x},t) \approx T_s^h(\vec{x},t) = \sum_{j=1}^{N} \chi_j(\vec{x}) T_{s_j}(t) \tag{2.6}$$

where $T_{s_j}(t)$ is the solid temperature variable at the jth node of the solid domain mesh.
In what follows, for the ease of presentation, the time variable t is omitted in u_j, p_j, T_{f_j}, T_{s_j}. We do so for the space variable $\vec{x}$ in ψ_j, φ_j and χ_j.

2.3 Fluid domain

2.3.1 Governing equations

The general system of Navier-Stokes for Newtonian compressible fluids is given by the system (2.7). This system includes the continuity, the momentum and the energy equations. The derivation of these equations can be found in [5]:

$$\begin{cases} \dfrac{\partial \rho_f}{\partial t} + \nabla.\ (\rho_f\ \vec{u}) = 0 & \text{(2.7a)} \\ \dfrac{\partial\ (\rho_f\ \vec{u})}{\partial t} + (\rho_f \vec{u}.\ \nabla)\,\vec{u} + \nabla p - \mu\ \Delta\vec{u} - \left(\zeta + \dfrac{\mu}{3}\right)\nabla\left(\nabla.\,(\vec{u})\right) = \rho_f \vec{f} & \text{(2.7b)} \\ \dfrac{\partial\left(\rho_f c_{p_f} T_f\right)}{\partial t} + \vec{u}.\nabla\left(\rho_f\ c_{p_f} T_f\right) - div\left(k\nabla T_f\right) = 0 & \text{(2.7c)} \end{cases}$$

In the system (2.7), ρ_f stands for the fluid density, $\frac{\partial}{\partial t}$ the partial derivative in time, μ the fluid dynamic viscosity, ζ the bulk viscosity, $\vec{f}$ the vector of body forces per

unit mass acting on the fluid (such as the gravitational acceleration vector $\vec{g}$ when the fluid weight is the only body force), c_{p_f} the fluid specific heat and k the fluid conductivity. The variables $\vec{u} = \vec{u}(\vec{x},t)$, $p = p(\vec{x},t)$, and $T_f = T_f(\vec{x},t)$ are the velocity, the pressure and the temperature of the fluid flow at time t and position $\vec{x} \in \Omega_f$, respectively. In the momentum equation (2.7b), the term $\mu\,\Delta\vec{u}$ is the viscous dissipation. The non-linearity of the momentum equation is due to the convective acceleration term, $(\rho_f \vec{u}.\,\nabla)\,\vec{u}$. The energy equation (2.7) is coupled to the fluid flow equations (2.7a), (2.7b) through the convective part $\vec{u}.\nabla\left(\rho_f\ c_{p_f} T_f\right)$.
In forced convection, there are two basic assumptions. First, the viscous dissipation, $\mu\ \Delta\vec{u}$, is neglected due to small changes of velocities in the flow. Second, the changes of fluid properties (density, viscosity, specific heat and conductivity, etc.) are neglected. These assumptions are valid when the changes of velocities are low compared to heat transfer [6], and when temperature rises are still small. As a result of these assumptions, the energy equation (2.7) reduces to convection-conduction equation that can be solved separately from the fluid flow part (2.7a), (2.7b). In addition, the term $\vec{u}.\nabla\left(\rho_f\ c_{p_f} T_f\right)$ is no longer non-linear since there are no longer velocity variable to solve but instead will be imported from the fluid solver.
In natural convection, however, fluid flow and heat transfer are coupled through the Boussinesq approximation [7], [8]. This approximation assumes that the fluctuations in density are related to gravity and result principally from thermal effects. This means that the density variations are neglected in continuity and energy equations except when they are related to the gravitational term ($\vec{f} = \vec{g}$ in (2.7b). The state equation of Boussinesq approximation is given by:

$$\rho_f(T) \;=\; \rho_0\left[1 - \beta\,(T - T_0)\right] \tag{2.8}$$

where ρ_0 denotes the density at a reference temperature T_0, and β the thermal expansion coefficient.
Combining equations (2.8) and (2.7b) yields the following system [7]:

$$\begin{cases} \nabla.\,(\vec{u}) = 0 & \text{(2.9a)} \\ \rho_0 \dfrac{\partial\,(\vec{u})}{\partial t} + \rho_0\,(\vec{u}.\nabla)\,\vec{u} + \nabla p - \mu\Delta\vec{u} = -\ \rho_0\beta\,(T_f - T_0)\,\vec{g} & \text{(2.9b)} \\ \rho_0 c_{p_f} \dfrac{\partial\,(T_f)}{\partial t} + \rho_0 c_{p_f}\ \vec{u}.\nabla T_f - \lambda\Delta T_f = 0 & \text{(2.9c)} \end{cases}$$

The system (2.9) constitutes the Navier-Stokes equations for a "weakly" compressible fluid in natural convection problem. Since the temperature is present in the momentum equation (2.9b), and the non-linear convective term in the energy equation (2.9), the fluid flow and heat transfer equations are solved in a coupled manner, by contrast to the forced convection problem.
Thereafter, the Navier-Stokes equations in (2.9) will be discretized in space using the FEM based on Galerkin approach [4].

2.3.2 Variational formulation

In order to derive the variational formulation, we multiply the continuity equation (2.9a) by a pressure test function p^*, the momentum equation (2.9b) by a velocity test function $\vec{u}^*$, and the energy equation (2.9) by a temperature test function T_f^*, and then we integrate over the domain Ω_f:

$$\left\{\begin{array}{l} \int_{\Omega_f} p^*\ \nabla.\left(\vec{u}\right)\ \mathrm{d}\Omega = 0 \\ \int_{\Omega_f} \left(\rho_0 \frac{\partial \vec{u}}{\partial t} + \rho_0 \left(\vec{u}.\nabla\right)\vec{u} + \nabla p - \mu\Delta\vec{u}\right).\vec{u}^*\ \mathrm{d}\Omega = \int_{\Omega_f} \left(-\ \rho_0\beta\left(T_f - T_0\right)\vec{g}\right).\vec{u}^*\ \mathrm{d}\Omega \\ \int_{\Omega_f} \left(\rho_0 c_{p_f} \frac{\partial T_f}{\partial t} + \rho_0 c_{p_f}\ \vec{u}.\nabla T_f - k_f \Delta T_f\right) T_f^*\ \mathrm{d}\Omega = 0 \end{array}\right. \tag{2.10}$$

Since the pressure is intended to be approximated over space of order 0, and the velocity and the temperature fields over space of order 1 (see § 2.1), then the terms ∇p, $\Delta\vec{u}$ and ΔT_f in the system (2.10) have to be transformed with the help of integration by parts (Green's and divergence formula) (Eqs. (2.11) and (2.12)).

$$\begin{aligned} &\int_{\Omega_f} \left(-\mu\Delta\vec{u} + \nabla p\right)\vec{u}^*\ \mathrm{d}\Omega \\ &= \mu \int_{\Omega_f} \nabla\vec{u}.\nabla\vec{u}^*\ \mathrm{d}\Omega - \mu \int_{\partial\Omega_f} \vec{n}.\left(\nabla\vec{u}.\vec{u}^*\right)\ \mathrm{d}\Gamma + \int_{\Omega_f} \left(\nabla.\left(p\ \vec{u}^*\right) - p\ \nabla.\left(\vec{u}^*\right)\right)\ \mathrm{d}\Omega \\ &= \mu \int_{\Omega_f} \nabla\vec{u}.\nabla\vec{u}^*\ \mathrm{d}\Omega - \mu \int_{\partial\Omega_f} \vec{n}.\left(\nabla\vec{u}.\vec{u}^*\right)\ \mathrm{d}\Gamma + \int_{\partial\Omega_f} \vec{n}.\left(p\ \vec{u}^*\right)\ \mathrm{d}\Gamma - \int_{\Omega_f} p\ \nabla.\left(\vec{u}^*\right)\ \mathrm{d}\Omega \\ &= \mu \int_{\Omega_f} \nabla\vec{u}.\nabla\vec{u}^*\ \mathrm{d}\Omega - \int_{\Omega_f} p\ \nabla.\left(\vec{u}^*\right)\ \mathrm{d}\Omega - \int_{\partial\Omega_f} \vec{n}.\left(\mu\nabla\vec{u} - p\ I\right).\vec{u}^*\ \mathrm{d}\Gamma \\ &= \mu \int_{\Omega_f} \nabla\vec{u}.\nabla\vec{u}^*\ \mathrm{d}\Omega - \int_{\Omega_f} p\ \nabla.\left(\vec{u}^*\right)\ \mathrm{d}\Omega - \int_{\partial\Omega_f} \vec{n}.\underline{\underline{\sigma}}.\vec{u}^*\ \mathrm{d}\Gamma \end{aligned}$$

$$\int_{\Omega_f} \left(-\mu\Delta\vec{u} + \nabla p\right)\vec{u}^*\ \mathrm{d}\Omega = \mu \int_{\Omega_f} \nabla\vec{u}.\nabla\vec{u}^*\ \mathrm{d}\Omega - \int_{\Omega_f} p\ \nabla.\left(\vec{u}^*\right)\ \mathrm{d}\Omega - \int_{\partial\Omega_f} \vec{n}.\underline{\underline{\sigma}}.\vec{u}^*\ \mathrm{d}\Gamma \tag{2.11}$$

where $\underline{\underline{\sigma}}$ is the Cauchy stress tensor. By taking $\vec{u}^*$ to be zero on the boundary $\partial\Omega_f$ (as assumed in (2.1), we deduce that:

$$\int_{\partial\Omega_f} \vec{n}.\underline{\underline{\sigma}}.\vec{u}^*\ \mathrm{d}\Gamma = 0\ \ \forall\vec{u}^* \in \mathcal{H}$$

We have also:

$$\begin{aligned}\int_{\Omega_f} -k\Delta T_f T_f^* \, \mathrm{d}\Omega &= k\int_{\Omega_f} \nabla T_f.\nabla T_f^* \, \mathrm{d}\Omega - \int_{\partial\Omega_f} k\vec{n}.\left(\nabla T_f.T_f^*\right) \, \mathrm{d}\Gamma \\ &= k\int_{\Omega_f} \nabla T_f.\nabla T_f^* \, \mathrm{d}\Omega + \int_{\partial\Omega_f} \left(-k\frac{\partial T_f}{\partial n}\right) T_f^* \, \mathrm{d}\Gamma \\ &= k\int_{\Omega_f} \nabla T_f.\nabla T_f^* \, \mathrm{d}\Omega + \int_{\partial\Omega_f} q_n T_f^* \, \mathrm{d}\Gamma \end{aligned} \tag{2.12}$$

where $q_n = -k\frac{\partial T_f}{\partial n}$ is the heat flux applied on the domain boundary $\partial\Omega_f$. We consider herein only the heat flux exchanged along the fluid-solid interface Γ^w:

$$q_n = -k\frac{\partial T_f}{\partial n} = q_s^w \quad \text{on } \Gamma^w \tag{2.13}$$

The term q_s^w is the heat flux to the wall from the solid at the fluid-solid interface Γ^w. It depends on the fluid as well as the solid temperatures, T_s, a solution of the energy equation in the solid domain (2.31). It is q_s^w that ensures the thermal coupling between the fluid and the solid problems. The coupling scheme types will be presented in Section 2.5.
Using the expressions (2.11) and (2.12) in the system (2.10), we deduce the variational problem of the system (2.9) as follows:

$$\left\{\begin{array}{ll} \text{Find } X = \{p, \vec{u}, T_f\} \in \mathcal{L}\times\mathcal{H}\times\mathcal{R} \text{ such that:} & \\ & \\ \int_{\Omega_f} p^*\nabla.\left(\vec{u}\right) \, \mathrm{d}\Omega = 0 & ; p^* \in \mathcal{L} \\ \rho_0\int_{\Omega_f} \frac{\partial\vec{u}}{\partial t}.\vec{u}^* \, \mathrm{d}\Omega + \rho_0\int_{\Omega_f}\left(\vec{u}.\,\nabla\right)\vec{u}.\vec{u}^* \, \mathrm{d}\Omega + \mu\int_{\Omega_f}\nabla\vec{u}.\nabla\vec{u}^* \, \mathrm{d}\Omega & \\ -\int_{\Omega_f} p\nabla.\left(\vec{u}^*\right) \, \mathrm{d}\Omega = -\rho_0\int_{\Omega_f}\beta\left(T_f - T_0\right)\vec{g}.\vec{u}^* \, \mathrm{d}\Omega & ; \vec{u}^* \in \mathcal{H} \\ \rho_0 c_{p_f}\int_{\Omega_f}\frac{\partial T_f}{\partial t}T_f^* \, \mathrm{d}\Omega + \rho_0 c_{p_f}\int_{\Omega_f}\vec{u}.\nabla T_f \;\; T_f^* \, \mathrm{d}\Omega + k_f\int_{\Omega_f}\nabla T_f.\nabla T_f^* \, \mathrm{d}\Omega & \\ = \int_{\Gamma^w} q_s^w T_f^* \, \mathrm{d}\Gamma & ; T_f^* \in \mathcal{R} \end{array}\right. \tag{2.14}$$

We define the following bilinear and trilinear forms:

$$a_u\left(\vec{u},\vec{u^*}\right)=\mu\int_{\Omega_f}\nabla\vec{u}.\nabla\vec{u^*}\ \mathrm{d}\Omega \qquad ;\vec{u},\vec{u^*}\in\mathcal{H} \tag{2.15}$$

$$a_T\left(T_f,T_f^*\right)=k\int_{\Omega_f}\nabla T_f.\nabla T_f^*\ \mathrm{d}\Omega \qquad ;T_f,T_f^*\in\mathcal{R} \tag{2.16}$$

$$a_0\left(p^*,\vec{u}\right)=\int_{\Omega_f}p^*\nabla.\left(\vec{u}\right)\ \mathrm{d}\Omega \quad ;\vec{u}\in\mathcal{H},p^*\in\mathcal{L} \tag{2.17}$$

$$b\left(T_f,\vec{u^*}\right)=-\rho_0\int_{\Omega_f}\beta\left(T_f-T_0\right)\vec{g}.\vec{u^*}\ \mathrm{d}\Omega \quad ;T_f\in R,\vec{u^*}\in\mathcal{H} \tag{2.18}$$

$$n_u\left(\vec{u},\vec{v},\vec{u^*}\right)=\rho_0\int_{\Omega_f}\left(\vec{u}.\nabla\right)\vec{v}.\vec{u^*}\ \mathrm{d}\Omega \qquad ;\vec{u},\vec{v},\vec{u^*}\in\mathcal{H} \tag{2.19}$$

$$n_T\left(\vec{u},T_f,T_f^*\right)=\rho_0 c_{p_f}\int_{\Omega_f}\vec{u}.\nabla T_f\ T_f^*\ \mathrm{d}\Omega \quad ;\vec{u},\ T_f,T_f^*\in\mathcal{H} \tag{2.20}$$

and

$$\left(q_s^w,T_f^*\right)_{\Gamma^w}=\int_{\Gamma^w}q_s^wT_f^*\ \mathrm{d}\Gamma \quad ;T_f^*\in\mathcal{R} \tag{2.21}$$

It follows from the system (2.14) and the equations (2.15) - (2.21) that the solution of the Navier-Stokes problem in the system (2.9) satisfies the following variational equations:

$$\left\{\begin{array}{l}\text{Find }\ (p,u,T_f)\in\mathcal{L}\times\mathcal{H}\times\mathcal{R}\text{ satisfying:}\\ \\ a_0\left(p^*,\vec{u}\right)=0 \qquad\qquad\qquad\qquad\qquad\qquad\qquad\qquad\qquad\qquad\qquad\qquad ;\ \ p^*\in\mathcal{L}\\ \left(\rho_0\partial_t\vec{u},\vec{u^*}\right)+a_u\left(\vec{u},\vec{u^*}\right)+n_u\left(\vec{u},\vec{u},\vec{u^*}\right)-a_0\left(p,\vec{u^*}\right)=b\left(T_f,\vec{u^*}\right) \ ;\ \ \vec{u^*}\in\mathcal{H}\\ \left(\rho_0c_{p_f}\partial_tT_f,T_f^*\right)+a_T\left(T_f,T_f^*\right)+n_T\left(\vec{u},T_f,T_f^*\right)=\left(q_s^w,T_f^*\right)_{\Gamma^w} \ ;\ \ T_f^*\in\mathcal{R}\end{array}\right. \tag{2.22}$$

where $\partial_t\vec{u}$ is the partial derivative with time.

2.3.3 Discrete detailed model

The problem is to determine the fluid variables, p, $\vec{u}=(u_1,u_2,u_3)$ and T_f of the system (2.9). To do that, we suppose that (2.22) hold for each $p^*\in\mathcal{L}_h$ for the pressure, $\vec{u^*}\in\mathcal{H}_h$ for the velocity, and $T^*\in\mathcal{R}_h$ for the temperature. Using the fact that these test functions are arbitrary, we choose them in the space spanned by the

shape functions, ψ_1 to ψ_m, φ_1 to φ_N, and χ_1 to χ_l, respectively.

$$\begin{cases} p^* = \psi_i;\ i = 1, \cdots, l & \text{(2.23a)} \\ \vec{u}^* \equiv \varphi_i;\ i = 1, \cdots, M & \text{(2.23b)} \\ T_f^* = \chi_i;\ i = 1, \cdots, N & \text{(2.23c)} \end{cases}$$

The substitution of (2.3) - (2.5) and (2.23a) - (2.23c) into the variational formulation (2.22) yields the so-called *Galerkin formulation*:

$$\begin{cases} \text{Find } \left(p^h, u^h, T_f^h\right) \in \mathcal{L}_h \times \mathcal{H}_h \ \times \mathcal{R}_h \text{ satisfying:} \\ \\ a_0\left(\psi_i, u^h\right) = 0 & ;\quad i = 1, \ldots, l \\ \left(\rho_0 \partial_t u^h, \varphi_i\right) + a_u\left(u^h, \varphi_i\right) + n_u\left(u^h, u^h, \varphi_i\right) - a_0\left(p^h, \varphi_i\right) = b\left(T_f^h, \varphi_i\right) & ;\quad i = 1, \ldots, M \\ \left(\rho_0 c_{p_f} \partial_t T_f^h, \chi_i\right) + a_T\left(T_f^h, \chi_i\right) + n_T\left(u^h, T_f^h, \chi_i\right) = \left(q_s^w, \chi_i\right)_{\Gamma^w} & ;\quad i = 1, \ldots, N \end{cases} \tag{2.24}$$

Using the equations (2.3) - 2.5 and given the linearity of the inner product, the derivative and the integral operators, we now rewrite (2.24) as:

$$\begin{cases} \sum_{j=1}^{M} u_j a_0\left(\psi_i, \varphi_j\right) = 0 & ; i = 1, \ldots, l \\ \sum_{j=1}^{M} \left(\dot{u}_j \left(\rho_0 \varphi_j, \varphi_i\right) + u_j \left(a_u\left(\varphi_j, \varphi_i\right) + n_u\left(\varphi_j, \sum_{k=1}^{M} u_k \varphi_k, \varphi_i\right)\right)\right) & \\ - \sum_{j=1}^{l} p_j a_0\left(\psi_j, \varphi_i\right) = \sum_{j=1}^{N} T_{f_j} b\left(\chi_j, \varphi_i\right) & ; i = 1, \ldots, M \\ \sum_{j=1}^{N} \dot{T}_{f_j}\left(\rho_0\, c_{p_f}\, \chi_j, \chi_i\right) + T_{f_j}\left(a_T\left(\chi_j, \chi_i\right) + n_T\left(\sum_{k=1}^{N} u_k \varphi_k, \chi_j, \chi_i\right)\right) & \\ = \left(q_s^w, \chi_i\right)_{\Gamma^w} & ; i = 1, \ldots, N \end{cases} \tag{2.25}$$

The formulation (2.25) can also be written as:

$$\begin{cases} \sum_{j=1}^{M} u_j \left(L_f\right)_{ij} = 0 & ; i = 1, \ldots, l \\ \sum_{j=1}^{M} \left(C_{fu}\right)_{ij} \dot{u}_j + \left(\left(K_{fu}\right)_{ij} + N_{fu}\left(\sum_{k=1}^{M} u_k \varphi_k\right)_{ij}\right) u_j & \\ - \sum_{j=1}^{l} \left(L_f\right)_{ji} p_j = \sum_{j=1}^{N} \left(B_f\right)_{ji} T_{f_j} & ; i = 1, \ldots, M \\ \sum_{j=1}^{N} \left(C_{fT}\right)_{ij} \dot{T}_{f_j} + \left(\left(K_{fT}\right)_{ij} + \left(N_{fT}\left(\sum_{k=1}^{M} u_k \varphi_k\right)\right)_{ij}\right) T_{f_j} & \\ = \left(Q_s\right)_i & ; i = 1, \ldots, N \end{cases} \tag{2.26}$$

with

$$\begin{cases} (L_f)_{ij} = a_0(\psi_i, \varphi_j) & ; i = 1 \dots l, j = 1 \dots M \\ (B_f)_{ij} = b(\chi_i, \varphi_j) & ; i = 1, \dots, N, j = 1, \dots, M \\ (C_{fu})_{ij} = (\rho_0 \varphi_j, \varphi_i) & ; i = 1, \dots, M, j = 1, \dots, M \\ (K_{fu})_{ij} = a_u(\varphi_j, \varphi_i), & ; i = 1, \dots, M, j = 1, \dots, M \\ (N_{fu}(u))_{ij} = n_u(\varphi_j, u, \varphi_i) & ; i = 1, \dots, M, j = 1, \dots, M \\ (C_{fT})_{ij} = \left(\rho_0 c_{p_f} \chi_j, \chi_i\right) & ; i = 1, \dots, N, j = 1, \dots, N \\ (K_{fT})_{ij} = a_T(\chi_j, \chi_i) & ; i = 1, \dots, N, j = 1, \dots, N \\ (N_{fT}(u))_{ij} = n_T(u, \chi_j, \chi_i) & ; i = 1, \dots, N, j = 1, \dots, N \end{cases} \tag{2.27}$$

and

$$(Q_s)_i = (q_s^w, \chi_i)_{\Gamma^w} \quad ; i = 1, \dots, N \tag{2.28}$$

The discrete formulation in (2.26) leads to a system of $l+M+N$ non-linear equations with $l + M + N$ unknowns forming the unknown nodal variables vector $[\mathbf{P}\ \mathbf{U}\ \mathbf{T_f}]^T$. We write the system (2.26) in matrix form as follows:

$$\begin{pmatrix} 0 & 0 & 0 \\ 0 & C_{fu} & 0 \\ 0 & 0 & C_{fT} \end{pmatrix} \begin{pmatrix} 0 \\ \dot{\mathbf{U}} \\ \dot{\mathbf{T}}_\mathbf{f} \end{pmatrix} + \begin{pmatrix} 0 & L_f & 0 \\ -{L_f}^T & K_{fu} + N_{fu}(U) & -{B_f}^T \\ 0 & 0 & K_{fT} + N_{fT}(U) \end{pmatrix} \begin{pmatrix} \mathbf{P} \\ \mathbf{U} \\ \mathbf{T_f} \end{pmatrix} = \begin{pmatrix} 0 \\ 0 \\ Q_s \end{pmatrix} \tag{2.29}$$

The problem (2.29) can be equivalently written as:

$$\begin{cases} L_f \mathbf{U} = 0 & \text{(2.30a)} \\ C_{fu}\dot{\mathbf{U}} + K_{fu}\mathbf{U} + N_{fu}(\mathbf{U})\mathbf{U} - {L_f}^T\mathbf{P} - {B_f}^T\mathbf{T_f} = 0 & \text{(2.30b)} \\ C_{fT}\dot{\mathbf{T}}_\mathbf{f} + K_{fT}\mathbf{T_f} + N_{fT}(\mathbf{U})\mathbf{T_f} = Q_s & \text{(2.30c)} \end{cases}$$

In the discrete system (2.30), (L_f, B_f, C_{fu}, K_{fu}, C_{fT}, K_{fT}) are the constant operators, and (N_{fu}, N_{fT}) the non-linear operators depending on the the velocity vector U. This problem is coupled to the solid problem through the rate of flux (power) vector Q_s (Section 2.5).

Solving scheme of the fluid discrete model

Several algorithms have been proposed to obtain a solution of the non-linear fluid problem (2.30). The most used numerical methods are iterative. The fluid flow and energy equations are commonly solved in a sequential manner. Indeed, the fluid flow equations (2.30a) - 2.30b are first solved to obtain the unknowns $\mathbf{U}$ and $\mathbf{P}$ [1]. Then, the discrete temperature equation can be solved according to the equation (2.30c) [1].

Examples of sequential procedures include the velocity-pressure methods based on the well-known SIMPLE algorithm proposed by Patankar and Spalding [9]. In SIMPLE algorithm, the coupled system formed of the discrete continuity and momentum equations (2.30a), (2.30b) are first solved, in which the computed velocity field is corrected using a pressure-correction equation derived from the continuity equation. Then, the iteration step is completed by solving the discrete energy equation (2.30c) for $\mathbf{T_f}$. Other improved SIMPLE algorithms have been proposed, such as the SIMPLER method (revised SIMPLE) introduced by Patankar [1], or also the SIMPLEC method proposed by Van Doormaal and Raithby [10], and many other pressure-based algorithms as stated in [11]. Alternative techniques, referred to as "Direct" methods, are to obtain a simultaneous solution of a linearized forms of the system equations (2.30a) - (2.30c) using an iterative algorithm such as the Newton-Raphson method. Such a simultaneous solution requires large computer time and storage and becomes very difficult to handle in large problems. This can be even more difficult for coupled fluid-solid problem as the vector Q_s depends on the solid temperature, an output of the thermal solid problem.

2.4 Solid domain

2.4.1 Governing equations and variational formulation

The thermal conduction inside the solid domain Ω_s is described by the following energy equation:

$$\rho_s c_{p_s} \frac{\partial T_s}{\partial t} - \nabla.(k_s \nabla T_s) = 0 \quad \in \Omega_s \times]0, t[\tag{2.31}$$

where T_s is the solid temperature, k_s the solid thermal conductivity, c_{p_s} the solid specific heat, and ρ_s the solid density. We assume that the material properties ρ_s, k_s, c_{p_s} are constants. The volumetric internal sources are neglected in (2.31). We recall that the solid temperature is defined in the space function $\mathcal{R} \subset H^1(\Omega_s)$ (Section 2.1) with:

$$H^1(\Omega_s) \quad = \quad = \left\{ v \in L^2(\Omega_s),\ \partial_{x_i} v \in L^2(\Omega_s),\ 1 \leq i \leq d \right\}$$

We multiply the energy equation in (2.31) by an arbitrary temperature test function, T_s^*, defined in $\mathcal{R}$:

$$\int_{\Omega_s} (\rho_s c_{p_s} \frac{\partial T_s}{\partial t} - k_s \Delta T_s)\, T_s^* \, \mathrm{d}\Omega \quad = \quad 0 \tag{2.32}$$

where $\Delta T_s = \nabla.(\nabla T_s)$.
Applying the integration by parts on the term $\int_{\Omega_s} k_s \Delta T_s \, T_s^* \, \mathrm{d}\Omega$ in the same way as in the fluid problem, the equation (2.32) can be equivalently stated as:

$$\int_{\Omega_s} \rho_s c_{p_s} \frac{\partial T_s}{\partial t} T_s^* \, \mathrm{d}\Omega + \int_{\Omega_s} k_s \, \nabla T_s . \nabla T_s^* \, d\Omega + \int_{\partial\Omega_s} q_n T_s^* \, \mathrm{d}\Gamma \;\; = \;\; 0 \tag{2.33}$$

The term q_n is given by:

$$q_n = -k_s \frac{\partial T_s}{\partial n} = \begin{cases} -q^{imp} & \text{on } \Gamma_s^i \\ q_f^w & \text{on } \Gamma^w \end{cases} \tag{2.34}$$

where q_f^w is the heat flux to the wall from fluid and q^{imp} the imposed heat flux on Γ_s^i. The variational problem of the energy equation (2.31) may be then written as follows:

$$\begin{cases} \text{Find } T_s \in \mathcal{R} \text{ such that:} \\ \\ \displaystyle\int_{\Omega_s} \rho_s c_{p_s} \frac{\partial T_s}{\partial t} T_s^* \, \mathrm{d}\Omega + \int_{\Omega_s} k_s \, \nabla T_s . \nabla T_s^* \, d\Omega = \int_{\Gamma^w} \left(-q_f^w\right) T_s^* \, \mathrm{d}\Gamma \\ \displaystyle + \int_{\Gamma_s^i} \left(q^{imp}\right) T_s^* \, \mathrm{d}\Gamma \qquad\qquad ; T_s^* \in \mathcal{R} \end{cases} \tag{2.35}$$

The formulation (2.35) can be defined based on the same notations used in the fluid domain:

$$\begin{cases} \text{Find } \; (p, u, T_f) \in \mathcal{L} \times \mathcal{H} \times \mathcal{R} \text{ satisfying:} \\ \\ \left(\rho_s c_{p_s} \partial_t T_s, T_s^*\right) + a_T \left(T_s, T_s^*\right) = \left(-q_f^w, T_s^*\right)_{\Gamma^w} + \left(q^{imp}, T_s^*\right)_{\Gamma_s^i} \quad ; \quad T_s^* \in \mathcal{R} \end{cases} \tag{2.36}$$

The forms a_T and $(\ ,\ )_{\Gamma^w}$ in the weak formulation (2.36) were defined in equations (2.16) and (2.21), respectively. The form $(\ ,\ )_{\Gamma_s^i}$ is defined in the same way as $(\ ,\ )_{\Gamma^w}$.

2.4.2 Discrete detailed model

In order to determine the discrete system of the energy equation (2.31), we proceed in the same way as in the fluid problem. The substitution of the the test function T_s^* by $\chi_{i, i=1,\cdots,N}$ and the solid temperature T_s by (2.6), results in the discrete equations written in matrix form as:

$$C_s \dot{\mathbf{T}}_\mathbf{s} + K_s \mathbf{T}_\mathbf{s} \;\; = \;\; Q \tag{2.37}$$

with

$$Q \;\; = \;\; Q_f + Q^{imp} \tag{2.38}$$

In the discrete system (2.37), C_s, K_s are the heat capacity and the conductivity matrices, $\mathbf{T_s}$ the nodal solid temperature vector, and $\dot{\mathbf{T}}_\mathbf{s}$ the time derivative of $\mathbf{T_s}$. The vector Q^{imp} is the external rate of flux applied on the solid and Q_f the rate of heat flux that ensures the coupling to the fluid problem (2.30). These operators are given by:

$$\left\{\begin{array}{lcll} (C_s)_{ij} & = & (\rho_s\, c_{p_s}\chi_j, \chi_i) & ; i = 1, \ldots, N, j = 1, \ldots, N \\ (K_s)_{ij} & = & a_T\,(\chi_j, \chi_i) & ; i = 1, \ldots, N, j = 1, \ldots, N \\ (Q^{imp})_i & = & (q^{imp}, \chi_i)_{\Gamma_s^i} & ; i = 1, \ldots, N \end{array}\right. \tag{2.39}$$

and

$$(Q_f)_i \;=\; \left(-q_f^w, \chi_i\right)_{\Gamma^w} \quad ; i = 1, \ldots, N \tag{2.40}$$

We note that matrices C_s and K_s are *symmetric* as they results from symmetric and bilinear forms, i.e. the scalar inner product and a_T in (2.39).

2.5 Coupling between fluid and solid model

The fluid and solid problems are coupled by the presence of heat exchange between both domains along the fluid-solid interface Γ^w. The heat exchange through the *fluid-to-solid* interface given in (2.34), is modelled using the following Newton's law:

$$q_f^w \;=\; h\,(T_s^w - T_f) \quad \text{on } \Gamma^w \tag{2.41}$$

The parameter h is the convective heat transfer coefficient. For the *solid-to-fluid* interface, the heat exchange given in (2.13) is written as:

$$q_s^w \;=\; h\left(T_f^w - T_s\right) \quad \text{on } \Gamma^w \tag{2.42}$$

In (2.41) and (2.42), T_s^w and T_f^w are the wall (interface) surface temperatures in the solid side and the fluid side, respectively. Besides the temperatures variables, the heat transfer coefficient is also essential to compute the coupled problem. In what follows, we will explain how the heat transfer coefficient is determined in both forced and natural convection.

2.5.1 Convective heat transfer coefficient

Determining the value of the heat transfer coefficient is the major part in thermal convection mechanism. The convective heat transfer coefficients are estimated using empirical correlations of dimensionless numbers. The heat transfer coefficient, h, is often calculated from the Nusselt number, N_u (a dimensionless number), according to the following equation:

$$Nu = \frac{hL}{k_f} \tag{2.43}$$

In (2.43), L is a characteristic length parameter of the fluid flow and k_f the thermal conductivity of the fluid.

- In forced convection, the Nusselt number is expressed as a function of the Reynolds number and the Prandtl number, $N_u = f\left(R_e, P_r\right)$. The correlations of these dimensionless numbers is available in various cases including typical geometries, different fluids, flow conditions (laminar/turbulent), etc. For example, the Nusselt number for a laminar flow over a flat plate is given by the following correlation [12]:

$$N_u \;=\; 0.332\; R_e^{\frac{1}{2}}\; P_r^{\frac{1}{3}} \quad P_r \leq 0.6 \tag{2.44}$$

- In natural convection, the Nusselt number is generally a function of the Prandtl number and the Grashof number (or sometimes the Rayleigh number such that $R_a = G_r\; P_r$), $N_u = f\left(G_r, P_r\right)$. Similarly, in a laminar flow over a flat plate the correlation expression of the Nusselt number is [12]:

$$N_u \;=\; \frac{0.508\; P_r^{\frac{1}{2}}\; G_r^{\frac{1}{4}}}{\left(0.952 + P_r\right)^{\frac{1}{4}}} \tag{2.45}$$

The dimensionless numbers expressions of R_e, P_r and G_r are still the same and are given in equations (2.46), (2.47), and (2.48), respectively.

$$R_e = \frac{|\text{inertia term}|}{|\text{viscous term}|} = \frac{|\rho_f\left(\vec{u}.\nabla\right)\vec{u}|}{|\mu\Delta\vec{u}|} = \frac{\rho_f V\; L}{\mu} \tag{2.46}$$

$$P_r = \frac{|\text{momentum diffusivity}|}{|\text{thermal diffusivity}|} = \frac{\nu}{\alpha} = \frac{\mu}{\rho_f}\frac{}{k}\rho_f c_{p_f} = \frac{\mu c_{p_f}}{k} \tag{2.47}$$

$$G_r = \frac{|\text{buoyancy force}|}{|\text{viscous force}|} = \frac{g\;\Delta\rho_f L^3}{\rho_f \nu^2} = \frac{{\rho_f}^2\; g\;\beta\left(T_w - T_f\right)L^3}{\mu^2} \tag{2.48}$$

where V is a characteristic velocity scale, g the acceleration due to gravity, β the thermal expansion coefficient of the fluid, and T_w the temperature at the fluid-interface temperature (the wall temperature) in the solid side.

- In **forced convection** (2.46) - (2.47), the heat transfer coefficient, h, depends only on the geometry, and the flow parameters and nature (laminar/turbulent regime, velocity profiles). As the changes of velocities are assumed low and those of fluid properties are neglected, h is constant in forced convection problem.

- In **natural convection** (2.48) - (2.47), h depends on the solid temperature that constitutes an output of the solid thermal problem. Therefore, h should be determined at each time iteration in the coupled fluid-solid problem.

2.5.2 Coupling scheme for coupled fluid-solid problem

The coupling between the solid and fluid domains can be either of "weak" or "strong" nature. Under weak coupling method, we proceed to the sequential analysis of each phenomena separately, coupled together by means of temperature and heat flux continuity along the fluid-solid interface. In strong coupling, however, we deal with the simultaneous solutions of all the system of equations in both fluid and solid domains.

Weak coupling

In weak coupling scheme, separate models for fluid and solid domains are considered. The coupling is achieved by applying the wall conditions on the fluid-solid interface as given in (2.49) and (2.50). These conditions include the continuity of temperature (2.49), and the heat flux (2.50), exchanged along the fluid-solid interface (wall) Γ^w.

$$T_f^w = T_s^w \quad \text{on } \Gamma^w \tag{2.49}$$

$$q_f^w = h\,(T_s^w - T_f) = -q_s^w \quad \text{on } \Gamma^w \tag{2.50}$$

Fig. 2.3 shows an illustration of the weak coupling scheme. In fact, prior to the calculation of h, the wall temperature in the solid side, T_s^w, has to be estimated by solving the heat conduction problem (2.31). T_s^w is then applied as boundary condition to the so-called computational fluid dynamics (CFD) solver. Then, the convection coefficient, h, can be calculated as explained in § 2.5.1. The fluid temperature, T_f, is obtained by solving the Navier-Stokes equations (2.9). The convective heat flux, q_s^w, can be then applied as a boundary condition to the solid domain on the fluid-solid interface Γ^w. Therefore, an updated solid temperature can be computed, so that an updated T_s^w. Iterations continue until the interface temperature and heat flux values from both solvers were close enough.

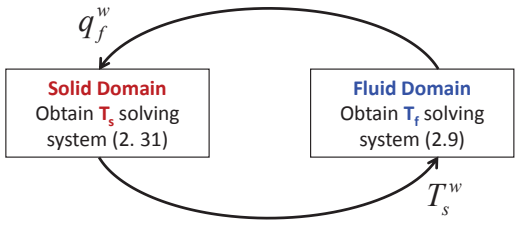

Figure 2.3. Schematic illustration of weak coupling process.

Strong coupling

The strong coupling scheme consists in calculating simultaneously the fluid and the solid temperatures according to the discretized systems (2.30) and (2.37), respec-

tively. To do that, it is necessary to discretize the terms Q_{s_i} (2.40) and Q_{f_i} (2.28) using the expressions (2.41) and (2.42), respectively [13]. Replacing the fluid and solid temperatures by their approximations in the equations (2.5) and (2.6), results in:

$$Q_{f_i} = \left(-q_f^w, \chi_i\right)_{\Gamma^w} = -h\left(\sum_{j=1}^{j=l}\chi_j T_{s_j}^w, \chi_i\right)_{\Gamma^w} + h\left(\sum_{j=1}^{j=l}\chi_j T_{f_j}, \chi_i\right)_{\Gamma^w} \quad ; i = 1, \ldots, N \tag{2.51}$$

$$Q_{s_i} = \left(q_s^w, \chi_i\right)_{\Gamma^w} = h\left(\sum_{j=1}^{j=l}\chi_j T_{f_j}^w, \chi_i\right)_{\Gamma^w} - h\left(\sum_{j=1}^{j=l}\chi_j T_{s_j}, \chi_i\right)_{\Gamma^w} \quad ; i = 1, \ldots, N \tag{2.52}$$

where $T_{s_j}^w$ and $T_{f_j}^w$ are the variables T_s and T_f at the jth fluid-solid interface node Γ^w, respectively. If they can be reached by means of the projection functions $\mathscr{P}_s\left(\vec{x}\right)$ and $\mathscr{P}_f\left(\vec{x}\right)$ [13], respectively:

$$T_{s_j}\mathscr{P}_s\left(\vec{x}\right) = T_{s_j}^w \tag{2.53}$$

$$T_{f_j}\mathscr{P}_f\left(\vec{x}\right) = T_{f_j}^w \tag{2.54}$$

Eqs. (2.56) and (2.56) take then the following forms:

$$Q_{f_i} = \underbrace{-\int_{\Gamma^w} h\sum_{j=1}^{j=N}\chi_i\chi_j\ \mathscr{P}_s\left(\vec{x}\right)}_{\left(K_{fs}\right)_{ij}}\ T_{s_j}\ \mathrm{d}\Gamma + \underbrace{\int_{\Gamma^w} h\sum_{j=1}^{j=N}\chi_i\chi_j}_{\left(K_{ff}\right)_{ij}}\ T_{f_j}\ \mathrm{d}\Gamma \quad ; i = 1, \ldots, N \tag{2.55}$$

and

$$Q_{s_i} = \underbrace{\int_{\Gamma^w} h\sum_{j=1}^{j=N}\chi_i\chi_j\ \mathscr{P}_f\left(\vec{x}\right)}_{\left(K_{sf}\right)_{ij}}\ T_{f_j}\ \mathrm{d}\Gamma - \underbrace{\int_{\Gamma^w} h\sum_{j=1}^{j=N}\chi_i\chi_j}_{(K_{ss})_{ij}}\ T_{s_j}\ \mathrm{d}\Gamma \quad ; i = 1, \ldots, N \tag{2.56}$$

Or equivalently, in the matrix form:

$$\begin{pmatrix} Q_f \\ Q_s \end{pmatrix} = \begin{pmatrix} K_{ff} & K_{fs} \\ K_{sf} & K_{ss} \end{pmatrix}\begin{pmatrix} T_f \\ T_s \end{pmatrix} \tag{2.57}$$

A fully coupled scheme of the fluid (2.30) and solid (2.37) problems seems to be difficult to handle especially when dealing with large models. In this solving scheme,

a solution of the fluid flow equations is generally obtained in a first place for the reasons explained in § (2.3.3). Then, the heat transfer problems in both fluid and solid domains, coupled together within the flux system (2.57), are solved simultaneously. The non-linear forms are linearized based on an iterative algorithm such as the Newton-Raphson method.

2.5.3 The FE solid model of linear and non-linear problems

If we substitute the vector Q_f into the discrete solid model (2.37), we obtain

$$C_s\dot{\mathbf{T}}_\mathbf{s} + K_s\mathbf{T}_\mathbf{s} - K_{fs}(h)\,\mathbf{T}_\mathbf{s} = Q^{imp} + K_{ff}(h)\,\mathbf{T}_\mathbf{f} \tag{2.58}$$

The system (2.58) involves the operators K_{ff}, K_{fs}, K_{sf} and K_{ss} that are dependent on the convective heat transfer coefficient h as shown through the equations (2.55) - (2.56). The heat flux vector Q^{imp} involves the heat flux densities $q^{imp} = q^{imp}(t)$ and is defined in (2.39).

- When **natural convection** is involved, **the coefficient h is, in turn, a function of $\mathbf{T_s}$ and $\mathbf{T_f}$** as it was stated in the Grashof expression (2.48), i.e. $h = h(T_s, T_f)$. Hence, the solid discrete model takes the following non-linear form:

$$C_s\dot{\mathbf{T}}_\mathbf{s} + K_{NL}(\mathbf{T_s}, \mathbf{T_f}) = Q^{imp} \tag{2.59}$$

  where $K_{NL}(\mathbf{T_s}, \mathbf{T_f}) = K_s\mathbf{T_s} - K_{fs}(h)\,\mathbf{T_s} - K_{ff}(\mathbf{T_s}, \mathbf{T_f})\,\mathbf{T_f}$ is a non-linear functions of $\mathbf{T_s}$ and $\mathbf{T_f}$.

- In the case of **forced convection**, however, the coefficient h is constant as aforementioned in the section 2.5.1, so that for the operators $K_{fs}(h) = K_{fs}$ and $K_{ff}(h) = K_{ff}$. The discrete solid model (2.58) can be then reduced to the following linear system:

$$C_s\dot{\mathbf{T}}_\mathbf{s} + K_{LIN}\mathbf{T_s} = Q^{imp} + K_{ff}\mathbf{T_f} \tag{2.60}$$

  with $K_{LIN} = K_s - K_{fs}$ is a constant conductivity matrix.

- In a pure heat **conduction problem**, the discrete model is written as:

$$C_s\dot{\mathbf{T}}_\mathbf{s} + K_s\mathbf{T_s} = Q^{imp} \tag{2.61}$$

In the above model, we should also introduce the boundary conditions of the solid problem in addition to the heat flux vector, Q^{imp}. For instance, if a convective boundary condition is imposed on an interface Γ_s^{conv} of the solid domain, then both the load vector (second member term in the FE model) and the conductivity matrix are affected and the FE model can be written as:

$$C_s\dot{\mathbf{T}}_\mathbf{s} + K_s^{cond}\ \mathbf{T}_\mathbf{s} + K_s^{conv}\ \mathbf{T}_\mathbf{s} \ = \ Q^{imp} + Q^{conv} \tag{2.62}$$

In the model (2.62), $K_s = K_s^{cond} + K_s^{conv}$, $K_s^{conv} = (K_s^{conv})_i = (h\chi_i, \chi_j)_{\Gamma_s^{conv}}$, and $Q^{conv} = (Q^{conv})_i = (hT_{amb}, \chi_i)_{\Gamma_s^{conv}}$, with $i, j = 1, \cdots, N$, T_{amb} the ambient temperature and h the imposed heat transfer coefficient. In the case of a Dirichlet boundary condition, a constant imposed temperature, the columns and rows belonging to the Dirichlet nodes (nodes on which the constant temperature is applied) are crossed out from the conductivity and capacity matrices. The FE model can be then generalized as follows:

$$C_s\dot{\mathbf{T}}_\mathbf{s} + K_s\mathbf{T}_\mathbf{s} \ = \ Q^{imp} + Q^{conv} + f^{Dirichlet} \tag{2.63}$$

The dimension of all vectors and matrices in (2.63) is equal to N reduced by the number of Dirichlet nodes, n_{BCs} (nodes on which the constant temperature is applied), $N = N - n_{BCs}$. We note that the aforementioned boundary conditions are introduced in the same way in the first two configurations of coupled problems.
The load vector, i.e. the second member in the FE model, can written in a separate form $E\ U(t)$ with $U(t)$ is the input signal and E a constant matrix that maps physical locations of the heat flux densities and boundary conditions to the FE nodes. The three configurations together within the corresponding FE model form are summarized in Table 2.1, in which we restitute the time variable of the time-dependent variables.

2.6 Conclusion

In this chapter, we derived a finite element model of a thermally coupled fluid-solid problem starting from the partial differential equations of both fluid and solid domains. We detailed different configurations including the forced and the natural convection, as well as a pure heat conduction problem. We also deduced the corresponding discrete reference models for each configuration. The obtained discrete models will play a key role in the choice of the reduced model form in the identification process of both linear and non-linear systems. Prior to that, we will develop the state of the art on the model order reduction methods. This is the focus of the next chapter.

Linear problem	Non-linear problem
$C_s\dot{\mathbf{T}}_\mathbf{s}(t) + K_{LIN}\mathbf{T}_\mathbf{s}(t) = FU(t)$	$C_s\dot{\mathbf{T}}_\mathbf{s}(t) + K_{NL}(\mathbf{T}_\mathbf{s}(t), \mathbf{T}_\mathbf{f}(t)) = E\,U(t)$
Conduction (2.61): $K_{LIN} = K_s$, $F = E$, $U(t) = \left[q^{imp}(t) \quad BCs\right]^T$	Natural convection (2.59): $K_{NL}(\mathbf{T}_\mathbf{s}(t), \mathbf{T}_\mathbf{f}(t))$ a quadratic function of $\mathbf{T}_\mathbf{s}(t)$ and $\mathbf{T}_\mathbf{f}(t)$
Forced convection (2.60): $K_{LIN} = K_s - K_{fs}$, $F = \begin{pmatrix} E & K_{ff} \end{pmatrix}$, $U(t) = \left[q^{imp}(t) \quad BCs \quad T_f(t)\right]^T$	$K_{NL}(\mathbf{T}_\mathbf{s}(t), \mathbf{T}_\mathbf{f}(t)) = K_s\mathbf{T}_\mathbf{s}(t) - K_{fs}(\mathbf{T}_\mathbf{s}(t), \mathbf{T}_\mathbf{f}(t))\,\mathbf{T}_\mathbf{s}(t) - K_{ff}(\mathbf{T}_\mathbf{s}(t), \mathbf{T}_\mathbf{f}(t))\,\mathbf{T}_\mathbf{f}(t)$, $U(t) = \left[q^{imp}(t) \quad BCs\right]^T$
with $U(t)$ the $(N_{ex} \times 1)$ input vector F the $(N \times N_{ex})$ input matrix associated to the heat flux densities and the Boundary Conditions (BCs) and eventually $\mathbf{T}_\mathbf{f}(t)$ in the forced convection configuration $\mathbf{T}_\mathbf{s}(t)$ the $(N \times 1)$ nodal solid temperature vector $\dot{\mathbf{T}}_\mathbf{s}(t)$ the time derivative of $\mathbf{T}_\mathbf{s}(t)$ $\mathbf{T}_\mathbf{f}(t)$ the $(N \times 1)$ nodal fluid temperature vector	

Table 2.1
Summary table of the detailed FE model for linear and non-linear thermal problems.

References

[1] S.V. Patankar. *Numerical heat transfer and fluid flow.* Hemisphere Publishing Corporation, 1980.

[2] H.K. Versteeg and W. Malalasekera. *An introduction to Computational Fluid Dynamics - The Finite Volume Method.* John Wiley & Sons Inc., New York, 1995.

[3] D. Bessems. Development of an extended quadratic tetrahedron for finite element analysis of Navier-Stokes problems. Master's thesis, Eindhoven University

of Technology - Departement of Mechanical Engineering, 2003.

[4] G. Dhatt, G. Touzot, E. Lefrançois. *Méthode des éléments finis*. Hermès - Lavoisier, 2005.

[5] C. Hirsch. *Numerical Computation of Internal and External Flows (Second Edition) - The Fundamentals of Computational Fluid Dynamics*. 2007.

[6] F.M. White. *Viscous fluid flow*. McGraw-Hill, New York, 1991.

[7] An introduction to natural convection flows. `www.turbulence-online.com`. Chalmers University of Technology, Gothenburg, Sweden.

[8] W.M. Kays and M.E. Crawford. *Convective heat and mass transfer*. McGraw-Hill, Highstown, NJ, 1993.

[9] S.V. Patankar and D.B. Splading. A calculation procedure for heat mass and momentum transfer in three dimensional parabolic flows. *International journal of Heat and Mass Transfer*, 15:1787, 1972.

[10] J.P. Doormaal, G.D. Raithby. Enhancements of the SIMPLE method for predicting incompressible fluid flows. *Numerical Heat Transfer*, 7:147–163, 1984.

[11] B. Yu and H. Ozoe. A modified pressure-correction scheme for the SIMPLER method, MSIMPLER. *Numerical Heat Transfer, Part B*, 39:435–449, 2001.

[12] C.P. Kothandaraman. *Fundamentals of heat and mass transfer*. New Age International, 2006.

[13] D.E. Hryb and M.B. Goldschmit. Thermal interaction model between a fluid flow and a solid. *Latin American applied research*, 39, 2009.

Chapter 3

Model Order Reduction and Identification methods

This chapter provides the state of the art regarding Model Order Reduction (MOR) methods. By analogy with the vocabulary used in stochastic analysis community, MOR methods can be divided into two main categories namely, intrusive and non-intrusive MOR methods. The second category is known also as system identification methods. In the first section, we review MOR methods of intrusive nature classified into projection-based and variable separation-based methods. Then, in the second section, we focus on system identification methods. For the needs of the identification process, we consider two model structures, the polynomial and the state space forms, to describe the relationship between the input data and output results of the system of interest. The latter form is the adopted for the aimed applications in this work. Three identification methods are introduced and divided into two classes according to the model structure used to describe the system: On the one hand, the Prediction Error method (PEM) for the identification of polynomial models; On the other hand, the Modal Identification Method (MIM) and the Subspace method for the identification of state space models.

Contents

3.1 Intrusive Model Order Reduction methods

The need for Model Order Reduction (MOR) is not new, as testified by the article published in 1965 by Guyan [1] dealing with a static condensation method enabling to process large models with the limited computer resources available at that time. Since then, the computational power has dramatically increased but the size of simulation models has grown correlatively to meet the requirements of the increasingly complex applications. Today, numerous publications deal with the MOR methods and interesting overviews can be found for instance in the book of Antoulas [2] or the PhD thesis of Dumon [3]. The basic idea of MOR methods consists of replacing the original high-order model with a much smaller one, named a Reduced Order Model (ROM), while keeping the essential dynamics of the original behaviour. The purpose behind MOR is to reduce the computational time and storage resources required by simulation and control models. Depending on their properties or implementation methodologies, several MOR methods have been developed during the last decade. Hereafter, we briefly introduce some of them and and for that purpose we group them in two classes:

- Projection-based methods requiring access to the detailed discretized model to project operators onto the subspace spanned by the set of reduced-order basis model,

- Variables-separation based methods allowing an *a priori* construction of a separated representation of the solution.

3.1.1 Projection-based methods

We recall the FE model of the linear thermal model of order N stated in Chapter 2 (see Table 2.1).

$$C_s \dot{\mathbf{T}}_{\mathbf{s}}(t) + K_{LIN} \mathbf{T}_{\mathbf{s}}(t) = FU(t) \tag{3.1}$$

Projection-based methods perform an approximation of the $(N \times 1)$ nodal vector $\mathbf{T}_{\mathbf{s}}(t)$ by means of a reduced basis transformation $V = \{v_1, v_2, \ldots, v_n\} \in \mathbb{R}^{N \times n}$, with $n \ll N$.

$$\mathbf{T}_{\mathbf{s}}(t) = \sum_{i=1}^{n} v_i T_{r_i}(t) = V T_r(t), \quad V \in \mathbb{R}^{N \times n}. \tag{3.2}$$

In (3.2), $T_r(t) = (T_{r_1}(t), T_{r_2}(t), \ldots, T_{r_n}(t))^T$ is the new reduced state vector of dimension $n \ll N$. This latter is composed of the generalized coordinates $T_{r_i}(t)$ in the reduced basis V. By substituting (3.2) into the linear FE model and left-multiplying both side of (3.1) by a projection matrix W^T, with $W \in \mathbb{R}^{n \times N}$, we have

$$C_r\dot{T}_r(t) + K_r T_r(t) = F_r U(t) \tag{3.3}$$

The model (3.3) constitutes the Reduced Order Model (ROM) of order n. The operators $C_r = W^T C_s V$, $K_r = W^T K_{LIN} V$ and $F_r = W^T F$ are the reduced capacity, conductivity and input matrices with appropriate dimensions. The performed projection is referred to as the Petrov-Galerkin projection. This latter also constrains the residual resulting from the transformation (3.2) to be orthogonal to W, i.e. $W^T r(t) = 0$. In particular, when $W = V$, the process is called a Galerkin projection [4]. Hereafter, we will be interested in this particular case. The form and computation of the projection basis V depend on the reduction method. Below, we provide the most important features of some of these projection-based techniques.

Substructuring methods

The substructuring methods principle consists of decomposing the FE model into smaller substructures called super-elements in finite elements and a reduced model is derived for each substructure. Substructuring is useful when dealing with large complex problems, in particular when the different substructures are characterized by different physical behaviours. This is justified through the research works of Nachtergaele *et al.* [5] for a thermo-mechanical problem, Kropp and Heiserer [6] for a vibro-acoustic problem, etc. Substructures are also attractive for reusability strategies in which the components models are stored in libraries. The first substructuring approach was proposed by Guyan [1] named the Guyan method or also static reduction. Although it was originally introduced for structural mechanics problems, Guyan method is also valid for thermal problems. This method, however, shows difficulties in dynamic analysis in both mechanical [7] and thermal [8] [9] problems. To overcome the limitation of the Guyan method, Craig and Bampton [10] proposed a dynamic reduction now named the Craig-Bampton method. This method was also originally developed in structural dynamics. Both Guyan and Craig-Bampton methods are are now part of most commercial Finite Element packages and continue to be used and enhanced in many recent research works as shown in [11], [12], [13] for structural dynamics applications as well as [14] for a heat conduction-convection thermal problem. Other substructuring techniques, analogous to the Craig-Bampton method, referred to as Modal Synthesis, have been developed in thermal problems of buildings; see the publication [15] and the references therein. These methods derive a thermal reduced modal model of a system from those of its components. The Modal analysis-based method are presented in the next paragraph. Prior to that, we briefly review the Guyan and Craig-Bampton methods.

Guyan method The principle consists of partitioning the degrees of freedom (DOF) of the FE model as master DOFs (also called interface DOFs) and slave DOFs (or also internal DOFs) to eliminate further these latter. This reduces the

FE model to the master DOFs only. The transformation matrix V_{Guyan}, usually called the static reduction basis, takes the form (details can be found in [1]):

$$V_{Guyan} = \begin{bmatrix} -K_{LIN_{ss}}^{-1} K_{LIN_{sm}} \\ I_{N_m} \end{bmatrix} \tag{3.4}$$

where the subscripts $_m$ and $_s$ correspond to the master and slave DOFs, respectively, I_{N_m} is the identity matrix of dimension N_m, the number of master DOFs, $K_{LIN_{ss}}$ is the conductivity matrix defined by the slave DOFs. As it can be noticed, the derivation of the matrix V_{Guyan} requires the inversion of the matrix $K_{LIN_{ss}}$. Consequently, the larger the number of slave DOFs is, the more the computational cost and complexity are. Another limitation is related to the fact that the larger the number of master DOFs is, the larger the order of the ROM is, which contradict the MOR interest.

Craig-Bampton methods Here, the reduced basis, denoted V_{CB}, combines the static modes, derived by Guyan, and the dynamic modes obtained by means of an eigenvalue problem when the master (interface) DOFs are fixed. These dynamic modes are composed of a selection of eigenmodes in a predefined frequency range and are gathered in a matrix Φ. The basis V_{CB} takes the form:

$$V_{CB} = \begin{bmatrix} \Phi & -K_{LIN_{ss}}^{-1} K_{LIN_{sm}} \\ 0 & I_{N_m} \end{bmatrix} \tag{3.5}$$

The limitations of the Craig-Bampton method are similar to those of the Guyan method apart from what is related to the static aspect.

Modal methods

The first step in a Modal approach is to compute the eigenvalue problem of the FE model (Table 2.1). To do this, let consider the model (3.1) without the right-hand term:

$$\dot{\mathbf{T}}_{\mathbf{s}}(t) = A_T \mathbf{T}_{\mathbf{s}}(t) + B_T U(t) \tag{3.6}$$

with $A_T = -C_s^{-1} K_{LIN}$. The reduced basis $V = W = V_{Modal}$ is obtained by means of an eigenvalue problem defined as follows:

$$(A_T - s_k \, \mathbf{I_n}) V_{Modal_k} = 0 \qquad k = 1, 2, \cdots, n \tag{3.7}$$

where s_k is the *kth* eigenvalue of matrix A_T and $V_{Modal_k} \in \mathbb{R}^{(N \times 1)}, k = \{1, 2, \cdots, n\}$ the associated eigenvector (mode), such that $V_{Modal}^T V_{Modal} = \mathbf{I_n}$ and $V_{Modal}^T A_T V_{Modal} = diag(s_1, s_2, \cdots, s_n)$. Eq. (3.7) is the *homogeneous equation* associated to (3.1) since the right-hand term is a null vector. Hence, the solution of (3.7) made of the modes s_k and eigenvectors V_{Modal_k} is determined independently of the excitation. The eigenvalues are related to the time constants of the thermal problem by $\tau_k = -\frac{1}{s_k}, k =$

$\{1, 2, \cdots, n\}$. The thermal problem is supposed to be stable with real and negative eigenvalues, if the matrices C_s and K_{LIN} are symmetric. The reduced modal basis $V_{Modal} \in \mathbb{R}^{(N \times n)}$ is obtained by selection or truncation of the total modes of the problem according to a given criterion. Different criteria exist in the literature such as the truncation methods [16], [17]. The simplest and used truncation method used in commercial software is the Marshall method [16]. This method uses a temporal criterion for which the n greatest time constants of the thermal problem are retained. This means that only the slow thermal dynamics is well described in the reduced model. This may lead to significant errors in the estimation of transient regime in a specific case where the rapid modes, considered negligible, are strongly excited. This is typically the case when the temperature observations are co-localised with the heat source input. It is then essential to keep a large number of modes, which does not allow a significant reduction of the FE model. Da Silva in his thesis [18] showed that even with a large number of modes, the Marshall method fails to capture the rapid dynamics and that its combination with an energy criterion slightly improves the result. Other evaluation methods have been investigated such as the aggregation [19] and the energy criterion-based methods [20]. An exhaustive list of these methods is available in Lefèbvre book [21]. All these methods, though, are not optimal regarding the order of the reduced model [21].

Residual-based correction methods

In order to overcome the projection errors in modal approaches, it is common to enrich the modal basis by residual vectors computed in an iterative way. This procedure is referred to as "correction methods". For instance, Da Silva [18] in his thesis performs a Singular Value Decomposition (SVD) to select the residual vectors intended to enrich the modal basis in a linear thermal problem. The correction methods have been applied to substructuring reduction methods as well. The reader should refer to thesis of Bobillot [22] and Renaud [23] for a detailed description of these methods.

Limitations of the enriched reduced basis in a non-linear problem The construction of the enriched reduced basis may be quite time-consuming in a highly non-linear problem as the projection reduced basis and operators have to be updated at every time step in order to generate a ROM.

POD method

The POD method, also known as Karhunen-Loève Decomposition [24], [25], Principal Component Analysis (PCA) [26] or Singular Value Decomposition (SVD), has been widely and successfully applied for the simulation [27], reduction [28], [29] and control [30] of large-scale and non-linear CFD applications. It has also gained status in thermal problems such as the recent publication on the thermal management in data centers [31], linear structural dynamics [32], etc. However, it is less robust in non-linear structural dynamics and should be used carefully [33], [32]. The POD has been also combined with other MOR technique to enhance the reduced model precision. For instance, Kumar *et al.* in [34] enrich the POD basis with Ritz static modes in a structural dynamics problem with local non-linearities [34].

The approach is an *a posteriori* reduction method for finding a projection reduced basis $V = W = V_{POD}$ based on offline simulations of the detailed model for a specific time domain or parameters variation. The results of these simulations are gathered into a matrix named the "snapshots" matrix. If $T(x_i, t_j)$ denotes the recorded temperature at the i^{th} DOF in the FE model and time t_j, with $i = 1, \ldots, N$ and $j = 1, \ldots, N_{snap}$, N_{snap} being the number of time snapshots, the snapshots matrix of size $N \times N_{snap}$ is:

$$\Theta = \begin{bmatrix} T(x_1,t_1) & T(x_1,t_2) & \ldots & T\left(x_1,t_{N_{snap}}\right) \\ T(x_2,t_1) & T(x_2,t_2) & \ldots & T\left(x_2,t_{N_{snap}}\right) \\ \vdots & \vdots & & \vdots \\ T(x_N,t_1) & T(x_N,t_2) & \ldots & T\left(x_N,t_{N_{snap}}\right) \end{bmatrix} \tag{3.8}$$

The POD basis can be constructed based on an eigenvalue decomposition of a covariance matrix $\Sigma = \frac{1}{N}\,\Theta\Theta^T \in \mathbb{R}^{N\times N}$. This, however, may be computationally expensive when dealing with a high-order FE detailed model. In this context and if $Nsnap \ll N$, the POD basis can be computed using the method of snapshots proposed by Sirovich [35] that involves an N_{snap}-dimensional eigenvalue problem instead. In the same context, the SVD method is another appropriate method, for which the reduced basis V_{POD} is composed of n column vectors corresponding to some greatest singular eigenvalues. We refer the reader to the publication of Podvin [36] for a full description of these approaches. It should be noted that the accuracy of the reduced model is significantly dependent on the choice of snapshots. This shortcoming is even more relevant in a parametric study. In fact, in order to derive a reduced model adapted to the representation of some parameters effects (load positions, material properties, boundary conditions), it is essential to compute a set of snapshots associated to the selected parameters. This may lead to a prohibitive computational time, especially in the case of complex and high-dimensional problems.

3.1.2 A priori variable separation-based methods

The reduction methods in this class do not require known projection matrices neither preliminary computations of detailed model to construct the reduced basis of the ROM, but instead use an iterative procedure to build the basis under the form of a separate representation. Two well-known approaches of this type are the A Priori Hyper-Reduction (APHR) method introduced by Ryckelynck [37], [38] to handle thermo-mechanical problems and the Proper Generalized Decomposition (PGD) method developed by the LMT Cachan and Centrale Nantes research teams. Below we will briefly review the PGD method.

PGD method

The PGD method [39], [40] is a recent MOR method introduced first by Ladevèze [41] in the context of the LATIN method (LArge Time INcrement method) in order to reduce computational cost, both in terms of simulation time and memory requirement, in a non-linear mechanical problem. Then, it was extended and used in several fields of applications such as fluids, rheology, thermo-viscoelastic coupled problems, multi-scale mechanical problems, multidimensional problems, etc. (see Dumon thesis [3] for a full overview of the method up to 2011). Recent applications have been addressed to computational surgery simulations [42], [43] and high-dimensional stochastic problems [44], etc. The PGD appeared as a generalization of the POD method. Like the POD, its principle is to find an approximation of the unknown field in the form of a separated representation, for which each variable function involves one of the problem coordinates (space, time and eventually parameters in order to derive a parametric model). In the POD, the decomposition is made in an already known basis extracted *a posteriori* from several computed snapshots of the detailed models. On the contrary, the PGD computes the reduced basis *a priori*, i.e. without the need to generate costly snapshots, and based instead on only the operator of the differential equation and the right hand side term. The reduced basis determination consists of a non-linear problem addressed by different iterative algorithms such a the fixed point and Newton methods. We should mention that this is performed in an offline phase.
If we consider a temperature field $T(x,t)$, the solution in the separate representation is expressed as a finite sum of functional products (here of time and space):

$$T(x,t) \approx T_n(x,t) = \sum_{k=1}^{n} \Phi_k(x)\,\lambda_k(t) \tag{3.9}$$

where x and t are the space and time variables, n the order of the representation (number of modes). $\Phi_k(x)$ and $\lambda_k(t)$ are the *a priori* unknown space functions (space modes) and time functions (temporal modes), respectively.

The PGD method is also able to treat multidimensional problems in order to deliver a parametric model addressed for many engineering problems such as optimization,

inverse-method, real-time simulation-based control [45]. For example, parameters like material properties, boundary conditions, geometrical parameters can be included as additional coordinates in the separate representation (3.9). Let consider a set of N_p parameters $\mathbf{p} = \left\{p_1, p_2, \ldots, p_{N_p}\right\}$, then

$$T\left(x,t,\mathbf{p}\right) \approx T_n\left(x,t,\mathbf{p}\right) = \sum_{k=1}^{n} \Phi_k\left(x\right)\lambda_k\left(t\right)\Gamma_k\left(p\right) \quad \text{with } \Gamma_k\left(\mathbf{p}\right) = \prod_{i=1}^{N_p} \gamma_{k,i}\left(p_i\right) \tag{3.10}$$

where $\gamma_{k,i}\left(p_i\right)$ are the parameters functions.

Although very competitive in highly dimensional non-linear problems, PGD still have open topics such as the convection-dominated coupled problems [46] and the optimality of the reduced model order [44]. Moreover, the PGD is an intrusive approach as it is based on the local differential equations of the problem, which is a shortcoming in closed commercial software.

3.2 Non-intrusive Model Order Reduction methods: System identification methods

System identification has been used in many practical problems of control, diagnosis and supervision, prediction, detection and optimization. During several past decades, it has been extensively applied in the fields of automatic control systems [47], linear and non-linear structural dynamics [48], [49], thermal modelling of buildings [50], inverse modelling problems [51], etc. The identification problem consists in finding a mathematical model that best describes the relationship between the input and output data generated from either experimental measurements or numerical results of the system considered as a "black-box". In the identification procedure, the system input in a thermal problem is essentially composed of the external heat fluxes (or heat fluxes densities). It is also common for boundary conditions (BCs) to be modelled as external inputs. For instance, an imposed temperature, involved in the solid problem, may be considered in the system input. In addition, if a convection BC is involved then the ambient temperature may be also considered. In the case of a coupled fluid-solid problem, some additional fluid temperature measurements may be included in the input to the thermal solid system identification. These aspects will be more detailed in Chapters 4 and 5. The thermal output in power electronics are often limited to some critical phenomena such as the "hot spots" that are generally located at junction of power-handling components. In the identification process, a system can be characterized by (1) transfer functions, (2) a polynomial model, usually labelled as ARMA (Auto-Regressive with Moving Average) models in the literature, or (3) a state-space model. The correspondence between those three forms for a linear system is well-known in the discrete-time setting [52]. Polynomial and state space models, however, are not equivalent for

non-linear systems [53]. While transfer functions are restricted to linear systems, the others forms can be used to describe both linear and non-linear systems and they are the only forms adopted in control strategies [54]. As far as we are concerned with control applications, we will focus on the polynomial and state space models in the system identification process. After that, we will review the Prediction Error Method (PEM) of a Linear-Time-Invariant (LTI) SISO polynomial model, the ARMAX model in particular, as well as the Modal Identification Method and the Subspace method, both based on the state space form.

3.2.1 Model representations for the identification process

Polynomial structure : ARMA models

Let us consider for the identification problem of a Single-Input-Single-Output (SISO) Linear-Time-Invariant (LTI) system, the input-output relationship (3.11) coming from the observation of a N_{snap} sampled input-output data.

Let $\{U(t_k), Y(t_k)\}_{k=0,\ldots,N_{snap}-1}$ be a discrete sequence of the system input-output data driven by a white noise. The system is then described by the difference equation:

$$Y[k] + \sum_{i=1}^{n_a} a_i \, Y[k-i] \;=\; \sum_{j=1}^{n_b} b_j \, U[k-j] + \sum_{l=1}^{n_c} c_l \, e[k-l] + e[k] \tag{3.11}$$

where the notation $[k]$ stands for the $k+1^{th}$ term of a sequence and $t_k = k\Delta t$ with Δt denoting the sampling time. The sequence $\{e(t_k)\}_{k=0,\ldots,N_{snap}-1}$ denotes the white noise combining the unknown uncertainties and the measurement errors. The coefficients $a_i\,(i=1,\ldots,n_a)$, $b_j\,(j=1,\ldots,n_b)$ and $c_l, (l=1,\ldots,n_c)$ are the model parameters to identify.

Let us introduce a time delay d such that $Y[k-i] = d^i Y[k]$, and similarly for the sequences of U and e. The d-operator is equivalent to the inverse of the z-operator in the $\mathcal{Z}$-transform [55], i.e. $d = z^{-1}$. The equation (3.11) can be rewritten in a compact form as follows:

$$A(d)\,Y[k] \;=\; B(d)\,U[k] + C(d)\,e[k] \tag{3.12}$$

or equivalently

$$Y[k] \;=\; \frac{B(d)}{A(d)} U[k] + \frac{C(d)}{A(d)} e[k] \tag{3.13}$$

with

$$A(d) \;=\; 1 + a_1 d + \ldots + a_{n_a} d^{n_a} \tag{3.14}$$

$$B(d) = b_0 + b_1 d + \ldots + b_{n_b} d^{n_b} \tag{3.15}$$

$$C(d) = 1 + c_1 d + \ldots + c_{n_c} d^{n_c} \tag{3.16}$$

The model structure in (3.13) is referred to as the Auto-Regressive (AR) with Moving Average (MA) and eXogenous (X) (or external) input (ARMAX) [48] [52]. The order of the ARMAX model is (n_a, n_b, n_c), where n_a, n_b and n_c are the orders of the polynomials $A(d)$, $B(d)$ and $C(d)$. The ARMAX model is composed of a deterministic dynamics model from U to Y, i.e. $\frac{B(d)}{A(d)}$, and a stochastic disturbance model from e to Y, i.e. $\dfrac{C(d)}{A(d)}$. Thanks to the disturbance model, the ARMAX model provides some flexibility in the modelling of stochastic processes. The dynamic and disturbance models share the same set of poles of number n_a determined in the polynomial denominator $A(d)$. This coupling may represent a disadvantage but can be handled by having a good ratio between the input and the noise signal. The orders n_b, n_c determine the number of zeros of the dynamic and disturbance models, respectively. The ARMAX structure can lead to other model variants depending on what polynomials are used in (3.13). The common special cases of (3.13) are summarized in Table 3.1 [48]. The AR, standing for the simple Auto-Regressive model, is the case where the output Y depends only on its previous values, i.e. $B(d) = 0$ and $C(d) = 1$, i.e. $c_l = 0$ for $l = 1, \ldots, n_c$. The ARX model is a special case of the ARMAX model structure when $C(d) = 1$. The ARX model is considered as the simplest polynomial structure for closed-loop controlled system. The ARMA model is a special case of ARMAX when only the system output data is available, i.e. $\{U(t_k)\}_{k=0,\ldots,N_{snap}-1} = 0$. This model is helpful in the case of unknown or unmeasured input [56] [57].

Table 3.1
Common special cases of polynomial model in (3.13) [48].

Polynomials used in (3.13)	Name of model	Abbreviation
$A,\ B = 0,\ C = 1$	Auto-Regressive	AR
$A,\ B,\ C = 1$	Auto-Regressive with eXogenous	ARX
$A,\ C, B = 0$	Auto-Regressive Moving Average	ARMA
$A,\ B,\ C$	Auto-Regressive Moving Average with eXogenous	ARMAX

State space models

The interest in the state space models comes from the following reasons; They:

- require less parameters than the input-output polynomial based descriptions,
- are more adapted than the polynomial forms for model estimation as discussed in [58],
- and are particularly convenient for system theory (system transformation, simplification, analysis) and modern control applications.

The state space model form is deduced from the thermal discrete FE model of the solid domain of order N. The derivation of the FE model is detailed in Chapter 2 and the corresponding equations of both linear and non-linear problems are summarized in Table 2.1. The linear case is concerned with a heat conduction problem and a fluid-solid problem mainly governed by the forced convection. The non-linear model corresponds to the case of coupling with natural convection. Actually, The FE model is considered as a "black-box" with a given set of input and output data, U and Y of dimensions $(N_{ex} \times 1)$ and $(N_{obs} \times 1)$, respectively. For the purpose of identification, that model is transformed into a continuous-time state space model linking Y to U and is referred to as FE reference model.

Linear state space models For the linear thermal problem (Table 2.1), the FE model given in (3.1) takes the following state space form:

$$\begin{cases} \dot{\mathbf{T}}_{\mathbf{s}}(t) = A_T \mathbf{T}_{\mathbf{s}}(t) + B_T U(t) & \text{(3.17a)} \\ Y(t) = C_T \mathbf{T}_{\mathbf{s}}(t) & \text{(3.17b)} \end{cases}$$

where $A_T = -C_s^{-1} K_{LIN}$ is the $(N \times N)$ state matrix, $B_T = C_s^{-1} F$ the $(N \times N_{ex})$ input matrix that maps physical locations of the thermal inputs to the FE model nodes. The matrix C_T, of dimension $(N_{obs} \times N)$, is a pseudo-identity observation matrix used to select a part or the whole nodal temperature field $\mathbf{T}(t)$, i.e. $N_{obs} \leq N$. If N_{ex}, $N_{obs} \geq 1$, the system is called a MIMO state-space model.

As it was stated in Section 3.1 in the intrusive MOR approach, the FE reference model (3.17) is replaced by a ROM of order n (3.19) with $n \ll N$, by means of a reduced-basis change $V \in \mathbb{R}^{(N \times n)}$.

$$\mathbf{T}_{\mathbf{s}}(t) \;=\; V T_r(t) \tag{3.18}$$

$$\begin{cases} \dot{T}_r(t) = A_r T_r(t) + B_r U(t) & \text{(3.19a)} \\ Y(t) = C_r T_r(t) & \text{(3.19b)} \end{cases}$$

In (3.18) - (3.19b), $T_r(t)$ is the reduced state vector of dimension n, $A_r = V^T A_T V$, $B_r = V^T B_T$ and $C_r = C_T V$ are the associated reduced matrices of dimensions $(n \times n)$, $(n \times N_{ex})$ and $(N_{obs} \times n)$, respectively.

In the identification process, it is aimed to identify a ROM in the form of system (3.19) but based only on input and output data, $U(t)$ and $Y(t)$. Therefore, matrices A_r, B_r, C_r are not directly computed, as well as V and $T_r(t)$. The LTI state space ROM to be identified takes the form:

$$\begin{cases} \dot{X}(t) = AX(t) + BU(t) & \text{(3.20a)} \\ \hat{Y}(t) = CX(t) + DU(t) & \text{(3.20b)} \end{cases}$$

Note that $\hat{Y}(t)$ in (3.20) stands for an approximation of the system output (3.19b). For the sake of simplicity, we will consider the notation $\hat{Y}(t) = Y(t)$. In the observation equation (3.20b), a matrix D of dimension $(N_{obs} \times N_{ex})$, usually called the static gain matrix, can be considered in some identification methods to account for a static approximation of the ROM.

Observability and controllability In control theory, the linear state space model (3.20) should respect the observability and the controllability criteria:

- a system of order n is observable if the observability matrix

$$\Gamma_{obs} = [C, CA, CA^2, \ldots, CA^{n-1}]^T \in \mathbb{R}^{mn \times n} \quad (3.21)$$

  is of rank n. This means that the state of a system can be determined from a sufficient number of observations of the output. If the system is observable, one can always transform the state space model into a polynomial input-output model,

- a system of order n is controllable if the controllability matrix

$$\Gamma_{cont} = [B\ AB, A^2B, \ldots, A^{n-1}B] \in \mathbb{R}^{n \times np} \quad (3.22)$$

  has rank n. Controllability is also called reachability in the literature. The idea behind this criterion is that the system can be guided by any desired state if it is controllable.

Non-linear state space models For a non-linear problem, the general form of a ROM state space model is given by:

$$\begin{cases} \dot{X}(t) = f_{NL}(X(t), U(t)) & \text{(3.23a)} \\ Y(t) = g_{NL}(X(t), U(t)) & \text{(3.23b)} \end{cases}$$

where f_{NL} and g_{NL} are non-linear functions. In this work, some assumptions are made about the form of these functions. The function g_{NL} will be assumed to be linear. The non-linear state space model will take the following particular form:

$$\begin{cases} \dot{X}(t) = f_{NL}(X(t), U(t)) & \text{(3.24a)} \\ Y(t) = CX(t) + DU(t) & \text{(3.24b)} \end{cases}$$

The dependence of the function f_{NL} to the state vector $X(t)$ and the input vector $U(t)$ relies on the nature of the problem. This will be addressed in Chapter 5.

3.2.2 Prediction Error Method

Classical system identification methods based on input-output polynomial description have been well developed until the mid 1980s. They are generally comprised under the label of Prediction Error Methods (PEMs) [48], [59]. PEMs are well suited for the identification of Linear-Time-Invariant (LTI) polynomial forms such as the ARMA models introduced in the previous section. The PEM is based on the minimization of a parameter-dependent criterion and may be applied in both time and frequency domains. The PEM can be interpreted as the Maximum Likelihood method [60] when the disturbance white noise $e(t)$ in (3.13) is Gaussian [61]. PEM reduces to the classical least-squares (LSQ) method for the identification of the Auto-Regressive (AR) model. Another approach to estimate the AR model uses the Yule-Walker [62] equations-based methods. Examples of these methods are those proposed by Burg [63] and Levinson [48]. These methods are, however, limited to linear system identification. The estimation of the Auto-Regressive with eXogenous input (ARX) model also corresponds to a linear problem which is generally solved by analytical method such as the classical LSQ method [64] or also the Instrumental Variables Method (IVM) [65] which is a variation of LSQ method but allowing for more general classes of noise signals. Other methods have been proposed to estimate the parameters of non-linear polynomial models. Fung *et al.* in [66] combined the Recursive Extended Least-Squares (RELS) method and the Neural Network (NN) method to estimate the parameters of a non-linear ARMAX model, denoted NARMAX originally proposed by Leontaritis and Billing [67]. Another approach aimed at the identification of time-varying parameters of a non-linear ARX (NARX) model has been proposed by Zhou and Franck in [68] using the Modified Strong Tracking Filter (MSTF) algorithm.

For illustrative purposes, we will only develop the principle of PEM for the parameters estimation of a linear SISO ARMAX model. In polynomial model identification, two crucial steps have to be addressed:

- the selection of the model order, for example, the order (n_a, n_b, n_c) of the ARMAX model,

- the estimation of the model parameters.

Model order selection

The model order selection step plays an important role in the identification of polynomial models like the ARMAX model and its variants (Table 3.1). For instance, the order (n_a, n_b, n_c) of ARMAX model is not known *a priori* and has to be fixed before proceeding to the parameter estimation problem. For this purpose, many techniques have been studied in the literature. The most used approaches are those of statistical nature based on the model residuals information. Examples of these methods are the well-known Akaike Information Criterion (AIC) [52] [69], the corrected Akaike Information Criterion (AICC) [70], the Bayesian Information Criterion (BIC) [52] [71], the average error (AE) of the model residuals-based technique [72] and so on. These methods are referred to as "Information Criterion method" category and they proceed as follows: once the measured data set is available, a set of models of different orders are postulated and then the most accurate model is selected by minimizing a given criterion. These methods, however, may lead to an under-fitting or an over-fitting models depending on which criterion is used. Moreover, by their very nature, these methods necessitate a large amount of measured data, which increases the computation and memory requirements. Another category of order selection techniques include the linear algebraic methods. These methods are based on determinant and rank testing algorithms like the SVD-based method. In [73], for example, the AR and MA orders of the ARMA model are determined separately using an Information Criterion method (the minimum eigenvalue criterion; MDL) for the former and the SVD of a correlation matrix for the latter. Multi-stage estimation method also exists. This latter is based on the examination of the estimated poles and zeros of the dynamics model (ARX model), for instance, on the z-plane of the stability diagram. This is, however, restricted for system identification with low power spectrum density [56]. Thereafter, we will briefly introduce the PEM for the off-line identification of a linear SISO ARMAX model provided that the model order is determined.

Estimation of the model parameters

We assume that the order (n_a, n_b, n_c) of the SISO linear ARMAX model in (3.13) is known. Then, we can introduce the parameter vector θ composed of the polynomial coefficients of the scalar polynomials $A(d)$, $B(d)$ and $C(d)$ as follows:

$$\theta = \left[a_1, \ldots, a_{n_a}, b_0, b_1, \ldots, b_{n_b}, c_1, \ldots, c_{n_c}\right]^T \tag{3.25}$$

We also introduce a linear regression vector ξ defined as follows:

$$\begin{aligned} \xi[k, \theta] = & \left[-Y[k-1], \ldots, -Y[k-n_a], U[k], U[k-1], \ldots, U[k-n_b]\right. \\ & \left.\epsilon[k-1, \theta], \ldots, \epsilon[k-n_c, \theta]\right] \end{aligned} \tag{3.26}$$

Note that Therefore, the model structure in (3.13) can be equivalently rewritten in the following linear regression form:

$$Y[k] = \xi[k,\theta]\,\theta + e[k] \tag{3.27}$$

with

$$\epsilon[k,\theta] = Y[k] - \xi^T[k,\theta]\,\theta \tag{3.28}$$

Eq. (3.28) is referred to as the "prediction error equation" in which ϵ replaces the unknown white noise terms $e[k]$ based on the estimated residuals. An optimal estimate of the parameter vector $\hat{\theta} = \theta$ is obtained by minimizing the following quadratic norm criterion function:

$$V_{N_{snap}}(\theta) = \frac{1}{N_{snap}} \sum_{k=0}^{N_{snap}-1} |Y[k] - \xi[k,\theta]\,\theta|^2 \tag{3.29}$$

$$\hat{\theta} = \underset{\theta}{\operatorname{argmin}} \left\{ V_{N_{snap}} \right\} \tag{3.30}$$

In the equation (3.29), $V_{N_{snap}}(\theta)$ is a non-linear function of the parameter vector θ, called also the objective function. As stated before for the ARX model, i.e. $c_l = 0, l = \{1,\ldots,n_c\}$, the PEM reduces to a classical LSQ method as the regression vector ξ (3.26) includes only the input and output sampled data [64]. In this case, the parameter estimate is obtained in an analytic form and the solution is unique. For the identification of ARMA/ARMAX models, however, an iterative algorithm has to be applied in order to solve the non-linear minimization problem (3.30). Examples of iterative numerical methods are the Newton-based methods, gradient-based methods [74], etc. These techniques are known to be very sensitive to the initialization and may lead to local minima far from the true solution of the non-linear criterion function $V_{N_{snap}}$. Many researchers have worked on the local minima optimization problem. Hu *et al.* [75] proposed a Homotopy PEM-based approach or also Wang *et al.* who replaced the gradient-based algorithm by the Particle Swarm Optimization algorithm [76] to cite few. In addition, non-linear optimization techniques may require large computational cost especially when dealing with a high order objective function [77]. This issue is typically encountered when identifying MIMO systems. In fact, if the system has N_{obs} outputs and N_{ex} inputs, the scalar polynomials $A(d)$, $B(d)$ and $C(d)$ in the SISO linear ARMAX model (3.13) become full matrices. For example, the matrix $A(d)$ is defined as follows [56]:

$$A(d) = \begin{pmatrix} a_{11}(d) & \ldots & a_{1N_{obs}}(d) \\ \vdots & a_{ij}(d) & \vdots \\ a_{N_{obs}1}(d) & \ldots & a_{N_{obs}N_{obs}}(d) \end{pmatrix}, \tag{3.31}$$

$$a_{ij}(d) = 1 + a_{ij}^{(1)} d + \ldots + a_{ij}^{\left(n_{a_{ij}}\right)} d^{n_{a_{ij}}}$$

and similarly for the matrices $B(d)$ and $C(d)$ with their corresponding orders $n_{b_{ij}}$ and $n_{c_{ij}}$. Therefore, $n_{a_{ij}}$, $n_{b_{ij}}$ and $n_{c_{ij}}$ orders have to be selected and then the corresponding matrices coefficients to be estimated. For a real application, the number of the parameters might be very large leading to a complex and very time-consuming optimization problem. State-space models, however, require usually less parameters than the input-output based descriptions [59] and they are more preferred for MIMO system description. In fact, it has been shown that input-output polynomial models can be represented in a state space form by using some realization techniques. For instance, a MIMO ARMAX model can be written in a canonical state space form, also called the innovation representation [78] [79]. In order to perform the optimization problem, a canonical form has to be imposed *a priori*. However, it may be difficult to choose an appropriate canonical form since there exist many possible canonical forms for a MIMO polynomial model. This generally lead to an over-parametrized model structure [79] in addition to the aforementioned inherent inconveniences of the optimization methods. The industrial practice, though, consists in formulating the MIMO polynomial model in a modal form (a decoupled problem). Hence, the MIMO polynomial model can be separated into N_{obs} MISO (multiple-input single-output) models that are identified separately following the same procedure as for the identification of SISO models [56] [57]. This solution is still an approximation neglecting the cross-coupling between the data sets.

3.2.3 Modal Identification Method (MIM)

The Modal Identification Method (MIM) is a suited method for the identification of MIMO state space models. It was proposed by the ENSMA research team ([80]; 1997) to handle thermal problems. Their method identifies a multiple-input multiple-output reduced model in state-space description under modal form. Similarly to Prediction error method, MIM is based on the resolution of a non-linear parametric optimization problem. This latter is solved using a stochastic global optimization method, the Particle Swarm Optimization (PSO) in its latest version [81], [82]. This latter produces better parameter estimation in comparison with the Gradient-based optimization method. Historically, work until the early 2000s were mainly intended for linear heat transfer problems based on the superposition principle [80], [83]. The method has been then extended to non-linear case [84] and has been successively applied to several thermal applications such as non-linear diffusive thermal systems [85], [84], coupled heat convection and diffusion problems [86], [87], and inverse problems in order to estimate time-varying thermal inputs [88]. Latest contributions were concerned with the implementation of *off-line* identified ROM in closed-loop thermal control problems for diffusion-convection applications [81], [82]. For illustration purposes, we will review the MIM principle for a linear conduction problem.

Linear ROM structure The method identifies a Reduced Order Model (ROM) of a thermal problem (solid domain) into a state space model in a modal form (3.32). The ROM structure is deduced from that of the FE reference problem. The ROM is of order $n \ll N$, with N denoting the order of the reference model, i.e. the number of Degrees Of Freedom (temperature field) of the FE model. The state matrix A is a **diagonal matrix**, i.e. $A = (a)_i, i = 1, \ldots, n$ whose coefficients are the dominant eigenvalues of the ROM. The columns of the observation matrix, i.e. $C = (c)_{ji}, j = 1, \ldots, N_{obs}; i = 1, \ldots, n$, and the row vectors of the command matrix, i.e. $B = (b)_{ik}, i = 1, \ldots, n; k = 1, \ldots, N_{ex}$, are the corresponding eigenvectors and input vectors, respectively.

$$\begin{cases} \dot{X}(t) = AX(t) + BU(t) & \text{(3.32a)} \\ Y(t) = CX(t) & \text{(3.32b)} \end{cases}$$

Non-linear ROM structure A non-linear problem involving a linear time-dependent temperature conductivity in a heat conduction application [85] for instance, is identified in a parametric manner in the following state space model in a modal form:

$$\begin{cases} \dot{X}(t) = AX(t) + BU(t) + \Omega Z(X(t)) & \text{(3.33a)} \\ Y(t) = CX(t) & \text{(3.33b)} \end{cases}$$

The same features as in (3.32) are assumed for the matrices A, B and C. In addition, if a quadratic non-linearity is considered in the conduction problem, $Z(X(t))$ in (3.33) is a non-linear term constituted of $\frac{n(n+1)}{2}$ symmetric cross products of the state variables $X_i(t) X_j(t)$ with n the order of the reduced model. The operator Ω is the weighting matrix of the components in the vector $Z(X(t))$.

Input signals type For the identification of a linear model as described in (3.32), time-delayed step signals applied successively on the power components are used for the simulation of the detailed model. An example of these signals will be shown in Fig. 4.6. It is also assumed that the steady-regime is reached when moving from one step to another. The identified linear ROM will be then valid for any input power signals. For the identification of non-linear models such as (3.33), successive step levels are used on each power component before switching another one to account for different excitation levels. Moreover, a random noise is added in each steady step in order to exhibit large ranges of frequencies [85].

Besides the heat sources, MIM considers time-dependent boundary conditions (BCs) as time-delayed step signals. In fact, the BC is assumed constant until all the components are switched on before bringing a variation of a relatively low amplitude.

Although being very efficient, this type of identification input may require very time-consuming simulations (FE reference model) especially when dealing with high number of heated components, which may limit MIM applicability in practice.

Identification principle We propose to illustrate the MIM method on a linear thermal problem. The KIM method aims at identifying a ROM in the form of (3.32) based on N_{snap} discrete sequence of input-output data produced by the reference detailed model, $\{U(t_k), Y(t_k)\}_{k=0,\ldots,N_{snap}-1}$. The order of the ROM, n, is assumed unknown *a priori* and is iteratively increased in an optimization problem. This latter is based on a minimization problem of a mean squared residual function, called the cost function (3.35), between the response of the reference model and that of the ROM for the N_{snap} sampled data:

$$\hat{\theta} = \underset{\theta}{\operatorname{argmin}} \left\{ \mathcal{J}\left(\theta(n), (C)_{N_{obs}\times n}\right)\right\} \tag{3.34}$$

with

$$\mathcal{J}\left(\theta(n), (C)_{m\times n}\right) = \sum_{k=0}^{N_{snap}-1} \sum_{j=1}^{m} \left(Y_j(t_k) - \hat{Y}_j\left(\theta(n), (C)_{m\times n}, t_k\right)\right)^2 \tag{3.35}$$

In those equations, $Y_j(t_k)$ is the j^{th} reference output at time t_k and $\hat{Y}_j\left(\theta(n), (C)_{N_{obs}\times n}, t_k\right)$ the output estimated by the ROM of order n when the same input signal is applied. The parameter vector $\theta(n) = [a_i, b_{ik}], i = 1,\ldots,n; k = 1,\ldots,N_{ex}$ is constituted of the coefficients of the matrices A and B. The identification procedure is performed in two main phases:

- The matrices A and B are identified based on the state equation (3.32a). The coefficients in those matrices are collected into a parameter vector θ defined as $\theta(n) = [a_i, b_{ik}], i = 1,\ldots,n; k = 1,\ldots,N_{ex}$. The optimal parameter vector $\hat{\theta}$ is estimated through the optimization problem (3.34) using a gradient-type method [85] or more recently the PSO method [87]. In order to enhance the stability of the ROM, a constraint is used to enforce the coefficients in the diagonal state matrix A to be real and negative in the optimization algorithm (3.34).

- The matrix $(C)_{N_{obs}\times n}$ is estimated by a linear least-squares (LSQ) problem based on the observation equation (3.32b).

A summary of the MIM algorithm is given below.

Algorithm 3.1 Modal Identification Method algorithm

1: Collect output data $Y_{data} = (Y_j(t_k))_{j=1,\ldots,N_{obs}}$ from numerical or experimental results for $k = 0, \ldots, N_{snap} - 1$
2: Set order n=1 such as $n = dim(X)$
3: $l = 0$, initialize $\theta = [a_n^0, b_{nk}^0], k = 1, \ldots, N_{ex}$ (a and b are postulated using the PSO method or arbitrarily chosen for $l = 0$ in a gradient-type method)

   (a) Given the input signal $U \rightarrow$ Compute the state variable X through (3.32a)

   (b) Given $Y_{data} \rightarrow$ Compute $(C)^l_{N_{obs} \times n}$ by the LSQ method of (3.32b)

   (c) Compute the cost function $\mathcal{J}\left(\theta(n), (C)_{N_{obs} \times n}\right)$ through (3.35)

   (d) Compute the new parameters $\theta = \left[a_n^l, b_{nk}^l\right], k = 1, \ldots, N_{ex}$ solution of (3.34) using the PSO method or a gradient-type method; constraint on the coefficient a_n^l (real negative)

   (e) If satisfactory result OK, else $l \leftarrow l + 1$ and return to step 3.a

4: If satisfactory result OK, else $n \leftarrow n + 1$ and return to step 3

Remarks:

- In the first iteration of the optimization problem of each ROM order, the state variable in (3.32a) is not computed by means of an integration method. Instead, it can be can be computed in two manners depending on the nature of the detailed model response. If the system response reaches the steady state, then X is given by $X = A^{-1}B\bar{U}$ such that $\bar{U}$ refers to the static level of the input signal. However, in the case of a stationary response, X becomes an additional unknown variable to be identified simultaneously with the vector θ. This may be handled by a Variational Data Assimilation method for instance [89].

- Note that the identification algorithm of the non-linear ROM in 3.33 is similar to that used in the linear case but with additional parameters in the vector θ corresponding to the Ω terms. More details can be found in [85], [81].

3.2.4 Subspace identification method

Another method convenient for the identification of MIMO state space models is the Subspace identification method. It has emerged in the late 1980s (De Moor [90] and Moonen *et al* [91], [92]) as a good alternative to the non-linear optimization-based prediction-error methods for the identification of discrete-time linear MIMO sys-

tems. An exhaustive comparison between ARMAX and Subspace method is given in [93]. The Subspace method is indeed attractive, when compared with the MIM technique, since a state-space system can be directly identified from input-output data without optimization algorithms, which prevents convergence problems. Furthermore, it requires no iterative procedures and uses instead linear algebraic tools such as the QR decomposition (or equivalently the LQ decomposition), the Singular Value Decomposition and the Least-Squares method. This makes the subspace method numerically fast and robust. Moreover, it is useful for real-world data, usually containing noise disturbances. Several Subspace approaches have been developed, such as N4SID (Numerical algorithms for Subspace State Space System IDentification) [94], MOESP (Multi Output-Error State Subspace) [95], [96] and CVA (Canonical Variate Analysis) [97] as well as ORT (ORThogonal decomposition-based method) approach proposed by Picci and Katayama [98], [79]. The Subspace approaches have been also extended to the frequency domain [99] [100], as well as the continuous-time domain [101]. The extension of linear subspace methods to non-linear problems remains a distinct challenge. Significant contributions were proposed in this context, both in the discrete-time [102] and frequency [103], [104] domains for mechanical applications. The Subspace approaches have been also utilized for the identification of linear thermal models in building applications [93]. However, they still remain underused in thermal problems, especially for non-linear cases.

Subspace identification method principle By contrast to the Modal Identification Method, the Subspace method is concerned with the identification of discrete-time state-space models. These latter can be then mapped to the continuous-time domain using a bilinear transformation as proposed by McKelvey *et al.* in [99]. That transformation is valid only if the input signals are piecewise constant between the sampling instants, which refers to the zero-order-hold (ZOH) inter-sample assumption. Moreover the sampled input signal should respect the Shannon's principle.
The Subspace identification problem of a deterministic linear system is stated briefly as follows:
Given N_{snap} measurements of the input-output data, $U = (U[0], U[1], \ldots, U[N_{snap} - 1])$ and $Y = (Y[0], Y[1], \ldots, Y[N_{snap} - 1])$, find an appropriate order n and matrices of the ROM in discrete-time domain:

$$\begin{cases} X[i+1] = \tilde{A}_d X[i] + \tilde{B}_d U[i] & \text{(3.36a)} \\ \tilde{Y}[i] = \tilde{C}_d X[i] + \tilde{D}_d U[i] & \text{(3.36b)} \end{cases}$$

where subscript d stands for discrete-time, i the sampling instant $i \in \{0, 1, \ldots, N_{snap} - 1\}$, $U[i]$ the $N_{ex} \times 1$ input vector at time $t_i = i\Delta t$ with Δt denoting the sampling time, $Y[i]$ the $N_{obs} \times 1$ output vector at time t_i, $X[i]$ the $n \times 1$ state vector at time t_i and $\tilde{A}_d, \tilde{B}_d, \tilde{C}_d$ and $\tilde{D}$ are matrices of appropriate dimensions. The model $\Sigma_d = \left(\tilde{A}_d, \tilde{B}_d, \tilde{C}_d, \tilde{D}_d\right)$ is the discrete-time model to be identified of order n,

assumed unknown *a priori*.
First, for $i > n$ and N_{snap} sufficiently large, we construct the input and output block Hankel matrices $U\,[0|2i-1]$ and $Y\,[0|2i-1]$ (3.37) in which the data is partitioned in past (subscript p) and future data (subscript f). The number of block rows i is a user-defined index and can be set to $i = 2n/N_{obs}$ [105], where n is the maximum order of the ROM we aim to identify. The number of columns is set to $N_{snap}-2i+1$, such that all N_{snap} available data samples are used. The output block Hankel matrix $Y\,[0|2i-1]$ is defined in a similar way as for the input data with $Y_p = Y\,[0|i-1]$ and $Y_f = Y\,[i|2i-1]$. We define further the past input-output data as $W_p = (U_p\ Y_p)^T$.

$$\left(\begin{array}{ccc} U\,[0] & \dots & U\,[j-1] \\ \vdots & \ddots & \vdots \\ U\,[i-1] & \dots & U\,[i+j-2] \\ \hline U\,[i] & \dots & U\,[i+j-1] \\ \vdots & \vdots & \ddots \quad \vdots \\ U\,[2i-1] & \dots & U\,[2i+j-2] \end{array}\right) = \left(\begin{array}{c} U\,[0|i-1] \\ \hline U\,[i|2i-1] \end{array}\right) = \left(\begin{array}{c} U_p \\ \hline U_f \end{array}\right) \tag{3.37}$$

Then, the discrete-time state-space model is transformed into a Subspace model (3.38), denoted the "data equation" as it relates the input to the output data as follows:

$$Y_f \;=\; \Gamma_i\, X_f \;+ T_i\, U_f \tag{3.38}$$

where Γ_i and T_i are the extended observability and triangular Toeplitz matrices, expressed in terms of $\{\tilde{A}_d, \tilde{C}_d\}$ and $\{\tilde{A}_d, \tilde{B}_d, \tilde{C}_d, \tilde{D}_d\}$, respectively. The operator $X_f = (X\,[i]\,, X\,[i+1]\,, \dots, X\,[i+j-1])$ denotes the future state sequence; see [105] and [79] for more details. In the continuous-time domain, the data equation (3.38) construction can be interpreted as we introduced up to $i-1$ derivatives of the continuous-time ROM state space model given in (3.20).

Input signals requirements In the subspace method, the external input signals should respect the ***persistently exciting*** (**PE**) condition [79], [106]. That condition means that the signals should be linearly independent along the time samples. Thus, it is important to select uncorrelated inputs with each other in time. Unlike the MIM method, the step signals are not very convenient for Subspace approaches as it was already mentioned in [106]. However, they are known to be very efficient when performed with uncorrelated random signals type since they give the same weight for all the frequencies in the input spectrum band. This will be confirmed through the results on the numerical use case in Chapter 4, Section 4.2.3.

Comparison between three Subspace approaches In this paragraph, we give a brief overview of three Subspace approaches, proposed by Overschee and De Moor (1996) in [105], for the identification the linear MIMO state-space model (3.36):

- (1) MOESP (Multi Output-Error State Space) approach corresponding to function *Project* in [105].
- (2) SubSV based on *algorithm 3* in [105]. This latter is a robust subspace algorithm that was developed in [105] to identify combined deterministic-stochastic models. This algorithm works as well for deterministic models.
- (3) SubCVA based also on *algorithm 3* in [105] and corresponding to CVA (Canonical Variate Analysis) subspace approach.

The Matlab program of these three approaches is available online in [107].

The SubSV and SubCVA both combine orthogonal and oblique projection techniques performed by the LQ decomposition (Appendix B). The MOESP approach, however, uses only the orthogonal projection technique. A comparative diagram of the aforementioned Subspace approaches is presented in Fig. 3.1, in which similarities and differences are outlined.
The Subspace approaches algorithms are basically performed in the following steps (Fig. 3.1):

1. project the 'data equation" (3.38) onto $U_f^{\perp}$ in the MOESP approach (orthogonal projection) or onto W_p along U_f in both SubSV and SubCVA (oblique projection). The result is denoted $\mathcal{O}_i$. Note that an additional orthogonal projection of $\mathcal{O}_i$ onto $U_f^{\perp}$ is performed in both SubSV and SubCVA approaches,

2. determine the order n by inspection of the singular values of $W_1\mathcal{O}_iW_2$, where W_1 and W_2 are two weighting matrices. Specific choices of the weighting matrices together within the projection type lead to different identification algorithms and determine the state-space basis in which the ROM is obtained.

3. determine the ROM order by inspection of the singular values of $W_1\mathcal{O}_iW_2$, so that the extended observability Γ_i can be identified.

4. the unknown ROM discrete-time matrices are identified by means of a linear least-squares problem.

We mention that the conditioning of data matrices (block Hankel matrices) is improved through the extra orthogonal projection in SubSV and SubCVA as depicted in Fig. 3.1. The corresponding algorithms of these two Subspace approaches were judged to be robust in [105]. This result will be confirmed through the results of the comparative work between the three subspace approaches with respect to our developed method in Chapter 4.

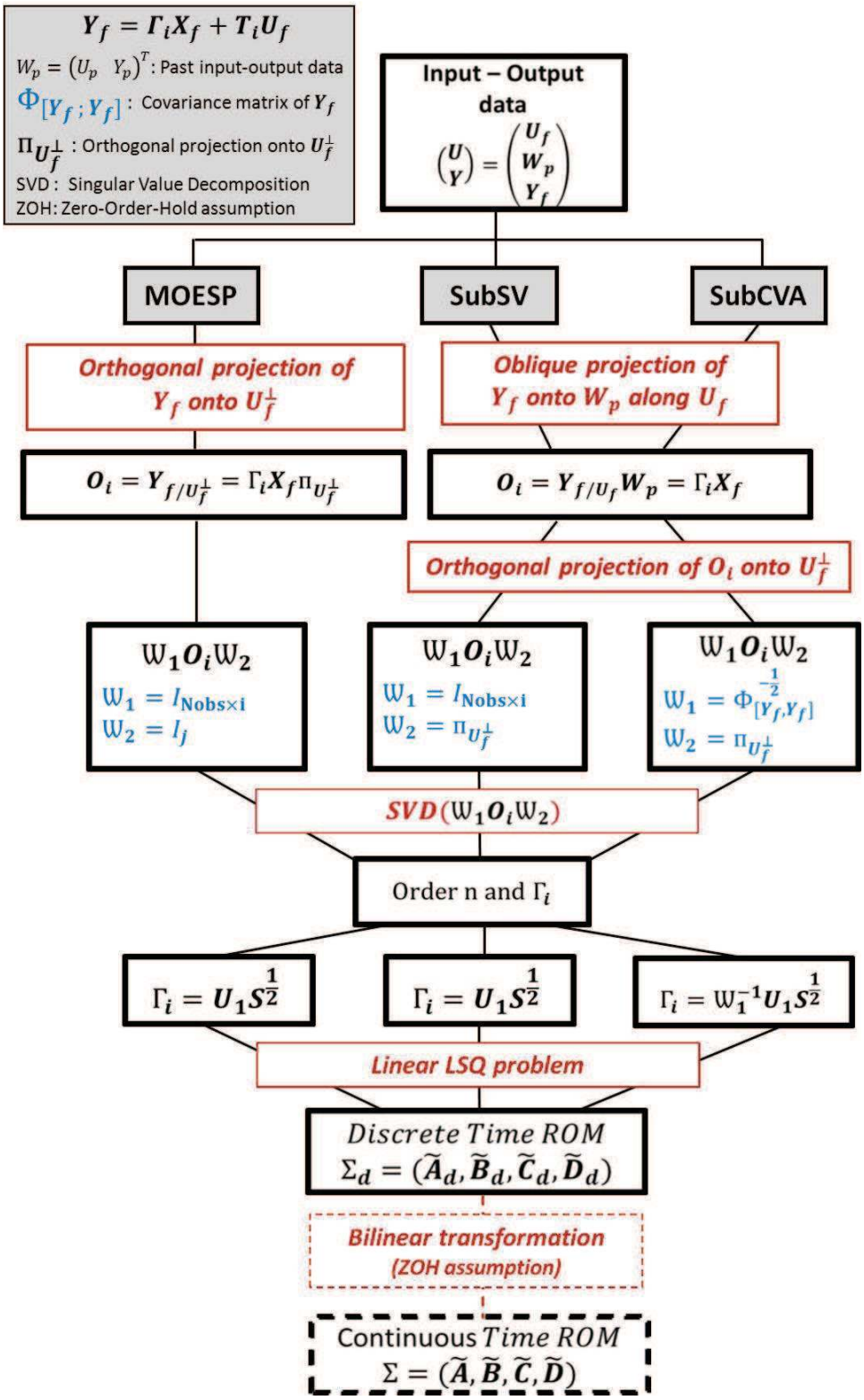

Figure 3.1. A comparative diagram of Subspace approaches (MOESP, SubSV and SubCVA)

3.3 Conclusion

In this chapter, we reviewed some existing model order reduction methods of intrusive and non-intrusive natures. In the first section, we introduced the principle and discussed the advantages and limitations of each of the intrusive methods. These latter are named so as they require access to the code solver to:

- project the original model operators onto an appropriate subspace like the projection-based reduction methods,
- or to act directly on the local differential equations of the problem like the *a priori* reduction methods.

With regard to the industrial needs, where the original model is considered as a "black-box" and the target software is inaccessible, the non-intrusive methods, i.e. system identification methods, are more suitable in this thesis. In this category, as stated in the literature, state space models are more convenient to deal with multiple-input multiple-output system with respect to the input-output ARMA models. Both prediction error-based methods and the modal identification method investigate non-linear optimization techniques, the former being based on the ARMA models and the latter applied to state space models. The subspace methods, however, are based on linear algebraic tools, such as the SVD and LQ decomposition method. This latter constitutes one of the key tool in the developed identification method in this work. The proposed method is developed in two stages. In the first stage, a new identification method referred to as "Kernel Identification Method" (KIM) is developed to derive linear compact thermal model in a state space form. Then, in the second stage, this method is extended to perform the identification of a non-linear state space model in the presence of natural convection. The next chapter focuses on the first stage dealing with the linear KIM method.

References

[1] R.J. Guyan. Reduction of stiffness and mass matrices. *AIAA Journal*, 3:380, 1965.

[2] A.C. Antoulas. *Approximation of Large-Scale Dynamical Systems*. Advances in Design and Control, Society for Industrial and Applied Mathematics, 2009.

[3] A. Dumon. *Réduction dimensionnelle de type PGD pour la résolution des écoulements incompressibles*. PhD thesis, Université de La Rochelle, 2011.

[4] D. Amsallem and C. Farhat. CME 345 : Model reduction. University Lecture - Standford University.

[5] P. Nachtergaele, D. Rixen and A. Steenhoek. Efficient weakly coupled projection basis for the reduction of thermo-mechanical models. *Journal of Computational and Applied Mathematics*, 234:2272–2278, 2010.

[6] A. Kropp and D. Heiserer. Efficient broadband vibro-acoustic analysis of passenger car bodies using an fe-based component mode synthesis approach. *Journal of Computational Acoustics*, 11:139–157, 2003.

[7] P. Koutsovasilis and M. Beitelschmidt. Comparison of model reduction techniques for large mechanical systems - A study on an elastic rod. *Multibody System Dynamics*, 20:111–128, 2008.

[8] L.B. Bushard. On the value of Guyan Reduction in dynamic thermal problems. *Computers & Structures*, 13:525–531, 1981.

[9] T. Bechtold, E.B. Rudnyi and J.G. Korvink. *Fast Simulation of Electro-Thermal MEMS: Efficient Dynamic Compact Models*. Microtechnology and MEMS, Springer-Verlag Berlin Heidelberg, 2007.

[10] R. Craig and M. Bampton. Coupling of Substructures for Dynamic Analysis. *AIAA Journal*, 6:1313–1319, 1968.

[11] V. Faucher and A. Combescure. A time and space mortar method for coupling linear modal subdomains and non-linear subdomains in explicit structural dynamics. *Computer methods in applied mechanics and engineering*, 192:509–533, 2003.

[12] D. Rixen. A dual Craig-Bampton method for dynamic substructuring. *Journal of Computational and Applied Mathematics*, 168:383–391, 2004.

[13] M. Mignolet, C. Soize and J. Avalos. Nonparametric stochastic modeling of structures with uncertain boundary conditions/coupling between substructures. *AIAA Journal*, 51:1296–1308, 2013.

[14] D. Botto, S. Zucca and M.M. Gola. Reduced-Order Models for the Calculation of Thermal Transients of Heat Conduction/Convection FE Models. *Journal of Thermal Stresses*, 30:819–839, 2007.

[15] P.O. Laffay, O. Quéméner, A. Neveu and B. Elhajjar. The Modal Substructuring Method : an efficient technique for large size numerical simulations. *Numerical Heat Transfer, Part B*, 60:278–304, 2011.

[16] S.A. Marshall. An approximate method for reducing the order of a linear system. *Control*, 10:642–643, 1966.

[17] L. Litz. State decomposition for singular perturbation order reduction - A modal approach. *International Journal of Control*, 34:937–954, 1981.

[18] F. Da Silva. *Méthodologies de réduction de modèles multiphysiques pour la conception et la commande d'une chaine de traction électrique*. PhD thesis, Ecole Centrale de Paris, .

[19] PhD thesis.

[20] G. Michailesco. *Approximation des systèmes complexes par des modèles de dimension réduite*. PhD thesis, Universitè Paris-Sud, 1979.

[21] G. Lefèbvre. *La méthode modale en thermique - Modélisation, simulation, mise en oeuvre, applications*. Ellipses Marketing, Paris, 2007.

[22] A. Bobillot. *Méthodes de réduction pour le recalage. Application au cas d'Ariane 5*. PhD thesis, Ecole Centrale de Paris, 2002.

[23] F. Renaud. *Etude de l'incidence des comportements dissipatifs dans les instabilités vibratoires des systèms de freinage*. PhD thesis, Ecole Centrale de Paris, 2011.

[24] K. Karhunen. Über lineare methoden in der wahrscheinlichkeitsrechnung. *Ann. Acad. Sci. Fennicae, ser. Al. Math. Phys*, 37:3–79, 1946.

[25] M.M. Loève. *Probability theory*. The University Series in Higher Mathematics, third ed., Van Nostrand, Princeton, NJ, 1963.

[26] B. C. Moore. Principal component analysis in linear systems: controllability, observability, and model reduction. *IEEE Transactions on Automatic Control*, 26:17–32, 1981.

[27] G. Berkooz, P. Holmes and J.L. Lumley. The proper orthogonal decomposition in the analysis of turbulent flows. *Annual Review of Fluid Mechanics*, 25:539–575, 1993.

[28] J.D. Rambo. *Reduced-order modeling of multiscale turbulent convection: Application to data center thermal management.* PhD thesis, Georgia Institute of Technology, 2006.

[29] C. Leblond, C. Allery and C. Inard. An optimal projection method for the reduced-order modeling of incompressible flows. *Computer Methods in Applied Mechanics and Engineering*, 200:2507–2527, 2011.

[30] M. Krasnyk, M. Mangold and A. Kienle. Reduction procedure for parametrized fluid dynamics problems based on proper orthogonal decomposition and calibration. *Chemical Engineering Science*, 65:6238–6246, 2010.

[31] R. Gosh and Y. Joshi. Error estimation in POD-based dynamic reduced-order thermal modeling of data centers. *International Journal of Heat and Mass Transfer*, 57:698–707, 2013.

[32] G. Kerschen, J-C. Golinval,A.F. Vakakis and L.A. Bergman. The method of proper orthogonal decomposition for dynamical characterization and order reduction of mechanical systems: an overview. *Nonlinear Dynamics*, 41:147–169, 2005.

[33] M. Amabili, A. Sarkar and M.P.Païdoussis. Reduced-order models for nonlinear vibrations of cylindrical shells via the proper orthogonal decomposition method. *Journal of Fluid and Structures*, 18:227–250, 2003.

[34] N. Kumar and T.D. Burton. On combined use of POD modes and Ritz vectors for model reduction in nonlinear structural dynamics. In *22nd Biennial Conference on Mechanical Vibration and Noise (ASME 2009).*

[35] L. Sirovich. Turbulence and the dynamics of coherent structures part i: Coherent structures. *Quarterly of Applied Mathematics*, 45:561–571, 1987.

[36] B. Podvin. Introduction à la décomposition orthogonale aux valeurs propres ou P.O.D.

[37] D. Ryckelynck. A priori hyperreduction method: an adaptative approach. *Journal of Computational Physics*, 202:346–366, 2005.

[38] N. Verdon, C. Allery, D. Ryckelynck and A. Hamdouni. An adaptive ROM approach for solving transfer equations. *Journal of Computational Mechanics/Revue Européenne de Mécanique Numérique*, 15:589–605, 2006.

[39] A. Ammar, B. Mokdad, F. Chinesta and R. Keunings. A new family of solvers for some classes of multidimensional partial differential equations encountered in kinetic theory modeling of complex fluids. *Journal of Non-Newtonian Fluid Mechanics*, 144:98–121, 2007.

[40] A. Nouy. A priori model reduction through proper generalized decomposition for solving time-dependent partial differential equations. *Computer Methods in Applied Mechanics and Engineering*, 199:1603–1626, 2010.

[41] P. Ladveze. *Nonlinear computational structural mechanics. New approaches and non-incremental methods of calculation*. Mechanical Engineering Series. Springer-verlag, 1999.

[42] E. Cueto, D. Gonzalez, I. Alfaro, C. Quesada and F. Chinesta. Model order reduction methods for computational surgery.

[43] S. Niroomandi, I. Alfaro, D. Gonzalez, E. Cueto and F. Chinesta. Model order reduction in hyperelasticity : a proper generalized decomposition approach. *International Journal for Numerical Methods in Engineering*, 96:129–149, 2013.

[44] O. Zahm, M. Billaud-Friess and A. Nouy. Goal-oriented low-rank approximation for high dimensional stochastic problems.

[45] F. Bordeu, F. Chinesta, E. Cueto, A. Leygue. Abaques numériques: Visualisation et post-Traitement de solutions variable séparée. Application au temps réel non Linaire.

[46] D. Bui, M. Hamdaoui and F. De Vuyst. POD-ISAT: A new and efficient reduced-order modeling method for the representation of parametrized finite element solutions. Application to aircraft air control systems. *International Journal for Numerical Methods in Engineering*, 00:1–21, 2010.

[47] K.J. Astrom and P. Eykhoff. System Identification - A Survey. *Automatica*, 7:123–162, 1971.

[48] L. Ljung. *System identification - theory for the user*. Prentice-Hall, Englewood Cliffs, New Jersey, 1987.

[49] G. Kerschen, K. Worden, A.F. Vakakis and J-C. Golinval. Past, present and future of nonlinear system identification in structural dynamics. *Mechanical Systems and Signal Processing*, 20:505–592, 2006.

[50] A. Allard. *A Linear Data-Driven System Identification Methodology for an Active/Passive Solar Thermal Storage System and Application to a Solar House*. PhD thesis, Concordia University, Montreal, Quebec, Canada, 2013. Department of Building, Civil and Environmental Engineering.

[51] G.A. Bekey. System Identification - an introduction and a survey. *Simulation*, 15:151–166, 1970.

[52] E.J. Hannan and M. Deistler. *The statistical theory of linear systems*. John Wiley & Sons Inc., New York, 1988.

[53] R.K. Pearson and U. Kotta. Nonlinear discrete-time models: state-space vs. I/O representations. *Journal of Process Control*, 2004.

[54] E. Meadows and J. Rawlings. *Nonlinear Process Control*. Prentice Hall, 1997. pp. 233310 (Chapter 5).

[55] The Z Transform. `http://lpsa.swarthmore.edu/ZXform/FwdZXform/FwdZXform.html`.

[56] S.M. Moore, J.C.S. Lai and K. Shankar. ARMAX modal parameter identification in the presence of unmeasured excitation-II: Theoretical background. *Mechanical Systems and Signal Processing*, 21:1601–1615, 2007.

[57] S.M. Moore, J.C.S. Lai and K. Shankar. ARMAX modal parameter identification in the presence of unmeasured excitation-II: Numerical and experimental verification. *Mechanical Systems and Signal Processing*, 21:1616–1641, 2007.

[58] M. Aoki. Complementary representation of multiple time series in state space innovation forms. *UCLA Economics Working Papers 628, UCLA Departement of Economics*, 1991.

[59] L. Ljung. *System identification - theory for the user (second ed.)*. Upper Saddle River, New Jersey: Prentice-Hall, 1999.

[60] K. J. Aström and T. Bohlin. Numerical identification of linear dynamic systems for normal operating records. In *The Proceedings of the 2nd IFAC Symposium on the Theory of Self-Adaptive Systems, Teddington, England*, pages 96–111, 1965.

[61] K.J. Aström. Maximum Likelihood and Prediction Error Methods. *Automatica*, 16:551–574, 2001.

[62] H. Monson. *Statistical Digital Signal Processing and Modeling*. John Wiley & Sons, 1996.

[63] S.M. Kay. *Modern Spectral Estimation: Theory and Application*. Prentice Hall, Englewood Cliffs, NJ, 1988. pp. 228-230.

[64] T. Söderström, B. Carlsson and S. Bigi. Least Squares Parameter Estimation of Continuous-Time ARX Models from Discrete-Time Data. In *IEEE transactions on Automatic Control*, volume 42, pages 659–673, 1997.

[65] T. Söderström and P. Stoica. *Instrumental variable method for system identification*. New York: Springer Verlag, 1983.

[66] E.H.K. Fung, Y.K. Wong, H.F. Ho and M.P. Mignolet. Modelling and prediction of machining errors using ARMAX and NARMAX structures. *Applied Mathematical Modelling*, 27:611–627, 2003.

[67] I.J. Leontaritis and S.A. Billings. Input-output parameter models for nonlinear systems. Part 1 : Deterministic nonlinear systems. Part 2 : Stochastic nonlinear systems. *International Journal of Control*, 41:303–344, 1985.

[68] D.H. Zhou and P.M. Franck. A real-time estimation approach to time-varying time delay and parameters of NARX processes. *Computers & Chemical Engineering*, 23:1763–1772, 2000.

[69] T. Söderström and P. Stoica. *System identification*. Prentice Hall, UK, 1989.

[70] C.M. Hurvich and C-L. Tsai. Regression and time series model selection in small samples. *Biometrika*, 76:297–307, 1989.

[71] S.D. Fassois. MIMO LMS-ARMAX identification of vibrating structures - part I: the method. *Mechanical Systems and Signal Processing*, 15:723–735, 2001.

[72] J.C-M. Yiu and S. Wang. Multiple ARMAX modeling scheme for forecasting air conditioning system performance. *Energy conversion & Management*, 48:2276–2285, 2007.

[73] M.S. Sadabadi, M. Shafiee and M. Karrari. Two-dimensional ARMA model order determination. *ISA Transactions*, 48:247–253, 2009.

[74] B. Bao, Y. Xu, J. Sheng and R. Ding. Least-squares based iterative parameter estimation algorithm for multivariable controlled ARMA system modelling with finite measurement data. *Mathematical and Computer Modelling*, 53:1664–1669, 2011.

[75] J. Hu, K. Hirasawa and K. Kumamaru. A homotopy approach to improving PEM identification of ARMAX models. *Automatica*, 37:1323–1334, 2001.

[76] B. Wang, N-L. Tai, H-Q. Zhai, J. Ye, J-D. Zhu and L-B. Qi. A new ARMAX model based on evolutionary algorithm and particle swarm optimization for short-term load forecasting. *Electric Power Systems Research*, 78:1679–1685, 2008.

[77] G.R. Sriniwas and Y. Arkun. A global solution to the nonlinear model predictive control algorithms using polynomial ARX models. *Computers & chemical Engineering*, 21:431–439, 1997.

[78] J.V. Candy. *Model-based signal processing*. Wiley-IEEE Press, 2005.

[79] T. Katayama. *Subspace methods for system identification*. Springer, 2010.

[80] D. Petit and R. Hachette, D. Veyret. A modal identification method to reduce a high-order model : application to heat conduction modelling. *International Journal of Modelling & Simulation*, 17(3):242–250, 1998.

[81] E. Videcoq, M. Girault and A. Piteau. Thermal control via state feedback using a low order model built from experimental data by the modal identification method. *International Journal of Heat and Mass Transfer*, 55:1679–1694, 2012.

[82] Y. Rouizi, Y. Favennec, Y. Jarny and D. Petit. Model reduction through identification - Application to some diffusion-convection problems in heat transfer, with an extension towards control strategies. *C. R. Mecanique*, 341:776–792, 2013.

[83] D. Petit and R. Hachette. Model reduction in linear heat condution : use of interface fluxes for the numerical coupling. *International Journal of Heat and Mass Transfer*, 41:3177–3189, 1998.

[84] Y. Favennec, M. Girault and D. Petit. The adjoint method coupled with the modal identification method for nonlinear model reduction. *Inverse Problems in Science and Engineering*, 14(2):153–170, 2006.

[85] M. Girault and D. Petit. Identification methods in nonlinear heat conduction. Part I: model reduction. *International Journal of Heat and Mass Transfer*, 48:105–118, 2005.

[86] Y. Rouizi, Y. Favennec, J. Ventura and D. Petit. Numerical model reduction of 2D steady incompressible laminar flows: Application on the flow over a backward-facing step. *Journal of Computational Physics*, 228:2239–2255, 2009.

[87] Y. Rouizi, M. Girault, Y. Favennec and D. Petit. Model reduction by the Modal Identification Method in forced convection: Application to a heated flow over a backward-facing step. *Journal of Thermal Sciences*, 49:1354–1368, 2010.

[88] M. Girault and D. Petit. Identification methods in nonlinear heat conduction. Part II: inverse problem using a reduced model reduction. *International Journal of Heat and Mass Transfer*, 48:119–133, 2005.

[89] W. Bouarifi. *Assimilation Variationnelle des conditions initiales par contrôle optimal et identification de paramètres par algorithmes génétiques dans le modèle ICARE*. PhD thesis, Faculté des Sciences et Techniques de Marrakech, 2009.

[90] B. De Moor, M. Moonen, L. Vandenberghe and J. Vandewalle. *Identification of linear state space models with SVD using canonical correlation analysis*, pages 161–169. North-Holland Publishing Co. Amsterdam, The Netherlands, 1988.

[91] M. Moonen, B. De Moor, L. Vandenberghe and J. Vandewalle. On- and off-line identification of linear state-space models. *International Journal of Control*, 49(1):219–232, 1989.

[92] M. Moonen and J. Vandewalle. QSVD approach to on- and off-line state-space identification. *International Journal of Control*, 51(5):1133–1146, 1990.

[93] L. Ferkl and J. Siroky. Ceiling radiant cooling: Comparison of ARMAX and subspace identification modelling methods. *Building and Environment*, 45:205–212, 2010.

[94] P. Van Overschee and B. De Moor. N4SID - Subspace algorithms for the identification of combined deterministic - stochastic systems. *Automatica*, 30(1):75–93, 1994.

[95] M. Verhaegen and P. Dewilde. Subspace model identification, Part 1: The output-error state-space model identification class of algorithms. *International Journal of Control*, 56(5):1187–1210, 1992.

[96] M. Verhaegen and P. Dewilde. Subspace model identification, Part 2: Analysis of the elementary output-error state space model identification algorithm. *International Journal of Control*, 56(5):1211–1241, 1992.

[97] W. E. Larimore. Canonical variate analysis in identification, filtering and adaptive control. In *The Proceedings of the 29th Conference on Decision and Control, Hawai, USA*, pages 596–604, 1990.

[98] G. Picci and T. Katayama. Stochastic realization with exogenous inputs and "subspace methods" identification. *Signal Processing*, 52(2):145–160, 1996.

[99] T. McKelvey, H. Akay and L. Ljung. Subspace-based multivariable system identification from frequency response data. *IEEE Transactions on Automatic Control*, 41:960–979, 1996.

[100] P. Van Overschee, B. De Moor, W. Dehandschutter and J. Swevers. A subspace algorithm for the identification of discrete-time frequency domain power spectra. *Automatica*, 33(12):2147–2157, 1997.

[101] A. Ohsumi, K. Kameyama and K. Yamaguchi. Subspace identification for continuous-time stochastic systems via distribution-based approach. *Automatica*, 38(1):63–79, 2002.

[102] S. L. Lacy and D. S. Bernstein. Subspace identification for non-linear systems with measured-input non-linearities. *International Journal of Control*, 78:906–926, 2005.

[103] J. P. Noël and G. Kerschen. Frequency-domain subspace identification for nonlinear mechanical systems. *Mechanical Systems and Signal Processing*, 40:701–717, 2013.

[104] J. P. Noël, S. Merchesiello and G. Kerschen. Subspace-based identification of a non-linear spacecraft in the time and frequency domains. *Mechanical Systems and Signal Processing*, 43:217–236, 2014.

[105] P. Van Overschee and P. B. De Moor. *Subspace identification for linear systems, Theory - Implementation - Applications*. Kluwer Academic Publishers, 1996.

[106] H. J. Palanthandalam-Madapusi, S. Lacy, J. B. Hoagg and D. S. Bernstein. Subspace-Based Identification for Linear and Nonlinear Systems. In *The Proceedings of the 2005 American Control Conference*, volume 4, pages 2320–2334, 2005.

[107] P. Van Overschee and P.B. De Moor. Available software for subspace identification. `http://homes.esat.kuleuven.be/~smc/sysid/software/`.

Chapter 4

Kernel Identification Method for Linear system identification

In this chapter, we propose a new non-intrusive MOR method named "Kernel Identification Method" for the identification of Linear-Time-Invariant state space models of a thermal multiple-input multiple-output system. A first small-scale use case of a heat conduction problem is proposed in order to illustrate the KIM in comparison with three Subspace approaches. Then, KIM is validated onto a large-scale industrial Valeo application dealing with a water cooled device simulated by a CFD software. KIM results are compared to those produced by the thermal impedance method used so far in Valeo.

Contents

4.1 Kernel Identification Method (KIM)

4.1.1 The Reduced Order Model (ROM) structure

Let us recall the FE reference model (3.17):

$$\begin{cases} \dot{\mathbf{T}}_{\mathbf{s}}(t) = A_T \mathbf{T}_{\mathbf{s}}(t) + B_T U(t) & \text{(4.1a)} \\ Y(t) = C_T \mathbf{T}_{\mathbf{s}}(t) & \text{(4.1b)} \end{cases}$$

The proposed method operates in continuous time-space, by processing discrete-time input data and output results produced by a 3D detailed finite element model. The ROM structure in KIM is deduced from that of the FE detailed model. The transition from the reference model to the ROM is explained in Section 3.2.1. In addition, KIM aims at identifying a ROM into a modal form defined as follows:

$$\begin{cases} \dot{X}(t) = \tilde{A} X(t) + \tilde{B} U(t) & \text{(4.2a)} \\ \tilde{Y}(t) = \tilde{C} X(t) + \tilde{D} U(t) & \text{(4.2b)} \end{cases}$$

with

$$\begin{cases} X = T_r \\ \tilde{A} = V_{Modal}^T \, A_T \, V_{Modal} \\ \tilde{C} = C_T \, V_{Modal} \end{cases} \quad \begin{cases} \dot{X} = \dot{T}_r \\ \tilde{B} = V_{Modal}^T \, B_T \end{cases} \tag{4.3}$$

The modal basis $V_{Modal} \in \mathbb{R}^{(N \times n)}$ in (4.3) is a solution of an eigenvalue problem of $\dot{\mathbf{T}}_{\mathbf{s}}(t) = A_T \mathbf{T}_{\mathbf{s}}(t)$. The eigenvalue problem is defined in (3.7) (see the Modal methods review on Page 80). We should note that V_{Modal} is not computed in order to deduce the new reduced state vector $X(t)$ in (4.2) as processed in an intrusive framework. In fact, the formulation within V_{Modal} only serves to expose the form of the reduced state matrix $\tilde{A}$. The matrix $\tilde{A}$ in (4.2) is identified into a diagonal form, i.e. $\tilde{A} = diag(a_1, a_2, \cdots, a_n)$ and its diagonal terms are the dominant eigenvalues (modes) of the FE reference problem, such that $a_i = -\frac{1}{\tau_i}, i = 1, \cdots, n$ with τ_i denoting the i^{th} time-constant. The corresponding eigenvectors are included into the columns of the $(N_{obs} \times n)$ observation matrix $\tilde{C}$. The main features of the ROM model are the followings:

- the ROM order n is at most equal to N_{obs}, with N_{obs} standing for the number of the observed points,
- the couple $\{\tilde{A}, \tilde{C}\}$ is independent of the excitation; it constitutes the kernel of the FE reference model (4.1),
- the $(N_{obs} \times n)$ reduced command matrix $\tilde{B}$, however, depends on the particular solution driven by the input U,
- the matrix $\tilde{D}$ is the static gain matrix contributing to a static correction of the ROM approximation.

We note $\Sigma = \left(\tilde{A}, \tilde{B}, \tilde{C}, \tilde{D}\right)$ the ROM linking the FE reference model observed results collected into Y to the input data U. In what follows, the time variable will be omitted for the sake of simplicity, so that $X(t) = X$, $Y(t) = Y$, $\tilde{Y}(t) = \tilde{Y}$ and $U(t) = U$.

4.1.2 KIM methodology

The method is referred to as the "Kernel Identification Method" since it identifies the kernel of the thermal problem through its eigenvectors and eigenvalues independent of the input and removes its stationary response thanks to a projection onto a space orthogonal to the space of input data. Hence, the implementation of the proposed method requires no iterative procedure and uses classical numerical algebraic tools instead. These tools include the orthogonal projection, computed by means of the LQ decomposition or more generally by the Householder decomposition [1], and the Least-Squares method. They are both described in Appendices A and B.

The initial step of KIM is to construct a model involving only input-output data as well as the reduced matrices to be identified, i.e. U, Y, $\tilde{A}, \tilde{B}, \tilde{C}$ and $\tilde{D}$. The equations from (4.4) to (4.7) detail how the KIM model is obtained. The reduced state equation (4.2b) enables to write

$$X = \left(\tilde{C}\right)^{\dagger} \left(\tilde{Y} - \tilde{D}\, U\right) \tag{4.4}$$

where $\left(\tilde{C}\right)^{\dagger}$ denotes the pseudo-inverse of matrix $\tilde{C}$.
The derivative of (4.2b) yields

$$\dot{\tilde{Y}} = \tilde{C}\dot{X} + \tilde{D}\dot{U} \tag{4.5}$$

Replacing $\dot{X}$ in (4.5) with the expression of the state equation (4.2a) gives

$$\dot{\tilde{Y}} = \tilde{C}\tilde{A}X + \tilde{C}\tilde{B}U + \tilde{D}\dot{U} \tag{4.6}$$

Finally, the combination of Eqs. (4.4) and (4.6) leads to

$$\dot{\tilde{Y}} = Z\tilde{Y} + WU + \tilde{D}\dot{U} \tag{4.7}$$

with

$$\begin{cases} Z = \tilde{C}\ \tilde{A}\ \left(\tilde{C}\right)^{\dagger} & \text{(4.8a)} \\ W = \tilde{C}\ \left(\tilde{B}\ -\ \tilde{A}\ \left(\tilde{C}\right)^{\dagger}\ \tilde{D}\right) & \text{(4.8b)} \end{cases}$$

Eq. (4.7) is **the reduced linear system of order $\mathbf{N_{obs}}$ to be solved**, in which the only unknown operators are the full matrices Z, W (Eqs. (4.8a) and (4.8b)) and $\tilde{D}$ of

dimensions $(N_{obs} \times N_{obs})$, $(N_{obs} \times N_{ex})$ and $(N_{obs} \times N_{ex})$, respectively. It is known that the solution Y consists of two parts. The first represents the homogeneous solution driven by the proper system, together within the initial values, the second the particular solution driven by the input U. The former, independent of the input data, relates to the kernel system $\{\tilde{A}, \tilde{C}\}$ as well as the operator Z. The latter pertains to the command matrix $\tilde{B}$. The static gain matrix $\tilde{D}$, however, contributes to a static correction of the approximation $\tilde{Y}$ in the ROM.

1- **The first key idea of KIM, is to project** (4.7) **on** $\mathbf{U}^{\perp}$, the orthogonal space to the row space of input data U, such that the projection of U onto $U^{\perp}$ is zero. The orthogonal projection aims to virtually suppress the particular solution driven by input U when identifying the system kernel. Thus, a generic reduced model is identified, valid afterwards for any signal input application. The projected KIM model on $U^{\perp}$ is written

$$\dot{\tilde{Y}}/U^{\perp} \;=\; Z\tilde{Y}/U^{\perp} + \tilde{D}\dot{U}/U^{\perp} \tag{4.9}$$

The terms $\dot{\tilde{Y}}/U^{\perp}$ $(= \dot{Y}/U^{\perp})$ and $\dot{U}/U^{\perp}$ are computed using the LQ decomposition if the matrix U is of full rank, or the Householder decomposition if U is rank-deficient (see Appendix B).

2- **The second key point comes from the *a priori* specification of the** Z **operator** that is assumed to be a **real symmetric matrix**. Thus, Z is diagonalizable, that is, $\mathcal{P}^{-1}\, Z\, \mathcal{P}$ is a diagonal matrix with N_{obs} distinct eigenvalues of Z on the diagonal. Since Z is symmetric, $\mathcal{P}$ is an orthogonal matrix, i.e. $\mathcal{P}^{-1} = \mathcal{P}^{T}$, whose columns vectors are the corresponding eigenvectors. Note that in the context of linear operators, the eigenvalues of a system are invariant under basis transformations. Hence, $\tilde{C} = \mathcal{P}$ and $\tilde{A} = diag\,(\tilde{a}_1, \cdots, \tilde{a}_n)$ with $n \leq N_{obs}$ (see the remark below). Therefore, $\tilde{C}$ is a square matrix, and in what follows we can write $\left(\tilde{C}\right)^{\dagger} = \tilde{C}^{-1}$. The opposite reciprocals of the eigenvalues (modes) $\tilde{a}_i$, $\{i = 1, \cdots, n\}$ are the ROM time-constants denoted τ_i, $\{i = 1, \cdots, n\}$ such that $\tilde{a}_i = -\frac{1}{\tau_i}$. Consequently, the problem results in N_{obs} decoupled first-order systems.

Remark: In the case of positive values in the diagonal of matrix $\tilde{A}$, these should be eliminated as well as the corresponding row and column vectors in matrices $\tilde{B}$ and $\tilde{C}$, in order to obtain a stable ROM. Moreover, such values would have significant physical meanings in the thermal problem.

Considering the previous key ideas, the next steps are the followings:

1. compute a least squares problem on (4.9) (Appendix A) to identify the matrix Z, assumed to be symmetric, and the static matrix $\tilde{D}$ (Appendix A),

2. compute the eigenvalue problem of Z to obtain the state matrix $\tilde{A}$ and the observation matrix $\tilde{C}$,

3. substitute the identified matrices $\tilde{A}$ and $\tilde{C}$ in (4.7) according to (4.8a) and (4.8b) such that $\left(\tilde{C}\right)^{\dagger} = \tilde{C}^{-1}$, and project the resulting system onto $\dot{U}^{\perp}$, the orthogonal space to the row space of derivative of input data $\dot{U}$,

4. compute a least squares problem on (4.10) to identify the command matrix $\tilde{B}$.

The projection of (4.7) onto $\dot{U}^{\perp}$ is given by:

$$\tilde{C}^{-1}\left(\dot{\tilde{Y}}/\dot{U}^{\perp} - \tilde{C}\tilde{A}\tilde{C}^{-1}\,\tilde{Y}/\dot{U}^{\perp} + \tilde{C}\tilde{A}\tilde{C}^{-1}\tilde{D}U/\dot{U}^{\perp}\right) \;=\; \tilde{B}U/\dot{U}^{\perp} \tag{4.10}$$

where the operator $\dot{U}^{\perp}$ is the orthogonal projection on $\dot{U}$. The projection on $\dot{U}^{\perp}$ allows to minimize the number of parameters in the least-squares problem.

In order to validate the identified ROM, heat sources signals different from those used in the identification step are applied. The ROM output is then computed through a numerical integration method. The initial state vector $\tilde{X}(t_0) = \tilde{X}(0)$ is determined using the ROM observation equation (4.2b) at time step $t_0 = 0$:

$$\tilde{X}\,(0) = \tilde{C}^{-1}\left(Y_{VAL} - \tilde{D}U_{VAL}\right)(0) \tag{4.11}$$

where Y_{VAL} is the observed temperatures results of the FE reference model simulated with the validation input data U_{VAL}.

ROM truncation criterion

A further reduction of the identified ROM $\Sigma = \left(\tilde{A}, \tilde{B}, \tilde{C}, \tilde{D}\right)$ can be obtained by retaining the most dominant eigenvalues in matrix $\tilde{A}$. To this end, the contribution of the eigenvalues is evaluated by inspection of the entries in the vector in (4.12):

$$diag\left(X_n X_n^T\right) \;=\; \{\sigma_1, \sigma_2, \cdots, \sigma_n\}^T \tag{4.12}$$

where X_n denotes a $(n \times N_{snap})$ matrix containing the identified state variables at different time steps. The eigenvalues are then sorted according to the decreasing order of the σ_i terms with $i \in [1, n]$ and $n \leq N_{obs}$ (see Remark on Page 114). The order of ROM is then decreased from n to k after the k greatest first values σ_i. The first k rows of the matrix $\tilde{B}$ and the first k columns of the matrix $\tilde{C}$ are only retained.

Precision criterion

The accuracy of identification results is computed through the norm $L2$ of the discrepancy, expressed as a percentage, between the response of the reference system described by (4.1) on the one hand, and the outputs of the ROM described by (4.2) on the other hand, when a specific input signal is applied.

$$\epsilon_{L_2} = \frac{1}{N_{obs}} \sum_{i=1}^{N_{obs}} \sqrt{\frac{\sum_{j=0}^{N_{snap}-1} \left(Y_i\left(t_j\right) - \tilde{Y}_i\left(t_j\right) \right)^2}{\sum_{j=0}^{N_{snap}-1} Y_i\left(t_j\right)^2}} \tag{4.13}$$

In this equation, $\tilde{Y}_i\left(t_j\right)$ is the estimated observed temperature produced by the ROM, $\Sigma = \left(\tilde{A}, \tilde{B}, \tilde{C}, \tilde{D}\right)$, at point (node) i at time t_j, and N_{snap} the number of time steps of the FE model simulation.

We can also evaluate the relative residual expressed as follows:

$$Res_i(t_j) = |\frac{Y_i(t_j) - \tilde{Y}_i(t_j)}{Y_i(t_j) - Y_i(t_0)}| \quad i = 1, \cdots, N_{obs} \quad j = 0, \ldots, N_{snap} - 1 \tag{4.14}$$

where $Res_i(t_j)$ is the relative residual at point i at time t_j and $Y_i\left(0\right)$ the i^{th} reference observed temperature at time $t = 0$. This evaluation is common in thermal design since the temperature variation constitutes an important information in reliability and lifetime prediction as illustrated in Fig. 1.3. Usually, a relative residual lower than 10 % could be considered acceptable, depending on the targeted application. The KIM algorithm is summarized below.

Algorithm 4.1 Kernel Identification Method algorithm

1: Generate the input $U_{N_{ex} \times N_{snap}}$ and output $Y_{N_{obs} \times N_{snap}}$ data from a numerical simulation (FE reference model).
2: Compute the orthogonal projections
$\dot{Y}/\ U^{\perp} \qquad Y/\ U^{\perp} \qquad \dot{U}/\ U^{\perp} \qquad U/\ U^{\perp} \equiv 0.$
3: Solve (4.9) by means of a Least-Squares method and diagonalization $\Longrightarrow$ ROM operators $\tilde{A}_{n \times n}, \tilde{C}_{N_{obs} \times n}$ and
$\tilde{D}_{N_{obs} \times N_{ex}}$, with $n = N_{obs}$.
4: Eliminate the positive diagonal terms in matrix $\tilde{A}$ as well as the corresponding row and column vectors in matrices $\tilde{B}$ and $\tilde{C}$, respectively. $\Longrightarrow$ A ROM of order $\mathbf{n \leq N_{obs}}$.
5: Arrange the diagonal coefficients in Matrix $\tilde{A}$ based on the $diag\left(X(t)\ X(t)^T\right)$ criterion in (4.12).
6: Truncate the ROM such that $\epsilon_{L_2} \leq \epsilon_{max}$ (4.13).
$\Longrightarrow X_k = X|_{(1:k), k \leq N_{obs}}$ and the corresponding ROM operators $\tilde{A}_k, \tilde{B}_k, \tilde{C}_k$ and $\tilde{D}_k (= D_k)$.

Observability and controllability
If the identified ROM is intended for closed loop control applications, it is necessary to verify its observability and controllability [2] particularly when the power input signals are different from those used in the identification step.

- On the one hand, the observability of the obtained ROM depends only on the coefficient matrices $\tilde{A}$ and $\tilde{C}$. This property is verified if and only if the observability matrix $\Gamma = [\tilde{C}, \tilde{C}\tilde{A}, \tilde{C}\tilde{A}^2; \cdots, \tilde{C}\tilde{A}^{n-1}]^T \in \mathbb{R}^{(N_{obs} \times n) \times n}$ has a full column rank of n, with n the order of the ROM and $(N_{obs} \times n)$ the dimension of matrix $\tilde{C}$.

- On the other hand, the ROM is controllable if and only if the controllability matrix $\zeta = [\tilde{B}\ \tilde{A}\tilde{B}, \tilde{A}^2\tilde{B}, \cdots, \tilde{A}^{n-1}\tilde{B}] \in \mathbb{R}^{n \times (n \times N_{ex})}$ has a full row rank of n, with $(n \times N_{ex})$ the dimension of matrix $\tilde{B}$.

4.1.3 Choice of KIM input

The input matrix U in the KIM model is composed of the heat sources applied to the power components and the boundary conditions (BCs). Below we detail the different requirements for both heat sources and the BCs.

Heat sources signals In the identification process, we should clearly distinguish between the identification input used to derive the ROM and the validation input that is composed of the power profiles (§ 1.2.1).
The choice of the heat sources signals in the identification input, i.e. the stimuli and their frequency content, has a crucial influence on the quality of system identification. Hence, they should be carefully selected, and the following requirements have to be considered:

- the input data (as well as the observed output) issued from the detailed model simulation should be resampled at a constant sample time dt (if this not was already the case) in order to ensure a fairly good estimation of the modes in the matrix $\tilde{A}$ using the least-squares method. If not, more importance would be given to over sampled laps time in the least squares problem,

- the frequency content $[0\ f_{ID_{max}}]$ should be included in that of the power profiles. This means that the maximum frequency is fixed such that $f_{ID_{max}} \leq f_{VAL_{max}}$ with $f_{VAL_{max}}$ denoting the maximum frequency the power profile for which electronics designers request a ROM. In addition, the sampling frequency $F_s = \frac{1}{dt}$ must respect the Shannon theorem, i.e. $f_{ID_{max}} \leq \frac{F_{s_{ID}}}{2}$, where $\frac{F_{s_{ID}}}{2}$ is the Nyquist frequency of discrete input signals,

- in order to identify a ROM valid afterwards for any input (in the linear case at least) given the same boundary conditions and respecting the aforesaid frequency condition, it is essential to separate the identification step from the validation one. However, if a ROM is required for specific power profiles, it is also possible, for KIM method, to identify the ROM directly on those power profiles. The power profiles in thermal simulations are often linearly dependent in time (an example is given in Section 4.3, Fig. 4.16). This means that unlike the Subspace method (Section 3.2.4), the KIM method should not necessarily respect the Persisting Exciting (PE) condition, i.e. the independence of the sources signals along the time samples. This will be proved through the industrial application in Section 4.3.

Boundary conditions The boundary conditions are also considered as inputs in the state space model (4.2) in accordance with the FE model form in the solid domain deduced in Section (2.5.3). Depending on the nature of the thermal problem, the BCs may include:

- in the case of a Dirichlet BC, the imposed temperature is assumed constant,

- if a convective BC is involved then the ambient temperature is considered and is assumed constant,

- if a coupled fluid-solid problem is investigated, some additional fluid temperature measurements may be included in the model input, in particular when the natural convection is involved. In the case of water cooled problem mainly governed by forced convection, however, the fluid temperature may be assumed constant. This case will be investigated in the industrial application in Section 4.3.

Remarks

- It is important to mention that the first two above-mentioned BCs may be varied in time during the detailed model simulation in order to ensure the independence between inputs. In doing so, a better numerical conditioning would be achieved in the identification process. This is particularly important when several boundary conditions are involved in the KIM model. This idea has been adopted in the Modal Identification Method (MIM) reviewed in Section 3.2.

- We should mention that the matrix U may not be of full-rank, like the case of $\dot{U}$ when a constant BC is considered, or even when linearly-dependent heat sources signals are involved. Consequently, in order to generate the matrices $U^{\perp}$ and $\dot{U}^{\perp}$ in (4.9) and (4.10), we use the *Householder QR decomposition* [3] (Appendix B). The rank deficiency in the least-squares problem leads also to an ill-conditioned problem. This latter is then performed by means of a generalized Least-Squares method [1] (Appendix A).

4.2 Application to a small-scale conduction problem and comparison with the Subspace method

4.2.1 The FE reference model

A 3D thermal FE model (Fig. 4.1) is used in order to evaluate the performance of KIM in comparison with the Subspace approaches (MOESP, SubSV and SubCVA) introduced in Section 3.2.4.
The model consists of nine cuboid sources partially embedded in a parallelepiped, each component being powered by a transient heat flux density input $U_i(t), \{i = 1, \ldots, 9\}$ (W/m^2) spread over its upper face. Convective BCs are applied to the upper (h_{Hi}) and lower (h_{Lo}) faces of the model with time-independent ambient temperature T_a to simulate a cooler. In the initial state the temperature of nodes is $T_i = T_a = 25\,^{\circ}\mathrm{C}$. The input matrix involved in the state space model is then $U = (U_1(t), U_2(t), \ldots, U_9(t), T_a)^T$. Materials characteristics are given in Table 4.1.

Despite its simplicity, this use case is representative of the thermal behaviour of a Printed Circuit Board substrate on which dissipating components are mounted. The simulation is carried out with a finite element model of size $N = 20236$, the mesh having 20236 nodes. The FE reference solution corresponds to the computed temperatures recorded at observation points **1** to **10** all placed at the center of the cubes $(Y_{i,\ (i=1,\cdots,N_{obs})})$ and at a point placed at the left bottom upper face of the model (Y_{10}) (Fig. 4.1). The reference solution is recorded at N_{snap} time steps.

Table 4.1
Material characteristics of FE reference model.

	Density Kg m^{-3}	Conductivity W $m^{-1}\,^{\circ}C^{-1}$	Specific Heat J $Kg^{-1}\,^{\circ}C^{-1}$
Upper part	1200	150	880
Lower part	1200	0.3	880

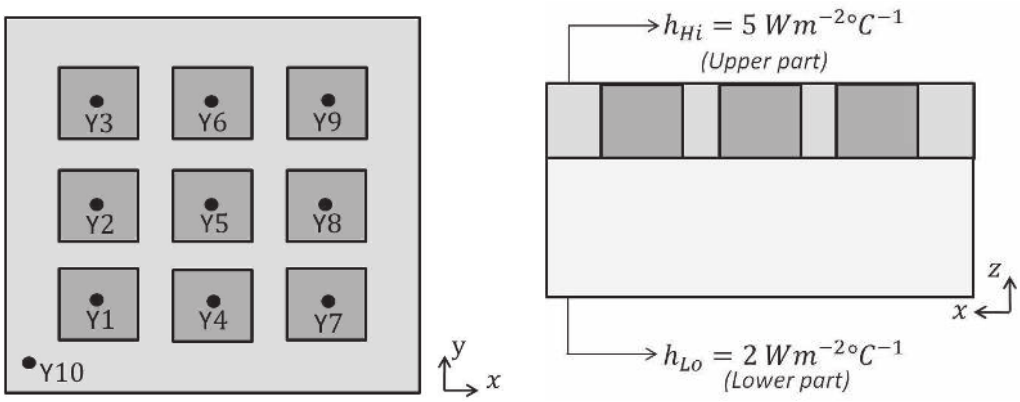

Figure 4.1. Reference model.

4.2.2 Tests description

The test cases are summarized in Table 4.2. Two heat sources signal types are carried out, complying with the input requirement described in § 4.1.3, in order to identify a ROM of the FE reference model:

(*i*) **signals of type 1** (Fig. 4.2(a)): time-delayed step signals applied **successively** on the upper faces of model components. This type is used in order to identify ROM1. We should mention that, this signals type together within a time-independent convective BC, do not follow the MIM hypothesis addressed to identification inputs, i.e. the temperature steady-regime is not reached for one component before switching on another one as it was mentioned in § 3.2.3 (Fig. 4.6).

(*ii*) **signals of type 2** (Fig. 4.3(a)): uncorrelated zero-mean random signals with offset applied simultaneously on the nine upper faces of components. This type is used in order to identify ROM2, as well as to validate both ROM1 and ROM2 (Table 4.2).

Identification input signals of type 1 and 2 are both sampled at time step $dt = 0.5$ s, then $F_{s_{ID}} = F_{s_{ID1}} = F_{s_{ID2}} = 1/dt = 2$ Hz. For the first type, the frequency spectrum becomes generally negligible after 5 df, with $df = 1/T$ and $T = 50$ s the time for which the step is non null. The second type, on the other hand, is filtered at $f_{ID_{max}} = 1$ Hz. Hence, the Shannon's principle is fulfilled for both signals types $f_{ID_{max}} \leq \frac{F_{s_{ID}}}{2}$. Their respective power spectra are shown in Figs. 4.2(b) and 4.3(b). The influence of these signals types on both KIM and Subspace methods will be investigated in Section 4.2.3.
In Table 4.2, test case 1 is concerned with the identification of ROM1 using the signals type 1 and test case 2 with the identification of ROM2 using the signals type 2. ROM1 and ROM2 are afterwards validated using the same input signals of type 2 different from those used in identification step, denoted validation (VAL)

inputs (Figs. 4.4(a), 4.4(b)). The validation inputs are sampled at $F_{s_{VAL}} = 1/3$ Hz and filtered up to $f_{VAL_{max}} = 0.15$ Hz $< f_{ID_{max}}$), which implies that the validation frequency range is included into that of the identification step.

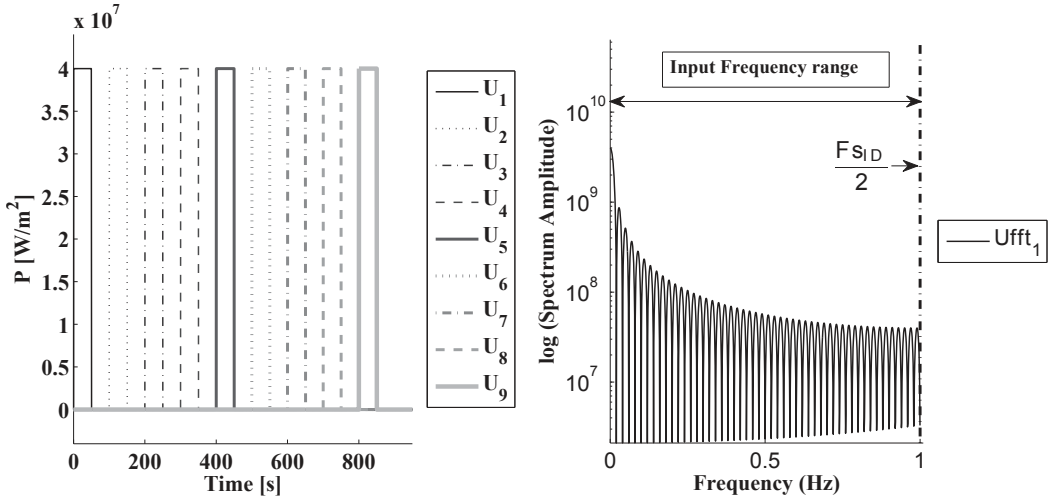

(a) Input signals. (b) Input spectrums.

Figure 4.2. (a) Identification input signals of **type 1 (time-delayed step signals)** and (b) the corresponding spectrum ($F_{s_{ID}} = 2$ Hz); for greater clarity, only the input spectrum applied on component 1 (Ufft_1) is illustrated in (b).

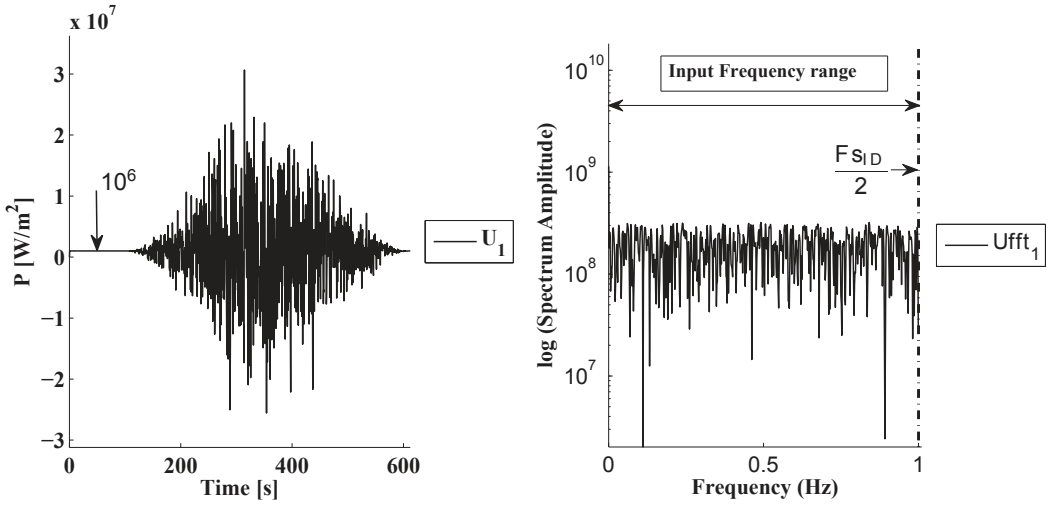

(a) Input signals. (b) Input spectrums.

Figure 4.3. (a) Identification input signals of **type 2 (uncorrelated zero-mean random signals with offset)** and (b) the corresponding spectrum ($F_{s_{ID}} = 2$ Hz); for greater clarity, only the input signal and spectrum applied on component 1 (U_1 and $Ufft_1$) are illustrated in (a) and (b), respectively.

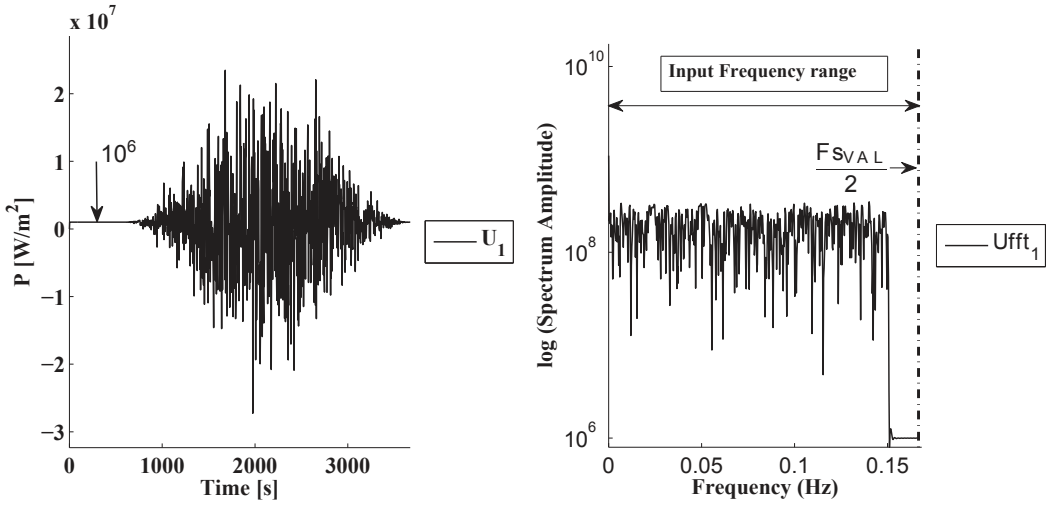

(a) Input signals. (b) Input spectrums.

Figure 4.4. (a) Validation input signals of **type 2 (uncorrelated zero-mean random signals with offset)** and (b) the corresponding spectrum ($F_{s_{VAL}} = 1/3$ Hz); for greater clarity, only the input signal and spectrum applied on component 1 (U_1 and $Ufft_1$) are illustrated in (a) and (b), respectively.

Table 4.2
Description of the tests ; two types of identification input signals and the resulting ROM, and one validation input to validate the ROMs.

	Test 1	Test 2
Identification input (heat sources signals)	**Signals of type 1** time-delayed step signals (Fig. 4.2(a)) signals spectrum (Fig. 4.2(b)) $\mathbf{N_{snap} = 1901}$ $\mathbf{F_{s_{ID1}}} = \mathbf{2}$ Hz	**Signals of type 2** uncorrelated zero-mean random signals with offset (Fig. 4.3(a)) signals spectrum (Fig. 4.3(b)) $\mathbf{N_{snap} = 1225}$ $\mathbf{F_{s_{ID2}}} = \mathbf{2}$ Hz
ROM identification	ROM1 of order $n1$ Figs. 4.5, 4.6 and 4.7(a), 4.7(b), and Tables 4.3 and 4.5	ROM2 of order $n2$ Figs. 4.8, 4.9 and 4.10(a), 4.10(b), 4.10(c), and Tables 4.4 and 4.5
Validation input (heat sources signals)	**signals of type 2** (Fig. 4.4(a)) spectrum (Fig. 4.4(b)) $\mathbf{f_{VAL_{max}}} = \mathbf{0.15}$ Hz $< \mathbf{F_{s_{VAL}}} = \mathbf{1/3}$ Hz ; $\mathbf{f_{VAL}} \subset \mathbf{f_{ID}}$	
ROM validation	Figs. 4.11(a) and4.11(b), and Table 4.6	Figs. 4.12(a) and 4.12(b), and Table 4.6

4.2.3 Results and Discussion: comparison to the Subspace method

Identification (ID) step

The accuracy of identified ROM is assessed by:

- computing the relative L2 norm error, as defined in (4.13), based on the discrepancies between the observed temperatures computed by the reference FE model at the 10 observation nodes, and the outputs of the ROM,

- verifying the numerical stability of relative error convergence depending on ROM order,
- examining the stability of its modes. On the one hand, KIM identifies a continuous-time ROM with modes placed on the diagonal of the state matrix $\tilde{A}$. The ROM is assumed stable if these diagonal terms are all negative. On the other hand, the subspace approaches identify iteratively a discrete-time ROM with a full state matrix. An eigenvalue decomposition is then performed on that matrix in order to compute the modes and compare them to those of KIM. In addition of being negative values, the modes have to be invariant regardless the ROM order. We should note that KIM is not concerned with the stability assessment since it identifies a ROM of order n and then truncates it by means of the criterion defined in (4.12).

Identification of ROM1 The identification relative error (4.13) on the estimated temperatures (at observation nodes $1, 2, \ldots, N_{obs} = 10$) is depicted in Fig. 4.5. Each of KIM, SubSV and SubCVA produce very good results. Even for order 1, the error ($\backsimeq 3.4\%$ for SubSV and lower than 10% for KIM and SubCVA) could be considered as acceptable, depending on the targeted application. Order 1 corresponds to the case where the lowest mode frequency (in absolute value), i.e. the largest time constant, only is retained. Unlike the other methods, MOESP approach produces significant error, the error being nearly constant at $\backsimeq 20\%$ for all ROM orders (up to 10). The relative error of ROM of order 10 for all methods is given in Table 4.3. As an example, the ROM response (fixed order as detailed in Table 4.3), is compared to the reference FE response in Fig. 4.6.

Figs. 4.7(a) and 4.7(b) show the stability diagram (identified modes versus ROM order) of the identified modes obtained by SubSV and SubCVA, respectively. Recall that KIM identifies a ROM of order equal to the number of observation points first, and then the model is truncated based on criterion in (4.12), so that it is not concerned with stability diagram and only modes of reduced model of order 10 are present (circle markers) in the other methods stability diagram. SubSV, SubCVA and KIM cover perfectly almost the same frequency band for ROM of order 10, except for the lowest frequency that is slightly different between Subspace approaches and KIM method. Moreover, the identified modes are all included into the bandwidth [0 , $\frac{F_{sID}}{2}$ Hz].

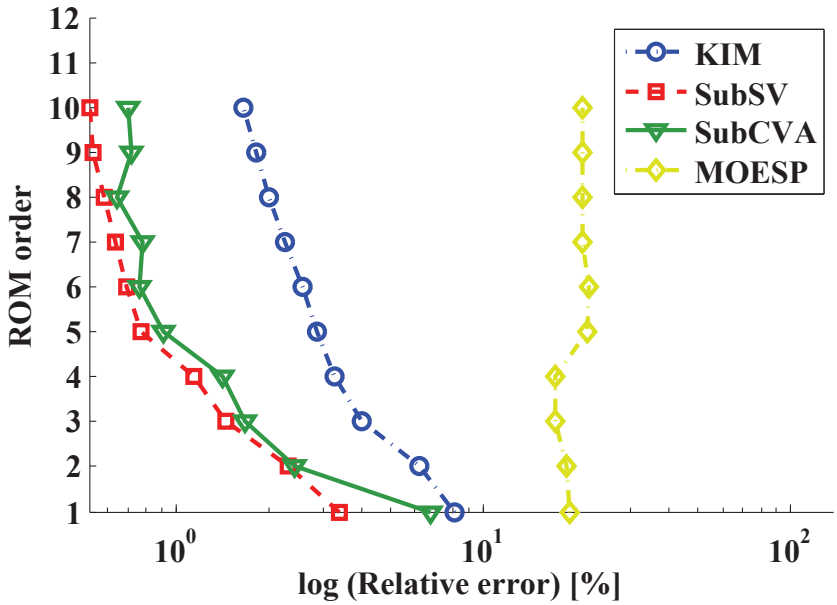

Figure 4.5. Identification relative error (4.13): L2-norm of the discrepancy between responses of the reference FE model and outputs of **ROM1**.

Table 4.3
ROM1 identification error (order 10)) based on all observation points (Eq. 4.13).

	KIM	SubSV	SubCVA	MOESP
Error ϵ_{L_2} (%)	1.6	0.5	0.7	21.0

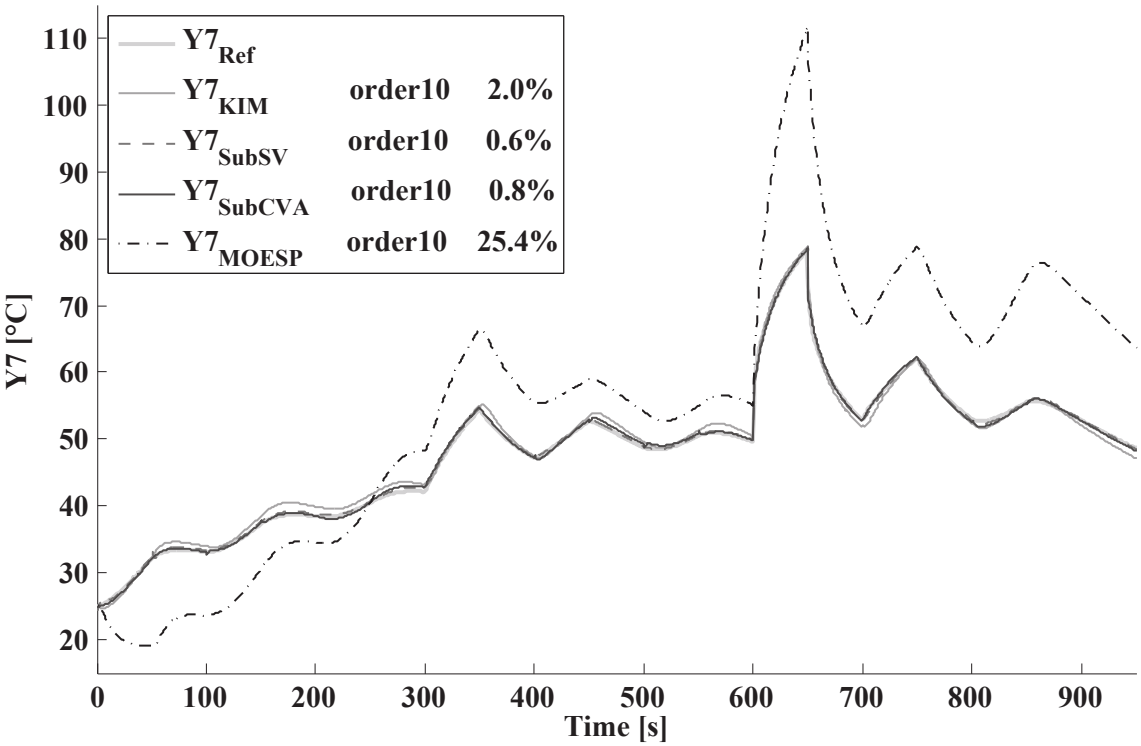

Figure 4.6. Identification of **ROM1**: comparison between the reference and estimated temperatures at point No. 7.

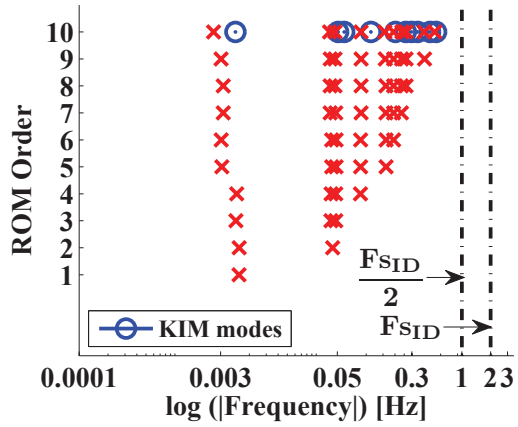

(a) SubSV stability diagram (Cross markers).

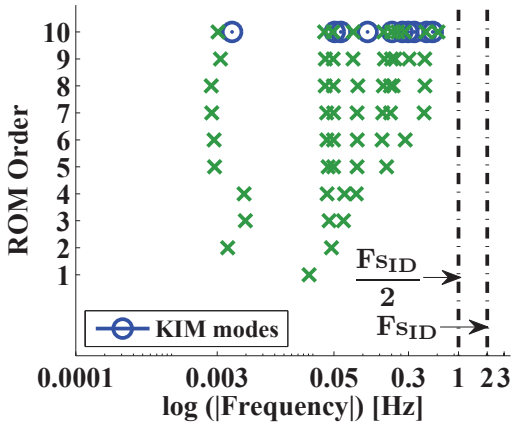

(b) SubCVA stability diagram (Cross markers).

Figure 4.7. Stability diagram of **ROM1** modes identified by (a) SubSV and (b) SubCVA in comparison with KIM modes (circle markers).

Identification of ROM2 The identification process is now carried out using the second type of heat sources signals. The most notable results in this test case are:

firstly, the significant enhancement of the ROM estimation obtained by MOESP approach (error 4 times lower than that obtained in test case 1; see Figs. 4.8, 4.9 and Table 4.4). Secondly, the identified modes obtained by SubSV and SubCVA (Figs. 4.10(a), 4.10(b)) become very stable in comparison with results of those of ROM1 (Figs. 4.7(a), 4.7(b)). The MOESP is very stable as well. One should also notice that KIM, SubSV and SubCVA yield very close low errors ($\backsimeq 1.5\%$ for ROM2 of order 1 and between 0.5% and 0.9% for order 10). Even though SubCVA and MOESP produces very stable modes (Fig. 4.10(c)), they still have no stable relative error convergence, on the contrary to the SubSV method (Fig. 4.8). Recall that KIM identifies a ROM of order equal to the number of observation points first, and then the model is truncated based on criterion in (4.12), so that it is not concerned with stability of relative error convergence. The limits of the identified frequency range, for both ROM1 and ROM2, are listed into Table 4.5. One observes that Subspace approaches produce almost the same frequency bandwidth (identical for SubSV and MOESP). Moreover, they identify almost the same lowest frequency value as KIM approach. The maximum range frequency is however different between KIM and Subspace approaches. Even so, the levels of errors are not necessarily very different except for the MOESP approach, as can be shown in Fig. 4.8 and Table 4.4. The MOESP approach appears to be less efficient than the SubSV and SubCVA methods. This may be explained by the additional use of an orthogonal projection in the SubSV and SubCVA as this can be noticed through the comparative diagram of these approaches (Fig. 3.1).

The lowest frequency, corresponding to the highest time-constant, has a much larger impact on the quality of reduced model. This can be further confirmed through the slight improvement of errors levels for Subspace and KIM methods when increasing the ROM2 order from 1 to 10 (see Fig. 4.8).

It is shown through Figs. 4.10(a), 4.10(b), 4.10(c) and Table 4.5 that Subspace approaches identify ROM2 frequencies exceeding the identification Nyquist frequency ($\frac{F_{s_{ID}}}{2} = 1$ Hz; see Table 4.2). In fact, the random signals used in the identification step was filtered to the maximum frequency of $f_{ID_{max}} = 1 \text{ Hz} \leq \frac{F_{s_{ID}}}{2}$. In practice, one cannot avoid filters imperfections from a theoretical point of view. To account for that gap between ideal theory and real practice, one should use a sampling frequency $F_{s_{ID}}$ that is a higher multiple of the highest frequency $f_{ID_{max}}$ in the signal than just the double of Nyquist frequency ($\frac{F_{s_{ID}}}{2}$). Under such precaution, the bilinear transformation, that maps the discrete-time identified model to the continuous-time domain, would not results in system modes exceeding the Nyquist frequency.

It is also shown from Figs. 4.10(a), 4.10(b), 4.10(c) and Table 4.5 that Subspace approaches favour the identification of higher frequencies in comparison with the KIM method (the identified frequency $f_{max}(KIM) \backsimeq 0.3$ Hz $< f_{max}(Subspace) \backsimeq 1.3, 1.5$ Hz). This is not surprising since the Subspace identification principle is derived through multiple derivations of input-output data in continuous-time domain

as it was mentioned in Section 3.2.4, which is equivalent to successive multiplication by jw in frequency domain, with j the complex variable and w the circular frequency variable. This aspect, however, is not detected in the identification using the time-delayed signals (Type 1), since they give greater weight for low frequencies values unlike random signals that give the same weight for all the input frequency band (see signals spectrum in Figs. 4.2(b) and 4.3(b)).

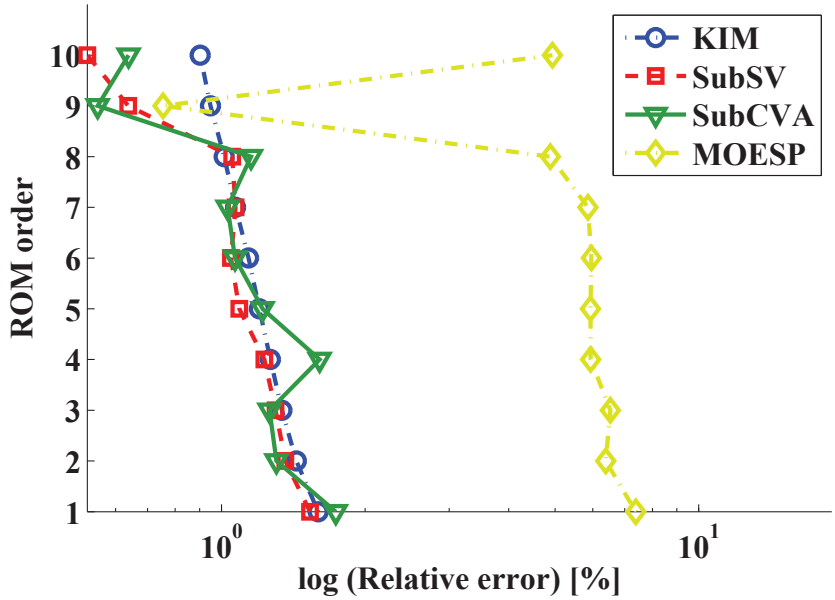

Figure 4.8. Identification relative error (4.13): L2-norm of the discrepancy between responses of the reference FE model and outputs of **ROM2**.

Table 4.4
ROM2 identification error (order 10) based on all observation points (Eq. 4.13).

	KIM	SubSV	SubCVA	MOESP
Error ϵ_{L_2} (%)	0.90	0.52	0.64	4.94

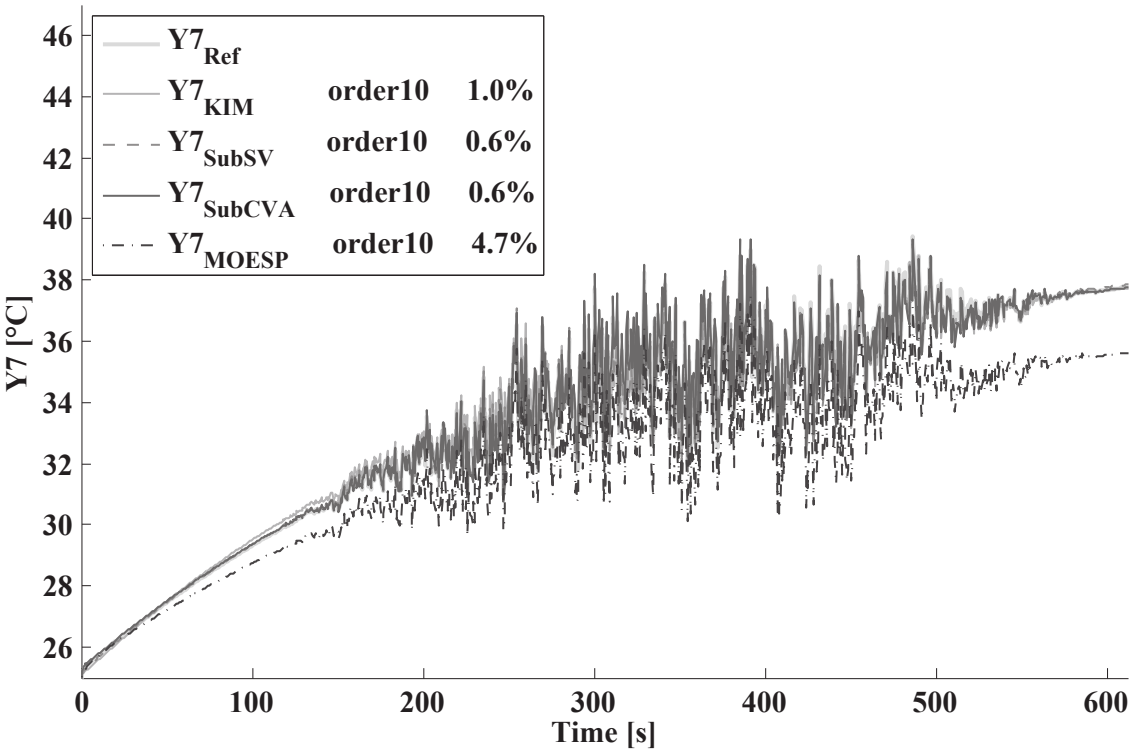

Figure 4.9. Identification of **ROM2**: comparison between the reference and estimated temperatures at point No. 7.

Table 4.5
Summary table of identified frequencies (all negative values) of ROM1 and ROM2 of order 10; comparison between KIM and Subspace approaches.

	ROM1		ROM2	
	$-f_{min}$	$-f_{max}$	$-f_{max}$	$-f_{max}$
KIM	0.0043	0.5382	0.0037	0.3122
SubSV	0.0025	0.5212	0.0033	1.2724
MOESP	0.0026	0.5277	0.0033	1.2723
SubCVA	0.0031	0.6112	0.0034	1.4488

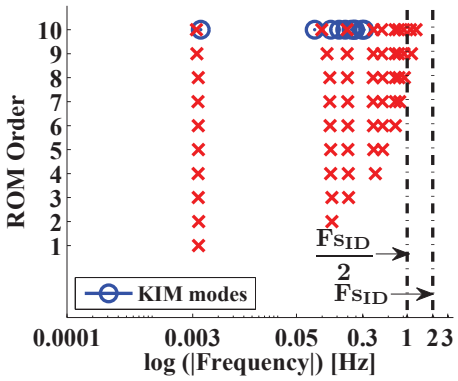

(a) SubSV stability diagram (Cross markers).

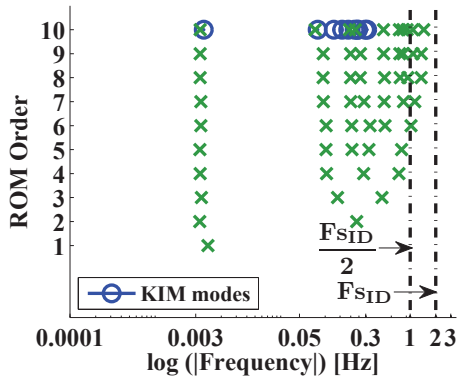

(b) SubCVA stability diagram (Cross markers).

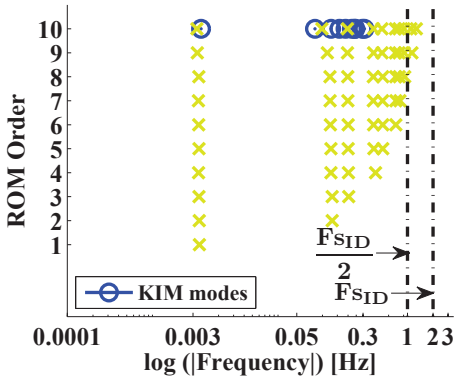

(c) MOESP stability diagram (Cross markers).

Figure 4.10. Stability diagram of **ROM2** modes identified by (a) SubSV, (b) SubCVA and (c) MOESP in comparison with KIM modes (circle markers).

Validation step

The validation step of ROM1 and ROM2 is performed using heat sources signals of type 2 (see Table 4.2 and Figs. 4.4(a), 4.4(b)). The ROM1 and ROM2 orders are selected at 10 for KIM and Subspace approaches. Fig. 4.11(a) show the ROM1 temperature estimation, obtained by each identification method at node 7, compared to those of the FE reference model at the same node. Their corresponding discrepancies are presented in Fig. 4.11(b). The ROM2 results are illustrated in a similar way in Figs. 4.12(a), 4.11(b). The Table 4.6 lists the validation step relative errors on the $N_{obs} = 10$ estimated temperatures for both ROM1 and ROM2.

When using ROM1, it is clear that KIM yields good results (maximum deviation of 2.6 °C for node 7 (Fig. 4.11(b))). Furthermore, the relative error, involving the N_{obs} temperatures , for KIM is $\backsimeq$ 2.4%, followed by SubCVA ($\backsimeq$ 2.4%) and SubSV ($\backsimeq$ 8.7%). The reason is that signals of type 1, time-delayed step signals used

for the identification of ROM1, are not very convenient for Subspace approaches (Section 3.2.4) since those signals give greater weight to low frequency range (see spectrum in Fig. 4.2(b)).

Now for the validation results of ROM2 of order 10 for KIM and Subspace approaches, we examine similarly the temperature estimation at node 7 and the corresponding discrepancies with FE reference observations (Figs. 4.12(a), 4.12(b)). Unlike ROM1, the SubSV and SubCVA approaches yield an excellent fit with the reference solution when using ROM2, followed by MOESP results (deviation of 7.5 °C for node 7). The relative error for ROM2 obtained by KIM method is of 2.8% and is almost equal to that obtained in ROM1 validation step (Table 4.6). Thus, KIM method works well for both identification signals types. The Subspace approaches, however, are more sensitive to the identification heat sources signals type and are, as aforementioned, more convenient with random signals, especially the MOESP approach.

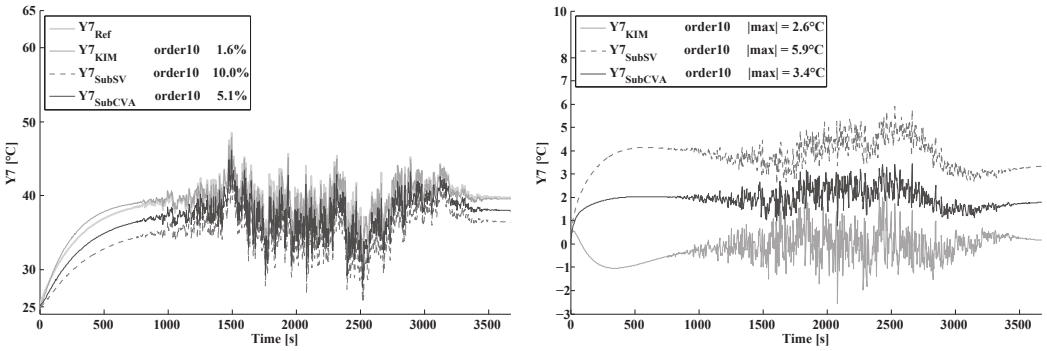

(a) Temperature estimation at point No. 7. (b) Temperature residual at point No. 7.

Figure 4.11. Validation of **ROM1**: (a) temperature estimation and (b) temperature residual at point No. 7.

Table 4.6
Comparison between the estimation error 4.13 for ROM1 and ROM2 (both of order 10), based on all observation points, when submitted to validation inputs different from those used in identification step.

		KIM	SubSV	SubCVA	MOESP
Error ϵ_{L_2} (%)	ROM1	2.4	8.7	4.1	–
	ROM2	2.8	2.9	2.4	7.8

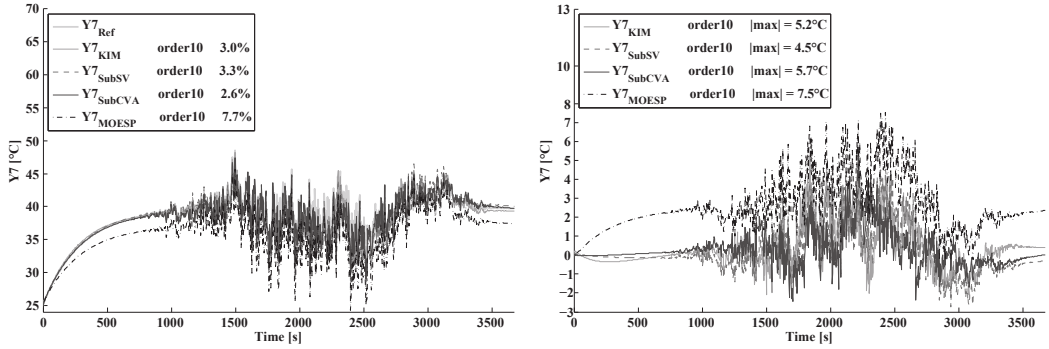

(a) Temperature estimation at point No. 7. (b) Temperature residual at point No. 7.

Figure 4.12. Validation of **ROM2**: (a) temperature estimation and (b) temperature residual at point No. 7.

4.3 Application to a large-scale water cooled CFD problem and comparison with the Zth method

4.3.1 The industrial model

In this section, we will apply KIM method on a large-scale industrial product in order to estimate the junction temperature of some electronic parts given a mission profile. The investigated application is a **water cooled CFD problem** involving conduction with constant material properties, internal and external natural convection, radiation, and a water cooling forced convection with $T_{coolant} = 105\,°\text{C}$. The problem, however, is **mainly governed by forced convection** and its thermal behaviour is approximately linear. A 3D Finite Volume (FV) model of almost 1 million cells allocated to both fluid and solid domains is carried out on the FloEFD software. The power module part consists of 51 power sources including 6 MOS, 6 Diodes, 3 capacitors and several PCB layout tracks (Fig. 4.13). The localisation of these power sources is depicted in Fig. 4.14. The thermal dissipated power (in watt) on the MOS and Diode components is located at the top of their respective Silicon dies.

The transient simulation is initialized by steady state results in which all the power sources are turned off allowing for a stabilized coolant flow at $t = 0$ s. The temperature cartography of the power module given in Fig. 4.15 shows an almost uniform temperature around the power components with values around $105\,°\text{C} \simeq T_{coolant}$. The transient simulation results showed that the thermal dissipated power applied on capacitors and layout have a negligible effect on the system thermal behaviour, with respect to those applied on MOS and Diode components. Therefore, in the identification process, we will consider only the MOS and Diode components as power sources even if the other sources are still active in the transient simulation.

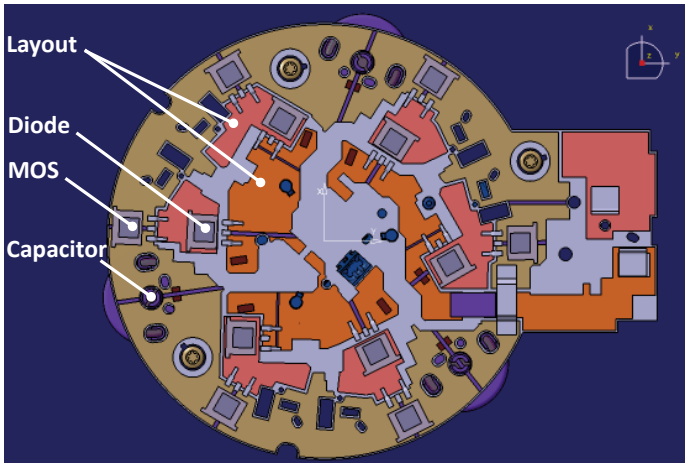

Figure 4.13. Top view of the power module composed of MOS, Diode, capacitors and layout placed on a substrate.

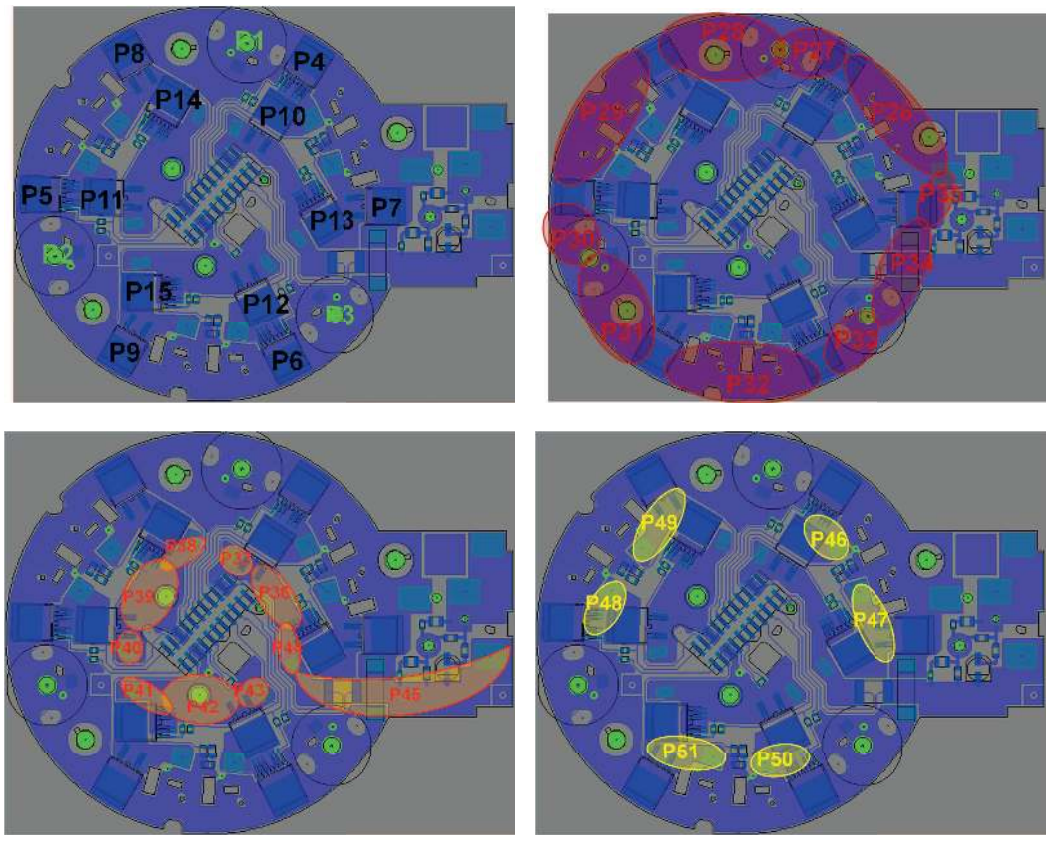

Figure 4.14. The localisation of the power sources; $P_{capacitor}$={P1, P2, P3}, P_{MOS}={P4, P5, P6, P13, P14, P15}, P_{Diode}={P7, P8, P9, P10, P11, P12} and layout (from P26 to P51).

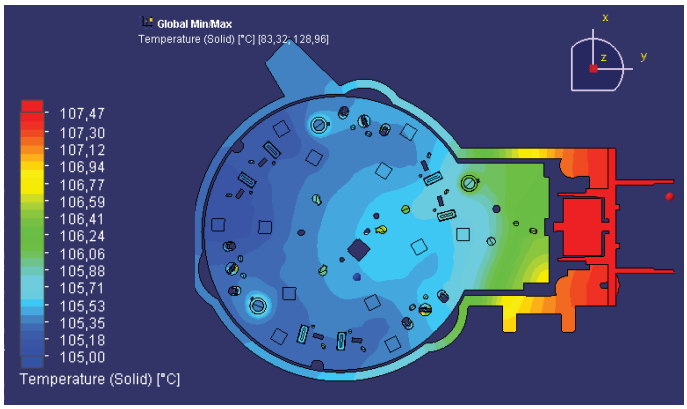

Figure 4.15. The temperature cartography of the steady state results.

In order to ensure convergence, FloEFD transient simulations are carried out with a variable sample time. Usually, small time steps are required for the initial transients (about microseconds) and during the power profiles changes like the switch on/off of a square signal. Consequently, the resulting input output data of the detailed model are not equidistantly sampled signals. The steady and transient simulations last around 12 hours and 6 hours, respectively. Before proceeding to the identification step, the input-output data are **resampled at constant time step** $dt = 0.05$ s resulting in $N_{snap} = 761$ sampling time steps in order to comply with the input sampling requirement described in § 4.1.3. The resampled power profiles applied on MOS and Diodes and their corresponding spectrum are given in Figs. 4.16(a) and 4.16(b), respectively. The recorded junction temperatures located at the top centre of the MOS and Diode components are presented in Fig. 4.17(b). This figure shows four different thermal behaviours; a similar behaviour for the MOS placed inside the substrate and another one for those placed at the boarder of substrate and similarly for Diode components. We can also detect from the figure 4.17(b) the hot spot which is located at point 11 of the MOS component.

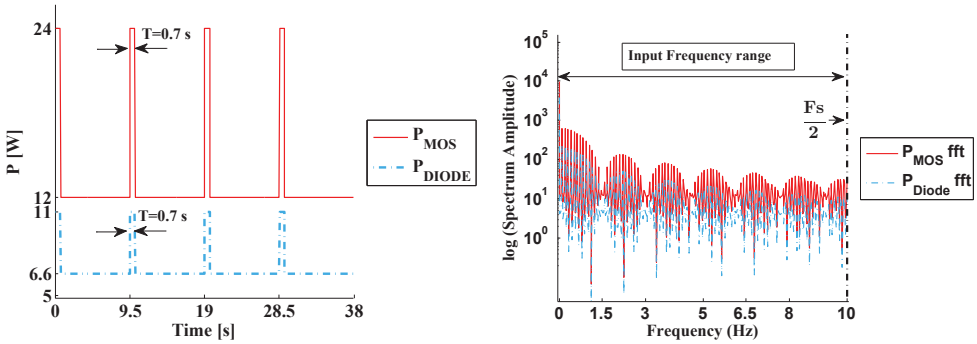

(a) Input signals. (b) Input spectrum.

Figure 4.16. (a) Power profiles signals and (b) the corresponding spectrum ($F_{s_{ID}} = 1/dt = 20$ Hz) applied to the MOS and Diode components in transient simulation.

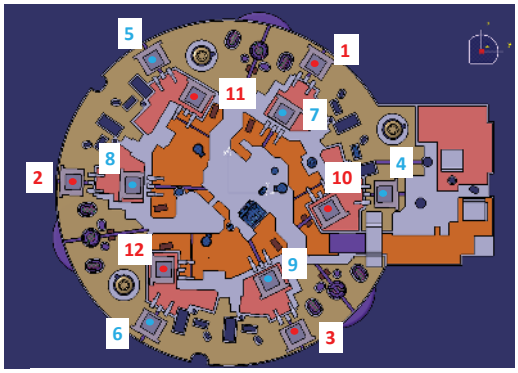

(a) The observations points.

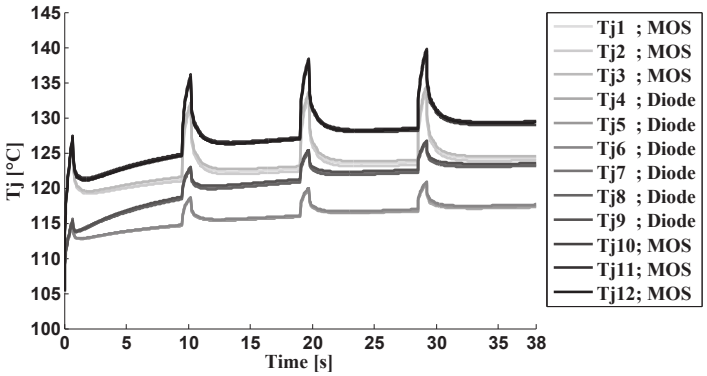

(b) The observed transient junction temperatures (hot spot at point 11).

Figure 4.17. The observed junction temperatures recorded at points located at the top center of the MOS and Diode components; Points 1, 2, 3, 10, 11, 12 for the MOS components and points from 4 to 9 for Diode components.

4.3.2 KIM results

By contrast to the first application in Section 4.2.1, **the KIM identification process in this example is based on the power profiles** for which electronics designers request a ROM. The input vector in the ROM is given by $U = (\mathrm{P_{MOS}}\ \mathrm{P_{Diode}}\ \mathrm{T_{coolant}})^T$ with P_{MOS} and P_{Diode} the power profiles shown in Fig. 4.16 and $T_{coolant}$ the water coolant temperature assumed constant over time of value 105 °C. As it was stated in § 4.1.3, this is possible since no other constant BCs are involved. Otherwise, the BCs should be varied in time into the transient simulation in order to distinguish between their different effects in the ROM. This is, however, outside the scope of this work.

The ROM output identified using only 12 observations, located at the junction of MOS and Diode components, shows significant errors with respect to the reference solution. The relative residual reaches up to 20 % at the hot spot for instance (results not shown here). Actually, the problem being strongly decoupled due the water forced convection, those 12 observation points seem insufficient to well cover the identified frequency range. This fact is illustrated by the modes (pink square markers) in Fig. 4.19 when compared to those identified when $N_{obs} = 71$ observation points are used in the identification procedure. The solution is therefore to consider additional observations points chosen arbitrarily in the proximity to the MOS and Diode components on the substrate, resulting in a total of 71 observation points for instance. Their localisation appears in Fig. 4.18.

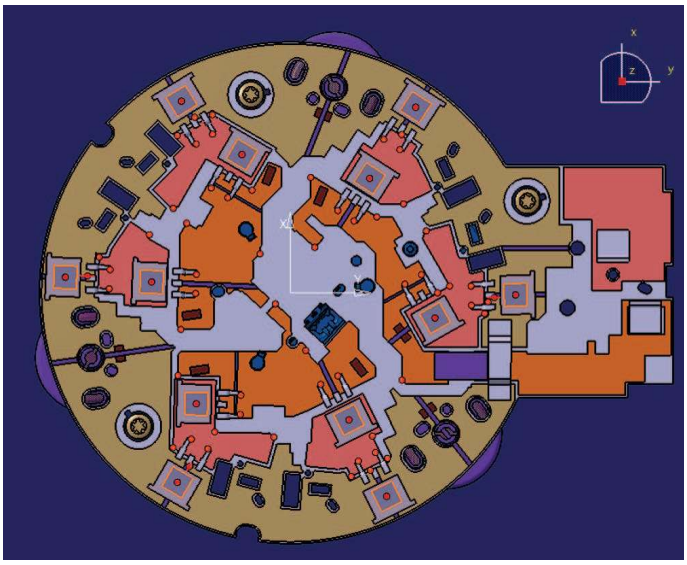

Figure 4.18. The 71 observation points used in KIM identification.

From Fig. 4.19, it should be also noticed that only some modes are retained (up to 8 modes (pink square markers) when 12 observations points are used and 35 modes (blue circle markers) for the 71 observation points) prior to the truncation

step according to the equation (4.12)) in KIM algorithm. The remaining modes are rejected because they exhibit positive eigenvalues, i.e. negative time constants, which lead to unstable model. The row and columns vectors of matrices $\tilde{B}$ and $\tilde{C}$ corresponding to the rejected modes in the diagonal matrix $\tilde{A}$ are also eliminated. It is worth mentioning that the increased number of observation points does not affect the computational time of the transient simulation.

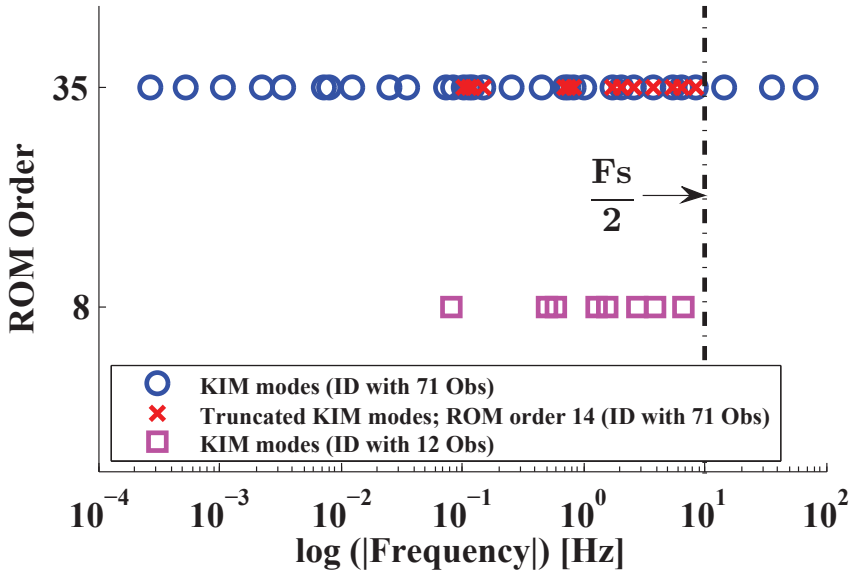

Figure 4.19. Comparison between the modes identified based on 12 observations points on MOS and Diode components (square markers) and those based on 71 observations points (circle markers). The selected ROM corresponds to the truncated modes (cross markers).

In order to check the behaviour of the identified reduced model, we apply the same power profiles depicted in Fig. 4.16. Fig. 4.20 shows the evolution of the relative error (4.13) computed on the estimated temperatures (points from 1 to 12 when $N_{obs} = 71$) when the model order is decreased based on the truncation criterion (4.12). The ROM of order 14 is selected as the error becomes stable from this order (of about 0.46 %). The corresponding modes are presented in red cross markers in Fig. 4.19. A lower order could be acceptable at cost of the error degradation. Fig. 4.21(a) shows the ROM temperature estimation for instance at points 11 (the hot spot on MOS component) and 6 (on Diode component) compared to the transient simulation output at these same points. The corresponding relative residuals starting from the 16^{th} time step defined in (4.14), are also presented in Fig. 4.21(b). The ROM yields good results, in particular at the temperature peaks (Fig. 4.21(a)), which constitute an important information in reliability management. In addition, the relative residuals do not exceed 6.5 % at both points 11 and 6; Fig. 4.21(b)). The targeted application in this study requires a relative residual lower than 10 % which is fully respected by the outputs of the ROM of order 14. A

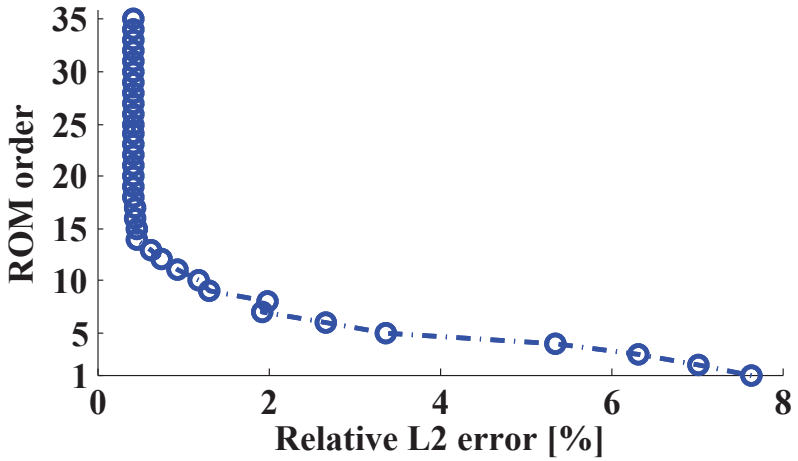

Figure 4.20. Identification relative error (4.13): L2-norm of the discrepancy between the temperatures output of the transient simulation and outputs of ROM located at points 1 to 12 (Fig. 4.17(a)) when $N_{obs} = 71$.

summary of KIM results is given in Table 4.7.

Table 4.7
Summary table of KIM results.

ID input	$U = (\mathrm{P_{MOS}}\ \mathrm{P_{Diode}}\ \mathrm{T_{coolant}})^T$ $\mathrm{P_{MOS}}$ and $\mathrm{P_{Diode}}$: Power profiles ($F_s = 10$ Hz, $T = 0.7$ s) (Fig. 4.16) $T_{coolant} = 105\,^{\circ}\mathrm{C}$: constant BC
Processed frequency band	between 0 and (about $5\Delta f = \frac{5}{T} = 7.14$ Hz or $7\Delta f = \frac{7}{T} = 10$ Hz)
3D simulations time (Hours)	$\simeq 18$
Number of observation points for identification	$N_{obs} = 71$
ROM order	**14**
f_{min} (Hz)	0.10
f_{max} (Hz)	8.59
τ_{min} (s)	0.12
τ_{max} (s)	9.80
L2 relative error ϵ_{L_2} (%)	0.46
Max (relative residual) (%)	6.5

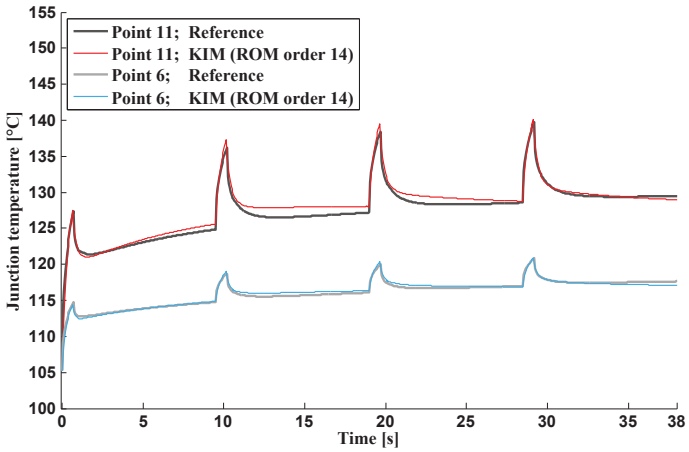

(a) The junction temperature at points 11 and 6.

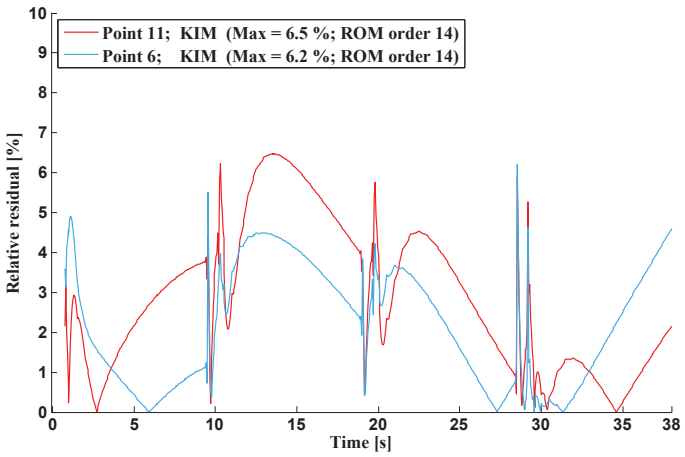

(b) The relative residual between the reference solution and the ROM output.

Figure 4.21. Comparison between the detailed model output (reference) and the ROM (of order 14) output at points 11 (hot spot on MOS component) and 6.

It should be noted that, being interested in only observed temperatures at the junction of MOS and Diode components (output of ROM; Fig. 4.17(a)), the obtained matrices $\tilde{C}$ and $\tilde{D}$ in the ROM of order 14 can be further reduced by selecting only the row vectors corresponding to these points.

4.3.3 Comparison between KIM and Zth methods

The thermal impedance (Zth) method was well described in Chapter 1. In this application, the identification process is as follows:

- the reference temperature is set to the water coolant temperature, i.e. $T_{ref} = T_{coolant} = 105\,^{\circ}\mathrm{C}$,

- the thermal model is reduced to the following points:
  - 1 junction temperature located at point 11 (the hot spot on MOS component).
  - 12 power injection points placed on the MOS and Diode components (power sources from P_4 to P_{15} as shown in Fig. 4.14). Unlike KIM, the other power sources are assumed inactive.
- the reduced model is identified based on step signals applied **in turn** on the 12 power sources. The step amplitude is chosen around the average level of the actual power profile over time. Here, an amplitude of 12 W is applied on the MOS components and 6.8 W on the Diode components,
- 12 transient simulations are carried out, each one taking around 3.3 Hours. Like KIM, all the above transient simulations are initialized from the same steady state results where all the power sources are turned off.

In Fig. 4.22(a), we compare the junction temperature at point 11 produced by the detailed model on the one hand, and the reduced model output produced by KIM (ROM of order 14) and Zth methods at the same point on the other hand. It is clear that KIM produces better results with respect to the Zth method. In addition, Fig. 4.22(b) shows that the Zth relative residual oscillates globally between 8 % and 12.3 % with a 10 % average at the temperature peaks. For KIM, the maximum is 6.5 %. Least but not least, the Zth method in this example underestimate the junction temperature as shown in Fig. 4.22(a), which may be critical in the thermal management of power modules. Nonetheless, we cannot conclude that KIM systematically overestimates the reference solution as this has not been verified on other examples.

Another important point concerns the time cost of the identification process. As it was already stated, the Zth method requires as many detailed model simulations as the number of active power sources considered in the identification step. The comparison of computational time cost for both methods is given in Fig. 4.23 using only one solver. Here, the identification process of KIM is more than 3 times faster than that of the Zth method (18.1 Hours for KIM against 57.4 Hours for Zth method). In fact, KIM takes benefits from the following two features:

- by contrast to the Zth method, KIM is based on a single simulation of the detailed model (3D transient simulation). Hence, KIM is even more favourable as the number of power sources gets higher,
- the power profiles to process in the targeted application are used directly as the identification input together with the BC (here the water coolant temperature $T_{coolant}$). Consequently, the identification (ID) and the validation (VAL) steps

are combined into one same step as it can be noticed in Fig. 4.23. We should mention that the time corresponding to the model identification step with the KIM method does not appear in this figure as it is very small compared to the simulation with the power profiles.

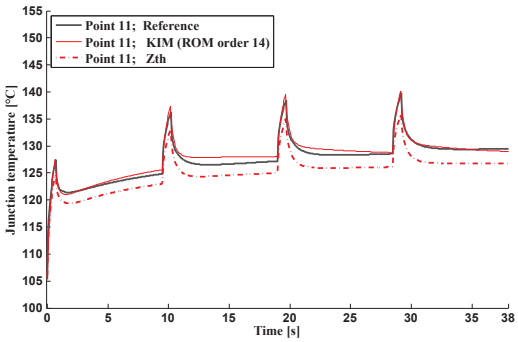

(a) The junction temperature at point 11.

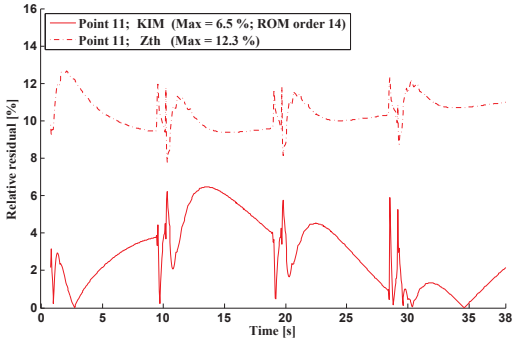

(b) The relative residual in temperature between the reference and the estimation results at point 11.

Figure 4.22. Comparison between KIM and Zth methods at point 11 (hot spot on MOS component).

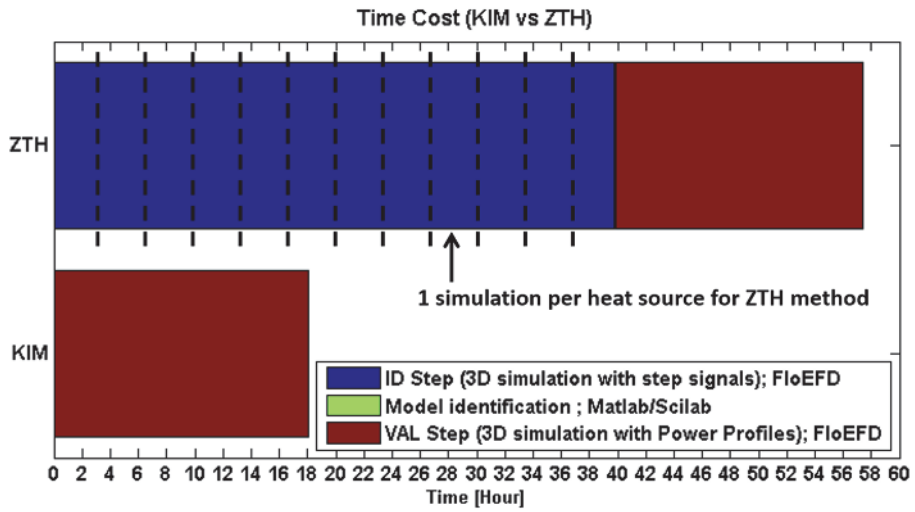

Figure 4.23. Comparison between KIM and Zth methods in computational time cost.

4.3.4 Use of the reduced model produced by KIM

The identified ROM produced by KIM is intended for two application types for the purpose of the power electronics thermal management.

On the one hand, KIM would allow for the use of the reduced model in reliability and lifetime prevision applications that are usually carried out in 0D thermal-electrical like-SPICE simulators. By contrast to the Zth method that provides a transfer function (the thermal impedance), KIM identifies a reduced model in a state space form. Therefore, as a perspective, the state space model should be converted into a transfer function [4] in order to be exploited in the aforesaid applications. The equivalent transfer function can be then transformed into an RC network as we already explained for the Zth method in Section 1.2.3.

On the other hand, the thermal reduced model in the state space form is aimed to be implemented in a system command law for real-time temperature control (the Derating; § 1.1.2). An example of the positioning of the thermal reduced model in a command law of a control process was shown in Fig. 1.5. In the present paragraph, we will focus on the second application, i.e. the real-time control application. In this context, the ROM block in the command part permits to link the junction temperatures located at the most dissipating power sources (MOS and Diode components here) to the thermal inputs including the thermal dissipated on the power components and the water coolant temperature. The final objective through the application is to control in real-time the junction temperatures by adjusting the water coolant temperature. A Simulink demonstrator of the ROM block is given in Fig. 4.24. The procedure consists of two main steps:

- first, an identification process delivers a ROM (here of order 14) based on the thermal input vector given by $U = (\mathrm{P_{MOS}}\ \mathrm{P_{Diode}}\ \mathrm{T_{coolant}})$ with $T_{coolant} = 105\,^{\circ}\mathrm{C}$ a constant BC (Section 4.3.2),

- then, the identified ROM is implemented in the command law to provide an accurate estimation of the temperature variables when the same input vector U is applied except the water coolant temperature that is different from that used to identify the ROM. For instance, the results present in Fig. 4.25 are computed in Simulink demonstrator with the identified ROM of order 14 (Table 4.7) when $T_{coolant}$ is decreased to $90\,^{\circ}\mathrm{C}$.

In order to validate the ROM output computed with $T_{coolant} = 90\,^{\circ}\mathrm{C}$ in Simulink, the same detailed simulation as in Section 4.3.1 is performed except that the water cooling forced convection temperature $T_{coolant}$ is set to $90\,^{\circ}\mathrm{C}$ for both the steady and transient simulations. The comparison between the reference and Simulink results is depicted in Fig. 4.25. In comparison with the ROM behaviour in Fig. 4.21, the ROM computed in Simulink with $T_{coolant} = 90\,^{\circ}\mathrm{C}$ produces greater error level when compared with the associated reference solution at point 11. This is due to the

use of a coolant temperature different from that used to identify the ROM. Even though, the error is still acceptable as the relative residual error does not exceeds 10 %, which complies with the targeted accuracy in this example.

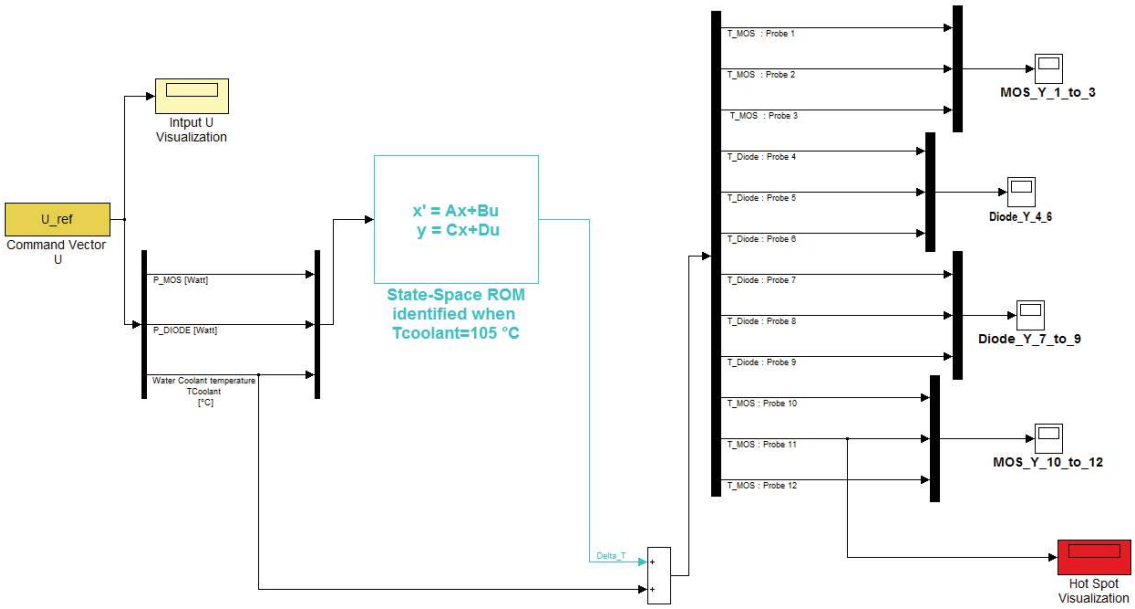

Figure 4.24. A Simulink demonstrator of the use of the ROM identified by KIM in a Derating application.

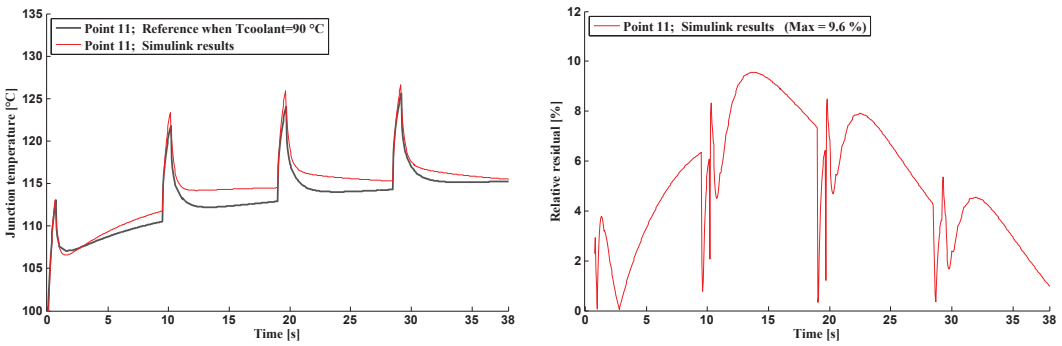

(a) The junction temperature at point 11.

(b) The relative residual in temperature between the reference and the estimation results at point 11.

Figure 4.25. Comparison between reference (detailed model simulation) and Simulink results at point 11 (hot spot on MOS component) when $T_{coolant} = 90\,°\mathrm{C}$. The input used in Simulink is $U = (\mathrm{P_{MOS}}\ \mathrm{P_{Diode}}\ \mathrm{T_{coolant}})$ with $T_{coolant} = 90\,°\mathrm{C}$ a constant BC in the ROM of order 14.

As a perspective, we could also consider the dissipated power as an adjustable variable for the real-time temperature control. In this case, it is essential for KIM to identify the thermal reduced model based on generic power sources signals, i.e. the stimuli and the frequency range. The idea consists in collecting some power profiles intended for some functioning configurations and to analyse the associated spectrum from which an averaged spectrum is deduced. The resulting signals may be linearly time-dependent which can be efficiently handled by KIM as it was demonstrated through the present application. Another possible solution consists in identifying the reduced model based on time delayed power sources signals as it was investigated in the first example in this chapter at the cost of higher computational time, especially for large-scale 3D models.

4.4 Conclusion

In this chapter, we proposed a new method named "Kernel Identification Method" (KIM) enabling the identification of reduced order models of linear thermal systems. The reduced model is identified in a continuous Linear Time Invariant state space form. Designed in a non-intrusive framework, this method is implemented as an offline tool that post-processes the inputs and outputs of a detailed reference model considered as a black-box. The non-intrusive framework is aimed at allowing its implementation independently of the software involved for the simulation of the detailed model. The main features of KIM can be described as follows:

i. ***the identification of the ROM in a modal formulation***, leading to a diagonal state space matrix formed of the dominants eigenvalues (opposite reciprocals of time-constants) of the thermal problem. The ROM then results into decoupled first-order systems, which plays a key role regarding the extension of the proposed method to the identification of non-linear systems, as proven in the next chapter,

ii. ***the identification of the system kernel independently of the excitation, i.e. the input data***. This feature is performed using an orthogonal projection onto the orthogonal space to the row space of the input data matrix built from the dissipated power signals and boundary conditions. Performed by means of a LQ decomposition, the underlying principle of the related orthogonal projection is to virtually suppress the particular solution driven by the input during the identification of the system proper dynamics,

iii. ***the simplicity of its implementation*** because of its combination of well-known algebraic tools, such as the LQ decomposition and the Least-Squares method.

KIM is successfully applied to two application examples: (1) a small-scale linear conduction problem of a Finite Element test case composed of nine dissipating sources and (2) a large-scale water cooled CFD problem mainly governed by forced convection of a Valeo product.

In the first example, KIM is compared to three Subspace approaches (SubSV, SubCVA and MOESP) on two types of dissipated power signals used in the identification step, the time-delayed step signals applied successively on the power components and the uncorrelated random signals applied simultaneously on those components. Both KIM and SubSV show very satisfactory results for both types of signals. The SubCVA and MOESP approaches, however, are more sensitive to the identification signals types, in particular MOESP that shows significant errors when using the time-delayed step signals. In addition, the Subspace method imposes the Persistently Exciting (PE) condition to the identification inputs, which means that they should be linearly independent in time. This condition is also respected by KIM in this first example, but not in the second.

In this second example, the identification and validation steps are combined into one. The power profiles provided by the electronics designers, for which a reduced model has to be produced, are used as input in the identification process. The thermal input also involves the time-independent water coolant temperature as a boundary condition. The main results drawn from this example are first the very satisfactory agreement between the reference and reduced model output. Compared to the Zth method, KIM shows better results in accuracy and time cost in the identification process. By contrast to the Zth method, the computational time of the detailed model in KIM identification process is unaffected by the number of the power sources. This advantage becomes even more efficient when dealing with a high number of heat sources. KIM is robust with regard to the existence of the time-independent water coolant temperature into the thermal input vector. A Simulink demonstrator is implemented in order to insert the reduced model block in the command system part for real-time temperature control. Keeping the reduced model identified by KIM, the water coolant temperature can be modified to keep the junction temperatures with the allowable maximum temperature in the power system part.

In the next chapter, we deal with the extension of KIM for the identification of non-linear reduced order models applicable to configurations dominantly governed by natural convective. Other identification methods are also investigated.

References

[1] T. Katayama. *Subspace methods for system identification*. Springer, 2010.

[2] R. E. Kalman. Mathematical description of linear dynamical systems. *SIAM Journal on Control*, 1:152–192, 1963.

[3] P. Businger and G. H. Golub. *Linear least squares solutions by Householder transformations*. in Wilkinson and Reinsch, Linear Algebra, Springer Verlag, 1971.

[4] E.J. Hannan and M. Deistler. *The statistical theory of linear systems*. John Wiley & Sons Inc., New York, 1988.

Chapter 5

Nonlinear System Identification

This chapter suggests two perspective methods for the identification of reduced models of non-linear thermal systems involving natural convection. The first proposed method deals with an extension of the Kernel Identification Method. This method is of non-parametric nature as it identifies a non-linear reduced model represented in a tabular form without knowing the non-linearity nature. Its behaviour is illustrated on a linear FE test case and is validated for the identification of single input single output reduced models. The second method is based on the Unscented Kalman Filter method. Its behaviour is investigated on both small and large scale test cases. Potential perspectives based on each of these proposed methods will be provided.

Contents

5.1 Introduction

Non-linear system identification methods can be divided into two categories; parametric and non-parametric methods. On the one hand, if the structure of the system model is assumed *a priori*, more specifically if the non-linearity expression is guessed, the identification is parametric. In this category, the identification results in a parameter estimation problem that calls generally for a non-linear optimization problem such as the the Prediction-Error based Methods (PEM) based on ARMA models class. In the non-linear case for example, the polynomial NARMAX model is considered for power electronics systems as shown in [1]. Unfortunately, PEM encounters inherent difficulties for MIMO systems as it was already pointed out in Section 3.2.2. Another optimization-based identification method is the Modal Identification Method (MIM) reviewed in Section 3.2.3. This method deals satisfactorily with non-linear conduction problems based on MIMO reduced state space models. The model (3.33) is an example of a ROM form with a quadratic guessed non-linearity. In non-linear problems involving natural convection, however, the non-linearity nature related to the heat transfer coefficient evolution is difficult to predict *a priori*, as we shall see later. In this case, non-parametric methods, in which any or little *a priori* information is available on the model structure, appear to be more convenient than the first category. An example of a non-parametric method includes step or impulse transient-response analysis such as the thermal impedance method reviewed in Section 1.2. We should mention that the thermal impedance method, also called the Zth method, has proved to be very useful when carefully utilized in some non-linear cases involving temperature-dependent material properties and radiation, but not in the case of natural convection (see Section 1.2.5 for an illustration in natural convection). Another classical non-parametric method is the Volterra series based-method [2] which is a generalization of the linear convolution integral in time domain of non-linear systems. The Volterra-based representation can be also transformed into the frequency domain, which is analogous to linear frequency response analysis in the linear case. For more details on Volterra series, see [3], [4] and the references therein. In practical problems, only a finite Volterra series can be used, referred to as "Truncated Volterra series". In this case, the analysis may become complex when a very high number of Volterra series must be retained to obtain the required accuracy [3].

In this work, we propose two methods for the identification of non-linear systems involving natural convection. Prior to that, we explain the derivation of the non-linear reduced model to be identified from the reference detailed model. After that, we propose a new non-parametric identification method as an extension of the KIM approach, in which the model is represented in a tabular form as a result of several linear reduced models identified for different power levels. In its present state, the method successfully identifies a SISO non-linear state space model. The methodology is illustrated on a non-linear 10-Degrees Of Freedom (DOF) FE model. The next stage for this method, which is out of the scope of this work, should be

addressed to the extension of the above method to the processing of MIMO models. In this context, we also propose another KIM-based method but of semi-parametric nature. The idea consists in: (1) applying the KIM method on the non-linear reference solution produced by the detailed model to identify a linearized behaviour of the non-linear system; (2) selecting some non-linear terms to be considered in the approximation of the non-linear part of the model; (3) performing a classical identification method, such as the least-squares method, to identify the parameters associated to the selected non-linear terms in a polynomial structure. In the last section, we propose a Kalman Filter-based identification method. The 10-DOF FE model is first used in a linear case, i.e. without natural convection, to validate the method in the linear case. We show the difficulties encountered regarding the initialization and the setting of the Kalman parameters in large-scale linear problems. This will enable us to outline some interesting research paths for the method enhancement in the linear case as well as the method extension to the non-linear case by combining it with KIM method.

5.2 The non-linear reference problem and the ROM form

Let us recall the FE model form of a non-linear system cooled by natural convection deduced in (2.58):

$$C_s\dot{\mathbf{T}}_\mathbf{s} + K_s\mathbf{T}_\mathbf{s} - K_{fs}(h)\,\mathbf{T}_\mathbf{s} = Q^{imp} + K_{ff}(h)\,\mathbf{T}_\mathbf{f} \tag{5.1}$$

where C_s and K_s are the heat capacity and the conductivity matrices of dimension $(N \times N)$ with N the number of DOF in the FE model. Thermal properties (thermal conductivity k_s, specific heat c_{p_s} and solid density ρ_s) are assumed temperature- and time-independent. The notation $\mathbf{T_s} = [T_{s_1}(t)\ T_{s_2}(t)\ \ldots\ T_{s_N}(t)]^T$ stands for the nodal temperature vector in the solid domain, $\dot{\mathbf{T}}_\mathbf{s}$ is the time derivative of the this vector. Similarly, $\mathbf{T_f}$ stands for the temperature vector in the fluid domain at the mesh nodes if a finite elements method is used (or eventually at the mesh cells if a finite volume method is adopted). The $(N \times 1)$ operator Q^{imp} designates the source vector of dimension N. The coupling operators $K_{fs}(h)$ and $K_{ff}(h)$ are linear functions of the heat transfer coefficient h as this can be noticed through (2.56). Recall that for the resolution of the solid problem, the heat transfer coefficient depends, in turn on the solid temperature $\mathbf{T_s}$, i.e. $h = h(\mathbf{T_s})$ (see § 2.5.1. If the meshes that approximate the solid and the fluid domains are coincident through the solid-fluid interface, we can write $K_{ff}(h) = -K_{fs}(h) = h(\mathbf{T_s})\,\mathcal{L}$ with $\mathcal{L}$ denoting a $(N \times N)$ constant matrix. Substituting this latter into (5.1) yields

$$\dot{\mathbf{T}}_\mathbf{s} = -C_s^{-1}K_s\mathbf{T_s} - C_s^{-1}\mathcal{L}h(\mathbf{T_s})(\mathbf{T_s} - \mathbf{T_f}) + C_s^{-1}Q^{imp} \tag{5.2}$$

This model can be transformed in a non-linear state space model linking Y to U as follows:

$$\begin{cases} \dot{\mathbf{T}}_\mathbf{s} = A_{NL}\left(\mathbf{T}_\mathbf{s}\right) + B_{NL}\left(\mathbf{T}_\mathbf{s}, U\right) & \text{(5.3a)} \\ \tilde{Y} = C\mathbf{T}_\mathbf{s} & \text{(5.3b)} \end{cases}$$

with

$$A_{NL}\left(\mathbf{T}_\mathbf{s}\right) = -C_s^{-1}K_s\mathbf{T}_\mathbf{s} - C_s^{-1}\mathcal{L}h\left(\mathbf{T}_\mathbf{s}\right)\mathbf{T}_\mathbf{s}$$

and

$$B_{NL}\left(\mathbf{T}_\mathbf{s}\right) = C_s^{-1}\mathcal{L}h\left(\mathbf{T}_\mathbf{s}\right)\mathbf{T}_\mathbf{f} + C_s^{-1}Q^{imp}$$

.

In (5.3), U is the $(N_{ex} \times 1)$ vector grouping the thermal inputs, the dissipated power (or eventually power densities) and the boundary conditions. In a natural convection problem, the boundary conditions may concern some temperature of fluid stream in the proximity to the solid interface. The matrix C of dimension $(N_{obs} \times N)$ with $N_{obs} \leq N$, permits to select a part or the whole solid temperature $\mathbf{T}_\mathbf{s}$, and this selection is gathered into the $(N_{obs} \times 1)$ output vector Y.

One can notice that rather than assuming a single non-linear operator in $\mathbf{T}_\mathbf{s}$ and U, two non-linear operators are instead considered, A_{NL} and B_{NL} non-linear functions of $\mathbf{T}_\mathbf{s}$, and $\mathbf{T}_\mathbf{s}$ and U, respectively. The reason behind this choice is that the proposed non-linear identification methods in this work are based on the KIM approach. This latter, in fact, allows to identify the kernel of the thermal problem (the homogeneous solution) independently of the input excitation. We shall see later more details on the non-linear identification KIM-based methods.

The non-linearity of A_{NL} and B_{NL} in $\mathbf{T}_\mathbf{s}$ is related to the variation of the heat transfer coefficient throughout the transient simulation in natural convection problem. The operator B_{NL} include the coupling between the input and the solid temperature. Besides, if an electrical non-linear behaviour is involved, B_{NL} also includes a non-linearity in U. In fact, the law of the power dissipated by Joule effect in power components (semiconductors) may vary over time in transient simulations due to semiconductor saturation for example.

System (5.3) is the reference detailed model of order N. Based on the form of the reference model, we assume the following form for the reduced order model (ROM) of order $n \ll N$ (the ROM derivation based on reduced basis change is described in Section 3.2.1):

$$\begin{cases} \dot{X} = \tilde{A}_{NL}\left(X\right) + \tilde{B}_{NL}\left(X, U\right) & \text{(5.4a)} \\ \tilde{Y} = \tilde{C}_{NL}\left(X\right) + \tilde{D}U & \text{(5.4b)} \end{cases}$$

with

$$\begin{cases} \tilde{A}_{NL}(X) & = & V^T(X)\ A_{NL}(V(X)X) \\ \tilde{B}_{NL}(X,U) & = & V^T(X)\ B_{NL}(V(X)X,U) \\ \tilde{C}_{NL}(X) & = & CV(X) \\ \tilde{D} & & \text{a static correction} \end{cases} \tag{5.5}$$

In (5.5), X is the $(n \times 1)$ reduced state variable and $V(X) \in \mathbb{R}^{(N \times n)}$ the reduced basis change composed of a set of non-linear modes from an intrusive point of view. It should be noted that this reduced basis may also consist of linear modes, i.e. $V(X) = V$, in which the non-linear modes are represented by a combination of the linear modes. This results then in an invariant observation matrix, $\tilde{C}_{NL} = \tilde{C}$. Note the $(N_{obs} \times N_{ex})$ constant added matrix $\tilde{D}$ in the observation equation (5.4b), the static gain matrix, contributing to a static correction to the ROM approximation as in the linear case.

In order to identify the ROM in (5.4), a parametric method would guess *a priori* the nature of the non-linearity in $\tilde{A}_{NL}$, $\tilde{B}_{NL}$ (and eventually $\tilde{C}_{NL}$) in the reference model (5.3). In natural convection, this is more complicated. Actually, as it was already stated in Chapter 2, Section 2.5.1, the heat transfer coefficient h in natural convection depends on the Grashof number Gr, which is in turn a linear function of the temperature difference between the solid and the fluid along the interface. The relationship between h and Gr generally depends on the geometry and flow conditions of the model (see § 2.5.1. For instance, the example given in (2.45) applied to a laminar flow over a flat plate shows that h is function of $G_r^{1/4}$. Therefore, we propose a non-parametric method as an extension of KIM.

5.3 Non-parametric Extended Kernel Identification Method

In this section, we propose a non-parametric KIM-based identification method of non-linear models involving natural convection. We attempt to identify a reduced model represented in a tabular for.

5.3.1 The method principle

The non-linear identification method proposed in this section aims at identifying a non-parametric reduced model in the form:

$$\begin{cases} \dot{X} = \tilde{A}_{NL}(X) + \tilde{B}_{NL}(X)\,U & \text{(5.6a)} \\ \tilde{Y} = \tilde{C}X + \tilde{D}U & \text{(5.6b)} \end{cases}$$

The model (5.6) constitutes a particular case of that presented in (5.4). In the identification process, the model (5.6) is represented in a tabular form. Actually,

based on the observed temperature issued from the reference non-linear model, the KIM approach is used to identify as much linear reduced models as the number of power levels carefully chosen to cover different operating points of the system. The linear ROM identified for a power level $\phi_i, i = 1, \cdots, N_p$ is noted (A^i, B^i, C^i, D^i). Below are the assumptions imposed on the proposed ROM form (5.6):

- the operators $\tilde{C}$ and $\tilde{D}$ in the observation equation (5.6b) are assumed full invariant matrices. This means that the non-linearity here does not influence the spatial dependence of the thermal flux,

- the operators $\tilde{A}_{NL}$ and $\tilde{B}_{NL}$ in the state equation (5.6a) are **non-linear functions of the state vector X identified in a tabular form**. We shall see later the methodology illustrated on a 10-DOF FE model,

- the non-linear operator $\tilde{A}_{NL}$ is assumed a diagonal matrix in which the ith diagonal element, i.e. the opposite inverse of the ith time-constant, is expressed as a function of the associated ith variable in the state vector X_i. The matrix form is defined as follows:

$$\tilde{A}_{NL} = \begin{pmatrix} -\dfrac{1}{\tau_1(X_1)} & & \\ & \ddots & \\ & & -\dfrac{1}{\tau_n(X_n)} \end{pmatrix} \tag{5.7}$$

- the non-linear function $\tilde{B}_{NL}$ is a full matrix. The elements of the ith row vector are expressed as functions of the associated ith variable in the state vector X_i. The coupling terms between the model state and the input are not considered, at least in the present state of the method.

As a result of the assumed ROM structure (5.6) together within the modal form adopted in KIM, the non-linear model is made up of a reduced number of decoupled first-order systems. We should also mention that this is possible thanks to the modal form adopted in the KIM approach.

In a first stage, we should mention that in comparison with the KIM algorithm on page (116) in a linear problem, the positive terms in the state matrix as well the corresponding row and column vectors in the observation and command matrices of each linear ROM are not eliminated. In addition, the modes are arranged based on the criterion in (4.12) but are not truncated. Once the linear reduced models are identified while considering the aforementioned points, hereafter are the next steps in the identification process:

1. **Modes Tracking based on the Modal Assurance Criterion (MAC)**. This technique, commonly used in mechanical dynamics [5], consists in associating modes, i.e. column vectors in observation matrix in each linear ROM, between them for different power levels. In fact, for a given power level ϕ_1 the identified modes would be $\lambda_{i_{\phi_1}}(\phi_1)$ and for another power level ϕ_2 the identified modes would be $\lambda_{i_{\phi_2}}(\phi_2)$ and i_{ϕ_1} need not be equal to i_{ϕ_2}. The MAC [6] here provides a measure, varying between 0 and 1, of the correlation between mode shapes from different power levels. The modes with the highest MAC value (near 1) are considered as corresponding mode shapes in the different linear ROMs. The MAC expression is given by:

$$\mathrm{MAC}\left(\mathrm{C}^{\phi_1}_{\mathrm{i}_{\phi_1}}, \mathrm{C}^{\phi_2}_{\mathrm{i}_{\phi_2}}\right) = \frac{\left({}^tC^{\phi_1}_{i_{\phi_1}}\ C^{\phi_2}_{i_{\phi_2}}\right)^2}{\left({}^tC^{\phi_1}_{i_{\phi_1}}\ C^{\phi_1}_{i_{\phi_1}}\right)\ \left({}^tC^{\phi_2}_{i_{\phi_2}}\ C^{\phi_2}_{i_{\phi_2}}\right)} \tag{5.8}$$

   where:

$$\begin{cases} C^{\phi_1}_{i_{\phi_1}} \text{ the } i_{\phi_1}\text{th column vector in matrix } \tilde{C} \text{ for a power level } \phi_1 \\ C^{\phi_2}_{i_{\phi_2}} \text{ the } i_{\phi_2}\text{th column vector in matrix } \tilde{C} \text{ for a power level } \phi_2 \end{cases}$$

2. **Analysis of the evolution of the state variables and the operators parameters with the power levels**.

3. **Determine the dependence of the time-constants and the terms in the command matrix with the state variables according to the values** $(\min(X) + \max(X))/2$ **computed in each block, i.e. for each power level**. In order to establish those dependences, the evolution of the state variables along with the total time **should be strictly monotonous**.

4. **Truncation of the linear ROMs all at the same order** such that the error in the sense of least squares verifies $\epsilon_{L_2} \leq \epsilon_{max}$ (Eq. 4.13). Note that we can further truncate those linear ROMs so that the associated observation matrices are composed of only orthogonal modes. This can be verified through the MAC values.

5. **Resolution of the non-linear reduced model** (5.6) **by means of a numerical integration method** in which the function $\tilde{A}_{NL}(X)$ and $\tilde{B}_{NL}(X)$ are provided in a tabular form.

5.3.2 Illustration on a non-linear 10-DOF FE model

The FE model

A thermal transient problem is investigated and described by a FE model of dimension N. A transient dissipated power signal $\phi\, u(t)$ composed of N_p successive steps is applied on the DOF 1 with ϕ_k the kth power level and $u_k(t)$ the associated unitary signal at the time interval $[t_k\ t_{k+1}], k = 1, \cdot, N_p$ (Fig. 5.1(a)). The power vector of dimension N is written as $Q^{imp} = [\phi\, u(t)\ 0\ \cdots\ 0]^T$. The model is non-linear due to the presence of natural convection assumed localized at DOF number 10. Thus, the operators $K_{fs}(h)$ and $K_{ff}(h)$ present in (5.1) can be simplified to:

$$K_{ff}(h) \;=\; -K_{fs}(h) \;=\; h\mathcal{L} \;=\; h \begin{pmatrix} 0 & \cdots & 0 \\ \vdots & & \vdots \\ 0 & \cdots & 0 \\ 0 & \cdots & 1 \end{pmatrix}_{10\times 10} \tag{5.10}$$

Thereafter, we omit the subscript $_s$ for sake of simplicity. If we assume the fluid to be at ambient temperature at DOF 10, i.e. $T_f = T_a$, and substitute (5.10) in 5.1, we obtain:

$$C\dot{\mathbf{T}} + K\mathbf{T} + \mathcal{L}h\,(\mathbf{T} - T_a) \;=\; Q^{imp} \tag{5.11}$$

Here, we assume a linear function of the heat transfer coefficient h in the solid temperature localized at the 10th DOF given by:

$$h \;=\; h_0 + aT_{10} \tag{5.12}$$

where h_0 and a are constant coefficients and T_{10} the temperature at the DOF number 10. Replacing (5.12) in the model (5.11) gives the following reference FE model:

$$C\dot{\mathbf{T}} + K_{LIN}\mathbf{T} + K_{NL}(\mathbf{T}) \;=\; F \tag{5.13}$$

with:

$$\begin{cases} C = \rho\ c_p \begin{pmatrix} 1 & & \\ & \ddots & \\ & & 1 \end{pmatrix}\ ,\ K_{LIN} = k \begin{pmatrix} 2 & -1 & & 0 \\ -1 & 2 & \ddots & \\ & \ddots & \ddots & -1 \\ 0 & & -1 & 1 + \dfrac{h_0}{k} \end{pmatrix} & : (\mathrm{N} \times \mathrm{N})\ \text{matrices} \\ K_{NL}(\mathbf{T}) = \mathcal{L}\,(aT_{10} - aT_a)\,\mathbf{T}\ ,\ F = \left(Q^{imp} + Q^{conv}\right) & : (\mathrm{N} \times 1)\ \text{vectors} \\ Q^{imp} = [\phi\, u(t)\ 0\ \cdots\ 0]^T\ ,\ Q^{conv} = [0\ \cdots\ 0\ h_0 T_a]^T & : (\mathrm{N} \times 1)\ \text{vectors} \end{cases}$$

In the non-linear operator $K_{NL}(\mathbf{T})$, we note the quadratic non-linearity in $\mathbf{T}$, and the coupling term $T_a\mathbf{T}$ between the input, through the boundary condition,

and the reference problem states. In the non-linear reduced model (5.6), the former would be approximated by $A_{NL}(X)$ and the latter through $B_{NL}(X)U$ with U the $(N_{ex} \times 1)$ vector of the thermal inputs, $U = [\phi\, u(t)\ \ T_a]^T$.

Results and discussion

A special case is assumed by imposing $a = 0.1$ Wm^{-2}, $h_0 = 0$ Wm^{-2} °C^{-1} and $T_a = 0$ °C. This means that only the quadratic non-linearity related to natural convection is considered, i.e. the linear part $\mathcal{L}(aT_a)\,\mathbf{T}$ is a null matrix in K_{NL} (5.13). In addition, in its present state, the method has been investigated for single input single output (SISO) model, i.e. $N_{ex} = N_{obs} = 1$. The thermal input vector consists of the power signal $U(t) = \phi\, u(t)$. This latter is composed of $N_p = 6$ power levels with $\phi = [1\ 5\ 10\ 15\ 20\ 25]$ (W) over a total time $t = 165$ s discretized in $N_{snap} = 12376$ time steps (Fig. 5.1(a)). The observed temperature is localized at one DOF of the detailed model (5.13). Hence, $N_{obs} = 1$, which means that we can identify a ROM, $(A^i = a_i, B^i = b^i, C^i = c^i, D^i = d^i)$, of order up to $n = 1$ since we have $n = 1 <= N_{obs}$ in KIM method (see Section 4.1). In addition, we are concerned with a SISO model as only one thermal input is applied on the FE model (at DOF 1), i.e. $N_{ex} = 1$,. For each power level $\phi_i, i = 1, \cdots, N_p$, with N_p denoting the number of power levels, we obtain a linear ROM $(A^i = a_i, B^i = b^i, C^i = c^i, D^i = d^i)$ in which matrix C_i is the unity. Let consider the observed temperature at DOF 8 as a reference solution given in Fig. 5.1(b).

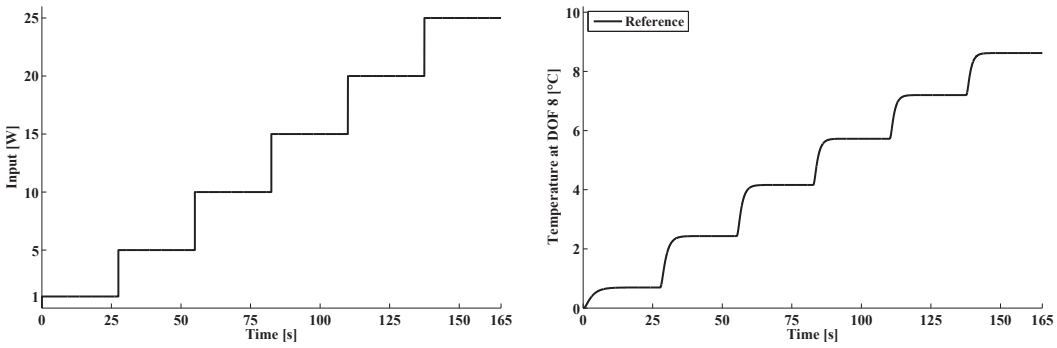

(a) Input signal applied at DOF 1 composed of $N_p = 6$ power levels.

(b) Reference solution observed at DOF 8.

Figure 5.1. Input-output data for the identification of the non-linear 10-DOF FE model (5.13) ($a = 0.1$ Wm^{-2}, $T_a = 0$ °C and $h_0 = 0$ Wm^{-2} °C^{-1}).

Fig. 5.2 depicts the evolution of a^i, $\tau^i = -1/a^i$, b^i and d^i with the power level ϕ. From Fig. 5.2(d), we can see the very low values of d^i, of order $\simeq 10^{-4}$. In addition, the contribution of $\tilde{D}U$ is then negligible with respect to both terms $\tilde{C}X$ and $\tilde{B}U$. Hence, the matrix $\tilde{D}$ is assumed invariant and fixed at value $\simeq 3.77\ 10^{-4}$. This is consistent with the choice of the non-linear ROM form in (5.6). **In what follows,**

the last identified value of matrix $\tilde{D} = d$, obtained in the ROM identified with power level $\Phi = 25$ s, will be used in the non-linear model (5.6). By contrast to the matrix $\tilde{D}$, the terms a^i and b^i, given in Figs. 5.2(a) and 5.2(c), show greater variation with the input power levels. The evolution of τ^i, depicted in Fig. 5.2(b), is deduced from that of the a^i such that $\tau^i = -1/a^i$. We also present the state variables identified in each time interval, which results in the global state variable evolution with time given in Fig. 5.3. In order to deduce the non-linear operators $\tilde{A}_{NL}(X) = -1/(\tau(X))$ as well as $\tilde{B}_{NL}(X)$, it is essential that the identified state variable be strictly monotonous which is the case as this can be noticed from Fig. 5.3. The dependence of the time-constants and matrix $\tilde{B}_{NL}$ are given in Figs. 5.4(a) and 5.4(b), respectively. In order to check the behaviour of the identified non-linear reduced model, we apply the same signal used in the identification step given in Fig. 5.1(a). The matrix $\tilde{D} = d$ in this non-linear reduced model is assumed constant and takes an almost null value identified for the last power level ($d = -3.77\ 10^{-4}$). In Fig. 5.5(a), we compare the evolution with time of the temperature at DOF 8 produced by the 10-DOF model and **the linear ROM identified by KIM over the whole time interval** on the one hand, and **the non-linear ROM** (5.6) **identified on the 6 time intervals**. The associated absolute residuals are given in Fig. 5.5(b). We can see that the linear ROM provides a linearized behaviour of the problem while the non-linear ROM gives very satisfactory results (an absolute residual has a maximum of $0.2428\,^{\circ}\mathrm{C}^{-1}$).

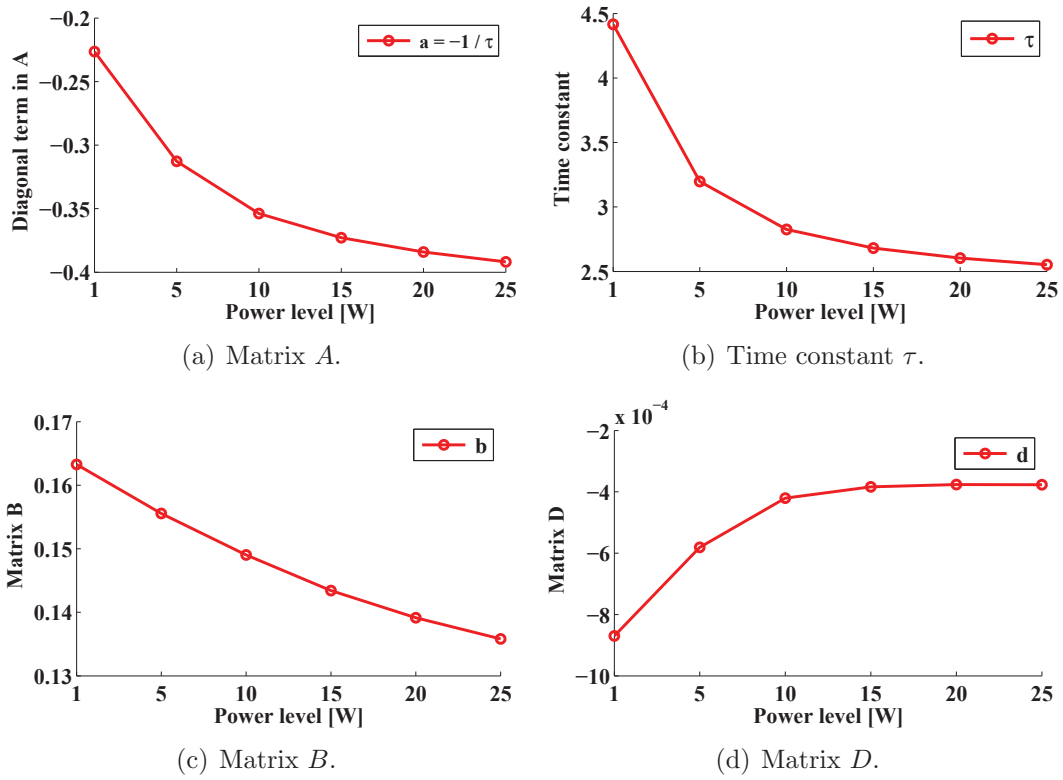

(a) Matrix A.

(b) Time constant τ.

(c) Matrix B.

(d) Matrix D.

Figure 5.2. Evolution of the matrices terms in the linear identified ROMs with the power level of input $\phi = \{\phi_i\}, i = 1, \cdots, 6$.

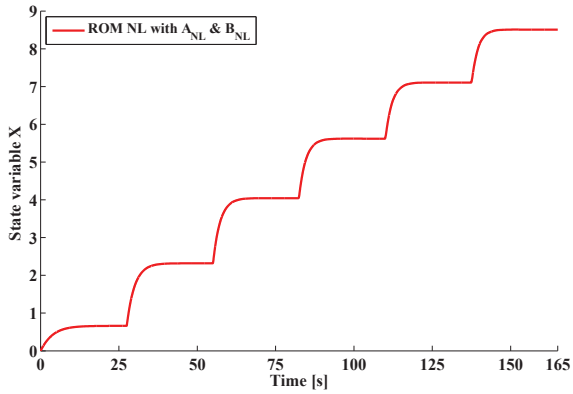

Figure 5.3. Identified state variable X resulting from those obtained over the 6 time intervals with 6 different power levels.

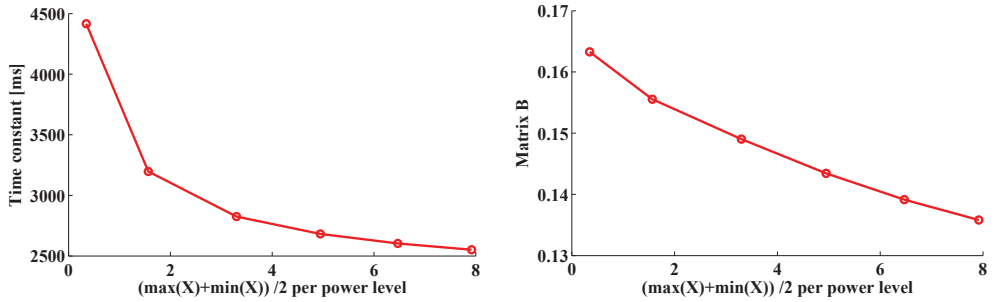

(a) Dependence of the time-constant on the state variable, i.e. $\tau(X)$; matrix $\tilde{A}_{NL}$ is defined as $\tilde{A}_{NL}(X) = -1/(\tau(X))$.

(b) Dependence of the command matrix with the state variable, i.e. $\tilde{B}_{NL}(X)$.

Figure 5.4. Identified non-linear ROM (5.6); $\tilde{A}_{NL}$ and $\tilde{B}_{NL}$ state variable X, $\tilde{C}$ unity matrix and $\tilde{D}$ invariant matrix of value $\simeq 3.77\ 10^{-4}$.

In Figs. 5.5(a) and 5.5(b), we also present the output of the non-linear ROM having a particular form. In this latter, only $\tilde{A}_{NL}(X)$ is considered while the command matrix is assumed constant and takes the values identified for either the first or the last power level, $B = B^1$ and $B = B^6$, respectively. The results show the contribution of the non-linear operator $\tilde{B}_{NL}(X)$ in the non-linear ROM. For instance, the non-linear ROM output when $\tilde{B}_{NL}$ is set to the first identified value B^1 shows a significant error (green dashed-dotted curve in Figs. 5.5(a) and 5.5(b)).

We should note that the extended KIM method has been also performed on the DOF 1, a collocated point with the power source. The non-linear ROM (5.6) shows good results (not shown here) as well and confirms the conclusion regarding the command matrix stating that its dependence to the state variable clearly contributes to the non-linear ROM.

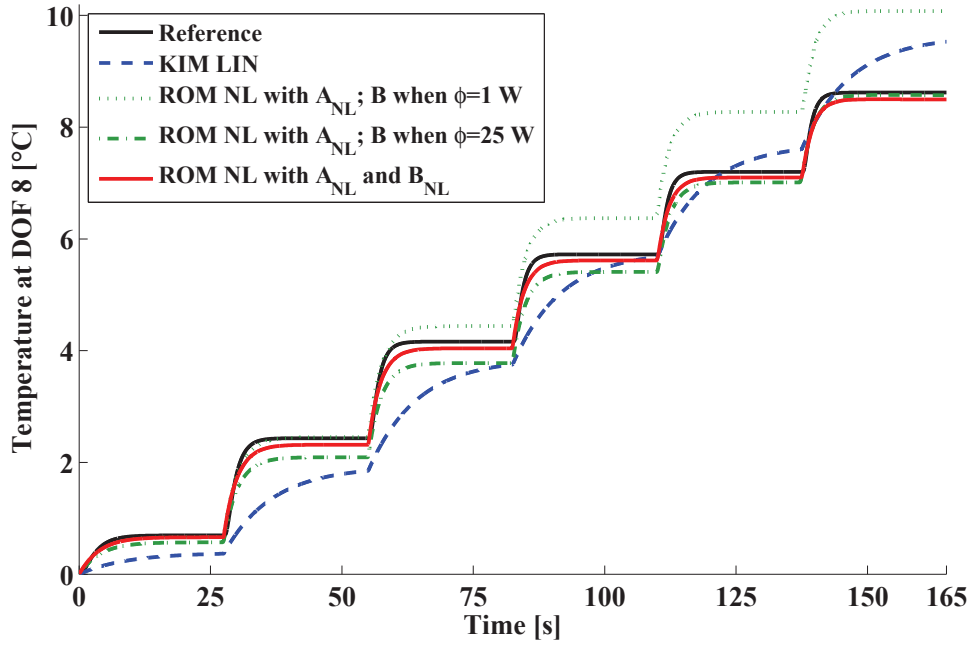

(a) Temperature at DOF 8.

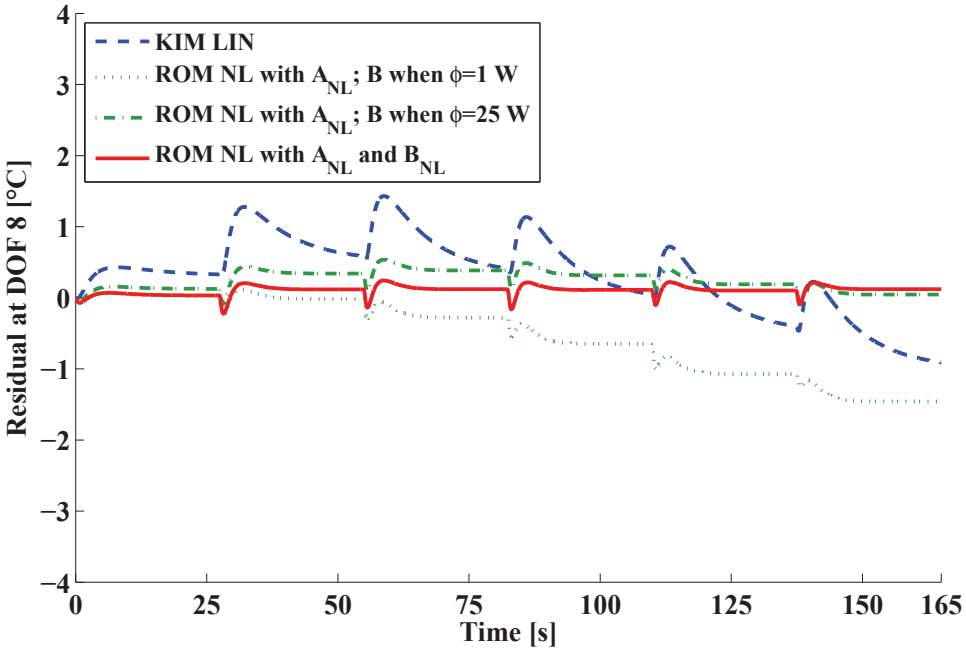

(b) Absolute residual between the reference and the ROM output at DOF 8.

Figure 5.5. Comparison between the reference model (solid black line) and the linear ROM identified by KIM, on the one hand, and the non-linear ROM identified by the non-parametric extended KIM.

5.3.3 Synthesis and perspectives

An extended KIM approach for the identification of non-linear problems governed by natural convection is proposed. The method is of non-parametric nature as it identifies a non-linear reduced model represented in a tabular form without knowing the non-linearity nature. This method calls as much KIM approach as the number of power levels investigated to cover different operating points of the system. The result method is evaluated on a 10-DOF FE model and successfully identifies a non-linear single input single output reduced model. In this case, only the state and command matrices are assumed dependent on the state variable whereas the observation and static matrices are assumed invariant. We should note that the reduced model behaviour is checked by applying the same input signal as the one used for the identification. Thus, prior to the use of the reduced model, it is essential to verify its validity for an excitation other than the one used for the identification. We should note that in order to obtain a fine estimation of the non-linear operators dependencies in the non-linear reduced model, it is essential to perform KIM on small time intervals. Nevertheless, as the KIM method is based on the least-squares method, these time intervals should respect a minimum length that depends on the number of the parameters to identify. In fact, the minimum length becomes larger as the number of observation points as well as the number of inputs involved in the identification step increases.

Future work should address the extension of the method to the processing of multiple-input multiple-output models. For this purpose, the non-linear reduced model form should be re-established to consider other dependency on the state and/or input variables of the model operators. We propose below another interesting research path regarding the identification of MIMO models based on the KIM approach as well.

Non-linear semi-parametric KIM-based method In a parametric identification method, the nature of a non-linear model is assumed *a priori* and the whole associated non-linear terms are considered in the identification process. The model (3.33) is an example of a ROM form with a quadratic guessed non-linearity. In non-linear problems involving radiative heat transfer, however, higher non-linear order terms, i.e. fourth order, should be considered. Consequently, the identification process results in an excessively computational time and may encounter convergence problems because of the high number of parameters to identify. Moreover, as we have already stated above, in non-linear problems involving natural convection, the non-linearity nature is difficult to predict *a priori* because of the dependence of the heat transfer coefficient on the model geometry and flow conditions. The original idea in the proposed method first consists in detecting the non-linear terms that have to be considered in the non-linear part of the reduced model, along with the characterisation of the involved non-linearity. Then, the identification process follows. Based on this idea, we refer this approach as a semi-parametric identification method. Below,

we develop the principle of this perspective method.

Let us consider a non-linear system with three inputs and two outputs described by a non-linear state-space reduced model of order $n = 3$ as follows:

$$\begin{cases} \begin{Bmatrix} \dot{X}_1 \\ \dot{X}_2 \\ \dot{X}_3 \end{Bmatrix} = \tilde{A} \begin{Bmatrix} X_1 \\ X_2 \\ X_3 \end{Bmatrix} + \tilde{B} \begin{Bmatrix} U_1 \\ U_2 \\ U_3 \end{Bmatrix} + \begin{Bmatrix} \alpha_1 X_1^2 + \alpha_2 X_1^2 U_1 U_3 \\ \beta U_1^2 \\ \gamma X_2^2 \end{Bmatrix} & \text{(5.15a)} \\ \begin{Bmatrix} \tilde{Y}_1 \\ \tilde{Y}_2 \end{Bmatrix} = \tilde{C} \begin{Bmatrix} X_1 \\ X_2 \\ X_3 \end{Bmatrix} + \tilde{D} \begin{Bmatrix} U_1 \\ U_2 \\ U_3 \end{Bmatrix} & \text{(5.15b)} \end{cases}$$

where $X = [X_1, X_2, X_3]^T$ is the state variable of the reduced model, $\dot{X}$ the drivative of X with time, $U = [U_1, U_2, U_3]^T$ the input vector and $\tilde{Y} = \left[\tilde{Y}_1, \tilde{Y}_2\right]^T$ an approximation of the reference solution produced by a non-linear detailed model of the system under study. The matrices $\tilde{A}$, $\tilde{B}$, $\tilde{C}$, $\tilde{D}$, of appropriate dimensions, define the linear part of the reduced model. We should note that in the identification process, the non-linear terms present in the state equation (5.15a), together with the linear part, are unknown. The model (5.15) is only given to expose the proposed method principle. To begin with, as proceeded in KIM approach (Section 4.1), we substitute $\dot{X}$ by (5.15a) into the derivative of the observation equation (5.15b). Hence, we obtain:

$$\begin{Bmatrix} \dot{\tilde{Y}}_1 \\ \dot{\tilde{Y}}_2 \end{Bmatrix} = \tilde{C}\tilde{A} \begin{Bmatrix} X_1 \\ X_2 \\ X_3 \end{Bmatrix} + \tilde{C}\tilde{B} \begin{Bmatrix} U_1 \\ U_2 \\ U_3 \end{Bmatrix} + \tilde{C} \begin{Bmatrix} \alpha_1 X_1^2 + \alpha_2 X_1^2 U_1 U_3 \\ \beta U_1^2 \\ \gamma X_2^2 \end{Bmatrix} + \tilde{D} \begin{Bmatrix} \dot{U}_1 \\ \dot{U}_2 \\ \dot{U}_3 \end{Bmatrix} \tag{5.16}$$

In a first step, the linear KIM approach is applied on the non-linear reference solution to obtain a linearized behaviour of the system. This approximation corresponds to the linear part in (5.16):

$$\begin{Bmatrix} \dot{\tilde{Y}}_1 \\ \dot{\tilde{Y}}_2 \end{Bmatrix} = \tilde{C}\tilde{A} \begin{Bmatrix} X_1 \\ X_2 \\ X_3 \end{Bmatrix} + \tilde{C}\tilde{B} \begin{Bmatrix} U_1 \\ U_2 \\ U_3 \end{Bmatrix} + \tilde{D} \begin{Bmatrix} \dot{U}_1 \\ \dot{U}_2 \\ \dot{U}_3 \end{Bmatrix} \tag{5.17}$$

The residual dR defined as the difference between the derivative of the reference observation and the derivative of the linearized reduced model output is given by:

$$[dR\,(t)]_{2\times N_{snap}} = \begin{Bmatrix} dR_1\,(t) \\ dR_2\,(t) \end{Bmatrix}_{2\times N_{snap}} = \tilde{C}_{2\times 3} \begin{Bmatrix} \alpha_1 X_1^2 + \alpha_2 X_1^2 U_1 U_3 \\ \beta U_1^2 \\ \gamma X_2^2 \end{Bmatrix}_{3\times N_{snap}} \tag{5.18}$$

or, equivalently:

$$\left[\left(\tilde{C}\right)^{\dagger} dR\left(t\right)\right] \;=\; \left\{\begin{matrix} dR_1\left(t\right) \\ dR_2\left(t\right) \end{matrix}\right\}_{3\times N_{snap}} \;=\; \left\{\begin{matrix} \alpha_1 X_1^2 + \alpha_2 X_1^2 U_1 U_3 \\ \beta U_1^2 \\ \gamma X_2^2 \end{matrix}\right\}_{3\times N_{snap}} \tag{5.19}$$

where $\left(\tilde{C}\right)^{\dagger}$ denotes the pseudo-inverse of the constant observation matrix identified by the linear KIM method. Let us denote

$$dR^c \;=\; \left(\tilde{C}\right)^{\dagger} dR \tag{5.20}$$

the $(3 \times N_{snap})$ left-hand term in (5.19).

The second step consists in determining which of the state and input variables have to be considered in the identification of the residual dR^c. For this purpose, we first normalize the operator dR^c and the state and input variables, $V = X$ or $V = U$:

$$dr_j^c \;=\; \frac{dR_j^c}{\sqrt{{}^t dR_j^c \; dR_j^c}} \quad j = 1,2,3$$

$$v_i \;=\; \frac{V_i}{\sqrt{{}^t V_i \; V_i}} \quad i = 1,2,3$$

A logarithm-based indicator W is then computed as follows:

$$W_{ji} \;=\; W\left(dR_j^c, V_i\right) \;=\; {}^t \log\left(r_j^c\right) \; \log\left(v_i\right) \quad i,j = 1,2,3 \tag{5.21}$$

Based on this indicator, we can conclude that the more W_{ji} tends towards an integer value m, the more V_i contributes to the operator dR_j^c within the power m. For instance in the model (5.19), assume we have $W\left(dR_1^c, X_1\right) = 2$, $W\left(dR_1^c, U_1\right) = 1$ and $W\left(dR_1^c, U_3\right) = 1$. In this case, the identification of the term dR_1^c should be focused on the following non-linear terms: X_1^2, $X_1^2 U_1$, $X_1^2 U_3$, $X_1^2 U_1 U_3$ and $U_1 U_3$. Let us denote these non-linear terms by $T_{NL,i}$.

Remarks:

- We should note that the logarithm-based indicator (5.21) has not been tested yet. In fact, further development regarding the choice of the norm used to normalize dR^c, X and U should be investigated to ensure (1) the domain of definition of the logarithm function in (5.21) (2) values greater than 1 for the normalized variables dr^c and v, which means positive values for the indicator W_{ji}.

- In the above example, if instead we have $W\left(dR_1^c, X_1\right) = 2.5$, then both variables X_1^2 and X_1^3 should be taken into account in the non-linear terms selection. Thus, X_1^3 $X_1^3 U_1$, $X_1^3 U_3$ and $X_1^3 U_1 U_3$ are the additional non-linear terms to be considered in $T_{NL,i}$. The selection should be then refined in the following step.

The third step, aims at further reducing the number of the selected non-linear terms above by retaining only the most contributing ones to the residual among the whole terms in $T_{NL,i}$. To this end, the operator dR^c is compared to each non-linear term $T_{NL,i}$ by means of a normal scalar product-based indicator as follows:

$$\mathcal{I}_{ji} = \frac{{}^t dR_j^c \; T_{NL,i}}{\sqrt{\left({}^t dR_j^c dR_j^c\right)\left({}^t T_{NL,i} T_{NL,i}\right)}} \tag{5.22}$$

The more $\mathcal{I}_{ji}$ is closest to 1, the more $T_{NL,i}$ should be retained among the selected non-linear terms in the second step.
If the residual corresponding to the difference between the obtained reduced model output and the reference solution is still significant, then we should start again the steps 2 and 3 to select other non-linear terms. This procedure is performed in an iterative manner until a given error level is reached.

Once the non-linear terms are selected according to steps 2 and 3, the constant parameters α_1, α_2, β and γ in (5.19) can be identified in a least-squares problem for example. Note that the linear operators $\tilde{A}$, $\tilde{B}$, $\tilde{C}$ and $\tilde{D}\,\tilde{C}$ identified by KIM in the first step are also updated together within the non-linear terms in the least-squares problem. For the same purpose, a Kalman Filter-based identification method may be also used. This will be the focus of the next chapter, but rather intended to identify state-space models.

5.4 Identification based on Kalman Filter method

In this section, we suggest a Kalman Filter (KF) based method for real-time identification. The challenging task through this study is to develop an *on-line* method for a simultaneous estimation of state and parameters based on the "real-world" input-output data issued from the system under study. This latter is identified into a state space form with the model operators entries as unknown parameters. The estimation problem leads to non-linear state space models, even for linear problems. Several approaches based on Kalman Filters were developed to deal with non-linear models. In our work, we have focused on two techniques, namely the Extended Kalman Filter (EKF) and Unscented Kalman Filter (UKF) proposed by Sorenson [7], and Julier and Uhlman [8], [9], respectively. These two Kalman variants have been extensively used in several areas of application such as signal processing [10], active control [11], target tracking [12], inverse problems [13], etc. In our publication [14], we have studied the EKF and UKF method for the identification of a linear multiple-input multiple-output state space model both evaluated on a 10-DOF FE linear model. Even if they show equivalent performance in this linear case, the UKF presents a crucial advantage with respect to the EKF regarding the method implementation as

well as its extension to the processing of non-linear problems. In addition, the UKF can provide a better estimation than EKF for a wide class of non-linear systems as stated in [9] and [15]. In fact, the EKF applies the standard Kalman Filter to non-linear models by a first-order linearization of the non-linear operators. However, in practice, the use of EKF has two well-known drawbacks [16], [9]. First, linearization can produce highly unstable filters if the assumptions of local linearity are violated. Second, the derivation of the Jacobian matrices is non-trivial in most applications and often lead to significant implementation difficulties, especially when the model construction step starts from a continuous state-space form. The UKF addresses the aforementioned EKF issues by using a deterministic sampling approach namely, the *Unscented Transform* that we shall describe later in more details. The UKF, in fact, improves the approximation order of the EKF and also avoids the computation of Jacobian operators. A comparative study between EKF and UKF for state and parameter estimation of a thermal transient problem was published in [14]. The produced simulation results show that the EKF is more sensitive to the process and measurement noise levels than the UKF. The simple implementation of UKF with regard to the extension to non-linear systems processing is also highlighted. In what follows, we will focus only on the UKF approach. But before that, we describe the derivation of the reduced UKF model.

5.4.1 Setting of the UKF model

As assumed in the KIM approach, we aim to identify a reduced order model (ROM) in a continuous-time state space form. We first develop the identification of linear models in a continuous-time state space form as introduced in Section 4.1. We recall that model form below:

$$\begin{cases} \dot{X}(t) = \tilde{A}X(t) + \tilde{B}U(t) & \text{(5.23a)} \\ \tilde{Y}(t) = \tilde{C}X(t) + \tilde{D}U(t) & \text{(5.23b)} \end{cases}$$

where X is the $(n \times 1)$ reduced state vector, U the $(N_{ex} \times 1)$ thermal input vector consisting of the power (or power density) sources and BCs, and Y the $(N_{obs} \times 1)$ output vector gathering the observed temperatures. In its present state, the proposed method considers **a full state matrix** $\tilde{A}$ as opposed to the KIM approach in which matrix $\tilde{A}$ is identified in a modal form. The operators $\tilde{B}$ and $\tilde{C}$ are assumed full matrices as well. Furthermore, **the operator $\tilde{D}$ is assumed a null matrix**, which reduced the number of parameters to identify by $N_{obs} \times N_{ex}$. The parameters to identify in the matrices $\tilde{A}$, $\tilde{B}$ and $\tilde{C}$ are gathered in a $(p \times 1)$ vector θ as follows:

$$\begin{aligned} \theta \;=\; & [a_{11}, \cdots, a_{1n}, \cdots, a_{n1}, \cdots, a_{nn}, b_{11}, \cdots, b_{1N_{ex}}, \cdots, \\ & b_{n1}, \cdots, b_{nN_{ex}}, c_{11}, \cdots, c_{1n}, \cdots, c_{N_{obs}1}, \cdots, c_{N_{obs}n}]^T \end{aligned} \tag{5.24}$$

For the state and parameter estimation problem, we consider an *augmented* (or also extended) state vector $X^a = [X\ \theta]^T$ of dimension $n + p$, whose distribution is

assumed to be Gaussian random variable. The resulting extended dynamical model reads:

$$\begin{cases} \dot{X}^a = \tilde{f}\left(X^a, U\right) & \text{(5.25a)} \\ Y = \tilde{h}\left(X^a\right) & \text{(5.25b)} \end{cases}$$

where $\tilde{f}$ and $\tilde{h}$ are the non-linear evolution and observation functions, respectively. In order to apply the UKF approach, the functions $\tilde{f}$ and $\tilde{h}$ are converted into the discrete functions $\tilde{F}$ and $\tilde{H}$, respectively, by means of an implicit numerical integration method; the Dormand-Prince method [17], [18]. The model (5.25) is then transformed into the following non-linear recursive (discrete-time) state space model:

$$\begin{cases} X^a_{k+1} = \tilde{F}_k\left(X^a_k, U_k, \right) + w_k & \text{(5.26a)} \\ Y_k = \tilde{H}_k\left(X^a_k\right) + v_k & \text{(5.26b)} \end{cases}$$

with the initial condition $X^a_0 = \left[X_0\ \theta_0\right]^T$. The indices $_k$ and $_{k+1}$ in (5.26) represent the quantities at time instants $t_k = (k)\,\Delta t$ and $t_{k+1} = (k+1)\,\Delta t$ with Δt denoting the time sampling, w and v the process and the observation noises assumed to be uncorrelated zero-mean Gaussian white noises with time-invariant covariance matrices Q and R, i.e. $w \sim \mathcal{N}\left(0, Q\right)$ and $v \sim \mathcal{N}\left(0, R\right)$.

We should note that the extension to the processing of non-linear problems would be handled by assuming the same reduced model form (5.23) but with time-varying parameters in the ROM operators. This constitutes a key advantage enabling to circumvent the difficulty related to the choice of the non-linear reduced model form in the non-linear case.

5.4.2 The UKF algorithm

The UKF algorithm is based on a deterministic sampling technique known as the Unscented Transform (UT), proposed by Julier and Uhlmann [8],[9]. The idea of UT is to form $2n+1$ samples that capture exactly the mean and covariance of the original distribution of X^a. This sample set is given by the so-called *sigma-points*. If the random state variable X^a defined by its mean

$$\hat{X}^a \;=\; E\left[X^a\right]$$

and covariance

$$P^X \;=\; E\left[\left(X^a - \hat{X}^a\right)\left(X^a - \hat{X}^a\right)^T\right]$$

with $E\left[.\right]$ representing the expectation operator. The *sigma-points* denoted $\left\{\mathcal{X}_i\right\}_0^{2n} = UT\left(\hat{X}^a, P_X\right)$ with their respective weights are given by:

$$\begin{aligned}
\mathcal{X}_0 &= \hat{X}^a & ; \quad \omega_0 &= \frac{\kappa}{(n+\kappa)} \\
\mathcal{X}_i &= \hat{X}^a + \left[\sqrt{(n+\kappa)P^X}\right]_i & ; \quad \omega_i &= \frac{1}{2\,(n+\kappa)} \\
\mathcal{X}_{i+n} &= \hat{X}^a - \left[\sqrt{(n+\kappa)\,P^X}\right]_i & ; \quad \omega_i &= \frac{1}{2\,(n+\kappa)}
\end{aligned} \tag{5.27}$$

with $i = 1, \cdots, n$ and $\left(\sqrt{.}\right)_i$ the ith column vector of the matrix square root and is derived via the Cholesky factorisation. The parameter κ is a scaling parameter used to control estimation properties. In our study, κ is set to zero. The data set $\{\mathcal{X}_i\}_0^{2n}$ is then propagated by the non-linear operators $\tilde{F}$ and $\tilde{H}$. The mean and covariance of the transformed variable are estimated from those of the sigma-points.

Assume now that the sigma-points are given, as well as $\hat{X}_0^a$ and P_0^X, denoting the initial mean and covariance of the state X^a. The UKF algorithm is performed in three recursive steps:

- a sampling step for the *sigma-points* generation,

- a prediction step consisting in a resolution of one time step (step k) of the model (5.26) for each *sigma-point* and computation of the mean value and covariance predictions denoted $\hat{X}_k^{a^-}$ and P_k^X for the state variable X^a, and $\hat{Y}_k^{a^-}$ and P_k^Y for the observation variable Y_k,

- a correction step to update the prediction for the state mean and covariance taking into account a new observation Y_k. The Kalman gain K_k acts as a weight of the innovation $z_k = Y_k - \hat{Y}_k$.

The UKF algorithm is summarized below.

Algorithm 5.1 Unscented Kalman Filter algorithm

1: **Sampling step**
Generation of $2n+1$ *sigma-points*:
$\{\mathcal{X}_{i,k-1}, \omega_i\}_{\{i=0\cdots 2n\}} = UT\left(\hat{X}^a_{k-1}, P_{k-1}\right)$

2: **Prediction step**

(a) State mean prediction:
$\mathcal{X}^-_{i,k} = F_k\left(\mathcal{X}_{i,k-1}, U_{k-1}\right)$ and $\hat{X}^{a^-}_k = \sum_{i=0}^{2n} \omega_i \mathcal{X}^-_{i,k}$

(b) State covariance prediction:
$P^-_k = \sum_{i=0}^{2n} \omega_i \left(\mathcal{X}^-_{i,k} - \hat{X}^{a^-}_k\right)\left(\mathcal{X}^-_{i,k} - \hat{X}^{a^-}_k\right)^T + Q$

3: **Correction step**

(a) Measurement update: $\mathcal{Y}_{i,k} = H_k\left(\mathcal{X}^-_{i,k}\right)$

(b) Measurement prediction: $\hat{Y}_k = \sum_{i=0}^{2n} \omega_i \mathcal{Y}_{i,k}$

(c) Innovation covariance: $P^Y_k = \sum_{i=0}^{2n} \omega_i \left(\mathcal{Y}_{i,k} - \hat{Y}_k\right)\left(\mathcal{Y}_{i,k} - \hat{Y}_k\right)^T + R$

(d) Cross covariance: $P^{XY}_k = \sum_{i=0}^{2n} \omega_i \left(\mathcal{X}^-_{i,k} - \hat{X}^{a^-}_k\right)\left(\mathcal{Y}_{i,k} - \hat{Y}_k\right)^T + R$

(e) Updated state mean and Covariance:

- Kalman Gain matrix: $K_k = P^{XY}_k {P^Y_k}^{-1}$
- Innovation (Residual term): $z_k = Y_k - \hat{Y}_k$; Y_k denoting the new observation at step k.
- State update: $\hat{X}^a_k = \hat{X}^{a^-}_k + K_k z_k$
- Covariance update: $P^X_k = P^{X^-}_k - K_k P^Y_k K^T_k$

5.4.3 Illustration on a linear 10-DOF FE model

The UKF method performance is investigated on the same FE model of 10 DOF as described in § 5.3.2, but this time in a linear case where $\mathcal{L}$ is a null matrix in (5.11). Initial conditions consist of a uniform temperature $T_0 = T_a = 25\,^{\circ}\mathrm{C}$, with T_a denoting the ambient temperature. The forcing term $\phi u\,(t)$ is a square signal applied at DOF 1 (Fig. 5.6(a)). The simulation results regarding the observed temperature are depicted in Fig. 5.6(b).

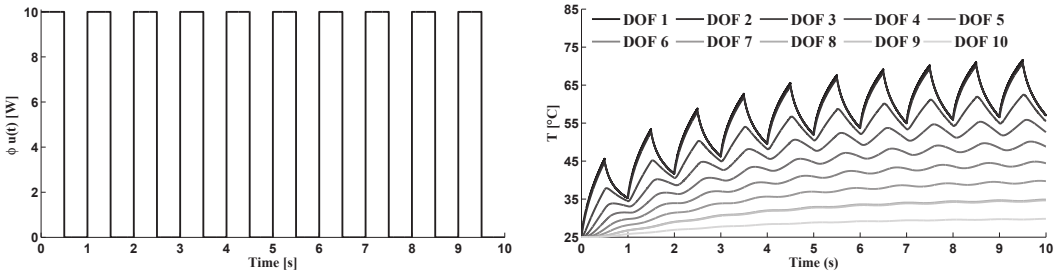

(a) Square power signal applied at DOF 1.

(b) Evolution of the temperature at all DOFs of the FE model.

Figure 5.6. Simulation results of the 10-DOF FE model.

As a first step, the Singular Value Decomposition (SVD) (Section 3.1.1) is applied on the whole observations at the FE model at all time steps in order to determine the minimum number of modes required to capture the essential dynamics of the reference model in the ROM. Fig. 5.7(a) shows that the first two singular values are much greater than the rest (the numerical values are 2061, 463.3, 130.2, ...). The Proper Orthogonal Modes (POM) contribution is also dominated by the first two modes as shown in Fig. 5.7(b). Hence, the reference model can be represented by a ROM of order 2 to be identified by the UKF method.

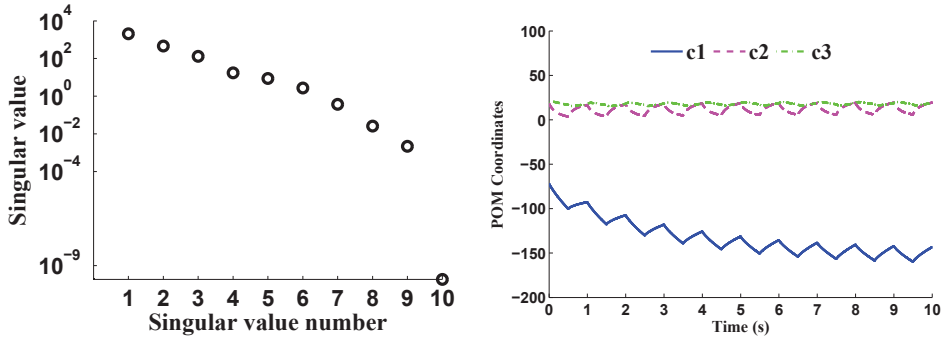

(a) Singular values.

(b) Coordinates of the first three Proper Orthogonal Modes (POM), $c_i, i = 1, 2, 3$.

Figure 5.7. Singular Value Decomposition (SVD) computed on the 10-DOF FE model.

UKF application

Now we apply the UKF in order to identify a ROM of order 2 using:

- two thermal inputs composed of the power source applied at DOF 1 depicted in Fig. 5.6(a) and the ambient temperature T_a assumed as a time-invariant boundary condition, i.e. $N_{ex} = 2$,

- two observed temperature collected at DOF 1 and 8 of the FE reference model (Fig. 5.6(b)), i.e. $N_{obs} = 2$.

The resulting *augmented* state vector is then of dimension $n^a = n\,(1 + n + N_{ex} + N_{obs}) = 14$ and takes the form:

$$X^a = [X_1,\, X_2,\, \theta] \tag{5.28}$$

with

$$\theta = [a_{11},\, a_{12},\, a_{21},\, a_{22},\, b_{11}, b_{12},\, b_{21},\, b_{22},\, c_{11},\, c_{12},\, c_{21},\, c_{22}] \tag{5.29}$$

The state and observation noise covariance matrices are assumed time-independent diagonal matrices set as $Q = \sigma_w^2 I_{n^a}$ and $R = \sigma_v^2 I_{N_{obs}}$, with σ_w^2 and σ_v^2 denoting the state and observation noise variances, respectively. The initial state estimate covariance is also assumed diagonal set as $P_0 = p_0 I_{n^a}$, where $p_0 = \left[p_0^X, p_0^A, p_0^B, p_0^C\right]$ is a vector of dimension n^a standing for the initial error variances of X, $\tilde{A}$, $\tilde{B}$ and $\tilde{C}$, respectively.

In what follows, we shall compare the UKF results for the following two cases:

- **case 1**: the estimation is based on **the temperature delta evolution** $T\,(t) - T_a$, such that $T_a = T_0 = T\,(0)$, as a reference observed data,

- **case 2**: the estimation is based on **the temperature evolution** $T\,(t)$ as a reference observed data.

The discrete reference data, i.e. input-output results of the FE model, is sampled in $N_{snap} = 1112$ time steps with constant sampling time $\Delta t = 0.009\ s$. The UKF entries, Q, R and P_0, as well as the initial estimate of X^a, used in the both cases are summarized in Table 5.1. Note that the initial estimate of the ROM state variable is computed as $X\,(0) = \tilde{C}_0^{\dagger} Y\,(0)$ with $\tilde{C}_0^{\dagger}$ denoting the pseudo-inverse of the initial estimate of matrix $\tilde{C}$.

Table 5.1
The UKF parameters used in both case 1 and case 2.

	Case 1	Case 2
UKF entries		
σ_w	10^{-10}	10^{-12}
σ_v	10^{-5}	10^{-5}
p_0^X	$10^{-5}\,[1,\ 1]$	$10^{-8}\,[1,\ 1]$
p_0^A	$10^{-5}\,[1,\ 1,\ 1,\ 1]$	$10^{-5}\,[1,\ 1,\ 1,\ 1]$
p_0^B	$10^{-5}\,[1,\ 1,\ 1,\ 1]$	$10^{-6}\,[1,\ 1,\ 1,\ 1]$
p_0^C	$10^{-5}\,[1,\ 1,\ 1,\ 1]$	$10^{-9}\,[1,\ 1,\ 1,\ 1]$
Initialization		
θ_0	$[-0.3,\ 2,\ 0.1,\ -6,\ 37,\ -16,\ 5,\ 2,\ 3,\ -1,\ 0.7,\ 2]$	
$X(0)$	$\tilde{C}_0^{\dagger} Y\,(0)$ [1]	

Results and discussion The performance of the UKF in both case 1 and case 2 is measured by: (1) evolution of the identified parameters; and (2) comparison of the reference observed and estimated temperature at the same observation points corresponding to the DOFs 1 and 8 of the FE model.
Fig. 5.8 shows good parameter identification results with low variance distribution of order 10^{-5} or 10^{-6} at the last time instants for both cases (variances not not shown in Fig. 5.8). However, we can notice that these parameters, constituting the ROM matrices, are not identically identified. Actually, there may exist an infinity of reduced models since any norm is imposed on the observation matrix $\tilde{C}$. This latter corresponds, in fact, to a restriction of a reduced projection basis to the observation points. Therefore, in order to ensure unicity of the ROM, a norm constraint should be imposed on matrix $\tilde{C}$ in the UKF algorithm. By contrast to the ROM operators, the eigenvalues of the state matrix $\tilde{A}$, i.e. the opposite reciprocal of time-constants, are invariant parameters of the thermal problem. In Fig. 5.9, we present the dominant time-constants identified in the cases 1 and 2. The lowest time-constant, equals $\simeq 0.24$ s, is identically identified in both cases. This time-constant corresponds to the collocated observation points with the applied power sources. The other dominant time-constant, however, is differently identified in the two cases, equals 4 s in case 1 and 2.55 s in case 2. This high value of time-constant should concern the low dynamics associated to observation points far from those collocated with the power sources, for example DOF 8.

[1] $\dagger$ stands for the pseudo-inverse of matrix $\tilde{C}_0$. Here, $\tilde{C}_0$ being a square matrix, $\tilde{C}_0^{\dagger} = \tilde{C}_0^{-1}$

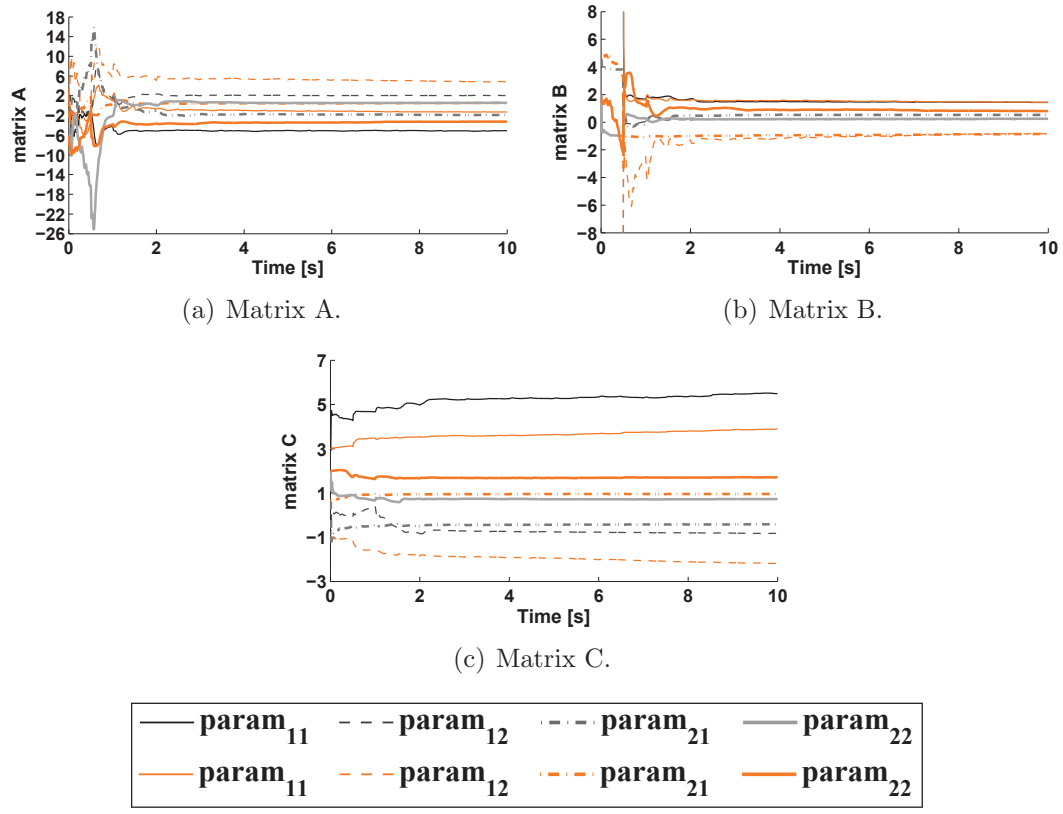

(a) Matrix A.

(b) Matrix B.

(c) Matrix C.

Figure 5.8. Identified parameters of the ROM; **case 1** (gray color) and **case 2** (orange color).

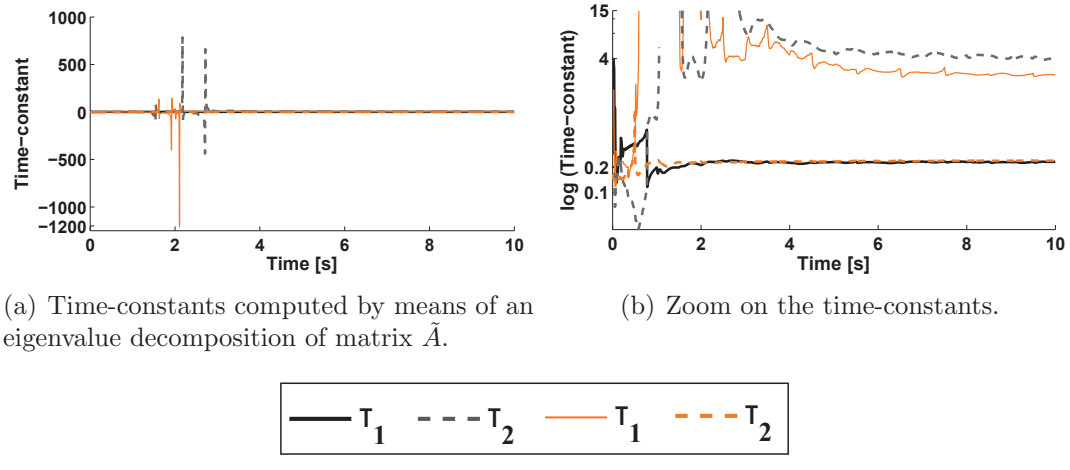

(a) Time-constants computed by means of an eigenvalue decomposition of matrix $\tilde{A}$.

(b) Zoom on the time-constants.

Figure 5.9. Identified time-constants (invariant parameters); **case 1** (gray color) and **case 2** (orange color).

In Figs. 5.10 and 5.11, we compare the reference and the ROM output at the DOFs 1 and 8 for both cases. In the view of real-time implementation, we evaluate the results of the ROM identified at different time instants, $t = 2,\ 4,\ 6,\ 8,\ 10$ s. In case 1, we obtain good identification at both DOFs 1 and 8 except those using the ROM identified at time instants 2 s and 4 s. This is consistent with the results shown in Fig. 5.9, where the large time-constant value, corresponding to the slow dynamics, is still not converged until the time instant 4 s.

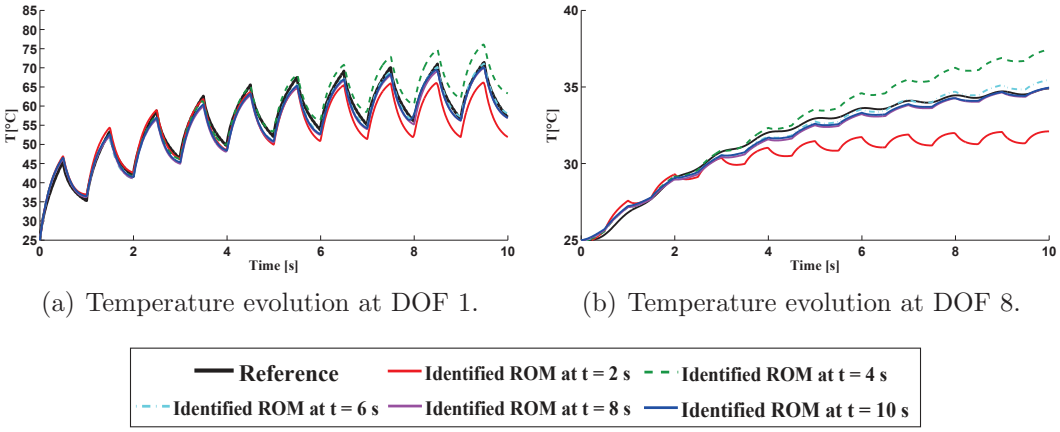

(a) Temperature evolution at DOF 1. (b) Temperature evolution at DOF 8.

Figure 5.10. **Case 1**: Comparison between the reference temperature and the ROM output identified at different time instants (t=2, 4, 6, 8 and 10s), all observed at the DOFs 1 (left) and 8 (right).

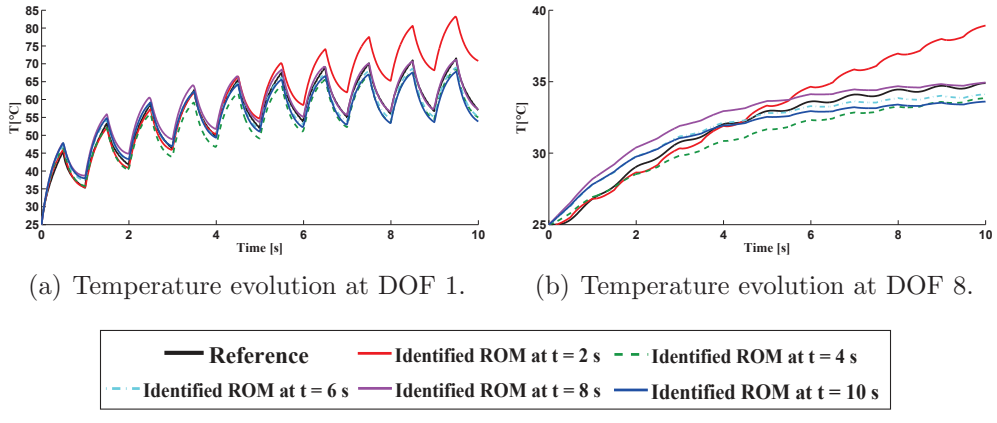

(a) Temperature evolution at DOF 1. (b) Temperature evolution at DOF 8.

Figure 5.11. **Case 2**: Comparison between the reference temperature and the ROM output identified at different time instants ($t = 2\,, 4\,, 6\,, 8\,, 10$ s), all observed at the DOFs 1 (left) and 8 (right).

The identification results obtained in case 2 are less satisfactory than in case 1, especially at the DOF 8 (Fig. 5.11(b)). The reason behind this is that the large time-constant is not well identified as this was already stated in Fig. 5.9(b), or eventually a ROM of order 2 is not sufficient in this case.

To sum up, the UKF estimation appears less efficient for the identification at the first time steps. This is a major drawback for thermal applications in electronics. In order to circumvent this issue in real-time implementation, the UKF method may be combined with a second identification method such as the KIM method for example, both intended to run in parallel. An error criterion on the UKF results would enable the switching between the two methods. In parallel with the UKF method, KIM is used to identify a ROM using first time instants data. Then, based on an error criterion of the UKF results, the identification process is switched to be performed by this latter enabling then the identification of the slower dynamics.

Sensitivity study A sensitivity study of the UKF estimation performed on the investigated 10-DOF model has been analysed with respect to (1) the state model covariance $Q = \sigma_w^2 I_{n^a}$ representing the confidence in the UKF model, (2) the observation noise covariance $R = \sigma_v^2 I_{n^a}$ representing the confidence in the measurements and (3) the initial state estimate covariance P_0 representing the confidence in the initial state estimate of X^a. This analysis shows that the choice of the UKF entries, Q, R and P_0, significantly impacts the UKF results ([14] for detailed results). The main conclusions are:

- The quotient σ_w/σ_v should be small enough, of order $\simeq 10^{-5}$ or 10^{-6} , in order to attribute sufficient confidence in the UKF model (5.26), that is to successfully identify the ROM parameters.

- The initial state covariance should be sufficiently large, of order $\simeq 10^{-5}$, 10^{-6}, to account for the unknown parameters values *a priori*. This means that a low confidence is accorded in the initial state.

5.4.4 UKF limitations illustrated on a large-scale 3D model

The initialization of the UKF state vector x^a becomes particularly difficult for higher ROM orders and eventually with a larger number of inputs and observations. For illustration purpose, the same UKF estimation procedure is performed on a simplified industrial large-scale 3D model (116505 DOFs). The model consists of 4 power components, 2 Igbts and 2 Diodes, mounted on a PCB. The boundary condition consists of the imposed temperature $T_{imp} = 90\,^{\circ}\mathrm{C}$ at the bottom face of the model. The initial temperature for all DOFs is set to $T_0 = T_{imp} = 90\,^{\circ}\mathrm{C}$. More details on this model are available in DaSilva thesis [19].

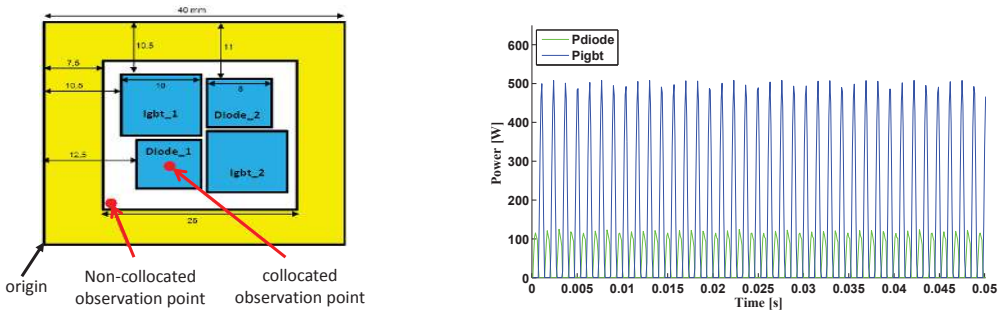

(a) Large-scale model of 116505 DOFs [19]. (b) Input signals.

Figure 5.12. Large-scale model composed of 2 Diodes and 2 Igbts mounted on the PCB.

For the UKF estimation, 4 observation points placed on the top center of the power components, and 1 observation point placed on the top of the PCB, are considered, i.e. $N_{obs} = 5$. Note that $Diode_1$ and $Diode_2$ on the one hand, $Igbt_1$ and $Igbt_2$ on the other hand, have similar thermal behaviour (see Fig. 5.12(a) for observation points locations). The thermal input vector is composed of the applied power sources on the components Igbts and Diodes (Fig. 5.12(b)) and the boundary condition T_{imp} assumed constant along time ($N_{ex} = 3$). The order of the ROM, $n = 5$, is determined by means of the SVD as proceeded above in the case of the 10-DOF FE model. Hence, the UKF state vector X^a is composed of $n\,(1 + n + Nex + Nobs) = 70$ variables to be identified. A *Matlab Identification Toolbox* is used to initialize the ROM matrices constituting the parameter vector θ. The range of values of the UKF entries, including the state model, the observation and the initial state estimate covariances, is set by means of a sensitivity analysis. In this example, the UKF estimation is based on the reference temperature delta evolution at the observation points, i.e. $Y\,(t) = Y_{ref}\,(t) - T_0$ with $Y_{ref}\,(t)$ denoting the reference temperature. The discrete data used in the identification process consists of $N_{snap} = 501$ time steps with a constant sampling time $\Delta t = 10^{-4}$. The state, observation covariances Q and R are diagonal matrices with variance values $\sigma_w = 10^{-12}$ and $\sigma_v = 10^{-3}$, respectively. The initial state estimate covariance is diagonal as well defined as $P_0 = 10^{-8} I_{n^a}$. In order to check the behaviour of the ROM, we apply the same power signals presented in Fig. 5.12(b). In Fig. 5.13, we compare the evolution with time of the temperature produced by the 3D detailed model and reduced model at observation points $Diode_1$, $Igbt_1$ and the one placed on the PCB. We can see from this figure that the identification results are not optimal. This typically the case of the collocated observation points with the sources, where the absolute residual reaches up to $\sim 11.5\,°\mathrm{C}$ for a temperature raise of about $35\,°\mathrm{C}$ at $Igbt_1$ and $Igbt_2$.

The eigenvalue value decomposition of the identified state matrix $\tilde{A}$ allows to obtain the eigenvalues corresponding to the opposite reciprocal of the time-constants of the thermal problem. Two conjugate complex eigenvalues with negative real part

are obtained among the 5 values. The reason behind this is that the UKF estimation lacks a constraint on matrix $\tilde{A}$. For instance, in order to ensure real eigenvalues, i.e real time-constants, we can impose a symmetry constraint on the state matrix $\tilde{A}$ in the UKF algorithm. Another solution consists in identifying a diagonal state matrix $\tilde{A}$ in the ROM. Nonetheless, the difficulty of the initialization step cannot be avoided.

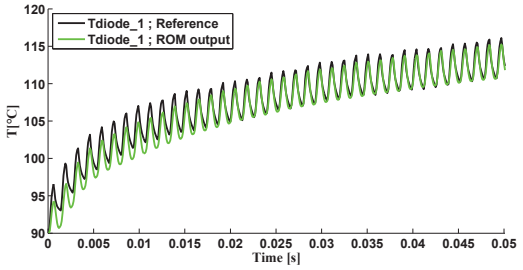

(a) Temperature evolution at the top center of Diode_1.

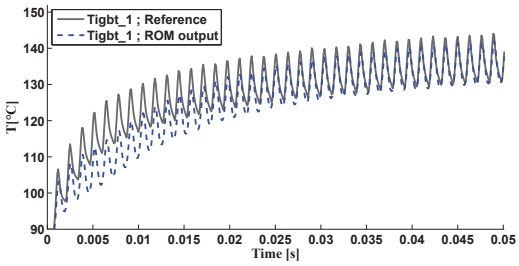

(b) Temperature evolution at the top center of Igbt_1.

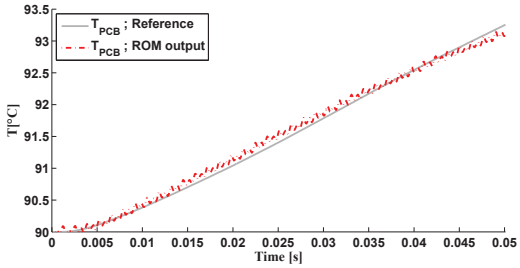

(c) Temperature evolution at the non-collocated observation point on the PCB.

Figure 5.13. Large-scale model: identified ROM based on the reference temperature delta evolution ($T(t) - T_a$); Comparison between the reference temperature and the ROM output identified at the last time instants ($t = 0.5$ s).

5.4.5 Synthesis

The proposed "Unscented Kalman Filter" (UKF) method aims at identifying linear reduced state space models. The objective behind this proposal is to perform a real-time identification of linear models before the extension to the processing of non-linear models. In this section, the UKF method is evaluated on two linear test cases: (1) a 10-DOF FE model and (2) a simplified industrial large-scale model. In both cases, the order of the reduced model is fixed by means of the Singular Value Decomposition method. A sensitivity analysis enables to fix the range values of the UKF parameters including the state model, observation model and initial state estimate covariance matrices. The initialization of the UKF state vector, however, becomes more difficult to set as the number of parameters to identify increases. In the large scale model for example, a Matlab Identification Toolbox is

used to overcome the initialization difficulty. The main conclusions drawn from the identification results in both cases are:

- The UKF estimation based on the temperature delta provides better results than the direct use of the temperature evolution as a reference observation. However, this is only possible when dealing with linear problems. In the non-linear problem, the identification should be performed directly on the temperature evolution as a reference output data.

- The UKF method identifies better the small time-constants corresponding to the collocated observation with the power excitation.

- The UKF estimation at the first time steps fails to capture the slow dynamics of the reference solution. Consequently, the UKF method cannot be implemented for real-time identification at the first time steps.

5.5 Conclusion

This chapter constitutes an exploratory study of two identification methods for the processing of non-linear problems mainly governed by natural convection. In such problems, it is difficult to predict the non-linearity form as the convective heat transfer coefficient depends on several model parameters (model geometry, flow conditions, etc.). Therefore, our choice has deliberately focused on non-parametric identification methods. In this context, two methods are suggested:

- an extended Kernel Identification Method for the identification of non-linear reduced state space models, in which the non-linear operators dependences are obtained by applying KIM method on several discrete time intervals with constant power level on each one. The method applied on a non-linear FE test case shows good results for the identification of single input single output reduced models. The next step should be its extension to the processing of multiple-input multiple-output models. In this same context, we propose another KIM-based identification method but of semi-parametric. This method consists in using the the KIM method to first identify a linear reduced model corresponding to a linearized behaviour of the system. The residual resulting from this approximation is identified iteratively by selecting only some non-linear terms based on a two specific indicator.

- a Kalman-based identification method using the variant Unscented Kalman Filter for an instantaneous identification of state variables and parameters of the reduced state space model. Before testing to the non-linear case, the method is studied for the linear case. An advantage of this method with

regard to the extension to the non-linear case is that the same model form is considered but with time-varying parameters. The UKF estimation shows good results evaluated on the same FE test case investigated in the extended KIM method but in a linear case. A second large-scale model representative of an industrial application reveals the following conclusions: (1) the Kalman parameters including the state, the observation and the intial state estimate covariance matrices should be judiciously chosen to ensure convergence of the UKF algorithm, (2) the initialization step may become very difficult to handle as the number of the number of the reduced model parameters to identify increases, and finally (3) the UKF method is more efficient once the initial time steps are passed over.

A potential perspective path in addition to the extended KIM method consists in combining the UKF approach with the linear KIM method for the identification of non-linear state space models. The idea is to first apply the KIM approach at the first time steps corresponding to a first power level, and then continue the identification process by means of the UKF method on continuously increasing power levels to fournish a finer estimation of the non-linear reduced model with time-varying parameters. In comparison with the extended KIM approach, the UKF method would allow finer estimation of the model parameters instead of an estimation on some discrete intervals.

References

[1] K.T. Chau and C.C. Chan. Nonlinear identification of power electronic systems. *SIAM Journal on Control*, 1:152–192, 1995.

[2] W.J. Rugh. *Nonlinear System Theory - The Volterra/Wiener Approach*. The Johns Hopkins University Press, 1981.

[3] L.L. Li and S.A. Billings. Volterra series truncation and reduction in the frequency domain for weakly nonlinear system. Technical report, Department of Automatic Control and Systems Engineering, University of Sheffield, UK, 2006.

[4] D.M. Storer. *Dynamic analysis of non-linear structures using higher order frequency response functions*. PhD thesis, The University of Manchester, 1991.

[5] R. Towner and J. Band. An analysis technique/automated tool for comparing and tracking analysis modes of different Finite Element models. In *53rd AIAA/ASME/ASCE/AHS/ASC Structures, Structural Dynamics and Materials Conference*, 2012.

[6] R.J. Allemang. The modal assurance criterion: Twenty years of use and abuse. *Sound and Vibration,*, 37:14–23, 2003.

[7] H.W. Sorenson. Least-squares estimation: from Gauss to Kalman. *IEEE Spectrum*, 7:63–68, 1970.

[8] S.J. Julier and J.K. Uhlmann. A general method for approximating nonlinear transformations of probability distributions. Technical report, University of Oxford, Departement of Engineering Science, 1996.

[9] S.J. Julier and J.K. Uhlmann. A new extension of the Kalman Filter to nonlinear systems. In *The Proceedings of AeroSense: The 11th Int. Symp. on Aerospace/Defence Sensing, Simulation and Controls*, pages 182–193, 1997.

[10] J-L. Dion, C. Stephan, G. Chevallier and H. Festjens. Tracking and removing modulated sinusoidal components: A solution based on the kurtsis and the Extended Kalman Filter. *Mechanical Systems and Signal Processing*, 38:428–439, 2013.

[11] M. Bisgaard, A. Cour-Harbo and J.D. Bendtsen. Adaptive control system for autonomous helicopter slung load operations. *Mechanical Systems and Signal Processing*, 18:800–811, 2010.

[12] S. Pan, H. Su, J. Chu and H. Wang. Applying a novel extended Kalman filter to missiletarget interception with APN guidance law: A benchmark case study. *Control Engineering Practice*, 18:159–167, 2010.

[13] K.M. Neaupane and M. Sugimoto. An inverse boundary value problem using the Extended Kalman Filter. *Mechanical Systems and Signal Processing*, 29:121–126, 2003.

[14] F. Abid, G. Chevallier, J-L. Blanchard and J-L. Dion. System identification using Kalman Filters. In *The Proceedings of the Society for Experimental Mechanics*, volume 7, pages 561–573, 2013.

[15] D.G. Khairnar, S.N. Merchant and U.B. Desai. Nonlinear target identification and tracking using UKF. In *The Proceedings of the 2007 IEEE International Conference on Granular Computing*, page 761, 2007.

[16] J.J. LaViola and K. Joseph. A comparison of unscented and extended Kalman filtering for estimating quaternion motion. In *The Proceedings of the 2003 American Control Conference*, pages 2435–2440, 2003.

[17] J.R. Dormand and P.J. Prince. A family of embedded Runge-Kutta formulae. *Journal of Computational and Applied Mathematics*, 6:19–26, 1980.

[18] J.H. Mathews and K.D. Fink. *Numerical methods using MATLAB*. Prentice Hall, 2004.

[19] F. Da Silva. *Méthodologies de réduction de modèles multiphysiques pour la conception et la commande d'une chaine de traction électrique*. PhD thesis, Ecole Centrale de Paris, .

General conclusion and perspectives

The objective of this research thesis is to develop a method producing reduced order models for estimating the thermal behaviour of power electronics systems in mechatronics products. Moreover, this method must speed up the transient thermal simulations of such products. In the first chapter, we presented a technical overview of power electronics systems summarizing the common practices in thermal management including both reliability and control assessments. In this chapter, we also reviewed the thermal impedance method constituting the currently used method in Valeo in order to estimate the junction temperature of power components. This method, being based on the superposition principle, cannot be extended to the processing of non-linear systems, in particular those cooled by natural convection. The investigated industrial example in this chapter shows the difficulties encountered in such problems, which fully justified the motivations of the search of an alternative model order reduction method. In the second chapter, we presented a mathematical background of thermally coupled fluid-solid problems and derive a discrete detailed model of such problems by means of a Finite Element Method. Actually, the derived detailed model constituted a reference model for the developed reduction method to deal with thermal problems mainly governed by conduction and forced or natural convection.

In chapter 3, we provided the state of art regarding Model Order Reduction (MOR) techniques classified into intrusive and non-intrusive methods. Intrusive methods require access to the source code of solvers to project the reference detailed model onto an appropriate subspace or to act directly on the local differential equations of the problem. Examples of projection-based methods are substructuring methods, Modal methods and Proper Orthogonal Decomposition. Examples of methods acting on the problem equations are the *a priori* variable separation-based methods including the Proper Generalized Decomposition. Non-intrusive methods, also known as identification methods, consists in finding a mathematical model that best describes the relationship between the input and output data of the system of interest. Examples of these are the Prediction Error Methods based on the polynomial ARMA models, the Modal Identification Method and the Subspaces methods identifying state space reduced models.

In the industrial context, the implementation of the reduction method must account for a double requirement: on the one hand, it should be based only on the processing of the input data and output results produced by a reference detailed model considered as a *black-box*; on the other hand, the reduced models should be represented in a behavioural form suitable for their insertion in command laws for real-time temperature control. In addition, the final purpose is to address the identification of non-linear problems in presence of natural convection. In such problems, the convective heat transfer coefficient depends on the geometry and flow conditions in the system. Hence, it is very difficult to postulate *a priori* the form of the non-linearity related to this coefficient, especially within a non-intrusive framework. For all the above reasons, our work has focused on **non-parametric identification methods** in order to produce **reduced models in state-space form**, a form particularly convenient form for a Simulink implementation and the further inclusion in command laws. To take up this challenge, we have first focused on Kalman Filter based-methods, the Unscented Kalman Filter (UKF) variant in particular, to perform a **real-time identification** of linear problems before the extension to the non-linear case. Even if the UKF method was validated on a linear test case, the setting up of UKF entries and the initialization of reduced model parameters remain difficult, especially when dealing with large-scale models. Consequently, our research work has focused on **offline identification methods for producing compact reduced models represented into a multiple-input multiple-output state space form**. In this context, a new identification method named "Kernel Identification Method" (KIM) has been introduced. The method development was performed in two separate stages. A first stage for the identification of linear problems followed by its extension to non-linear applications involving the natural convection.

In Chapter 4, we introduced the KIM method for the identification of linear reduced models in linear applications. In view of its extension to the non-linear case, the reduced model is identified in a modal form where the state matrix is assumed to be diagonal. The method is based on the Least-Squares method and uses the LQ decomposition to identify the kernel of the thermal problem independently of the thermal inputs. The kernel is in fact composed of the dominant eigenvalues, i.e. the opposite reciprocal of dominant time-constants, placed on the diagonal terms of the state matrix. The corresponding eigenvectors constitute the observation matrix. The linear KIM was successfully validated on two applications: (1) a small-scale linear conduction problem; and (2) an industrial large-scale water-cooled CFD problem mainly governed by forced convection. In these two applications, the thermal inputs considered in the reduced model are composed of the power sources signals and boundary conditions that are intended to be monitored in control applications. In the first application, KIM was compared to three Subspace approaches (SubSV, SubCVA and MOESP) that are well-documented in Overschee and De Moore (1996). The KIM method showed equivalent results with respect to the first two approaches that have already proved their practical performance in the literature. In the second

example, KIM was compared to the Thermal Impedance Method and showed better results in accuracy and especially in time cost. In fact, the Thermal Impedance method requires as much simulations of the detailed model as the number of the considered power sources in the identification process. By contrast, KIM can be directly performed on the validation inputs signals, which presents a significant advantage as the number of power components increases in mechatronic systems.

In Chapter 5, we proposed an exploratory study for the identification of non-linear reduced state space models. Besides the UKF method that showed some difficulties in the identification large-scale linear applications, we suggested an extension of the KIM method of non-parametric nature aimed at identifying a non-linear reduced model represented in a tabular form. This method must be applied on discrete time intervals with a constant power level on each one to provide satisfactory results. The derived multi-linear reduced models enables to determine the form of the non-linear operators in the reduced model, without knowing the non-linearity nature. The proposed method has been validated on a particular single-input single-output small-scale model. The next step should address its extension to the processing of multiple-input multiple-output problems. In this context, some questions that need to be further studied are: how many levels of the inputs should be involved in the identification step? How to choose the amplitude of these levels corresponding to each input?

An interesting future research area is the combination of the Kernel Identification Method and the Unscented Kalman Filter method for the identification of non-linear thermal problems involving essentially the natural convection. In a first stage, the KIM method could be applied on the first time steps with constant inputs levels. Then, the KIM results could be used for the initialization of the UKF estimation in order to identify a reduced model for the remaining time steps. The purpose of the KIM-UKF combination is to identify a non-linear reduced state space model with time-varying parameters. This should significantly improve the UKF estimation for which the initialization step is very difficult to set, especially when dealing with a high number of parameters to identify. Moreover, the UKF estimation should provide finer estimation of the reduced model with respect to the non-parametric extended version of KIM method. Finally, the previous questions related to the choice of the number and amplitudes of the inputs levels should be avoided as the UKF estimation provides an instantaneous estimation of the parameters at each time step. Consequently, this should allow for the application of other inputs signals in the identification step such as continuously increasing inputs levels to cover different operating points of the system.

Another promising method also based on the KIM approach needs further investigation. This method would be of semi-parametric nature, combining the KIM method for the identification of the linear part and a parametric approximation of some originally selected non-linear terms.

Appendix A

Least-Squares method

This appendix describes how the Least-Squares method (LSQ) have been implemented in order to identify the operator Z, a symmetric matrix, and $\tilde{D}$ and B, full matrices (See Section 4.1).

Let $x = (x_1, \ldots, x_l)^T$ and $y = (y_1, \ldots, y_m)^T$ be $l \times 1$ and $m \times 1$ real vectors, such that $m \geq l$, and F a $m \times l$ matrix.
Suppose that $l = 2$ and $m = 3$, then we can write:

$$\begin{Bmatrix} y_1 \\ y_2 \\ y_3 \end{Bmatrix} = \begin{bmatrix} F_{11} & F_{12} \\ F_{21} & F_{22} \\ F_{31} & F_{32} \end{bmatrix} \begin{Bmatrix} x_1 \\ x_2 \end{Bmatrix} \tag{A.1}$$

The goal herein is to identify the values of the coefficients in matrix F.
Let

$$\Theta = (F_{11}, F_{21}, F_{31}, F_{12}, F_{22}, F_{32})^T \tag{A.2}$$

denote the vector of unknown parameters in system (A.1).
Suppose that a data set is given $\{x^i, y^i\}$, where $i \in \{1 : N_{snap}\}$ stands for time instant and N_{snap} the total number of samples, then the system (A.1) is transformed into:

$$\mathcal{Y} = \mathcal{X}\,\Theta \tag{A.3}$$

where

$$\mathcal{Y} = \begin{bmatrix} y_1^1 \\ y_2^1 \\ y_3^1 \\ \vdots \\ y_1^{Nt} \\ y_2^{Nt} \\ y_3^{Nt} \end{bmatrix}, \; \mathcal{X} = \begin{bmatrix} x_1^1 & 0 & 0 & x_2^1 & 0 & 0 \\ 0 & x_1^1 & 0 & 0 & x_2^1 & 0 \\ 0 & 0 & x_1^1 & 0 & 0 & x_2^1 \\ \vdots & \vdots & \vdots & \vdots & \vdots & \vdots \\ x_1^{Nt} & 0 & 0 & x_2^{Nt} & 0 & 0 \\ 0 & x_1^{Nt} & 0 & 0 & x_2^{Nt} & 0 \\ 0 & 0 & x_1^{Nt} & 0 & 0 & x_2^{Nt} \end{bmatrix} \tag{A.4}$$

The solution of the least-squares problem is defined as:

$$\min_{\Theta \in \mathbb{R}^{(m \times l)}} \left\| \mathcal{X}\ \Theta\ -\ \mathcal{Y} \right\|, \qquad \mathcal{X} \in \mathbb{R}^{(m \times N_t) \times (l \times m)}, \qquad \mathcal{Y} \in \mathbb{R}^{(m \times N_t) \times 1} \tag{A.5}$$

and the least-squares estimate of $\hat{\Theta}$ is :

$$\hat{\Theta}\ =\ \mathcal{X}^{\dagger}\, \mathcal{Y} \tag{A.6}$$

where $()^{\dagger}$ denotes the pseudo-inverse and $\mathcal{X}^{\dagger} = (\mathcal{X}^T \mathcal{X})^{-1}\ \mathcal{X}^T$ is called the *Moore-Penrose inverse*, or the pseudo-inverse, of matrix $\mathcal{X}$.

It is known that the unicity of the solution produced by a least-square estimation requires the matrix $\mathcal{X}$ to be of full rank, i.e. its column vectors are linearly independent. When $\mathcal{X}$ is rank-deficient, we obtain an ill-conditioned least-squares problem, i.e. there exist many vectors $\hat{\Theta}$ that minimize $\left\| \mathcal{X}\ \Theta\ -\ \mathcal{Y} \right\|$. In that case, a generalized Least-Squares method of solving an ill-conditioned problem, named also the *Moore-Penrose generalized inverse*, is generally used [132], producing a minimum norm solution. The corresponding command in Matlab is ***pinv***.

In the Kernel Identification Method, the Least-Squares method (LSQ) is applied in order to identify the operator Z, a symmetric matrix, and $\tilde{D}$ and B, full non symmetric matrices (Chapter 4 Section ...).

Appendix B

The LQ decomposition

This appendix recalls the LQ decomposition technique, used for the computation of the projection onto a space orthogonal to the space of input data, U, a matrix of full rank in the investigated example in Chapter 4.
We state in the following the LQ decomposition definition: let $\mathcal{A} \in \mathbf{R^{p \times j}}$ and $\mathcal{B} \in \mathbf{R^{q \times j}}$ two given matrices of full rank p and q, respectively, i.e. their row vectors are linearly independent. We also assume that $j \geq max\,(p, q)$, which will always be the case in the identification methods described in this paper. $\mathcal{A}/\mathcal{B}$ is the orthogonal projection of the row space of $\mathcal{A}$ onto the row space of $\mathcal{B}$. $\mathcal{A}/\mathcal{B}^{\perp}$ is the projection of the row space of $\mathcal{A}$ onto $\mathcal{B}^{\perp}$, the orthogonal complement of the row space of $\mathcal{B}$, and

$$\mathcal{A} \;=\; \mathcal{A}/\mathcal{B} + \mathcal{A}/\mathcal{B}^{\perp} \tag{B.1}$$

or, equivalently

$$\mathcal{A} \;=\; \mathcal{A}\Pi_{\mathcal{B}} + \mathcal{A}\Pi_{\mathcal{B}^{\perp}} \tag{B.2}$$

where Π_B and $\Pi_{B^{\perp}}$ denote the projections of $\mathcal{A}$ onto $\mathcal{B}$ and $\mathcal{B}^{\perp}$, respectively.

The matrix representations of these projections can be easily computed via the LQ decomposition of $\begin{pmatrix}\mathcal{B}\\ \mathcal{A}\end{pmatrix}$, which is the numerical version of the Gram-Schmidt orthogonalization procedure. The actual computation of the LQ decomposition is performed by taking the transpose of the QR decomposition of the matrix $\begin{pmatrix}\mathcal{B}^T & \mathcal{A}^T\end{pmatrix} \in \mathbf{R^{j \times q+p}}$.
The LQ decomposition of $\begin{pmatrix}\mathcal{B}\\ \mathcal{A}\end{pmatrix}$ is given by

$$\begin{pmatrix}\mathcal{B}\\ \mathcal{A}\end{pmatrix} = L\;Q^T = \begin{pmatrix}L_{11} & 0\\ L_{21} & L_{22}\end{pmatrix}\begin{pmatrix}Q_1^T\\ Q_2^T\end{pmatrix} \tag{B.3}$$

where $L_{11} \in \mathbf{R^{q \times q}}$, $L_{21} \in \mathbf{R^{p \times q}}$, $L_{22} \in \mathbf{R^{p \times p}}$ with L_{11}, L_{22} lower triangular, and $Q_1 \in \mathbf{R^{j \times q}}$, $Q_2 \in \mathbf{R^{j \times p}}$ are orthogonal, i.e. $Q^T\;Q = \begin{pmatrix}Q_1^T\\ Q_2^T\end{pmatrix}\begin{pmatrix}Q_1 & Q_2\end{pmatrix} = \begin{pmatrix}\mathbf{I_q} & 0\\ 0 & \mathbf{I_p}\end{pmatrix}$.
Hence, we have

$$\begin{cases} \mathcal{B} &= L_{11}\, Q_1^T & \text{(B.4a)} \\ \mathcal{A} &= L_{21}\, Q_1^T \;+\; L_{22}\, Q_2^T & \text{(B.4b)} \end{cases}$$

It is shown in [144], [145] that if the matrices $\mathcal{A}$ and $\mathcal{B}$ are of full rank, the same holds for the matrix L and thus L_{11} is non-singular, implying $Q_1^T = L_{11}^{-}1\, \mathcal{B}$. Thus, it follows that

$$\mathcal{A} \;=\; L_{21}\, L_{11}^{-1}\, \mathcal{B} + L_{22}\, Q_2^T \tag{B.5}$$

Since Q_1 and Q_2 are orthogonal, it follows [132]:

$$\begin{cases} \mathcal{A}/\mathcal{B} &= L_{21}\, Q_1^T & \text{(B.6a)} \\ \mathcal{A}/\mathcal{B}^{\perp} &= L_{22}\, Q_2^T & \text{(B.6b)} \end{cases}$$

Note that if the matrix $\begin{pmatrix} \mathcal{B} \\ \mathcal{A} \end{pmatrix}$ is rank-deficient, which is typically the case when projecting onto an orthogonal space to the derivative of input data space (see Chapter 4), the LQ decomposition is computed using *elementary orthogonal Householder matrices* [162]. This consideration is taken into account in the Matlab command ***qr***.

General references

[1] J-L. Blanchard. CEE project reporting & visual management: FE-multiphysics Simulation use cases. 2009.

[2] B. Boehm. *Software Engineering Economics*. Prentice Hall, 1981.

[3] M.H. Rashid. *SPICE for Power Electronics and Electric Power, Third Edition*. CRC Press, Taylor & Francis Group, 2012.

[4] M.D. Gunzburger and J.S. Petersen. The reduced basis method in control problems. In *The Proceeding of Computation and Control, Birkhäuser, Berlin*, pages 211–218, 1993.

[5] J.M. Morelle. IML Mechatronic packaging technology, an innovative solution for automotive power electronics, Valeo presentation of the EC project HOPE. In ECPE Workshop, editor, *ECPE - HOPE Symposuim. Automotive power electronics - High density power electronics for hybrid traction, Germany*, 2008.

[6] P. Sardat. Power MOSFETs users guide. Technical report, VALEO: Group Electronic Expertise and Development Services, 2009.

[7] D. Newcombe D. Chamund. *IGBT module reliability*, 2010. DynexApplication Note.

[8] M. Held, P. Jacob, G. Nicoletti, P. Scacco, M.-H. Poech. Fast power cycling test for IGBT modules in traction application. In *The Proceeding of Power Electronics and Drive Systems*, 1997.

[9] P. D. T. O'Connor and A. Kleyner. *Practical reliability engineering - fifth edition*. John Wiley & Sons, Ltd, 2012.

[10] M. White, M. Cooper, Y. Chen and J. Bernstein. Impact of junction temperature on microelectronic device reliability and considerations for space applications. In *IEEE International Integrated reliability Workshop, CA, USA*, pages 133–136, 2003.

[11] A. Vassighi, M. Sachdev. Thermal runaway in integrated circuits. In *The Proceeding of Device and Materials Reliability (IEEE Transactions)*, volume 6, pages 300–305, 2006.

[12] Power module reliability - Mitsubishi electric. `http://www.mitsubishielectric.com/semiconductors/products/pdf/reliability/0512_e.pdf`.

[13] *Military Handbook, reliability prediction of electronic equipment*. the United States Department of Defense, 1990.

[14] *Recueil de Données de Fiabilité - Modèle universel pour le calcul de la fiabilite prévisionnelle des composants, cartes et équipements électroniques - RDF 2000 (UTEC 80810)*. Association Française de Normalisation (AFNOR), 2005.

[15] *Reliability methodology for Electronic Defense Systems - FIDES Guide (UTEC 80811)*. Association Française de Normalisation AFNOR), 2009.

[16] *Military standard. NASA standard Electrical, Electronic and Electromechanical (EEE) parts list*. National aeronautics and space administration. Washington, D.C. 20546, 1994.

[17] S. Roberts. Thermal derating of LEDs. `http://docs-europe.origin.electrocomponents.com/webdocs/0e28/0900766b80e289cf.pdf`, 2009. Recom Technical Support.

[18] NTC and PTC thermistors - reliable limiting of current surges. TDK EPCOS `http://www.epcos.com/epcos-en/374108/tech-library/articles/products---technologies/products---technologies/reliable-limiting-of-current-surges/172842`, 2012.

[19] S-H. Yu, D. Jang and K-S. Lee. Effect of radiation in a radial heat sink under natural convection. *International Journal of Heat and Mass Transfer*, 55:505–509, 2012.

[20] G.R. Wagner. A study of the maximum theoretical power dissipation of tablets under natural convection conditions. In *The Proceeding of the 20th international workshop on Thermal Investigations of ICs and Systems (THERMINIC)*, pages 1–5, 2014.

[21] S. S. Kang. Advanced cooling for power electronics. In *The proceeding of the 7th international conference on Integrated Power Electronics Systems (CIPS 2012), Nuremberg, Germany*, pages 1–8, 2012.

[22] J-L. Blanchard. Simulation électrique et thermohydraulique de systèmes mécatroniques en éléments finis. Seminaire NAFEMS France: Les defis de la Simulation Multiphysique: `http://www.nafems.org/events/nafems/2008/multiphysics_paris/`, 2008.

[23] A. Poppe. Thermal measurements and modelling - the transient and multichip issues. `http://cmp.imag.fr/conferences/therminic/therminic05/APoppe_Tutorial.pdf`, 2005. 11th THERMINIC workshop, Belgirate, Italy.

[24] *JEDEC Standard. Guidelines for Reporting and Using Electronic Package Thermal Information. JESD51-12*. JEDEC Solid State Technology Association 2005. Arlington, VA 22201-3834, 1999.

[25] V. Szekely and T. Van Bien. Fine structure of heat flow path in semiconductor devices: a measurement and identification method. *Solid-Slate Electronics*, 31:1363–1368, 1988.

[26] V. Szekely. On the representation of infinite length distributed RC one-ports. *IEEE Transactions on Circuits and Systems*, 38:711–719, 1991.

[27] M. Carmona, S. Marco, J. Palacn, and J. Samitier. A time-domain method for the analysis of thermal impedance response preserving the convolution form. *IEEE Transactions on components and packaging technology*, 22(2):238–244, 1999.

[28] P. Dubus, R. Leon, D. Le Guyader and L. Caves. Thermal pre-dimensioning methodology based on thermal impedance. In *The Proceedings of the 6th International Conference on Integrated Power Electronics Systems (CIPS 2010), Nuremberg, Germany*, pages 1–6, 2010.

[29] J.W. Sofia. Analysis of thermal transient data with synthesized dynamic models for semiconductor devices. *IEEE Components, Packaging, and Manufacturing Technology Society*, 18:39–47, 1995.

[30] F. Christiaens and E. Beyne. Transient thermal modeling and characterization of a hybrid component. In *The Proceeding of the 46th Electronic Components and Technology Conference, Orlando, FL*, pages 154–164, 1996.

[31] Y.C. Gerstenmaier and G. Wachutka. Calculation of the temperature development in electronic systems by convolution integrals. In *The Proceeding of the 16th Semiconductor Thermal Measurement and Management Symposium (SEMITHERM 2000) , San Jose, CA*, pages 50–59, 2000.

[32] P. Dubus and L. Caves. OD electro thermal models methodology. Technical report, VALEO: Group Electronic Expertise and Development Services, 2010.

[33] M. März, P. Nance. Thermal modeling of power-electronic systems. `http://peufeu.free.fr/audio/articles/Thermal%20modeling%20of%20power%20systems.pdf`. Accessed: 2014-08-29.

[34] F. N. Masana. A new approach to the dynamic thermal modelling of semiconductor packages. *Microelectronics Reliability*, 41(6):901–912, 2001.

[35] L. Weinberg. *Network analysis and synthesis.* McGraw-Hill, New-York, 1962.

[36] P.E. Bagnoli, C. Casarosa, M. Ciampi and E. Dallago. Thermal Resistance Analysis by Induced Transient (TRAIT) method for power electronic devices thermal characterizationpart I: Fundamentals and Theory. *IEEE Transactions on Power Electronics*, 13:1208–1219, 1998.

[37] J.-L. Blanchard. Technological development plan: model order reduction - bibliographic study. Technical report, VALEO: Group Electronic Expertise and Development Services, 2011.

[38] W.H. Press, S.A. Teukolsky, W.T. Vetterling, and B.P. Flannery. *Numerical recipes in C: The art of scientific computing, 2nd ed., Cambridge*. Cambridge University Press, 1992.

[39] D. Schweitzer. Thermal transient multisource simulation using cubic spline interpolation of Zth functions. In *The Proceedings of the 13th International Workshop on Thermal Investigations of ICs and Systems (THERMINIC 2006), Nice, Cte dAzur, France*, pages 123–127, 2006.

[40] R. Leon. Debrifing vd46. Technical report, VALEO: Group Electronic Expertise and Development Services, 2012.

[41] S.V. Patankar. *Numerical heat transfer and fluid flow*. Hemisphere Publishing Corporation, 1980.

[42] H.K. Versteeg and W. Malalasekera. *An introduction to Computational Fluid Dynamics - The Finite Volume Method*. John Wiley & Sons Inc., New York, 1995.

[43] D. Bessems. Development of an extended quadratic tetrahedron for finite element analysis of Navier-Stokes problems. Master's thesis, Eindhoven University of Technology - Departement of Mechanical Engineering, 2003.

[44] G. Dhatt, G. Touzot, E. Lefrançois. *Méthode des éléments finis*. Hermès - Lavoisier, 2005.

[45] C. Hirsch. *Numerical Computation of Internal and External Flows (Second Edition) - The Fundamentals of Computational Fluid Dynamics*. 2007.

[46] F.M. White. *Viscous fluid flow*. McGraw-Hill, New York, 1991.

[47] An introduction to natural convection flows. `www.turbulence-online.com`. Chalmers University of Technology, Gothenburg, Sweden.

[48] W.M. Kays and M.E. Crawford. *Convective heat and mass transfer*. McGraw-Hill, Highstown, NJ, 1993.

[49] S.V. Patankar and D.B. Splading. A calculation procedure for heat mass and momentum transfer in three dimensional parabolic flows. *International journal of Heat and Mass Transfer*, 15:1787, 1972.

[50] J.P. Doormaal, G.D. Raithby. Enhancements of the SIMPLE method for predicting incompressible fluid flows. *Numerical Heat Transfer*, 7:147–163, 1984.

[51] B. Yu and H. Ozoe. A modified pressure-correction scheme for the SIMPLER method, MSIMPLER. *Numerical Heat Transfer, Part B*, 39:435–449, 2001.

[52] C.P. Kothandaraman. *Fundamentals of heat and mass transfer*. New Age International, 2006.

[53] D.E. Hryb and M.B. Goldschmit. Thermal interaction model between a fluid flow and a solid. *Latin American applied research*, 39, 2009.

[54] R.J. Guyan. Reduction of stiffness and mass matrices. *AIAA Journal*, 3:380, 1965.

[55] A.C. Antoulas. *Approximation of Large-Scale Dynamical Systems*. Advances in Design and Control, Society for Industrial and Applied Mathematics, 2009.

[56] A. Dumon. *Réduction dimensionnelle de type PGD pour la résolution des écoulements incompressibles*. PhD thesis, Université de La Rochelle, 2011.

[57] D. Amsallem and C. Farhat. CME 345 : Model reduction. University Lecture - Standford University.

[58] P. Nachtergaele, D. Rixen and A. Steenhoek. Efficient weakly coupled projection basis for the reduction of thermo-mechanical models. *Journal of Computational and Applied Mathematics*, 234:2272–2278, 2010.

[59] A. Kropp and D. Heiserer. Efficient broadband vibro-acoustic analysis of passenger car bodies using an fe-based component mode synthesis approach. *Journal of Computational Acoustics*, 11:139–157, 2003.

[60] P. Koutsovasilis and M. Beitelschmidt. Comparison of model reduction techniques for large mechanical systems - A study on an elastic rod. *Multibody System Dynamics*, 20:111–128, 2008.

[61] L.B. Bushard. On the value of Guyan Reduction in dynamic thermal problems. *Computers & Structures*, 13:525–531, 1981.

[62] T. Bechtold, E.B. Rudnyi and J.G. Korvink. *Fast Simulation of Electro-Thermal MEMS: Efficient Dynamic Compact Models*. Microtechnology and MEMS, Springer-Verlag Berlin Heidelberg, 2007.

[63] R. Craig and M. Bampton. Coupling of Substructures for Dynamic Analysis. *AIAA Journal*, 6:1313–1319, 1968.

[64] V. Faucher and A. Combescure. A time and space mortar method for coupling linear modal subdomains and non-linear subdomains in explicit structural dynamics. *Computer methods in applied mechanics and engineering*, 192:509–533, 2003.

[65] D. Rixen. A dual Craig-Bampton method for dynamic substructuring. *Journal of Computational and Applied Mathematics*, 168:383–391, 2004.

[66] M. Mignolet, C. Soize and J. Avalos. Nonparametric stochastic modeling of structures with uncertain boundary conditions/coupling between substructures. *AIAA Journal*, 51:1296–1308, 2013.

[67] D. Botto, S. Zucca and M.M. Gola. Reduced-Order Models for the Calculation of Thermal Transients of Heat Conduction/Convection FE Models. *Journal of Thermal Stresses*, 30:819–839, 2007.

[68] P.O. Laffay, O. Quéméner, A. Neveu and B. Elhajjar. The Modal Substructuring Method : an efficient technique for large size numerical simulations. *Numerical Heat Transfer, Part B*, 60:278–304, 2011.

[69] S.A. Marshall. An approximate method for reducing the order of a linear system. *Control*, 10:642–643, 1966.

[70] L. Litz. State decomposition for singular perturbation order reduction - A modal approach. *International Journal of Control*, 34:937–954, 1981.

[71] F. Da Silva. *Méthodologies de réduction de modèles multiphysiques pour la conception et la commande d'une chaine de traction électrique*. PhD thesis, Ecole Centrale de Paris, .

[72] PhD thesis.

[73] G. Michailesco. *Approximation des systèmes complexes par des modèles de dimension réduite*. PhD thesis, Universitè Paris-Sud, 1979.

[74] G. Lefèbvre. *La méthode modale en thermique - Modélisation, simulation, mise en oeuvre, applications*. Ellipses Marketing, Paris, 2007.

[75] A. Bobillot. *Méthodes de réduction pour le recalage. Application au cas d'Ariane 5*. PhD thesis, Ecole Centrale de Paris, 2002.

[76] F. Renaud. *Etude de l'incidence des comportements dissipatifs dans les instabilités vibratoires des systèms de freinage*. PhD thesis, Ecole Centrale de Paris, 2011.

[77] K. Karhunen. Über lineare methoden in der wahrscheinlichkeitsrechnung. *Ann. Acad. Sci. Fennicae, ser. Al. Math. Phys*, 37:3–79, 1946.

[78] M.M. Loève. *Probability theory*. The University Series in Higher Mathematics, third ed., Van Nostrand, Princeton, NJ, 1963.

[79] B. C. Moore. Principal component analysis in linear systems: controllability, observability, and model reduction. *IEEE Transactions on Automatic Control*, 26:17–32, 1981.

[80] G. Berkooz, P. Holmes and J.L. Lumley. The proper orthogonal decomposition in the analysis of turbulent flows. *Annual Review of Fluid Mechanics*, 25:539–575, 1993.

[81] J.D. Rambo. *Reduced-order modeling of multiscale turbulent convection: Application to data center thermal management.* PhD thesis, Georgia Institute of Technology, 2006.

[82] C. Leblond, C. Allery and C. Inard. An optimal projection method for the reduced-order modeling of incompressible flows. *Computer Methods in Applied Mechanics and Engineering*, 200:2507–2527, 2011.

[83] M. Krasnyk, M. Mangold and A. Kienle. Reduction procedure for parametrized fluid dynamics problems based on proper orthogonal decomposition and calibration. *Chemical Engineering Science*, 65:6238–6246, 2010.

[84] R. Gosh and Y. Joshi. Error estimation in POD-based dynamic reduced-order thermal modeling of data centers. *International Journal of Heat and Mass Transfer*, 57:698–707, 2013.

[85] G. Kerschen, J-C. Golinval,A.F. Vakakis and L.A. Bergman. The method of proper orthogonal decomposition for dynamical characterization and order reduction of mechanical systems: an overview. *Nonlinear Dynamics*, 41:147–169, 2005.

[86] M. Amabili, A. Sarkar and M.P.Païdoussis. Reduced-order models for nonlinear vibrations of cylindrical shells via the proper orthogonal decomposition method. *Journal of Fluid and Structures*, 18:227–250, 2003.

[87] N. Kumar and T.D. Burton. On combined use of POD modes and Ritz vectors for model reduction in nonlinear structural dynamics. In *22nd Biennial Conference on Mechanical Vibration and Noise (ASME 2009).*

[88] L. Sirovich. Turbulence and the dynamics of coherent structures part i: Coherent structures. *Quarterly of Applied Mathematics*, 45:561–571, 1987.

[89] B. Podvin. Introduction à la décomposition orthogonale aux valeurs propres ou P.O.D.

[90] D. Ryckelynck. A priori hyperreduction method: an adaptative approach. *Journal of Computational Physics*, 202:346–366, 2005.

[91] N. Verdon, C. Allery, D. Ryckelynck and A. Hamdouni. An adaptive ROM approach for solving transfer equations. *Journal of Computational Mechanics/Revue Européenne de Mécanique Numérique*, 15:589–605, 2006.

[92] A. Ammar, B. Mokdad, F. Chinesta and R. Keunings. A new family of solvers for some classes of multidimensional partial differential equations encountered in kinetic theory modeling of complex fluids. *Journal of Non-Newtonian Fluid Mechanics*, 144:98–121, 2007.

[93] A. Nouy. A priori model reduction through proper generalized decomposition for solving time-dependent partial differential equations. *Computer Methods in Applied Mechanics and Engineering*, 199:1603–1626, 2010.

[94] P. Ladveze. *Nonlinear computational structural mechanics. New approaches and non-incremental methods of calculation*. Mechanical Engineering Series. Springer-verlag, 1999.

[95] E. Cueto, D. Gonzalez, I. Alfaro, C. Quesada and F. Chinesta. Model order reduction methods for computational surgery.

[96] S. Niroomandi, I. Alfaro, D. Gonzalez, E. Cueto and F. Chinesta. Model order reduction in hyperelasticity : a proper generalized decomposition approach. *International Journal for Numerical Methods in Engineering*, 96:129–149, 2013.

[97] O. Zahm, M. Billaud-Friess and A. Nouy. Goal-oriented low-rank approximation for high dimensional stochastic problems.

[98] F. Bordeu, F. Chinesta, E. Cueto, A. Leygue. Abaques numériques: Visualisation et post-Traitement de solutions variable séparée. Application au temps réel non Linaire.

[99] D. Bui, M. Hamdaoui and F. De Vuyst. POD-ISAT: A new and efficient reduced-order modeling method for the representation of parametrized finite element solutions. Application to aircraft air control systems. *International Journal for Numerical Methods in Engineering*, 00:1–21, 2010.

[100] K.J. Astrom and P. Eykhoff. System Identification - A Survey. *Automatica*, 7:123–162, 1971.

[101] L. Ljung. *System identification - theory for the user*. Prentice-Hall, Englewood Cliffs, New Jersey, 1987.

[102] G. Kerschen, K. Worden, A.F. Vakakis and J-C. Golinval. Past, present and future of nonlinear system identification in structural dynamics. *Mechanical Systems and Signal Processing*, 20:505–592, 2006.

[103] A. Allard. *A Linear Data-Driven System Identification Methodology for an Active/Passive Solar Thermal Storage System and Application to a Solar House*. PhD thesis, Concordia University, Montreal, Quebec, Canada, 2013. Department of Building, Civil and Environmental Engineering.

[104] G.A. Bekey. System Identification - an introduction and a survey. *Simulation*, 15:151–166, 1970.

[105] E.J. Hannan and M. Deistler. *The statistical theory of linear systems*. John Wiley & Sons Inc., New York, 1988.

[106] R.K. Pearson and U. Kotta. Nonlinear discrete-time models: state-space vs. I/O representations. *Journal of Process Control*, 2004.

[107] E. Meadows and J. Rawlings. *Nonlinear Process Control*. Prentice Hall, 1997. pp. 233310 (Chapter 5).

[108] The Z Transform. `http://lpsa.swarthmore.edu/ZXform/FwdZXform/FwdZXform.html`.

[109] S.M. Moore, J.C.S. Lai and K. Shankar. ARMAX modal parameter identification in the presence of unmeasured excitation-II: Theoretical background. *Mechanical Systems and Signal Processing*, 21:1601–1615, 2007.

[110] S.M. Moore, J.C.S. Lai and K. Shankar. ARMAX modal parameter identification in the presence of unmeasured excitation-II: Numerical and experimental verification. *Mechanical Systems and Signal Processing*, 21:1616–1641, 2007.

[111] M. Aoki. Complementary representation of multiple time series in state space innovation forms. *UCLA Economics Working Papers 628, UCLA Departement of Economics*, 1991.

[112] L. Ljung. *System identification - theory for the user (second ed.)*. Upper Saddle River, New Jersey: Prentice-Hall, 1999.

[113] K. J. Aström and T. Bohlin. Numerical identification of linear dynamic systems for normal operating records. In *The Proceedings of the 2nd IFAC Symposium on the Theory of Self-Adaptive Systems, Teddington, England*, pages 96–111, 1965.

[114] K.J. Aström. Maximum Likelihood and Prediction Error Methods. *Automatica*, 16:551–574, 2001.

[115] H. Monson. *Statistical Digital Signal Processing and Modeling*. John Wiley & Sons, 1996.

[116] S.M. Kay. *Modern Spectral Estimation: Theory and Application*. Prentice Hall, Englewood Cliffs, NJ, 1988. pp. 228-230.

[117] T. Söderström, B. Carlsson and S. Bigi. Least Squares Parameter Estimation of Continuous-Time ARX Models from Discrete-Time Data. In *IEEE transactions on Automatic Control*, volume 42, pages 659–673, 1997.

[118] T. Söderström and P. Stoica. *Instrumental variable method for system identification*. New York: Springer Verlag, 1983.

[119] E.H.K. Fung, Y.K. Wong, H.F. Ho and M.P. Mignolet. Modelling and prediction of machining errors using ARMAX and NARMAX structures. *Applied Mathematical Modelling*, 27:611–627, 2003.

[120] I.J. Leontaritis and S.A. Billings. Input-output parameter models for nonlinear systems. Part 1 : Deterministic nonlinear systems. Part 2 : Stochastic nonlinear systems. *International Journal of Control*, 41:303–344, 1985.

[121] D.H. Zhou and P.M. Franck. A real-time estimation approach to time-varying time delay and parameters of NARX processes. *Computers & Chemical Engineering*, 23:1763–1772, 2000.

[122] T. Söderström and P. Stoica. *System identification*. Prentice Hall, UK, 1989.

[123] C.M. Hurvich and C-L. Tsai. Regression and time series model selection in small samples. *Biometrika*, 76:297–307, 1989.

[124] S.D. Fassois. MIMO LMS-ARMAX identification of vibrating structures - part I: the method. *Mechanical Systems and Signal Processing*, 15:723–735, 2001.

[125] J.C-M. Yiu and S. Wang. Multiple ARMAX modeling scheme for forecasting air conditioning system performance. *Energy conversion & Management*, 48:2276–2285, 2007.

[126] M.S. Sadabadi, M. Shafiee and M. Karrari. Two-dimensional ARMA model order determination. *ISA Transactions*, 48:247–253, 2009.

[127] B. Bao, Y. Xu, J. Sheng and R. Ding. Least-squares based iterative parameter estimation algorithm for multivariable controlled ARMA system modelling with finite measurement data. *Mathematical and Computer Modelling*, 53:1664–1669, 2011.

[128] J. Hu, K. Hirasawa and K. Kumamaru. A homotopy approach to improving PEM identification of ARMAX models. *Automatica*, 37:1323–1334, 2001.

[129] B. Wang, N-L. Tai, H-Q. Zhai, J. Ye, J-D. Zhu and L-B. Qi. A new ARMAX model based on evolutionary algorithm and particle swarm optimization for short-term load forecasting. *Electric Power Systems Research*, 78:1679–1685, 2008.

[130] G.R. Sriniwas and Y. Arkun. A global solution to the nonlinear model predictive control algorithms using polynomial ARX models. *Computers & chemical Engineering*, 21:431–439, 1997.

[131] J.V. Candy. *Model-based signal processing*. Wiley-IEEE Press, 2005.

[132] T. Katayama. *Subspace methods for system identification*. Springer, 2010.

[133] D. Petit and R. Hachette, D. Veyret. A modal identification method to reduce a high-order model : application to heat conduction modelling. *International Journal of Modelling & Simulation*, 17(3):242–250, 1998.

[134] E. Videcoq, M. Girault and A. Piteau. Thermal control via state feedback using a low order model built from experimental data by the modal identification method. *International Journal of Heat and Mass Transfer*, 55:1679–1694, 2012.

[135] Y. Rouizi, Y. Favennec, Y. Jarny and D. Petit. Model reduction through identification - Application to some diffusion-convection problems in heat transfer, with an extension towards control strategies. *C. R. Mecanique*, 341:776–792, 2013.

[136] D. Petit and R. Hachette. Model reduction in linear heat condution : use of interface fluxes for the numerical coupling. *International Journal of Heat and Mass Transfer*, 41:3177–3189, 1998.

[137] Y. Favennec, M. Girault and D. Petit. The adjoint method coupled with the modal identification method for nonlinear model reduction. *Inverse Problems in Science and Engineering*, 14(2):153–170, 2006.

[138] M. Girault and D. Petit. Identification methods in nonlinear heat conduction. Part I: model reduction. *International Journal of Heat and Mass Transfer*, 48:105–118, 2005.

[139] Y. Rouizi, Y. Favennec, J. Ventura and D. Petit. Numerical model reduction of 2D steady incompressible laminar flows: Application on the flow over a backward-facing step. *Journal of Computational Physics*, 228:2239–2255, 2009.

[140] Y. Rouizi, M. Girault, Y. Favennec and D. Petit. Model reduction by the Modal Identification Method in forced convection: Application to a heated flow over a backward-facing step. *Journal of Thermal Sciences*, 49:1354–1368, 2010.

[141] M. Girault and D. Petit. Identification methods in nonlinear heat conduction. Part II: inverse problem using a reduced model reduction. *International Journal of Heat and Mass Transfer*, 48:119–133, 2005.

[142] W. Bouarifi. *Assimilation Variationnelle des conditions initiales par contrôle optimal et identification de paramètres par algorithmes génétiques dans le modèle ICARE*. PhD thesis, Faculté des Sciences et Techniques de Marrakech, 2009.

[143] B. De Moor, M. Moonen, L. Vandenberghe and J. Vandewalle. *Identification of linear state space models with SVD using canonical correlation analysis*, pages 161–169. North-Holland Publishing Co. Amsterdam, The Netherlands, 1988.

[144] M. Moonen, B. De Moor, L. Vandenberghe and J. Vandewalle. On- and off-line identification of linear state-space models. *International Journal of Control*, 49(1):219–232, 1989.

[145] M. Moonen and J. Vandewalle. QSVD approach to on- and off-line state-space identification. *International Journal of Control*, 51(5):1133–1146, 1990.

[146] L. Ferkl and J. Siroky. Ceiling radiant cooling: Comparison of ARMAX and subspace identification modelling methods. *Building and Environment*, 45:205–212, 2010.

[147] P. Van Overschee and B. De Moor. N4SID - Subspace algorithms for the identification of combined deterministic - stochastic systems. *Automatica*, 30(1):75–93, 1994.

[148] M. Verhaegen and P. Dewilde. Subspace model identification, Part 1: The output-error state-space model identification class of algorithms. *International Journal of Control*, 56(5):1187–1210, 1992.

[149] M. Verhaegen and P. Dewilde. Subspace model identification, Part 2: Analysis of the elementary output-error state space model identification algorithm. *International Journal of Control*, 56(5):1211–1241, 1992.

[150] W. E. Larimore. Canonical variate analysis in identification, filtering and adaptive control. In *The Proceedings of the 29th Conference on Decision and Control, Hawai, USA*, pages 596–604, 1990.

[151] G. Picci and T. Katayama. Stochastic realization with exogenous inputs and "subspace methods" identification. *Signal Processing*, 52(2):145–160, 1996.

[152] T. McKelvey, H. Akay and L. Ljung. Subspace-based multivariable system identification from frequency response data. *IEEE Transactions on Automatic Control*, 41:960–979, 1996.

[153] P. Van Overschee, B. De Moor, W. Dehandschutter and J. Swevers. A subspace algorithm for the identification of discrete-time frequency domain power spectra. *Automatica*, 33(12):2147–2157, 1997.

[154] A. Ohsumi, K. Kameyama and K. Yamaguchi. Subspace identification for continuous-time stochastic systems via distribution-based approach. *Automatica*, 38(1):63–79, 2002.

[155] S. L. Lacy and D. S. Bernstein. Subspace identification for non-linear systems with measured-input non-linearities. *International Journal of Control*, 78:906–926, 2005.

[156] J. P. Noël and G. Kerschen. Frequency-domain subspace identification for nonlinear mechanical systems. *Mechanical Systems and Signal Processing*, 40:701–717, 2013.

[157] J. P. Noël, S. Merchesiello and G. Kerschen. Subspace-based identification of a non-linear spacecraft in the time and frequency domains. *Mechanical Systems and Signal Processing*, 43:217–236, 2014.

[158] P. Van Overschee and P. B. De Moor. *Subspace identification for linear systems, Theory - Implementation - Applications*. Kluwer Academic Publishers, 1996.

[159] H. J. Palanthandalam-Madapusi, S. Lacy, J. B. Hoagg and D. S. Bernstein. Subspace-Based Identification for Linear and Nonlinear Systems. In *The Proceedings of the 2005 American Control Conference*, volume 4, pages 2320–2334, 2005.

[160] P. Van Overschee and P.B. De Moor. Available software for subspace identification. `http://homes.esat.kuleuven.be/~smc/sysid/software/`.

[161] R. E. Kalman. Mathematical description of linear dynamical systems. *SIAM Journal on Control*, 1:152–192, 1963.

[162] P. Businger and G. H. Golub. *Linear least squares solutions by Householder transformations*. in Wilkinson and Reinsch, Linear Algebra, Springer Verlag, 1971.

[163] K.T. Chau and C.C. Chan. Nonlinear identification of power electronic systems. *SIAM Journal on Control*, 1:152–192, 1995.

[164] W.J. Rugh. *Nonlinear System Theory - The Volterra/Wiener Approach*. The Johns Hopkins University Press, 1981.

[165] L.L. Li and S.A. Billings. Volterra series truncation and reduction in the frequency domain for weakly nonlinear system. Technical report, Department of Automatic Control and Systems Engineering, University of Sheffield, UK, 2006.

[166] D.M. Storer. *Dynamic analysis of non-linear structures using higher order frequency response functions*. PhD thesis, The University of Manchester, 1991.

[167] R. Towner and J. Band. An analysis technique/automated tool for comparing and tracking analysis modes of different Finite Element models. In *53rd AIAA/ASME/ASCE/AHS/ASC Structures, Structural Dynamics and Materials Conference*, 2012.

[168] R.J. Allemang. The modal assurance criterion: Twenty years of use and abuse. *Sound and Vibration,*, 37:14–23, 2003.

[169] H.W. Sorenson. Least-squares estimation: from Gauss to Kalman. *IEEE Spectrum*, 7:63–68, 1970.

[170] S.J. Julier and J.K. Uhlmann. A general method for approximating nonlinear transformations of probability distributions. Technical report, University of Oxford, Departement of Engineering Science, 1996.

[171] S.J. Julier and J.K. Uhlmann. A new extension of the Kalman Filter to nonlinear systems. In *The Proceedings of AeroSense: The 11th Int. Symp. on Aerospace/Defence Sensing, Simulation and Controls*, pages 182–193, 1997.

[172] J-L. Dion, C. Stephan, G. Chevallier and H. Festjens. Tracking and removing modulated sinusoidal components: A solution based on the kurtsis and the Extended Kalman Filter. *Mechanical Systems and Signal Processing*, 38:428–439, 2013.

[173] M. Bisgaard, A. Cour-Harbo and J.D. Bendtsen. Adaptive control system for autonomous helicopter slung load operations. *Mechanical Systems and Signal Processing*, 18:800–811, 2010.

[174] S. Pan, H. Su, J. Chu and H. Wang. Applying a novel extended Kalman filter to missiletarget interception with APN guidance law: A benchmark case study. *Control Engineering Practice*, 18:159–167, 2010.

[175] K.M. Neaupane and M. Sugimoto. An inverse boundary value problem using the Extended Kalman Filter. *Mechanical Systems and Signal Processing*, 29:121–126, 2003.

[176] F. Abid, G. Chevallier, J-L. Blanchard and J-L. Dion. System identification using Kalman Filters. In *The Proceedings of the Society for Experimental Mechanics*, volume 7, pages 561–573, 2013.

[177] D.G. Khairnar, S.N. Merchant and U.B. Desai. Nonlinear target identification and tracking using UKF. In *The Proceedings of the 2007 IEEE International Conference on Granular Computing*, page 761, 2007.

[178] J.J. LaViola and K. Joseph. A comparison of unscented and extended Kalman filtering for estimating quaternion motion. In *The Proceedings of the 2003 American Control Conference*, pages 2435–2440, 2003.

[179] J.R. Dormand and P.J. Prince. A family of embedded Runge-Kutta formulae. *Journal of Computational and Applied Mathematics*, 6:19–26, 1980.

[180] J.H. Mathews and K.D. Fink. *Numerical methods using MATLAB*. Prentice Hall, 2004.